PART 1. DYNAMIC RESPONSE OF PHASE BOUNDARIES IN THE EARTH TO SURFACE LOADING

PART 2. PLEISTOCENE GLACIATION AND THE VISCOSITY OF THE LOWER MANTLE

Thesis by

Richard John O'Connell

In Partial Fulfillment of the Requirements

For the Degree of

Doctor of Philosophy

California Institute of Technology

Pasadena, California

1969

(Submitted May 19, 1969)

ACKNOWLEDGMENTS

Throughout my graduate career, G. J. Wasserburg has generously given of his time, even when little was available, to answer questions, discuss problems, and give advice in general. In preparing Part 1 of this thesis under his guidance, I learned much about doing science beyond the mere mechanics of it. For all this I would like to thank him.

I would like to thank Don L. Anderson for discussions of Part 2 of this thesis, and for accepting partial responsibility for a student who rarely let him know what he was doing. Peter Goldreich pointed out to me that the non-hydrostatic bulge of the earth is no larger than the ellipticity of the equator, thus saving me from pursuing a study based on the assumption that the bulge was anomalously large.

During my studies I was supported as a Graduate Research Assistant by the California Institute of Technology and by a National Science Foundation Graduate Fellowship. Research for Part 2 of this thesis was supported by NASA contract NGL 05-002-069.

Most of all I would like to thank my wife Micheline, who, having left her home, family and friends to come to a foreign country and culture, constantly and patiently gave her loving support and encouragement, and who combined the best of two cultures in creating a welcome refuge to which it was always a temptation to retire.

ABSTRACT

Part 1. Analytic approximate solutions have been found for the response of a phase change to pressure loading. These solutions allow the behavior of the system to be analyzed in terms of simple parameters of the system. Different characteristic types of behavior are shown to obtain for short times and long times, and criteria for defining these characteristic time scales are given in terms of known parameters. The distribution of heat sources and convective heat transport are shown to generally have only minor influence on the solution, and may be neglected in many cases. The important parameters are the latent heat of the phase change, and the difference between the Clapeyron slope and the temperature gradient at the phase boundary; in addition the long term behavior is governed by the boundary conditions at the surface and at depth, and the relative positions of the surface, the phase boundary, and the lower boundary. The effect of thermal blanketing from sediments is included in the solution, and it depends primarily on the depth of the phase boundary and the average temperature gradient in the sediments. The effect of isostasy in conjunction with a phase change is shown to be of major importance; the existence of instabilities where the water depth increases with sedimentation are demonstrated. These solutions allow the history of a sedimentary basin to be calculated, and characterized in terms of certain types of behavior. The existence of oscillatory behavior is demonstrated, where repeated cycles of sedimentation and erosion take place. These oscillations can either decay or grow in amplitude, and expressions are given for their frequency and damping or growth

constants. A phase change mechanism can account for thicknesses of sediments which exceed the depth of the basin in which they were deposited by a factor of twenty or more. These solutions allow the discussion of the geological implications of phase changes in a quantitative manner. The consequences of a phase change can be accurately calculated. This will allow the more complete investigation of the role of phase changes in geologic processes.

Part 2. The non-tidal acceleration of the earth, revealed by astronomical observations and records of eclipses in antiquity, is attributed to the change in the earth's moment of inertia resulting from isostatic response to the most recent deglaciation and rise in sea level. The isostatic response time for a spherical harmonic deformation of degree two is calculated on this basis to be either $\sim$ 2000 years or $\sim$ 100,000 years. A correlation of the geopotential with the potential that would have existed following deglaciation indicates that any large scale anomalies resulting from deglaciation have already decayed. This rules out the 100,000 relaxation time; thus the relaxation time of the earth is $\sim$ 2000 years for degree two. Calculations of the relaxation time spectrum of a layered, gravitating spherical viscous earth model indicates that a model with a uniform mantle viscosity of $\sim 10^{22}$ poise, except for fine structure in the upper few hundred kilometers, can satisfy the relaxation time of 3000 years for degree two as well as the relaxation time of $\sim$ 4000 years for degree twenty which results from studies of uplift in Fennoscandia. A zone of high viscosity in the lower 800 km. of the mantle has a significant effect on the degree two relaxation time. This rules out any substantial increase in viscosity in the lower mantle. The calculated viscosity permits rapid polar wandering and convection in the lower mantle.

To my parents,

in appreciation of their loving and patient support

TABLE OF CONTENTS

PART I

DYNAMIC RESPONSE OF PHASE BOUNDARIES IN THE EARTH TO SURFACE LOADING

CHAPTER I

DYNAMICS OF THE MOTION OF A PHASE CHANGE BOUNDARY TO CHANGES IN PRESSURE

This chapter is a reprint of an article of the same title by R.J. O'Connell and G.J. Wasserburg in Reviews of Geophysics, volume 5, number 4, pages 329-410, published November, 1967.

REVIEWS OF GEOPHYSICS

VOLUME 5 NOVEMBER 1967 NUMBER 4

Dynamics of the Motion of a Phase Change Boundary to Changes in Pressure[1]

RICHARD J. O'CONNELL AND G. J. WASSERBURG

Charles Arms Laboratory of Geological Sciences
California Institute of Technology, Pasadena, California

Abstract. Because of the significance of both shallow and deep phase changes to geophysical problems, the dynamical response of a phase change to pressure loading was investigated. It was found that the characteristic behavior of the system may be analyzed in terms of simple parameters of the system by using analytic expressions that apply for the initial part and the final part of the motion of the phase boundary. These expressions are obtained from approximations based on generalizations of Neumann's solution for melting at a constant temperature or from simple physical approximations based on the over-all geometry of the model. The range of applicability of the approximations can be obtained from the approximations themselves. The analytic results compare very favorably with exact numerical solutions. The distribution of heat sources and convective heat transport are shown to be generally of minor importance on the motion of the phase boundary; the effect of convective heat transport can be estimated from the analytic approximation. The important parameters are the latent heat of the phase change and the difference in slope between the Clapeyron curve and the temperature distribution in the earth. In addition, the long-term motion depends primarily on the over-all geometry of the model and the boundary condition at depth. The analytic results indicate the time at which thermal blanketing by sediments becomes important and the effect of the rate of sedimentation on the response of the system; they also define slow and fast sedimentation and secular equilibrium. The effect of isostasy in conjunction with a shallow phase change is shown to be of major importance, and for certain cases the sediment thickness that can accumulate in a sedimentary basin may depend only on the sedimentation rate and not the initial depth of the basin. The analytic results permit a more physical discussion of the problem, since the functional dependence of the solution on the parameters may be seen. In addition, important results for a variety of models can be obtained by relatively simple calculations, without resorting to separate numerical solutions for each model considered.

[1] California Institute of Technology Contribution 1494.

NOTATION

t, time.
x, depth.
$T(x, t)$, temperature.
$M(t)$, location of phase boundary.
$b(t)$, location of lower boundary.
$-J(x, t)$, heat flux.
$P(x)$, pressure.
$\mathfrak{T}_c(P) = GP - F = T_c(x)$, Clapeyron temperature.
K_j, thermal conductivity in region 'j.'
ρ_j, density in region 'j.'
c_v, heat capacity at constant volume.
c_j, heat capacity c_v in region 'j.'
κ_j, thermal diffusivity in region 'j.'
A_j, heat production due to sources in region 'j.'
V_j, velocity in region 'j.'
L, latent heat of phase change.
S_j, entropy per gram of *phase* 'j.'
g, gravitational acceleration.
$\Theta(x, t) \equiv T(x, t) - T(x, 0)$, perturbation temperature.
$M_i \equiv M(0)$, initial location of phase boundary.
$M_f \equiv M(\infty)$, final location of phase boundary.
ΔP, pressure pulse.
$b_i \equiv b(0)$, initial location of lower boundary.
$b_f \equiv b(\infty)$, final location of lower boundary.
s, sediment thickness.
w, water depth.
$\tilde{\theta}$, $\tilde{\tau}$, $\tilde{\xi}$, tilde denotes approximation to corresponding quantity (θ, τ, ξ).

DIMENSIONLESS TERMS

$b_0 \equiv b(0)$
$T_0 \equiv [J(0, 0)/K_1]b_0$
$\xi \equiv x/b_0$, depth.
$\tau \equiv (\kappa_1/b_0^2)t$, time.
$\eta(\xi, \tau) \equiv T(x, t)/T_0$, temperature.
$\xi_m(\tau) \equiv M(t)/b_0$, location of phase boundary.
$\beta(\tau) \equiv b(t)/b_0$, location of lower boundary.
$\eta_c(\xi) \equiv T_c(P)/T_0$, Clapeyron temperature.
$\alpha_i \equiv \kappa_i/\kappa_1$, diffusivity.
$\sigma_i \equiv b_0^2 A_i/T_0 K_i$, heat sources.
$\nu \equiv (b_0/\kappa_1)V$, velocity.
$C \equiv L/c_1 T_0$, latent heat.
$\theta(\xi, \tau) \equiv \eta(\xi, \tau) - \eta(\xi, 0)$, perturbation temperature.
$\theta_c(\xi) \equiv \eta_c(\xi) - \eta(\xi, 0)$, reduced Clapeyron temperature.
$\gamma_i \equiv [J(0, 0)/K_i](b_0/T_0)$, temperature gradient.
$D \equiv (G\rho_1 g b_0/T_0) - \gamma_1$, reduced Clapeyron slope.
$E \equiv (F/T_0) - (G\,\Delta P/T_0)$, zero intercept of $\theta_c(\xi_m)$.
$W \equiv 1 - J(0, 0)/G\rho_1 g K_1$
$R \equiv \rho_s c_1 b_0/WK_1\, ds/dt$, sedimentary loading rate.
$r \equiv 4D/C\sqrt{\pi}$, rate constant for continuous sedimentation models.
$\tilde{\tau}^*$, see equation 36.
$\tilde{\tau}^{**}$, see equation 46.
$\tilde{\tau}_l$, see equation 44.
$\tilde{\tau}^\dagger$, see equation 48.
$\tilde{\tau}^{\dagger\dagger}$, see equation 49.
$\tilde{\tau}_R$, see equation 57.

1. INTRODUCTION

There is no doubt that phase changes are a significant feature of the earth's mantle; thus a response of a phase change to dynamical changes in pressure is of general geophysical interest. Although the discussion to be presented in this paper emphasizes shallow phase changes, the formal treatment developed is applicable to the more general problem.

The identification of the Mohorovicic discontinuity as a phase change has been shown to have important geological implications. *Lovering* [1958] and *Kennedy* [1959] have discussed such a phase change as a mechanism for uplifting or depressing relatively large areas of the earth's surface and have alluded to the pertinence of this mechanism to such questions as the formation of geosynclines, the elevation of plateaus, and the origin and permanence of mountain ranges.

The consequences of such a phase change result from the fact that the depth of the phase boundary is determined by the temperature and pressure in the earth; hence changes in either of these might change the equilibrium position of the phase boundary. If sediments are deposited on the surface, the resultant increase in pressure will tend to move the phase boundary upward, which, owing to the difference in density of the two phases, will cause the surface to subside. The conversion of a low density–high entropy phase to a high density–low entropy phase will result in the liberation of heat at the phase boundary. The removal of this extra heat will govern the rate of movement of the phase boundary.

Owing to the subsidence of the surface and the different thermal conductivities of the two phases, the new equilibrium position of the phase boundary may result in a final steady-state temperature distribution different from the initial distribution. This redistribution may extend to considerable depth and may therefore depend on thermal conditions deep in the earth. Since the new temperature distribution will partly determine the final equilibrium position of the phase boundary, it will affect its movement.

The presence of sediments on the formerly free surface will also affect the final temperature distribution, causing the temperature beneath the former surface to rise, which would tend to move the phase boundary deeper.

Thus there are basically two different effects: (1) an increase in pressure causes the surface to subside in response to the loading, and (2) the thermal blanketing of any deposited sediments would by itself cause the surface to rise in opposition to the loading. Modifying these two effects are (3) the fact that the latent heat must be removed from the vicinity of the phase boundary for the reaction to proceed, and (4) the final temperature distribution may require the redistribution of heat from the initial distribution.

MacDonald and Ness [1960] have already treated certain aspects of the dynamic problem; because of the possible importance of the problem, however, it was considered of interest to treat the problem in more detail in order to separate the effects of the various factors that together determine the solution.

Wetherill [1961] has treated some of the steady-state aspects of the problem, which predict the final location of the phase boundary after the deposition of a given thickness of sediments. He showed that, although the identification of the Moho as a single phase change cannot explain the differences between oceans and continents, response of a phase change to loading by sediments could result in considerable differences in crustal elevation. Further, the necessity to include isostasy in the solution to the dynamic problem was stressed, as well as the importance of the rate of erosion on uplifted regions. Finally, the possible importance of convective heat transport in the dynamic problem was pointed out.

Although the problem treated in this paper does not fully consider isostasy or

continuous sedimentation and erosion, it is still of considerable geophysical interest. The essential process that will be treated is the response of a phase change to changes in pressure; the effects of isostasy, sedimentation, and erosion will be primarily to modify the pressure response. Our first object is, therefore, to examine the response of a phase change to a given pressure pulse, and the dependence of this response on various parameters. To this end it is desirable to treat at first a highly simplified problem in order to separate various effects. We later consider the effect of the altered equilibrium temperature distribution on the movement of the phase boundary.

To formulate the problem in one dimension we represent the outer layers of the earth as an infinite plate of uniform thickness. We thus neglect the sphericity of the earth; this omission should not be serious, however, owing to the restricted thickness of the region considered (100–200 km).

The relevant equation is the equation of heat conduction

$$\rho c(DT/Dt) = \rho c[\partial T/\partial t + V(\partial T/\partial x)] = (\partial/\partial x)[K(\partial T/\partial x)] + A \qquad (1)$$

where
T = temperature.
K = thermal conductivity.
ρ = density.
c = heat capacity.
A = rate of radioactive heat production.
V = velocity of medium.

The boundary conditions to be satisfied are:

(*a*) $T = 0$ at the earth's surface.

(*b*) a boundary condition must be applied at the bottom of the region, i.e. at some depth in the earth. The exact condition is not known; however, it should be contained between the following extremes:

(1) Constant temperature at the bottom of the region $x = b$. This means that the temperature in regions below the depth $x = b$ will be unaffected by changes at depths less than b.

(2) Constant heat flux at depth $x = b$. This means that changes in temperature at shallow depth might cause changes at all depths to the earth's center.

Since the process would actually take place only in a restricted segment of the earth, the temperature at depth would be controlled by lateral flow of heat. Constant flux at $x = b$ implies that heat flows laterally. Constant temperature implies that no heat flows laterally.

Knowledge of the effect of the choice of the boundary condition on the solution to the problem would indicate possible limitations of the solution obtained from this model.

(*c*) At the phase boundary $M(t)$, the temperature must be continuous and will be given by the Clapeyron curve, which gives the temperature at which the two phases may coexist at a given pressure. The liberation of the latent heat of reaction at the phase boundary requires

$$\left[K(x)\frac{\partial T}{\partial x}\right]_{x=M^-(t)} - \left[K(x)\frac{\partial T}{\partial x}\right]_{x=M^+(t)} = -L\rho\frac{dM(t)}{dt} \tag{2}$$

where L = latent heat of phase change and ρ = density of region in which the coordinate system is fixed. Thus there will be a discontinuity in the heat flux at the phase boundary due to the evolution of heat.

We will assume that the stress distribution is always hydrostatic. Conservation of mass across the phase boundary will determine the velocity in the field equation 1. In addition, heat sources must be conserved across the phase boundary.

There are two major sources of difficulty in the problem. The first is the nonlinear condition (2) at the phase boundary. The second is the nonlinear term for convective heat transport in the heat equation. This term could conceivably be neglected if it were small enough. If so, the search for an analytic solution would be greatly simplified. Thus it is of interest to determine the magnitude and importance of the term $V(\partial T/\partial x)$ in the field equation.

The approach in this paper will be to analyze the problem in certain limiting cases. We will then show that these cases exhibit a simple behavior, which can be characterized in terms of simple functions of the physical constants. These relationships will be applied to the more general case, and it will be shown that this can be treated semiquantitatively with the approximate analytical expressions obtained.

2. STEADY-STATE BEHAVIOR

Before discussing the dynamics of the motion of a phase boundary subject to loading, it is of interest to develop the properties of the steady-state systems. Consider a layered system of two phases (1, 2) in hydrostatic equilibrium containing no heat sources at equilibrium. Let the Clapeyron curve be a straight line defined by $\mathfrak{I}_e(P) = GP - F$, let the initial depth of the transition be M_i, and let the initial total thickness of the layers be $b(0)$. The mass per unit area between the surface and the base of the lower layer is $m \equiv \rho_1 M_i + \rho_2(b(0) - M_i)$. The initial temperature is given by

$$T_i(x) = \begin{cases} \dfrac{J_i x}{K_1} = \dfrac{J_i P(x)}{K_1\rho_1 g}\,; & 0 \le x \le M_i \\ \dfrac{J_i M_i}{K_1} + \dfrac{J_i(x - M_i)}{K_2} & \\ \qquad = \dfrac{J_i P(M_i)}{K_1\rho_1 g} + \dfrac{J_i[P(x) - P(M_i)]}{K_2\rho_2 g}\,; & M_i \le x \le b(0) \end{cases} \tag{3}$$

where $-J_i$ is the initial heat flux at the surface $x = 0$. The initial pressure as a function of depth is

$$P_i(x) = \begin{cases} \rho_1 g x & 0 \le x \le M_i \\ \rho_1 g M_i + \rho_2 g(x - M_i) & M_i \le x \end{cases} \tag{4}$$

The initial position of the phase boundary is given by

$$M_i = \frac{F}{\rho_1 g(G - J_i/K_1\rho_1 g)}$$

$$P_i(M_i) = \frac{F}{(G - J_i/K_1\rho_1 g)} \tag{5}$$

$$T_i(M_i) = \frac{J_i F}{K_1\rho_1 g(G - J_i/K_1\rho_1 g)}$$

If we assume for simplicity that $K_1\rho_1 = K_2\rho_2$, then on the (P, T) plane, the initial temperature T_i is a straight line of slope $J_i/K_1\rho_1 g$. This is shown in Figure 1. The point of intersection of $T_i[x(P)]$ and $\mathfrak{T}_c(P)$ is very sensitive to the difference between the Clapeyron slope $[d\mathfrak{T}_c(P)/dP] = G$ and the temperature slope $[dT_i(P)/dP] = J_i/K_i\rho_1 g$.

Let us now consider the new state that will obtain for this system at the instant that a sudden pressure pulse ΔP is applied and maintained. This means that the pressure of every piece of matter is increased by ΔP and the temperature at that

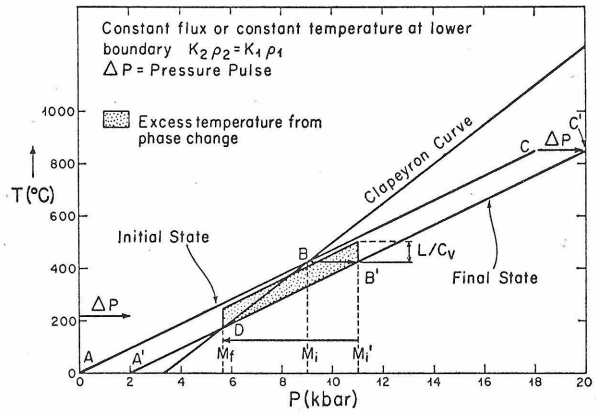

Fig. 1. Representation in the pressure-temperature plane of the effect of a pressure pulse ΔP on a phase change. The initial temperature distribution is shown by the line ABC. The phase boundary is originally at depth M_i, corresponding to point B. The pressure pulse increases the pressure at depth M_i; thus point B is moved to B' in pressure space, although the depth of the phase boundary is unchanged. The change in the temperature distribution due to the pressure pulse is represented by the translation of the line ABC into line $A'B'C'$ and of the point M_i to M_i'. The difference in pressure between the initial and final positions of the phase boundary corresponds to the arrow between M_i' and M_f. In order that the phase change move to its final position at M_f, the latent heat $L\rho(M_i - M_f)$ must be removed. The line displaced vertically by L/C_v is the increase in temperature that would occur if the phase change proceeded instantaneously in the region between M_f *to* M_i'.

instant remains constant. Hence, $P(x)$ is replaced by $P(x) - \Delta P$ in the expressions for $T(x)$.

$$T = \frac{J_i(P - \Delta P)}{K_1\rho_1 g}; \qquad P = \begin{cases} \rho_1 g x + \Delta P & 0 \leq x \leq M_i \\ \rho_1 g M_i + \rho_2 g(x - M_i) + \Delta P & M_i \leq x \leq b_i \end{cases} \tag{6}$$

This is the initial state translated by a distance ΔP in the (P, T) plane. In the (P, T) plane, the translated position of the initial phase boundary M_i is indicated by M_i' and corresponds to the motion of point B to B', as shown in Figure 1. If we assume the pressure pulse to be due to a load with no thermal impedance, then the final steady state will correspond to the translated line. The surface and bottom of the system correspond to points A' and C', respectively. The final equilibrium position of the phase change occurs at depth M_f, corresponding to point D in the diagram.

$$\begin{aligned} M_f &= M_i - \frac{G\,\Delta P}{\rho_1 g(G - J_i/K_1\rho_1 g)} = M_i\left(1 - \frac{G\,\Delta P}{F}\right) \\ P(M_f) &= P_i(M_i) - \frac{G\,\Delta P}{(G - J_i/K_1\rho_1 g)} = P_i(M_i)\left(1 - \frac{G\,\Delta P}{F}\right) \\ T(M_f) &= T_i(M_i) - \frac{GJ_i\,\Delta P}{K_1\rho_1 g(G - J_i/K_1\rho_1 g)} = T_i(M_i)\left(1 - \frac{G\,\Delta P}{F}\right) \end{aligned} \tag{7}$$

The fractional changes in the position, temperature, and pressure of the phase boundary at the new equilibrium position is thus $-(G\,\Delta P/F)$.

The difference between the new equilibrium temperature and the original unperturbed temperature as a function of position is defined by $\Theta(x, t) \equiv T(x, t) - T_i(x)$, and it is identically zero for the simple case under discussion.

The total heat energy per unit area that the system must lose to go from the initial to the final state is $L(M_f - M_j)\,\rho_1$. The temperature rise that a unit of matter would undergo if it instantaneously underwent the transition is L/c_v as shown in Figure 1. If $(L/c_vG) \geq \Delta P$, then no piece of matter will completely undergo the transition instantaneously, as this would drive it to a temperature above the Clapeyron curve. In this case the phase boundary will move at a rate determined by equation 2, if the transition is initiated at the initial interface, and the matter will never be superheated outside of its stability field. The possibility of mixtures of the two phases will not be considered here.

If the pressure pulse $\Delta P > (L/c_vG)$, there will exist a finite region that may spontaneously undergo the transition without intersecting the Clapeyron curve. If ΔP satisfies this condition, we will define the system to be overdriven. This is indicated by the region between M_i'' and M_i', corresponding to $P(M_i') - P(M_i'') = [(G\Delta P/F) - (L/c_vF)]\,P_i(M_i)$. M_i'' is the depth at which the Clapeyron curve intersects the top of the stippled region in Figure 1. The matter that is at pressures between $P(M_f)$ and $P(M_i'')$ is metastable and superpressured.

We have so far assumed that the agent causing the jump ΔP in pressure has no thermal impedance. If it has the same properties (i.e. ρ_1, K_1) as were initially above the phase boundary, then the final state will correspond to the initial state.

Immediately after the pressure pulse is applied, the phase boundary will move to shallower depths and lower pressures, approaching M_f, and will then reverse its motion and return to M_i. The addition of heat is then required to raise the temperature of the original material extending to the lower boundary, causing a long-term transient.

The behavior of the above system is greatly simplified because of the assumption that $K_1\rho_1 = K_2\rho_2$. We will now discuss the case in which the material properties are different in region 1, above the transition, and in region 2, below the transition. Let the lower boundary of region 2 be a distance $b(0)$ below the surface. We first consider the case in which the flux at the lower boundary is fixed. The initial temperature and pressure as a function of depth is given by equations 3 and 4, and the initial position and pressure at the phase boundary by equation 5. In the (P, T) plane, the initial temperature distribution consists of two straight line segments of slope $J_i/K_1\rho_1 g$ and $J_i/K_2\rho_2 g$ in regions 1 and 2, respectively. This is shown in Figure 2 for the case $K_2\rho_2 = 2K_1\rho_1$.

Immediately after the application of an increment ΔP in pressure, the T-P curve is translated to the right as stated earlier. The phase boundary moves to M_i', and the lower boundary $b(0)$ of region 2 moves from point C to C'. Since we have required that the flux at the lower boundary remain constant, the final state will have the same slope in regions 1 and 2 as the initial state. The difference between the final and initial states is markedly different than for the simple case where $\Theta(x, \infty) = 0$.

Here

$$\Theta(x, \infty) = T(x, \infty) - T_i$$

$$= \begin{cases} 0 & 0 \le x \le M_f \\ -J_i\left\{\frac{1}{K_1} - \frac{1}{K_2}\right\}(x - M_f) & M_f \le x \le M_i \\ -J_i\left\{\frac{1}{K_1} - \frac{1}{K_2}\right\}(M_i - M_f) & M_i \le x \le b(\infty) \end{cases} \tag{8a}$$

or as a function of pressure

$$\Theta = \begin{cases} 0 & \Delta P \le P \le P(M_f) \\ -J_i\left\{\frac{1}{K_1\rho_1 g} - \frac{1}{K_2\rho_2 g}\right\}[P - P(M_f)] & P(M_f) \le P \le P(M_i') \\ -J_i\left\{\frac{1}{K_1\rho_1 g} - \frac{1}{K_2\rho_2 g}\right\}[P(M_i') - P(M_f)] & P(M_i') \le P \le P(b(\infty)) \\ & = P_i(b(0)) + \Delta P \end{cases} \tag{8b}$$

P_f and M_f are given by equation 7.

Since the pressure on each unit of matter is assumed to be conserved after the pulse is applied, the time trajectories of each point are constrained to move vertically in the (P, T) plane. The propagation of the phase boundary under the assumptions given will proceed in the same manner as discussed for the simple

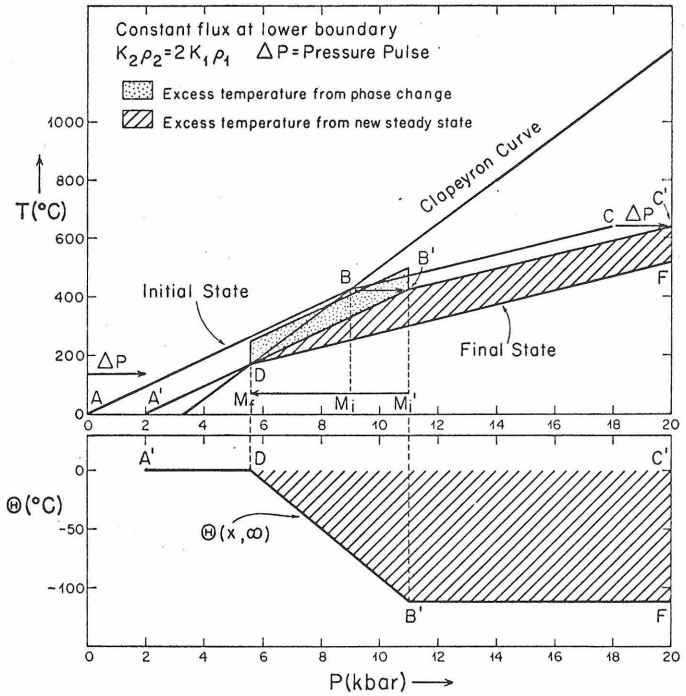

Fig. 2. Pressure temperature representation of the effects of a pressure pulse for constant flux at the lower boundary when the physical parameters of the two phases differ. The initial state shown by line ABC is translated to $A'B'C'$, owing to the pressure pulse. The final state is shown by line $A'DF$. Since the translated initial and final steady-state temperature distributions differ, the heat corresponding to the difference between the initial and final states (the hatched region) must be removed, as well as the latent heat, in order for the phase boundary to move from its initial position M_i' to its final position M_f. The lower curve shows the perturbation temperature $\Theta(x,\infty)$, which is the difference in temperature between the final and initial states $[\Theta(x,\infty) = T(x,\infty) - T(x,0)]$. $\Theta(x,\infty)$ is a continuous function comprised of three straight-line segments.

case $\rho_1 K_1 = \rho_2 K_2$. If the source of the pressure pulse has no thermal impedance, the excess heat per unit area corresponding to

$$-\int_{P(M_f)}^{P(b(0))+\Delta P} \Theta \frac{c_v\, dP}{g\rho}$$

must be removed in addition to the excess heat from the phase change.

If the source of the pressure pulse is a material of identical properties to region 1 and was initially at 0°C, then the phase boundary will move from M_i' toward M_f and then reverse and return to M_i; the final state will be the same as the initial state, except that heat will have to be added to the system to raise the temperature of the translated curve $A'B'C'$ of Figure 2 to the temperature of curve ABC, the heat being provided from below the lower boundary. In either

case, if the load has thermal impedance or if $K_1 \neq K_2$, the system will have a long-time transient to achieve the final steady state.

So far we have emphasized the (P, T) representation of the system. The dependence on spatial coordinates is fundamentally different, since $T_i(x)$ does not change as $P \rightarrow P + \Delta P$, but $\mathfrak{I}_c(P)$ as an implicit function of x will be changed. In addition, the total depth $b(t)$ from the surface to the lower boundary depends on time, whereas the pressure is fixed in the matter. Mass conservation requires that the quantity $\rho_1 M(t) + \rho_2[b(t) - M(t)]$ be constant, so that the change in depth of the lower boundary for the preceding case with constant flux is

$$b(\infty) - b(0) = -G\,\Delta P \frac{(\rho_2 - \rho_1)}{\rho_2\rho_1 g(G - J_i/K_1\rho_1 g)} = -\frac{M_i(\rho_2 - \rho_1)}{\rho_2}\frac{G\,\Delta P}{F} \tag{9}$$

It follows that an (x, T) representation of the foregoing problem is analogous to the (P, T) representation, except that the Clapeyron curve is displaced instead of $T_i(x)$ and there is a shift in the end point $b(t)$. The trajectory of a unit of matter is thus not constrained to move vertically in the (x, T) plane, since the spatial coordinate of a unit of matter is not conserved.

The next case of steady-state behavior that we wish to consider here is for the case of the lower boundary at depth b at constant temperature $T(b(t)) = T_b$. Since the flux is not conserved, it is convenient to use the other variables to define the position of the phase boundary.

The equations governing the position of the phase boundary are

$$J_i = \frac{T(b)}{(b_i/K_2) + M_i[(1/K_1) - (1/K_2)]} \qquad J_f = \frac{T(b)}{(b_f/K_2) + M_f[(1/K_1) - (1/K_2)]}$$

$$\frac{J_f}{J_i} = \frac{1}{1 - [(M_i - M_f)/\rho_2[(\rho_2/K_1)] - (\rho_1/K_2)][J_i/T(b)]}$$

$$M_i = F \Big/ \left\{\frac{1}{2}\left[G\rho_1 g - \frac{T(b)K_2}{b_i K_1} - \frac{FK_2}{b_i K_1}\left(1 - \frac{K_1}{K_2}\right)\right]\right.$$

$$\left. + \frac{1}{2}\left[\left(G\rho_1 g - \frac{T(b)K_2}{b_i K_1} - \frac{FK_2}{b_i K_1}\left(1 - \frac{K_1}{K_2}\right)\right)^2 + 4G\rho_1 g\left(1 - \frac{K_1}{K_2}\right)\frac{FK_2}{b_i K_1}\right]^{1/2}\right\}$$

$$M_f = (F - G\,\Delta P) \Big/ \left\{\frac{1}{2}\left[G\rho_1 g - \frac{T(b)K_2\rho_2}{K_1 m}\right.\right.$$

$$\left. - \frac{(F - G\,\Delta P)}{m}\rho_2\frac{K_2}{K_1}\left(\left(1 - \frac{K_1}{K_2}\right) + \left(1 - \frac{\rho_1}{\rho_2}\right)\frac{K_1}{K_2}\right)\right] \tag{10}$$

$$+ \frac{1}{2}\left\{\left[G\rho_1 g - \frac{T(b)K_2\rho_2}{K_1 m} - \frac{(F - G\,\Delta P)}{m}\frac{\rho_2 K_2}{K_1}\left[\left(1 - \frac{K_1}{K_2}\right) + \left(1 - \frac{\rho_1}{\rho_2}\right)\frac{K_1}{K_2}\right]\right]^2\right.$$

$$\left. + 4(F - G\,\Delta P)\frac{G\rho_2\rho_1 g}{m}\frac{K_2}{K_1}\left[\left(1 - \frac{K_1}{K_2}\right) + \left(1 - \frac{\rho_1}{\rho_2}\right)\left(\frac{K_1}{K_2}\right)\right]\right\}^{1/2}\right\}$$

$$T(M_i) = \frac{J_i M_i}{K_1} = \mathfrak{I}_c(P(M_i)) \qquad T(M_f) = \frac{J_f M_f}{K_1} = \mathfrak{I}_c(P(M_f))$$

$$m \equiv \rho_1 M_i + \rho_2(b_i - M_i) = \rho_1 M_f + \rho_2(b_f - M_f)$$

$$M_f^2\left(\frac{1}{K_1}-\frac{1}{K_2}\right)G\rho_1 g + M_f\left\{\frac{G\rho_1 g}{K_2}\left[b_i - \frac{(\rho_2-\rho_1)}{\rho_2}(M_i - M_f)\right]\right.$$
$$\left. - \frac{T(b)}{K_1} - \left(\frac{1}{K_1}-\frac{1}{K_2}\right)(-G\,\Delta P + F)\right\}$$
$$- \frac{1}{K_2}\left[b_i - \left(\frac{\rho_2-\rho_1}{\rho_2}\right)(M_i - M_f)\right](-G\,\Delta P + F) = 0$$

The expression for M_i is an explicit function of b_i and $T(b_i)$, and the expression for M_f is an implicit function of M_i through m.

If $(\rho_2/K_1) > (\rho_1/K_2)$ and $M_i > M_f$, the flux is increased and the temperature gradient is increased (see the expression for J_f/J_i). As a result, the temperature at the transition is increased above that which would obtain if $\rho_2 K_2 = \rho_1 K_1$, as in the first example. A schematic illustration of this case is shown in Figure 3. One of the fundamental effects of $(\rho_2/K_1) > (\rho_1/K_2)$ is that, to the low pressure side of point E (Figure 3), the temperature of the translated initial state is below the final state, and to the high pressure side of point E the reverse situation occurs. This means that in addition to the heat of the transition which must be removed,

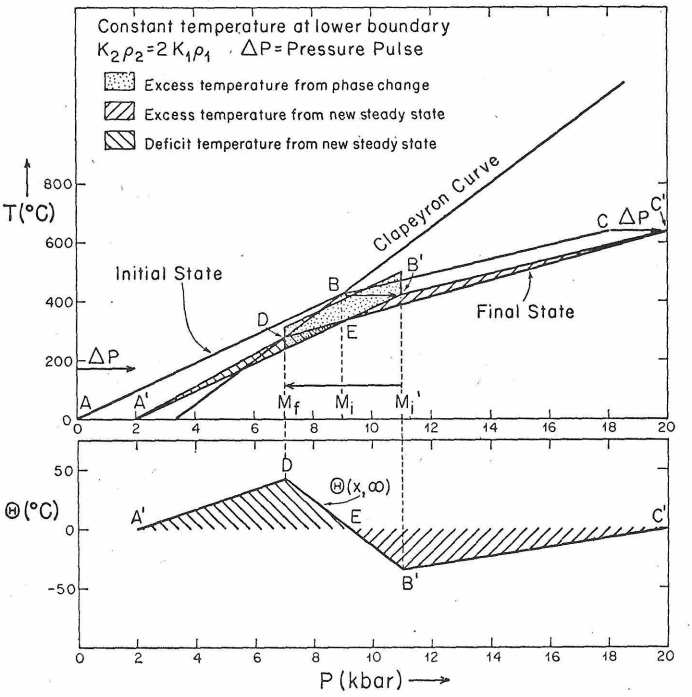

Fig. 3. Pressure temperature representation of the effect of a pressure pulse with a constant temperature at the lower boundary when the properties of the two phases differ. Besides the surplus heat in the region $EB'C'$, there is a heat deficit in the region $A'DE$ due to the difference between the translated initial state and the final state. The translated initial and final temperatures are the same at point E.

an additional amount of heat due to the excessive temperature must be removed from the right of point E. Some of this heat will go to the region to the left of E to fill in the temperature deficit. This has two major consequences. Firstly, a long-term temperature readjustment over the whole system must take place. Secondly, the kinetics of the motion of the phase boundary is somewhat enhanced because the heat lost at the front of the motion automatically tends to compensate for the difference between the initial and final states. This should be compared with the constant flux case where the system must radically alter the total heat content between initial and final states. Figure 3 shows $\Theta(x, \infty) = T_f - T_i$ for this case and illustrates the comments made above. Figure 4 shows a similar case in the (x, T) plane.

We have so far restricted the discussion to a source-free region. If sources of variable strength are present, the steady-state temperature distribution is defined by the field equation $(\partial/\partial x)[K(x)(\partial T(x)/\partial x)] + A(x) = 0$ and the boundary conditions. The position of the phase boundary is then defined by $T(M) = \mathfrak{I}_c(P(M))$,

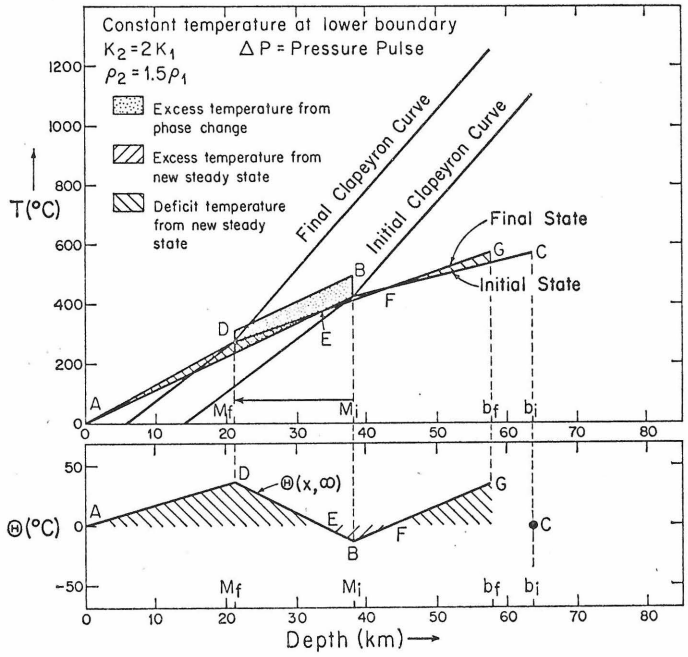

Fig. 4. A depth-temperature representation of the effect of a pressure pulse for constant temperature at the lower boundary. Both the densities and the conductivities in regions 1 and 2 are taken to be different. The initial temperature distribution is not changed by the pulse, but instead the Clapeyron curve is shifted. The initial and final Clapeyron curves are segmented in the (x,T) representation. The initial and final temperatures are given by the line segments ABC and ADG respectively. Points B and D correspond to the initial and final positions of the phase boundary. The lower boundary moves from C to G corresponding to depths b_i and b_f, respectively. Note that Θ is not defined in the region between G and C.

where $\mathfrak{I}_c(P)$ defines the Clapeyron curve. In investigating the possible positions of the phase boundary for various static loads, an additional constraint occurs from consideration of source conservation in regions into which the phase boundary may be displaced. Let $-$ and $+$ denote the low and high pressure side of the phase boundary, respectively; then $[A(M^-)/\rho(M^-)] = [A(M^+)/\rho(M^+)]$, i.e. A/ρ is continuous across the moving phase boundary in the direction of motion.

With regard to the phase transition, it is of course possible to utilize a simple two-layer model for ρ, K, c and to use an arbitrary source distribution subject to the above constraint. For the purpose of exhibiting the effects of sources, we will discuss the case of a simple two-layer model with $A_1/\rho_1 = A_2/\rho_2$.

The temperature distribution is then

$$T(x) = \begin{cases} \dfrac{J(0)x}{K_1} - \dfrac{A_1x^2}{2K_1}\,; & 0 \le x \le M \\ \dfrac{J(0)M}{K_1} - \dfrac{A_1M^2}{2K_1} + \left(\dfrac{J(0)}{K_2} - \dfrac{A_1M}{K_2}\right)(x - M) - \dfrac{A_1\rho_2}{2\rho_1K_2}(x - M)^2\,; & M \le x \le b \end{cases} \tag{11}$$

Here $J(0)$ is the flux at $x = 0$. The initial and final temperature distributions can be found by setting M equal to M_i and M_f, respectively, and $J(0)$ equal to J_i and J_f, respectively. For case of known flux, the expression for M is

$$M = \frac{F - G\,\Delta P}{\frac{1}{2}\rho_1 g\left\{\left(G - \dfrac{J(0)}{K_1\rho_1 g}\right) + \left[\left(G - \dfrac{J(0)}{K_1\rho_1 g}\right)^2 + 2(F - G\,\Delta P)\dfrac{A_1}{K_1\rho_1{}^2 g^2}\right]^{1/2}\right\}} \tag{12}$$

M_i can be obtained by setting $\Delta P = 0$ in the above equation. The effect of the sources is to decrease the depth M at which the phase transition takes place for a given flux.

As will be shown, the two-layer model does not fully exhibit the more general problem with sources because of the condition of source conservation.

More generally for an N layer model, where layer n lies between X_{n-1} and X_n, the temperature distribution is given by

$$T_n(x) = T_{n-1}(X_{n-1}) + \frac{J_{n-1}(X_{n-1})}{K_n}(x - X_{n-1}) - \frac{A_n}{2K_n}(x - X_{n-1})^2$$

$$X_{n-1} \le x \le X_n \quad \text{and} \quad X_0 \equiv 0$$

and

$$J_n(X_n) \equiv J_0(0) - \sum_{i=1}^{n}(X_i - X_{i-1})A_i \qquad n \ge 1$$

$T_n(x)$ is the temperature distribution in layer n which has material properties A_n and K_n.

For a two-layer model, the system is highly constrained, since the source strength in region 1 determines the strength in region 2. The simplest multilayer model which is not 'overconstrained' is with four layers. In the two neighboring regions in which the phase boundary may move, the relative source strengths are

fixed by the conservation condition. In the other two regions the source strengths may have arbitrary values. However, if the phase boundary M is at X_1 or X_2 and the sources in layers 3 and 4 are similar, then it is probably unnecessary to distinguish 3 and 4. Thus a three-layer model is sufficient for an approximate description of a system in which M is located at X_1, when A_1 and A_2 are similar in strength ($A_1/\rho_1 = A_2/\rho_2$) and A_3 is distinctly different, or when M is located at X_2 and A_1 and A_2 are distinct in strength, but A_2 and A_3 are similar ($A_2/\rho_2 = A_3/\rho_3$). These cases can correspond to M located in a high-source region or a low-source region.

In comparing the initial and final states of a system, it should be noted that the physical parameters in the regions $0 \leq x \leq M$ remain unchanged as a function of x. However, for $x \geq M$, the parameters will change, owing to the translational motion of material. This applies to the source strengths A_n as well as the conductivities. The function $\Theta(x, \infty) = T_f(x) - T_i(x)$ will contain several regions with discontinuities both in slope and in curvature due to the translation of the boundaries between the regions.

For a three-layer model with M at depth X_1 and for constant flux the expression for $\Theta(x, \infty) = T_f(x) - T_i(x)$ is, assuming $M_f \leq M_i$

$$\Theta(x, \infty) = T_{1f}(x) - T_{1i}(x) = 0 \qquad 0 \leq x \leq M_f$$

$$\Theta(x, \infty) = T_{2f}(x) - T_{1i}(x) = -J(0)\left(\frac{1}{K_1} - \frac{1}{K_2}\right)(x - M_f) + A_1 M_f^2\left(\frac{1}{K_2} - \frac{1}{2K_1} - \frac{\rho_2}{2\rho_1 K_2}\right) + \frac{A_1 M_f x}{K_2}\left(\frac{\rho_2}{\rho_1}\right) + \frac{A_1 x^2}{2}\left(\frac{1}{K_1} - \frac{\rho_2}{\rho_1 K_2}\right) \qquad M_f \leq x \leq M_i$$

$$\Theta(x, \infty) = T_{2f}(x) - T_{2i}(x) = -J(0)(M_i - M_f)\left(\frac{1}{K_1} - \frac{1}{K_2}\right) + \frac{A_1}{2K_1}(M_i^2 - M_f^2) - \frac{A_1}{K_2}[M_i^2 - M_f^2 - (M_i - M_f)x] + \frac{\rho_2 A_1}{2K_2\rho_1}[M_i^2 - M_f^2 - 2(M_i - M_f)x] \qquad M_i \leq x \leq X_{2f}.$$

$$\Theta(x, \infty) = T_{3f}(x) - T_{2f}(x) \qquad X_{2f} \leq x \leq X_{2i}$$

$$\Theta(x, \infty) = T_{3f}(x) - T_{3i}(x) \qquad X_{2i} \leq x \leq X_{3f}$$

where $\rho_1 M_i + \rho_2(X_{2i} - M_i) = \rho_1 M_f + \rho_2(X_{2f} - M_f)$ from the conservation of matter. The values of M_i and M_f are determined from the same equation 12 as the one-layer model for this case. The above equations may be compared with equations 10 for the source-free cases. The case with sources is shown in Figure 5.

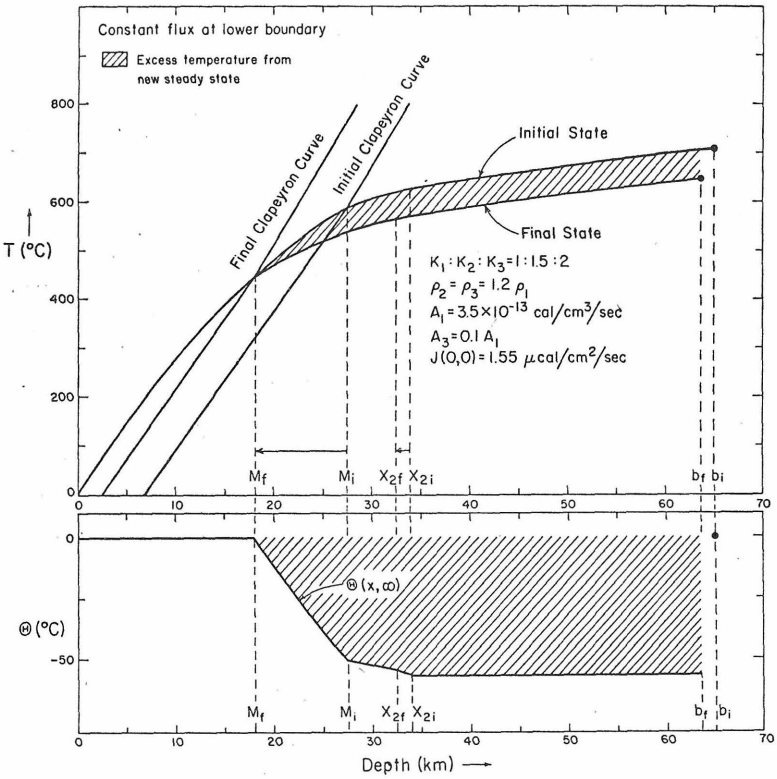

Fig. 5. Depth-temperature diagram similar to Figure 4 except for a three-layer model with sources and constant flux at the lower boundary. The boundary between layers 2 and 3, X_2, moves from X_{2i} to X_{2f} as the phase boundary moves from M_i to M_f. Note that there are discontinuities in $\partial\Theta/\partial x$ at both X_{2i} and X_{2f} due to the translation of the material in the region $X > M$. In addition $\partial^2\Theta/\partial x^2$ does not vanish for $M_f < x < M_i$ and $X_f < x < X_i$, owing to the different source strengths in the different layers. Nevertheless, the curvature is small in these two regions.

The discontinuities in $\Theta(x, \infty)$ due to the different conductivities in the different regions are apparent in Figure 5.

3. THE DYNAMIC PROBLEM

Formulation. In this section we treat the formulation of the dynamic problem in one dimension. We first exhibit the relevant equations and boundary conditions; we then reduce them to a convenient dimensionless form and introduce a dimensionless perturbation temperature relative to the initial steady state. These transformations in themselves result in a great simplification of the problem and allow significant general conclusions to be drawn.

For simplicity we consider a two-layer model with constant uniform properties, subject to a sudden pressure pulse. The geometry of the model is shown below.

$x = 0$—— surface

Region 1: $\rho_1, c_1, K_1, A_1, V_1 \equiv 0$; phase 1

$x \downarrow$ $M(t)$——

Region 2: $\rho_2, c_2, K_2, A_2, V_2$; phase 2

$b(t)$——

The surface of the earth is taken as $x = 0$, the phase boundary is at $x = M(t)$, corresponding to a point on the Clapeyron curve, and the lower boundary condition is imposed at $x = b(t)$, which is fixed in the matter in region 2. Since the coordinates are fixed in region 1, the velocity vanishes in this region.

We assume that the two phases coexist only among the plane $x = M(t)$; thus we do not consider mixtures of two phases along the Clapeyron curve. This implies that a new phase does not nucleate away from the plane $x = M(t)$.

The heat equation thus becomes

$$\begin{aligned} \frac{\partial T}{\partial t} &= \frac{K_1}{\rho_1 c_1}\frac{\partial^2 T}{\partial x^2} + \frac{A_1}{\rho_1 c_1} && 0 \le x \le M(t) \\ \frac{\partial T}{\partial t} + V_2\frac{\partial T}{\partial x} &= \frac{K_2}{\rho_2 c_2}\frac{\partial^2 T}{\partial x^2} + \frac{A_2}{\rho_2 c_2} && M(t) \le x \le b(t) \end{aligned} \tag{13}$$

The boundary equations become

$$T(0, t) = 0 \tag{14a}$$

$$T(b(t), t) = \text{constant}, \quad \text{or} \tag{14b}$$

$$J(b(t), t) = K_2 \left.\frac{\partial T}{\partial x}\right|_{x=b(t)} = \text{constant}$$

$$K_1 \left.\frac{\partial T}{\partial x}\right|_{x=M^-(t)} - K_2 \left.\frac{\partial T}{\partial x}\right|_{x=M^+(t)} = -L\rho_1 \frac{dM(t)}{dt} \tag{14c}$$

$$T(M(t), t) = \mathfrak{T}_c(P) \qquad \text{Clapeyron curve} \tag{14d}$$

The Clapeyron curve $\mathfrak{T}_c(P)$ is the integral of the Clausius Clapeyron equation

$$(d\mathfrak{T}_c/dP) = [(1/\rho_1) - (1/\rho_2)]/(S_1 - S_2) \tag{15}$$

where P = pressure and S_i = entropy per gram of phase i.

We now assume that the Clapeyron curve may be adequately represented by $\mathfrak{T}_c(P) = GP - F$ and defining $T_c(x) = \mathfrak{T}_c(P(x))$ we have

$$T_c(x) = G\rho_1 g x + G\,\Delta P - F \tag{16}$$

where g = acceleration due to gravity and ΔP = pressure pulse. The intersection of this curve for $\Delta P = 0$ with $T(x, 0)$ defines the initial position $M(0)$ of the phase boundary.

Similarly, the latent heat of the phase change L in (14c) is

$$L = T_c(S_1 - S_2) \tag{17}$$

which we take as constant. This assumption is not compatible with (15) ,if ρ_1 and ρ_2 are constant; however, this approximation should introduce no significant error unless $T(M_i) - T(M_f)$ is large.

Conservation of mass and heat sources requires

$$V_2 = [(\rho_2 - \rho_1)/\rho_2]\, dM/dt \tag{18a}$$

$$b(t) = b(0) - [(\rho_2 - \rho_1)/\rho_2](M(0) - M(t)) \tag{18b}$$

$$A_1/\rho_1 = A_2/\rho_2 \tag{18c}$$

We now introduce the dimensionless parameters, with $b_0 = b(0)$ and with T_0 an arbitrary temperature scaling factor.

$$\xi \equiv \frac{x}{b_0}, \qquad \tau \equiv \frac{K_1}{\rho_1 c_1 b_0^2}\, t, \qquad \eta(\xi, \tau) \equiv \frac{T(x, t)}{T_0}, \qquad \gamma_i \equiv \frac{J(0, 0) b_0}{K_i T_0}$$

$$\alpha \equiv \frac{K_2 \rho_1 c_1}{K_1 \rho_2 c_2}, \qquad \xi_m(\tau) \equiv \frac{M(t)}{b_0}, \qquad \beta(\tau) \equiv \frac{b(t)}{b_0}, \qquad C \equiv \frac{L}{c_1 T_0} \tag{19}$$

$$\sigma_i \equiv \frac{b_0^2 A_i}{T_0 K_i}, \qquad \eta_c(\xi) \equiv T_c(x)/T_0, \qquad \nu \equiv \frac{b_0}{\kappa_1} V_2$$

The equations become

$$\frac{\partial \eta}{\partial \tau} = \frac{\partial^2 \eta}{\partial \xi^2} + \sigma_1 \qquad 0 \le \xi \le \xi_m \tag{20a}$$

$$\frac{\partial \eta}{\partial \tau} = \alpha \frac{\partial^2 \eta}{\partial \xi^2} - \nu \frac{\partial \eta}{\partial \xi} + \alpha \sigma_2 \qquad \xi_m \le \xi \le \beta(\tau) \tag{20b}$$

subject to the boundary conditions

$$\eta(0, \tau) = 0 \tag{21a}$$

$$\eta(\beta(\tau), \tau) = \text{constant}, \quad \text{or} \tag{21b}$$

$$\left.\frac{\partial \eta}{\partial \xi}\right|_{\xi = \beta(\tau)} = \text{constant}$$

$$\left.\frac{\partial \eta}{\partial \xi}\right|_{\xi = \xi_m -} - \frac{K_2}{K_1} \left.\frac{\partial \eta}{\partial \xi}\right|_{\xi = \xi_m +} = -C \frac{d\xi_m}{d\tau} \tag{21c}$$

$$\eta(\xi_m(\tau), \tau) = \eta_c(\xi_m) = \frac{G \rho_1 g b_0}{T_0} \xi_m + \frac{G\, \Delta P}{T_0} - \frac{F}{T_0} \tag{21d}$$

as well as the conservation equations

$$\nu = [(\rho_2 - \rho_1)/\rho_2]\, d\xi_m/d\tau \tag{22a}$$

$$\beta(\tau) = 1 - [(\rho_2 - \rho_1)/\rho_2](\xi_m(0) - \xi_m(\tau)) \tag{22b}$$

$$K_1 \sigma_1/\rho_1 = K_2 \sigma_2/\rho_2 \tag{22c}$$

We define the perturbation temperature $\theta(\xi, \tau)$ and the reduced Clapeyron curve $\theta_c(\xi)$ to be

$$\theta(\xi, \tau) \equiv \eta(\xi, \tau) - \eta(\xi, 0)$$
$$\theta_c(\xi) \equiv \eta_c(\xi) - \eta(\xi, 0) \tag{23}$$

The reduced Clapeyron curve $\theta_c(\xi)$ depends only on the difference between $\eta_c(\xi)$ and $\eta(\xi, 0)$.

Both $\eta(\xi, 0)$ and $\eta(\xi, \tau)$ are continuous; hence $\theta(\xi, \tau)$ will be continuous. Continuity of heat flux requires that $\partial\eta(\xi, \tau)/\partial\xi$ and $\partial\eta(\xi, 0)/\partial\xi$ have discontinuities at $\xi_m(\tau)$ and $\xi_m(0)$, respectively. Hence $\partial\theta(\xi, \tau)/\partial\xi$ will have discontinuities at these two points.

From the initial condition of thermal equilibrium, it may be seen that

$$\left.\frac{\partial\eta(\xi, 0)}{\partial\xi}\right|_{\xi=\xi_m-(0)} - \frac{K_2}{K_1}\left.\frac{\partial\eta(\xi, 0)}{\partial\xi}\right|_{\xi=\xi_m+(0)} = 0$$
$$\eta(0, 0) = 0, \qquad \left.\frac{\partial\eta(\xi, 0)}{\partial\xi}\right|_{\xi=0} = \gamma_1 \tag{24}$$

For the case $\xi_m(\tau) \leq \xi_m(0)$, the problem as formulated for $\theta(\xi, \tau)$ is

$$\frac{\partial\theta}{\partial\tau} = \frac{\partial^2\theta}{\partial\xi^2}; \qquad 0 \leq \xi \leq \xi_m(\tau) \qquad \text{(region 1)} \tag{25a}$$

$$\frac{\partial\theta}{\partial\tau} = \alpha\frac{\partial^2\theta}{\partial\xi^2} - \nu\left[\frac{\partial\theta(\xi, \tau)}{\partial\xi} + \frac{\partial\eta(\xi, 0)}{\partial\xi}\right] + \alpha(\sigma_2 - \sigma_1);$$
$$\xi_m(\tau) \leq \xi \leq \xi_m(0) \qquad \text{(region 3)} \tag{25b}$$

$$\frac{\partial\theta}{\partial\tau} = \alpha\frac{\partial^2\theta}{\partial\xi^2} - \nu\left[\frac{\partial\theta(\xi, \tau)}{\partial\xi} + \frac{\partial\eta(\xi, 0)}{\partial\xi}\right]; \qquad \xi_m(0) \leq \xi \leq \beta(t) \qquad \text{(region 2)} \tag{25c}$$

subject to boundary conditions

$$\theta(0, \tau) = 0 \tag{26a}$$

$$\theta(\beta(\tau), \tau) = \eta(\beta(0), 0) - \eta(\beta(\tau), 0) \quad \text{or}$$
$$\left.\frac{\partial\theta(\xi, \tau)}{\partial\xi}\right|_{\xi=\beta(\tau)} = \left.\frac{\partial\eta(\xi, 0)}{\partial\xi}\right|_{\xi=\beta(0)} - \left.\frac{\partial\eta(\xi, 0)}{\partial\xi}\right|_{\xi=\beta(\tau)} \tag{26b}$$

$$\left.\frac{\partial\theta}{\partial\xi}\right|_{\xi=\xi_m-(\tau)} - \frac{K_2}{K_1}\left.\frac{\partial\theta}{\partial\xi}\right|_{\xi=\xi_m+(\tau)}$$
$$+ \left.\frac{\partial\eta(\xi, 0)}{\partial\xi}\right|_{\xi=\xi_m-(\tau)} - \frac{K_2}{K_1}\left.\frac{\partial\eta(\xi, 0)}{\partial\xi}\right|_{\xi=\xi_m+(\tau)} = -C\frac{d\xi_m}{d\tau} \tag{26c}$$

$$\left.\frac{\partial\theta}{\partial\xi}\right|_{\xi=\xi_m-(0)} - \left.\frac{\partial\theta}{\partial\xi}\right|_{\xi=\xi_m+(0)}$$
$$= -\left.\frac{\partial\eta(\xi, 0)}{\partial\xi}\right|_{\xi=\xi_m-(0)} + \left.\frac{\partial\eta(\xi, 0)}{\partial\xi}\right|_{\xi=\xi_m+(0)}; \qquad \tau > 0 \tag{26d}$$

$$\theta(\xi_m(\tau), \tau) = \theta_c(\xi_m) \equiv \frac{G\rho_1 g b_0}{T_0}\xi_m + \frac{G\,\Delta P(\tau)}{T_0} - \frac{F}{T_0} - \eta(\xi_m, 0) \tag{26e}$$

$$\theta(\xi, 0^+) = 0, \qquad \xi \neq \xi_m(0) \tag{26f}$$

The conservation equations (22) remain unchanged.

A comparison of the original field equations 13 with those obtained for the dimensionless perturbation temperature (25) shows that the equations for θ require the distinction of three regions, owing to the conditions 26*c* and 26*d* whereas the equations for T require only a distinction of two regions.

Region 3 arises for two reasons: (1) We have subtracted $\eta(\xi, 0)$, which has a discontinuous first derivative at $\xi_m(0)$, from $\eta(\xi, \tau)$. This leads to condition 26*d*. The extra term in condition 26*c* arises similarly. Both are due solely to different conductivities in regions 1 and 2.

(2) Heat sources are redistributed, owing to the volume change at the phase boundary, giving rise to a source term in the heat equation in region 3.

In spite of the complexity due to the addition of a third region with associated boundary conditions, it is obvious that field equations 25 are considerably simplified as compared with (13). There are no source terms in either regions 1 or 2. The source term appears only as the difference $\alpha(\sigma_2 - \sigma_1)$ in region 3, i.e., in the region between the initial and final position of the phase boundary. From this consideration for the two-layer model, it is evident that the presence of sources is of small importance in the dynamic equations, unless region 3 becomes large. As was seen in the discussion of the steady-state case, the presence of sources affects the initial and final positions of the phase boundary. The final steady-state temperature in region 3 will have a change in curvature, which will be small unless $\sigma_2 - \sigma_1$ is large and, in fact, will vanish if $\rho_2/K_2 = \rho_1/K_1$, as can be seen from (22*c*). This leads to the conclusion that the distribution of sources is of small importance in determining the dynamics of motion and the perturbation in the temperature.

This conclusion must be somewhat weakened for the case of multilayer or continuous models. Because of our choice of Eulerian coordinates for the representation of the problem, the source intensity must be considered as a function of time. The general equations corresponding to (13) for a nonuniform continuous medium with arbitrary time-independent sources are unchanged in the region $(0 \leq x \leq M(t))$, and hence the source term will still vanish in the perturbation temperature formulation. In some other regions for $x > M(t)$, there will be differences in source terms due to the effects of translation and the phase transition. It follows that the strong conclusion drawn for the model with two homogeneous layers must be weakened somewhat for the more realistic multi or continuous layer models.

However, following the argument given for the homogeneous two-layer model, we still conclude that for small motions of the phase boundary, the effects of the source distribution on the dynamics of the systems will still be small unless the differences between the source strengths is large.

Returning to the two-layer problem as formulated in (25) and (26), it is evident that the major complexities remain. These are the nonlinear condition (26*c*) at the phase boundary and the nonlinear term for convective heat transport in the heat equation in regions 2 and 3. In addition, it can be seen that the differences in thermal properties complicate the boundary conditions. From the above discussion it would appear that sources should not dominate the geophysical problem considered here. The important issue is the motion of the phase boundary,

which is governed by the nonlinear boundary condition 26c, and the Clapeyron curve.

The gutted problem. To isolate the effect of this nonlinear boundary condition, the following simplifications were made to define the gutted problem: (1) sources are neglected, $\sigma_1 \equiv 0$; (2) the thermal parameters in regions 1 and 2 are taken to be identical; (3) the densities of the two phases are set equal in the field equation and conservation equations; hence the velocity in region 2 vanishes and the lower boundary $\beta(\tau) = \beta(0) = 1$; and (4) the reduced Clapeyron curve is given by $\theta_c(\xi) = D\xi - E$; $0 < E < D$; thus the phases are assumed to have different densities only in the Clausius Clapeyron equation.

The gutted problem so defined may be summarized

$$\frac{\partial \theta}{\partial \tau} = \frac{\partial^2 \theta}{\partial \xi^2} \qquad 0 \leq \xi < \xi_m, \quad \xi_m < \xi \leq 1, \quad \tau > 0 \tag{27a}$$

$$\theta(0, \tau) = \theta(1, \tau) = 0, \qquad \tau \geq 0 \tag{27b}$$

$$\left.\frac{\partial \theta}{\partial \xi}\right|_{\xi=\xi_m^+(\tau)} - \left.\frac{\partial \theta}{\partial \xi}\right|_{\xi=\xi_m^-(\tau)} = C \frac{d\xi_m(\tau)}{d\tau} \tag{27c}$$

$$\theta(\xi_m(\tau), \tau) = D\xi_m(\tau) - E, \qquad \tau \geq 0 \tag{27d}$$

$$\theta(\xi, 0) = 0, \qquad \xi \neq \xi_m(0); \qquad \theta(\xi_m(0), 0) = D\xi_m(0) - E \tag{27e}$$

$$C, D, E \text{ constants}, \quad 0 < E < D; \quad 0 < \xi_m(0) < 1, \quad C > 0 \tag{27f}$$

$$D \equiv \frac{G\rho_1 g b_0}{T_0} - \frac{J(0,0)b_0}{K_1 T_0} \qquad E \equiv \frac{F}{T_0} - \frac{G\,\Delta P}{T_0}$$

$$C \equiv \frac{L}{c_1 T_0}$$

In comparing (25), (26), and (27), major simplifications are evident, including the disappearance of region 3. These simplifications make the problem more susceptible to analysis and permit the identification of characteristic parameters of the motion.

Some of the characteristics of the gutted problem are given in the appendix. It is shown (appendix 1) that, if $\xi_m(0) > E/D$, then (1) $E/D \leq \xi_m(\tau) < \xi_m(0)$, and (2) $\xi_m = E/D$ is the only equilibrium position for $\xi_m(\tau)$. Thus the phase boundary is constrained to move only in the region between the initial position and the zero of the reduced Clapeyron curve $\theta_c(\xi_m) = 0$, which is the final equilibrium position.

We may note here that the boundary condition (26c) can be rewritten in integral form: Integrating equation 26a

$$\int_0^1 \frac{\partial \theta}{\partial \tau}\, d\xi = \int_0^{\xi_m} \frac{\partial^2 \theta}{\partial \xi^2}\, d\xi + \int_{\xi_m}^1 \frac{\partial^2 \theta}{\partial \xi^2}\, d\xi = \left.\frac{\partial \theta}{\partial \xi}\right|_{\xi=\xi_m^-} - \left.\frac{\partial \theta}{\partial \xi}\right|_{\xi=0} + \left.\frac{\partial \theta}{\partial \xi}\right|_{\xi=1} - \left.\frac{\partial \theta}{\partial \xi}\right|_{\xi=\xi_m^+}$$

Using (26c), we then obtain

$$C \frac{d\xi_m}{d\tau} = -\frac{d}{d\tau} \int_0^1 \theta\, d\xi - \left.\frac{\partial \theta}{\partial \xi}\right|_{\xi=0} + \left.\frac{\partial \theta}{\partial \xi}\right|_{\xi=1}. \tag{28}$$

This expression is equivalent to the requirement that heat energy be conserved.

The characteristic behavior of the gutted problem is shown in Figure 6. The initial temperature distribution $\theta(\xi, 0)$ is zero everywhere except at $\xi = \xi_m(0)$, where $\theta(\xi_m(0), 0) = D\xi_m(0) - E$ and the phase transition is initiated. As the phase boundary moves, the temperature pulse becomes wider. The temperature of the phase boundary is constrained to lie on the reduced Clapeyron line of slope D. Because the boundary conditions require that the temperature at the ends be zero, the temperature θ rises from the end points to a point $\theta(\xi_m(\tau), \tau) = D\xi_m(\tau) - E$ on the reduced Clapeyron line and is restricted to lie below the reduced Clapeyron curve to the right of the phase boundary.

The temperature at the phase boundary continually decreases until the end point $\xi_m(\infty) = E/D$ is reached, and the perturbation temperature $\theta(\xi, \infty)$ is everywhere zero. As shown in appendix 1, the curvature of the perturbation temperature is always negative just behind the phase boundary. For the initial motion, the curvature in front of the pulse is positive and then becomes negative for long times.

This problem is essentially similar to the classical Stefan problem with these major exceptions: the temperature at the phase boundary is not constant, the thermodynamically unstable region is finite, and the displacement of the phase boundary is bounded.

Generalized Stefan problem. Many of the essential aspects of the gutted problem may be found by consideration of a modification of Neumann's solution to the Stefan problem as given by *Carslaw and Jaeger* [1959, chapter 11]. We will present the solution to this problem in dimensionless form and use it to define the asymptotic behavior of the gutted problem for short times. This discussion will be followed by a treatment for long times. These results will then permit the a priori assignment of values for the dimensionless parameters that characterize the problem and the dependence of the solution on these quantities.

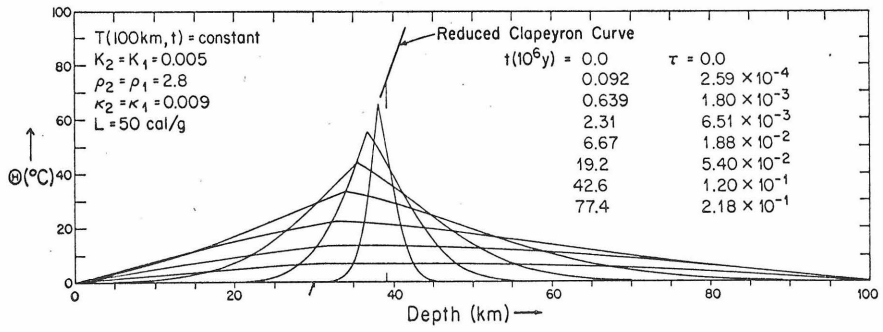

Fig. 6. Profiles of the perturbation temperature $\Theta(x,t)$ at selected times for the gutted problem obtained by the numerical solution for model 1. Each curve is the distribution at a specific time t or an equivalent dimensionless time τ, starting with $t = \tau = 0$. At $\tau = 0$, the temperature is zero everywhere except at M_i and is represented in the figure as an interrupted vertical line at a depth of 39 km. The peaks of all the profiles lie on the reduced Clapeyron curve, a portion of which has been omitted for clarity. $\Theta(x,\infty)$ is zero everywhere.

Consider a supercooled liquid phase 1 ($-\infty < \xi < \xi_m(0)$) initially in contact with a solid phase 2 ($\xi_m(0) < \xi < +\infty$). The two phases have identical parameters. Let us suppose that the initial temperature of both phases is zero and that the equilibrium temperature at which these two phases coexist is θ_s. Let C be the dimensionless heat liberated by the transition ($1 \rightarrow 2$). Then the solution to the problem, if the liquid begins freezing at the interface $\xi_m(0)$, is

$$\theta(\xi, \tau) = \frac{\theta_s}{(1 - \operatorname{erf} \lambda)}\left[1 + \operatorname{erf}\left(\frac{\xi - \xi_m(0)}{2\tau^{1/2}}\right)\right]; \quad \xi \leq \xi_m(\tau)$$
$$\theta(\xi, \tau) = \frac{\theta_s}{(1 + \operatorname{erf} \lambda)}\left[1 - \operatorname{erf}\left(\frac{\xi - \xi_m(0)}{2\tau^{1/2}}\right)\right]; \quad \xi \geq \xi_m(\tau) \tag{29}$$

$$\xi_m(\tau) - \xi_m(0) = -2\lambda\tau^{1/2} \tag{30}$$

where λ is the root of the transcendental equation

$$n(\lambda) \equiv \tfrac{1}{2}\pi^{1/2}\lambda e^{\lambda^2}[1 - (\operatorname{erf} \lambda)^2] = \theta_s/C \tag{31}$$

The function $n(\lambda)$ is shown in Figure 7, and it has a maximum value of 1 as

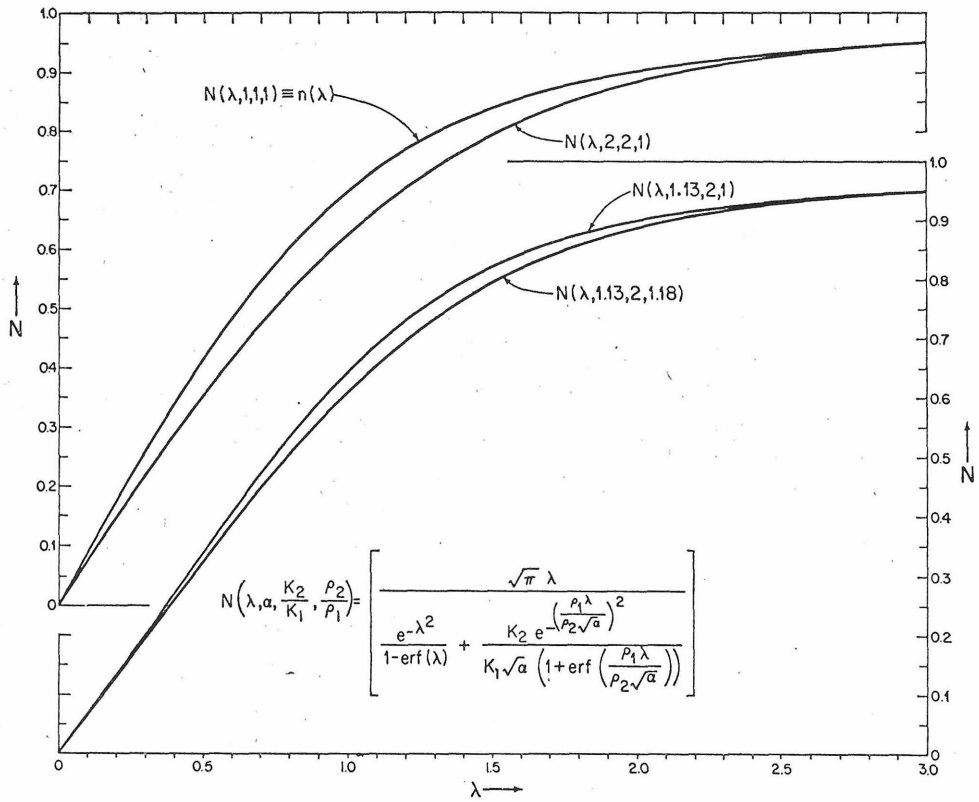

Fig. 7. The characteristic function $N(\lambda, \alpha, K_2/K_1, \rho_2/\rho_1)$ versus λ for the Stefan problem for various values of the arguments α, K_2/K_1, ρ_2/ρ_1. The characteristic function $n(\lambda)$ for the gutted problem is equal to $N(\lambda, 1, 1, 1)$. The two curves on the left should be read on the left-hand scale, the other curves on the right-hand scale. The scales on both sides are equal and offset by an integral number of scale divisions.

$\lambda \to \infty$. The temperature is bounded by $0 \leq \theta \leq \theta_s$, and the curvature is

$$\frac{\partial^2 \theta}{\partial x^2} \begin{cases} >0, & \xi \leq \xi_m(\tau) \\ <0, & \xi = \xi_m{}^+(\tau) \end{cases}.$$

These results are a special case of the theorem given in appendix 1. The heat flux at the lead edge of the phase boundary exceeds the flux at the back edge, as may be seen by

$$-\left.\frac{\partial \theta}{\partial x}\right|_{\xi=\xi_m-} \Big/ \left.\frac{\partial \theta}{\partial x}\right|_{\xi=\xi_m+} = \frac{1 + \operatorname{erf} \lambda}{1 - \operatorname{erf} \lambda} > 1$$

The half-width $(\xi_{1/2}{}^+ - \xi_{1/2}{}^-)$ of the temperature perturbation as defined by

$$\theta(\xi_{1/2}{}^-, \tau) = \theta_s/2 \qquad \xi_{1/2}{}^- < \xi_m$$
$$\theta(\xi_{1/2}{}^+, \tau) = \theta_s/2 \qquad \xi_{1/2}{}^+ > \xi_m$$

is

$$(\xi_{1/2}{}^+ - \xi_{1/2}{}^-) = \frac{[\xi_m(0) - \xi_m(\tau)]}{\lambda} \{\operatorname{erf}^{-1} [\tfrac{1}{2} + \tfrac{1}{2} \operatorname{erf} \lambda] + \operatorname{erf}^{-1} [\tfrac{1}{2} - \tfrac{1}{2} \operatorname{erf} \lambda]\} \qquad (32)$$

and therefore increases in proportion to the displacement or to $\tau^{1/2}$.

This problem corresponds to the gutted problem for an infinite region and for a constant transition temperature $\theta_c(\xi) = \theta_s$. Let us now consider the case of the gutted problem with a variable temperature $\theta_c(\xi_m)$ at the phase boundary. For the initial motion of the phase boundary, the relative change in $\theta_c(\xi_m)$ will be small. Hence the motion of the phase boundary should approximately be as though the temperature at the phase boundary were constant, and, in particular, the initial singularity in $d\xi_m/d\tau$ exhibited by the Neumann solution must also characterize the gutted problem.

If we substitute $\theta_c(\xi_m)$ for θ_s in equation 29 and thus interpret θ_c to be an explicit function of ξ_m and only an implicit function of time, we obtain the function $\tilde{\theta}_{SA}$, which is a solution to the heat flow equation and which satisfies the condition $\tilde{\theta}_{SA}(\xi_m, \tau) = \theta_c(\xi_m)$. Here

$$\begin{aligned} \tilde{\theta}_{SA} &\equiv \frac{\theta_c(\xi_m)}{[1 - \operatorname{erf} \lambda(\xi_m)]} \left[1 + \operatorname{erf}\left(\frac{\xi - \xi_m(0)}{2\tau^{1/2}}\right)\right] \qquad \xi \leq \xi_m(\tau) \\ \tilde{\theta}_{SA} &\equiv \frac{\theta_c(\xi_m)}{[1 + \operatorname{erf} \lambda(\xi_m)]} \left[1 - \operatorname{erf}\left(\frac{\xi - \xi_m(0)}{2\tau^{1/2}}\right)\right] \qquad \xi \geq \xi_m(\tau) \end{aligned} \qquad (33)$$

where we have defined $\lambda = \lambda(\xi_m)$ so that equation 30 becomes

$$\xi_m(\tau) - \xi_m(0) = -2\lambda(\xi_m)\tau^{1/2} \qquad (34a)$$

The boundary condition 27c becomes

$$\begin{aligned} -2C \frac{d}{d\tau} [\lambda(\xi_m)\tau^{1/2}] &= -\frac{C\lambda(\xi_m)}{\tau^{1/2}} - 2C\tau^{1/2} \frac{d\lambda(\xi_m)}{d\xi_m} \frac{d\xi_m}{d\tau} \\ &= -\frac{\theta_c(\xi_m)}{\tau^{1/2}(\pi^{1/2})} \left[\frac{2e^{-\lambda^2}}{(1 + \operatorname{erf} \lambda(\xi_m))(1 - \operatorname{erf} \lambda(\xi_m))}\right]. \end{aligned} \qquad (34b)$$

It should be noted that the boundary condition 27 can be numerically integrated directly for a given approximation $\tilde{\theta}$ to the temperature field

$$C\frac{d\xi_m}{d\tau} \approx \frac{\partial\tilde{\theta}}{\partial\xi}\bigg|_{\xi_m+} - \frac{\partial\tilde{\theta}}{\partial\xi}\bigg|_{\xi_m-}$$

Boundary condition 34*b* may be rewritten in the form

$$n(\lambda) = \frac{\theta_e(\xi_m)}{C}\left[1 - \frac{d\log\lambda}{d\log(\xi_m(0) - \xi_m(\tau))}\right] \tag{35}$$

It is evident that (33) and (35) are not exact solutions to the generalized Stefan problem and that a particular functional form for the temperature field is assumed. Nonetheless, they satisfy the field equations and obey the constraint $\theta_e(\xi_m) = \tilde{\theta}_{SA}(\xi_m, \tau)$ and have the characteristic singularity of the simple Stefan problem. It therefore appears useful to apply this general Stefan-type approximation (SA) to the gutted problem. This functional form must be valid in the neighborhood of $\tau = 0$ because of the singularity that obtains at this time. If $|(d\log\lambda)/[d\log(\xi_m(0) - \xi_m)]| \ll 1$, then the time derivative of λ is negligible compared with $d\xi_m/d\tau$, and we may obtain the roots $\lambda(\xi_m)$ from the simple equation $n(\lambda) = \theta_e(\xi_m)/C$. Within the scheme of the SA an estimate of the error, resulting from neglecting the term $(d\log\lambda)/[d\log(\xi_m(0) - \xi_m)]$, may be obtained by evaluating this from the expression

$$\frac{d\log\lambda}{d\log(\xi_m(0) - \xi_m)} \approx \frac{(\xi_m - \xi_m(0))D}{\lambda C[dn(\lambda)/d\lambda]}.$$

When this term is neglected we define the general Stefan approximation to be of type 1 (SA1).

From physical considerations, it would appear that the approximation SA1 does not take into account the redistribution of heat behind the phase boundary. That is, the temperature behind the phase boundary is always less than $\theta_e(\xi_m)$ in the SA1 approximation. This suggests that the instantaneous velocity calculated from SA1 is too great.

Another estimate of the solution that will tend to compensate for this effect is to include the apparent excess heat behind the phase boundary $D[\xi_m(0) - \xi_m(\tau)]$ with the latent heat C. This yields a second Stefan approximation SA2, where the expression for the temperature remains unchanged but C is replaced by $C + D[\xi_m(0) - \xi_m(\tau)]$ in the characteristic equation 35.

Termination of Stefan-like behavior. From the equation

$$\frac{d\xi_m}{d\tau}\left(D - \frac{\partial\theta}{\partial\xi}\bigg|_{\xi=\xi_m}\right) = \frac{\partial^2\theta}{\partial\xi^2}\bigg|_{\xi=\xi_m}$$

given in appendix 1, it is evident that at a time τ^* and position $\xi_m{}^*$, when $(\partial\theta/\partial\xi)_{\xi=m} = D$, there is an inflection point at $\xi_m{}^*$ at the phase boundary, and the curvature changes sign from positive to negative. This is a fundamental change in the nature of $\theta(x, \tau)$; it cannot happen in the Stefan approximation and is proof that the solution is not exact. This condition when applied to the Stefan problem thus gives

a criterion for the change from behavior predicted by the Stefan approximation to a behavior where $(\partial^2\theta/\partial\xi^2) < 0$ over the major part of the space.

Inserting $\tilde{\theta}_{SA}$ into the above expression, we obtain an estimate $\tilde{\tau}^*$ of the time τ^* when the curvature of θ changes sign and when the Stefan approximation would deviate from the correct solution. Thus

$$\left.\frac{\partial\theta}{\partial\xi}\right|_{\xi_m-} \cong \left.\frac{\partial\tilde{\theta}_{SA}}{\partial\xi}\right|_{\xi_m-} = D = \frac{\theta_c(\xi_m{}^*)e^{-\lambda^{*2}}}{(1 - \operatorname{erf}\lambda^*)(\pi)^{1/2}(\tilde{\tau}^*)^{1/2}}$$

or

$$(\tilde{\tau}^*)^{1/2} = \frac{(D\xi_m(0) - E)}{D\{\pi^{1/2}(1 - \operatorname{erf}\lambda^*)e^{\lambda^{*2}} + 2\lambda^*\}} = \frac{(D\xi_m(0) - E)}{Dp(\lambda^*)} \tag{36}$$

and

$$\begin{aligned}\xi_m{}^* \equiv \xi_m(\tilde{\tau}^*) &= \xi_m(0) - \frac{2\lambda(D\xi_m(0) - E)}{D\{(\pi)^{1/2}(1 - \operatorname{erf}\lambda^*)e^{\lambda^{*2}} + 2\lambda^*\}} \\ &= \xi_m(0) - \frac{2\lambda^*(D\xi_m(0) - E)}{p(\lambda^*)D}\end{aligned} \tag{37}$$

where

$$p(\lambda) \equiv (\pi)^{1/2}(1 - \operatorname{erf}\lambda)e^{\lambda^2} + 2\lambda. \tag{38}$$

The value of λ^* to be used in (36) and (37) is determined from the characteristic equation for SA1

$$h_1(\lambda^*) \equiv n(\lambda^*) + \lambda^{*2}(\operatorname{erf}\lambda^* + 1) = \frac{D\xi_m(0) - E}{C} \tag{39}$$

or for SA2

$$h_2(\lambda^*) \equiv \frac{n(\lambda^*) + \lambda^{*2}(\operatorname{erf}\lambda^* + 1)}{1 - \lambda^{*2}(\operatorname{erf}\lambda^* + 1)} = \frac{D\xi_m(0) - E}{C} \tag{40}$$

The values of λ^* and $(\tau^*)^{1/2}$ for case 1 are less than the respective values for SA2. It would appear that the estimates of τ^* and $\xi_m{}^* \equiv \xi_m(\tau^*)$ determine the end of the Stefan behavior in terms of the constants of the problem. Graphs of the functions of $h_i(\lambda)$ and $p(\lambda)$ are presented in Figure 8. In terms of the dimensional parameters of the system, the termination of the Stefan behavior is therefore given by

$$\begin{aligned}h_i(\lambda^*) &= \frac{\{G\rho_1 g - [J(0,0)/K_1]\}M(0) + G\,\Delta P - F}{L/c_1} \\ (\tilde{t}^*)^{1/2} &= \left(\frac{\rho_1 c_1}{K_1}\right)^{1/2}\left[\frac{M(0) - M(\infty)}{p(\lambda^*)}\right] \\ M(0) - M(t^*) &\cong 2\lambda^*(\tilde{\tau}^*)^{1/2}b_0 = 2\lambda^*\left(\frac{K_1}{\rho_1 c_1}\right)^{1/2}(\tilde{t}^*)^{1/2}\end{aligned} \tag{41}$$

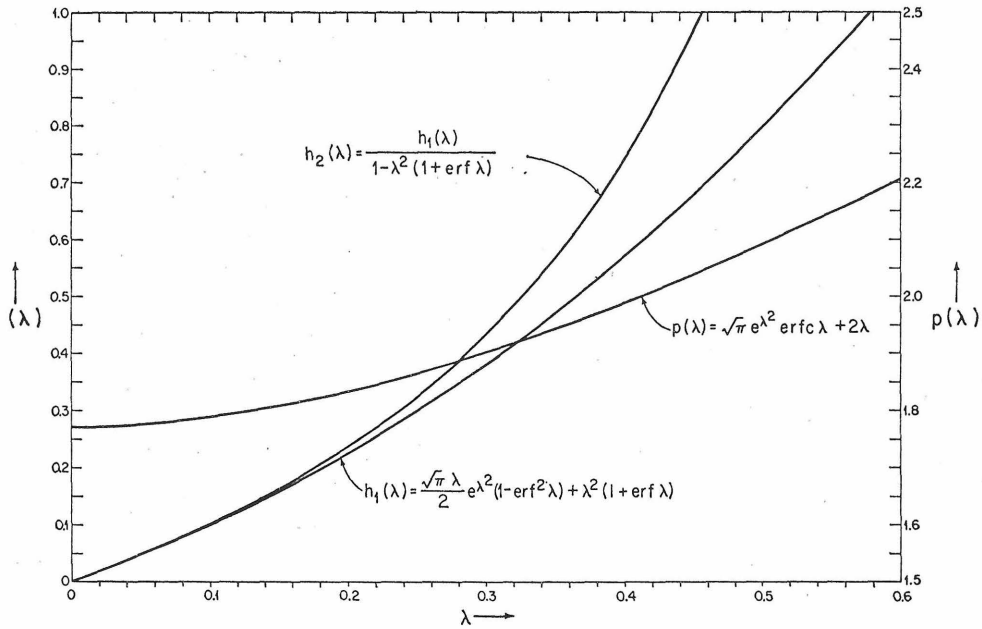

Fig. 8. The functions $p(\lambda)$, $h_1(\lambda)$, $h_2(\lambda)$ versus λ. The value of $\tilde{\lambda}_i^*$ is determined from $h_i(\tilde{\lambda}_i^*) = (1/C)[D\xi_m(0) - E]$. $\tilde{\tau}^*$ is then determined by $\tilde{\tau}_i^{*1/2} = [\xi_m(0) - E/D]/p(\tilde{\lambda}_i^*)$. h_i is read on the on the left-hand scale and p on the right-hand scale.

Long-time behavior. In the previous section the effects of the boundaries at $\xi = 0$ and $\xi = 1$ were neglected. At times when these are important, the SA type of treatment is clearly not applicable. The boundaries will be significant when the energy liberated at the moving phase boundary has diffused over the entire region and caused the temperature field to rise uniformly from the exterior boundaries to the phase boundary, rather than in the type of sharply peaked temperature distribution that characterizes the initial motion.

An estimate for the long-time behavior of $\xi_m(\tau)$ can be obtained by approximating the temperature $\theta(\xi, \tau)$ with a quasi-steady-state distribution (QSSA)

$$\begin{aligned} \tilde{\theta}_{ss}(\xi, \tau) &\equiv \left(\frac{D\xi_m(\tau) - E}{\xi_m(\tau)}\right)\xi \qquad && 0 \le \xi \le \xi_m(\tau) \\ \tilde{\theta}_{ss}(\xi, \tau) &\equiv \left(\frac{D\xi_m(\tau) - E}{1 - \xi_m(\tau)}\right)(1 - \xi) \qquad && \xi_m(\tau) \le \xi \le 1 \end{aligned} \tag{42}$$

Inspection of Figure 6, showing the temperature distribution for the gutted problem, indicates the essential validity of this approximation for sufficiently long times. Substituting $\tilde{\theta}_{ss}$ into the integral form of the boundary condition 28 yields

$$C\frac{d\xi_m}{d\tau} = -\frac{D}{2}\frac{d\xi_m}{d\tau} - \frac{D(\xi_m - E/D)}{\xi_m(1 - \xi_m)}$$

The first term on the right-hand side of this equation is due to the change in temperature of the phase transition and the resulting change in the total distribution.

The second term corresponds to the heat flux out of the region at the boundaries. If we had used the differential form of the boundary condition (27*c*), we would have neglected the first term.

For the long times under consideration, $\partial^2\theta/\partial\xi^2 = (\partial\theta/\partial\tau) < 0$, whereas for the approximation used $\partial^2\tilde{\theta}_{ss}/\partial\xi^2 = \partial\tilde{\theta}_{ss}/\partial\tau = 0$. Thus we have under-estimated the magnitude of $\partial\theta/\partial\xi$ at the boundaries. The effect of $\partial^2\theta/\partial\xi^2$ in the integral should be very small. Hence we expect that the approximation $\tilde{\theta}_{ss}$ will underestimate the velocity of the phase boundary.

If, as ξ_m approaches E/D, $[1/(\xi_m - E/D)]\ (d\xi_m/d\tau) \rightarrow -1/\tau_l = \text{constant}$, it follows that the asymptotic behavior is exponential. From $\tilde{\theta}_{ss}$ we obtain

$$\xi - E/D \cong \text{constant} \exp\left\{\frac{-\tau}{[(C/D) + \frac{1}{2})(E/D)(1 - (E/D)]}\right\}. \tag{43}$$

We expect that the long-term behavior for the gutted problem will exhibit this functional form. This can be characterized by the dimensionless relaxation time

$$\tau_l \approx \tilde{\tau}_l = [(C/D) + \tfrac{1}{2})(E/D)(1 - (E/D)] \tag{44}$$

In this time the distance of the phase boundary from its final position will reduce by a factor $1/e$.

For $C = 0$, the movement will be controlled by the decay of the temperature distribution alone. This may be compared with the long-term relaxation of a slab of unit thickness with zero surface temperature and constant initial temperature which has a dimensionless relaxation time $1/\pi^2$. The analogous form of the gutted problem is the symmetrical case $E/D = \frac{1}{2}$, which yields $\tilde{\tau}_l = \frac{1}{8}$. The difference of these two values is an indication of the accuracy of the quasi-steady-state temperature approximation used.

In terms of the geophysical parameters

$$\tilde{t}_l = \frac{\rho_1 c_1}{K_1}\left\{\frac{L/c_1}{b_0[G\rho_1 g - (J(0, 0)/K_1)]} + \frac{1}{2}\right\}M_f[b_0 - M_f] \tag{45}$$

Taking the values of the parameters $K_1/\rho_1 c = 0.01$ cm^2/sec, $b_0 = 100$ km, $M_f = 30$ km, $L/c_1 = 75$°C, we see that the latent heat will not dominate unless $G\rho_1 g - (J(0, 0)/K_1) \leq 1.5$°C/km; thus, neglecting the latent heat, $\tilde{t}_l = 33 \times 10^6$ years. This is approximately the thermal relaxation time for the slab between $x = 0$ and $x = 30$ km, and it therefore appears that the long-term effects for cases of this type are little influenced by the thermodynamic parameters.

The time at which the motion of the phase boundary becomes exponential is defined as τ^{**}. This will be approximately the time at which the temperature distribution becomes essentially linear. We may estimate this time τ^{**} after which the long-term behavior predicted by the QSSA will apply by considering the limiting case of a slab with ends at zero temperature which was initally at a constant temperature. The linear behavior will dominate when all but the lead time-dependent terms in the Fourier representation of the solution are negligible [*Carslaw and Jaeger*, 1959, p. 100]. This will certainly be the case for $\pi^2\tau/(1 - \xi_m)^2 > 2$ for which the deviation from a linear distribution is less than 10%.

Hence

$$\tau^{**} \approx \tilde{\tau}^{**} = 2(1 - E/D)^2/\pi^2 \tag{46}$$

For times approaching τ^{**}, the QSSA should be a very good approximation. We have assumed above that the phase boundary is closer to $\xi = 0$ than to $\xi = 1$. If this is not the case, then the above expression for τ^{**} should be modified accordingly.

If the phase boundary is far enough removed from the boundaries of the region, so that we may regard it as infinite, we can obtain an estimate of the limiting behavior as ξ_m approaches E/D from the Stefan approximation.

For small values of λ, $n(\lambda) \approx (\pi^{1/2}/2)\ \lambda$. Then $\lambda = (2/\pi^{1/2})\ (D/C)\ [\xi_m - (E/D)]$ and $d\xi_m/d\tau = -\lambda/\tau^{1/2} = (-2/\pi^{1/2})\ (D/C)\ (\xi_m - E/D)\tau^{-1/2}$. Hence

$$\xi_m - E/D \approx \text{constant exp}\ [-(4/\pi^{1/2})(D/C)\tau^{1/2}] \tag{47}$$

This type of long-term behavior may be of significance for a phase change deep in a planetary interior, for instance.

4. NUMERICAL RESULTS

Since exact analytic solutions to the problems defined in the last section have not been found, the problems were solved numerically. An implicit method using standard finite difference equations was used in an iterative scheme to determine the motion of the phase boundary (appendix 2). The solution obtained was stable with respect to changes in the space and time steps. The method was also used to solve the Stefan problem for short times.

The numerical solutions to the gutted problem and the Stefan problem were obtained using both the integral and differential forms of the boundary conditions. The solutions by either of the two methods were in satisfactory agreement for both cases, indicating that no serious errors were accumulated in the partial derivatives near the phase boundary.

The solutions so obtained enabled us to determine the validity of the approximations to the gutted problem, to identify the more important parameters, and to extend the approximations to more complex cases.

The parameters of the models for which numerical solutions have been obtained are given in Tables 1 and 2. The models generally increase successively in complexity in order to illustrate the dependence of the solution on the parameters of the model.

In general these models have been constructed to represent some specific aspects of the problem in a reasonable manner; they are not intended to be taken as realistic representations of the complete geophysical problem. Thus, the parameters used are usually in the range of geophysical interest, although their exact values may have been chosen to facilitate comparisons among different models.

In discussing the numerical results we will compare the temperature distribution, position of the phase boundary, and the various parameters τ^*, τ^{**}, τ_l, $\xi_m(\tau^*)$, etc., with the estimates obtained from the approximate theory given in

TABLE 1. Parameters Describing Models

Parameter	Model: Units	1	2	3	4	5	6	7	8	9	10	11	12	13	14	15	16	17	18–20
K_1	$\frac{\text{cal}}{\text{cm/sec °C}}$	0.005	0.005	0.005	0.005	0.005	0.005	0.005	0.005	0.005	0.005	0.005	0.005	0.005	0.005	0.005	0.005	0.005	0.005
K_2		0.005	0.005	0.005	0.010	0.010	0.010	0.010	0.010	0.010	0.010	0.010	0.005	0.010	0.010	0.010	0.010	0.010	0.005
κ_1	$\frac{\text{cm}^2}{\text{sec}}$	0.0089	0.0089	0.0089	0.0089	0.0089	0.0089	0.0089	0.0089	0.0089	0.0089	0.0089	0.0089	0.0089	0.0089	0.0089	0.0089	0.0089	0.0089
κ_2	,,	0.0089	0.0089	0.0089	0.018	0.018	0.018	0.018	0.018	0.010	0.010	0.010	0.0089	0.018	0.010	0.010	0.010	0.010	0.0089
ρ_1	g/cm³	2.8	2.8	2.8	2.8	2.8	2.8	2.8	2.8	2.8	2.8	2.8	2.8	2.8	2.8	2.8	2.8	2.8	2.8
ρ_2		2.8	2.8	2.8	2.8	2.8	2.8	2.8	2.8	2.8	3.3	3.3	2.8	3.3	3.3	3.3	3.3	3.3	2.8
$J(0, 0)$	$\frac{\mu\text{cal}}{\text{cm}^2\text{ sec}}$	0.62	0.62	0.62	0.62	0.62	0.62	0.62	0.62	0.62	0.62	0.62	0.62	0.62	1.01	1.50	0.53	0.19	0.62
$b(0)$	km	100	100	100	100	100	200	100	100	100	100	100	95	95	100	100	100	100	100
B_0C_0*		*T*	*T*	*J*	*J*	*T*	*T*	*T*	*T*	*T*	*T*	*T*	*T*	*T*	*T*	*T*	*T*	*T*	*T*
G	°C/kbar	75	75	75	75	75	75	75	60	75	75	75	75	75	75	75	100	75	75
F	°C	320	320	320	320	320	320	320	160	320	320	320	320	320	167	170	274	658	320
ΔP	kbar	1.0	1.0	1.0	1.0	1.0	1.0	1.0	1.0	1.0	1.0	1.0	1.0	1.0	1.0	1.0	0.75	1.0	0
L	cal/g	50	15	15	15	15	15	30	15	15	15	15	15	15	15	15	15	15	15
V_2†		0	0	0	0	0	0	0	0	0	0	finite	finite	finite	finite	finite	finite	finite	0
A_i/ρ_i	$\frac{10^{-12}\text{ cal}}{\text{g sec}}$	0	0	0	0	0	0	0	0	0	0	0	0	0	0.36	1.25	0	0	0
$J(b(0), 0)$	$\frac{\mu\text{cal}}{\text{cm}^2\text{ sec}}$	0.62	0.62	0.62	0.62	0.62	0.62	0.62	0.62	0.62	0.62	0.62	0.62	0.62	0.0	0.05	0.53	0.19	0.62
Sediments	km	0	0	0	0	0	0	0	0	0	0	0	3.64	3.64	0	0	0	0	0

* Boundary condition at lower boundary. *T*: constant temperature; *J*: constant flux.

† Velocity in lower layer. If finite, $V_2 = [(\rho_2 - \rho_1)/\rho_2]dM(t)/dt$.

TABLE 2. Dimensionless Parameters Describing Models

Model	b, km	T_0, °C*	C	D	E	$\xi_m(0)$	$\xi_m(\infty)$	γ_1	t/τ, 10^6 yr
1	100	1000	0.250	0.8193	0.245	0.3906	0.2991	1.24	355
2	100	1000	0.075	0.8193	0.245	0.3906	0.2991	1.24	355
3	100	1000	0.075	0.8193	0.245	0.3906	0.2991	1.24	355
4	100	1000	0.075	0.8193	0.245	0.3906	0.2991	1.24	355
5	100	1000	0.075	0.8193	0.245	0.3906	0.3238	1.24	355
6	200	2000	0.0375	0.8193	0.1225	0.1953	0.1573	1.24	1420
7	100	1000	0.150	0.8193	0.245	0.3906	0.3238	1.24	355
8	100	1000	0.075	0.4096	0.100	0.3906	0.3047	1.24	355
9	100	1000	0.075	0.8193	0.245	0.3906	0.3238	1.24	355
10	100	1000	0.075	0.8193	0.245	0.3906	0.3268	1.24	355
11	100	1000	0.075	0.8193	0.245	0.3906	0.3268	1.24	355
12	100†	1000	0.075	0.8193	0.245	0.3906	0.3335	1.24	355
13	100†	1000	0.075	0.8193	0.245	0.3906	0.3454	1.24	355
14	100	1000	0.075	‡	0.092	0.3906	0.3244	‡	355
15	100	1000	0.075	§	0.095	0.3925	0.3550	§	355
16	100	1000	0.075	1.6755	0.583	0.3925	0.3550	1.063	355
17	100	1000	0.075	1.6755	0.583	0.3925	0.3507	0.384	355
18–20	100	1000	0.075	0.8193	0.320‖	0.3906	¶	1.24	355

* These values for T_0 have been arbitrarily chosen to make comparison between different models easier. T_0 is not necessarily the temperature at the lower boundary.

† Note, however, that the lower boundary condition was fixed at $x = 95$ km. The discrepancy is due to the sediments on the surface.

‡ Compare model 11, which is a no-source approximation for this model.

§ Compare models 16 and 17, which are no-source approximations for this model.

‖ $E(0)$, since E is time dependent.

¶ Not determined, since E is time dependent.

section 3. It will be seen that the Stefan and long time approximations are extremely successful. In the subsequent discussion the approximate theory will be extended to apply to more complicated cases as they arise.

Gutted problem. We will first consider the numerical results for the most elementary cases that correspond to the gutted problem. Models 1 and 2 are examples of the gutted problem, and model 3 is a slight variation of it.

As we are neglecting sources in these cases, it is necessary to neglect the heat that would be produced by them. For this reason the artifically low value of 0.62 μcal/cm^2 sec is used for the surface heat flux $J(0, 0)$. A Clapeyron curve was chosen which is compatible with the results of *Ringwood and Green* [1964]. This yields a depth for the phase boundary that is near that of the continental Moho. The initial temperature distribution and Clapeyron curve for models 1, 2, and 3 may be seen in Figure 9*a*. Some results for model 3 which illustrate the nature of the temperature distribution are presented in Figure 9*b*, which shows the actual temperature and perturbation temperature after the motion has gone 60% of the total possible displacement. The shape of the perturbation temperature ⊙ illustrates the 'short time' behavior discussed in the section on the gutted problem. Its similarity with the form for the generalized Stefan problem is evident. The

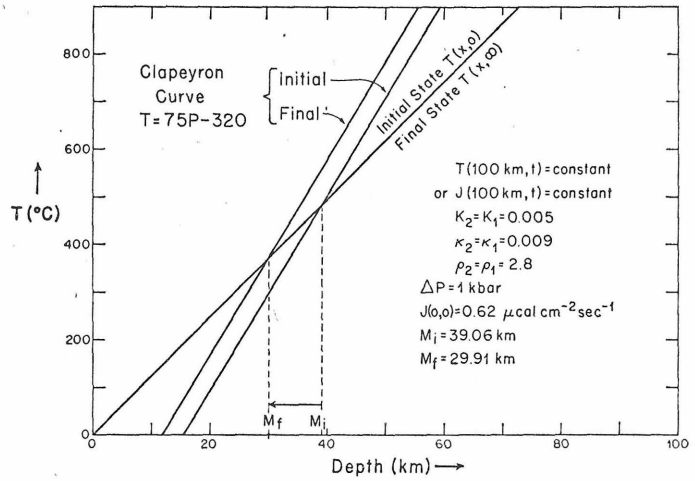

Fig. 9*a*. Initial and final temperature distribution and Clapeyron curves for models 1, 2, and 3. For constant temperature at the lower boundary, the problem reduces to the gutted problem.

general effect of this phase transition is to generate a narrow region of anomalously high temperature.

The development of the temperature distribution with time for model 1 is shown in Figure 6. The initial sharp peak decreases in height and becomes broader with time until it is limited by the effects of the boundaries. The illustration shows segments of the reduced Clapeyron curve. This line passes through the points of the temperature profile where there is a discontinuity in the slope. The singularity in the initial temperature is shown by the interrupted vertical line.

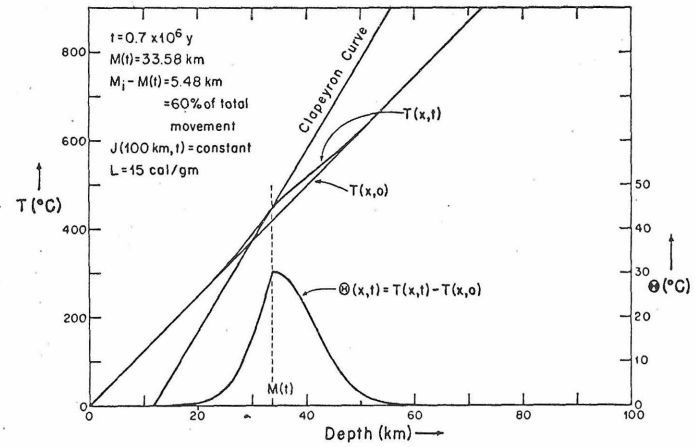

Fig. 9*b*. Typical temperature distribution for model 3 at a time t after the pressure pulse was applied, showing the relation between the temperature $T(x,t)$, the initial temperature $T(x, 0)$, the final Clapeyron curve, and the perturbation temperature $\Theta(x, t)$.

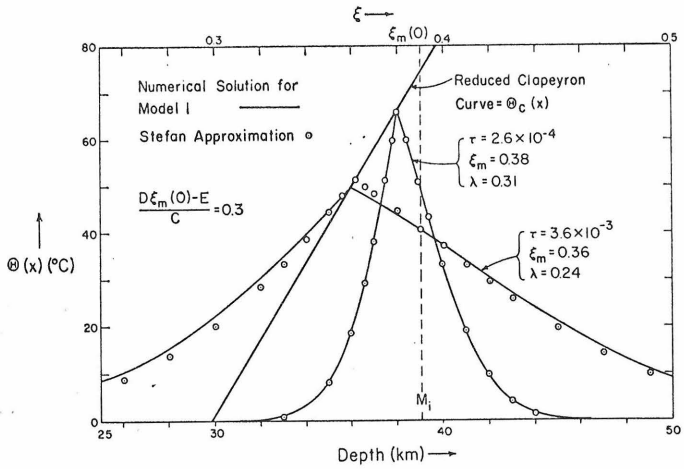

Fig. 10. Profiles of the perturbation temperature comparing the Stefan approximation (SA1) and the numerical solution for model 1 at the same time, for two different times. The solid curves show the numerical solution; the separate points indicate the Stefan approximation.

A comparison of the shapes of the temperature profile for the gutted problem and the Stefan approximation SA1 at two different times may be seen in Figure 10. The agreement for $\tau = 2.6 \times 10^{-4}$ is remarkably good. Since for this model $(1/C)\,[D\xi_m(0) - E] = 0.3$, the initial value of λ and the initial velocity are not too great, and we would not except the Stefan approximation to be in serious error. The agreement for $\tau = 3.6 \times 10^{-3}$ is not so good as in the previous case, primarily because there is a slight error in the time dependence of the location of the phase boundary using the Stefan approximation. With this error taken into consideration, the agreement may be regarded as very satisfactory.

The position of the phase boundary with time is shown in Figure 11. This figure shows two curves: (1) the logarithm of the displacement from the *initial* position versus the logarithm of time in order to illustrate the behavior for times when the position of the boundary changes rapidly; and (2) the logarithm of the distance of the boundary from its *final* position in order to illustrate the behavior when the position changes slowly with time.

Examination of the first curve shows that the slope $[d \log (\xi_m(0) - \xi_m(\tau))]/(d \log \tau)$ is initially slightly greater than $\frac{1}{2}$ and decreases smoothly as time increases, until it equals zero when the phase boundary attains its equilibrium position. In spite of the changing slope, the departure of the curve from a straight line of slope $= \frac{1}{2}$ is quite small for the first 20–25% of the motion.

Several points for the Stefan approximation are shown, and it may be seen that the agreement between the numerical solution and the approximation is satisfactory. The point (ξ_m^*, τ^*) at which the Stefan behavior begins to break down is shown as well. The Stefan approximation remains good well beyond this point even though the criterion that determines equation 36 is violated. Thus the change in curvature of the temperature distribution at this time is a subtle

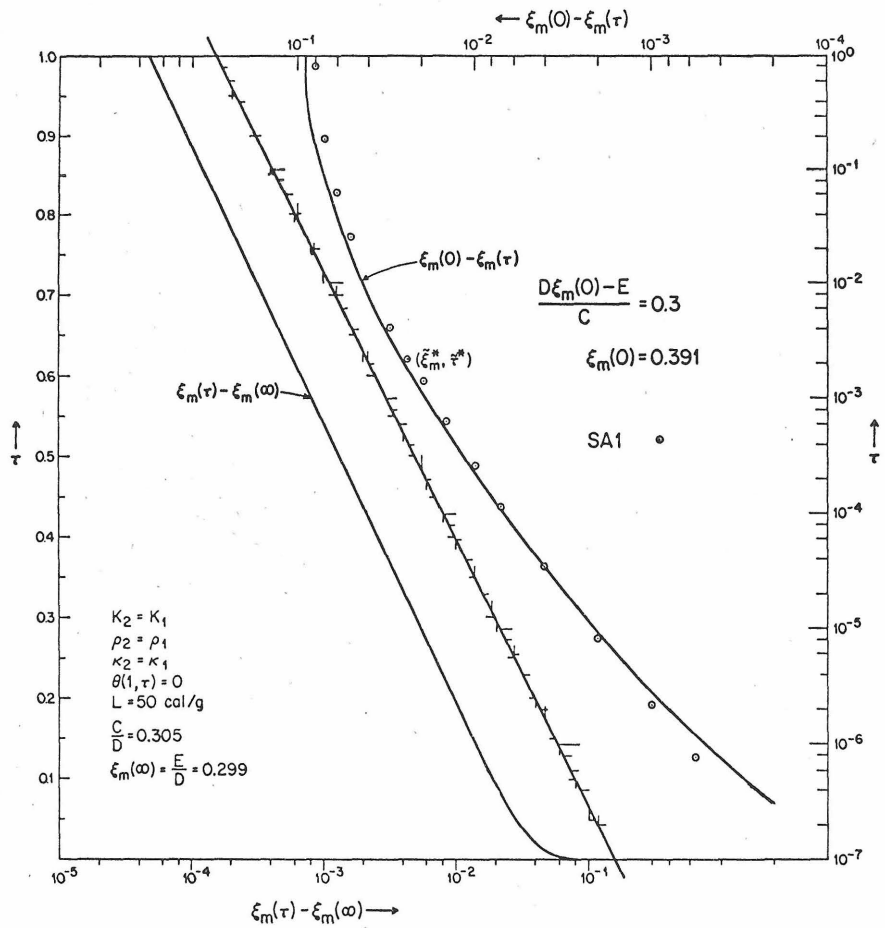

Fig. 11. Model 1. The curve on the right shows the nature of the initial motion of the phase boundary as shown by a plot of log $(\xi_m(0) - \xi_m(\tau))$ versus log τ. Selected points for the Stefan approximations are indicated. These include $(\xi_m(\tilde{\tau}_1^*), \tilde{\tau}_1^*)$ as calculated from the Stefan approximation. The curve on the left shows the nature of the long-term motion as shown by a plot of log $(\xi_m(\tau) - \xi_m(\infty))$ versus τ. Note that the two curves are separated by the heavy diagonal line with tick marks and have different scales.

criterion and does not appear to have a serious influence on the solution. This may be confirmed by examination of Figure 6, where the general shape of the temperature profile is the same after τ^* ($\tau = 6.51 \times 10^{-3}$) as before ($\tau = 1.80 \times 10^{-3}$). It would thus appear that the approximation SA1 continues to be accurate until the effects of the boundaries of the region significantly interfere.

The above comparison between the numerical results and the Stefan approximation indicates that the criterion at τ^* provides a very strict limit to the cessation of Stefan behavior and should be generally applicable in predicting the range of application of the Stefan approximation.

The preceding discussion was concerned with the motion of the phase boundary for times such that the boundaries of the region were not felt. The

motion of the phase boundary for long times is best shown by the curve on the left of Figure 11, which shows the logarithm of the distance of the phase boundary from its final position plotted against time. The curve is linear for long times in agreement with the exponential behavior predicted by the quasi-steady-state approximation (QSSA); the departure from linearity is due to the nonapplicability of the quasi-steady-state approximation. This may be confirmed by examination of the temperature profiles for $\tau < 0.02$. The logarithmic derivative $(d/d\tau)$ as $\tau \to \infty$, $d[\log (\xi_m - E/D)]/d\tau = 1/\tau_l$ for model 1 is given in Table 3 and may be compared with that calculated from QSSA, also in Table 3. The agreement between the actual and theoretical values is quite satisfactory considering the simplicity of the theoretical model.

An estimate of the time τ^{**} when the QSSA is dominant was here defined for the numerical solution when the logarithmic slope

$$\frac{1}{(\xi_m(\tau) - \xi_m(\infty))} \frac{d\xi_m(\tau)}{d\tau}$$

last departed by 20% from the asymptotic value as $\tau \to \infty$. The comparison of the theoretical and numerical values may be seen in Table 3.

In model 1 we have considered a case in which the term $d(\log \lambda)/d[\log(\xi_m(0) - \xi_m)]$ in (35), which is neglected in the SA1 approximation, has not been very large. We next consider the limiting case $(1/C)\ [D\xi_m(0) - E] = 1.0$ in model 2. This corresponds to the maximum pressure pulse which can be applied without overdriving the system and for which in the corresponding Stefan case $\lambda(\xi_m(0)) \to \infty$.

A representative example of the temperature distribution may be seen in Figure 9*b*. The peak is not as pointed as it would be for model 1, which may be attributed to the more rapid motion of the phase boundary for this case. Nevertheless, the general shape of the curve is similar to that for model 1.

The location of the phase boundary with time may be seen in Figure 12, which is analogous to Figure 11 for model 1. The general shape of the curves are, of course, similar for the two cases.

This model provides a more severe test for the Stefan approximation because of the singularity in λ. Comparison of SA1 with the numerical results for times significantly after $\tau = 0$ indicates that it is a fairly reasonable approximation to the temperature field. A comparison between the positions of the phase boundary calculated from the Stefan approximation (SA1 and SA2) and the numerical results are also shown in Figure 12.

It may be seen that for the initial motion $(\xi_m(0) - \xi_m(\tau)) \lesssim 0.01$, $\lambda \gtrsim 1.5$), the position of the phase boundary as calculated from either SA1 or SA2, overestimates the displacement. Both Stefan approximations are intrinsically unsatisfactory because their error lies primarily in approximating the temperature field. Exact integration of equation 34*b* would result in an even greater motion of the phase boundary for short times. This is undoubtedly because the motion of the phase boundary is so rapid that it is controlled to a large extent by the decay of the former temperature peak. For short times, SA2 is the better approximation for this case because it includes some of the effects of the redistribution of heat.

TABLE 3. Time and Position Criteria Obtained from Both the Stefan Approximation and Numerical Solution

Model	τ^*	$\xi_m(\tau^*)$	$\bar{\tau}_1^*$	$\tilde{\xi}_m(\bar{\tau}_1^*)$	τ_2^*	$\tilde{\xi}_m(\bar{\tau}_2)$	$\bar{\tau}\dagger$	$\tilde{\xi}_m(\bar{\tau}\dagger)$	$\bar{\tau}\dagger\dagger$	$\tilde{\xi}_m(\bar{\tau}\dagger\dagger)$	τ_1	$\bar{\tau}_1$	τ^{**}	$\bar{\tau}^{**}$
1	0.00252	0.3635	0.00241	0.3659	0.00243	0.3672	...	...	...	...	0.1510	0.1688	0.1060	0.0996
2	0.00106	0.3429	0.00176	0.3420	0.00200	0.3497	...	...	...	...	0.1148	0.1240	0.1129	0.0996
3	0.00106	0.3429	0.00176	0.3420	0.00200	0.3497	...	...	...	...	0.4260	0.2817	0.3488	0.2987
4	0.00126	0.3458	0.00172	0.3406	0.00191	0.3467	3.15×10^{-4}	0.3555	0.00154	0.3396	0.5003	0.4403	0.0481	0.1493
5	0.00126	0.3458	0.00172	0.3406	0.00191	0.3467	3.15×10^{-4}	0.3555	0.00154	0.3396	0.0875	0.1036	0.0241	0.0463
6	0.00032	0.1729	0.00043	0.1703	0.00048	0.1734	7.88×10^{-5}	0.1778	0.00039	0.1698	0.0828	0.0837	0.0567	0.0719
7	0.00184	0.3559	0.00213	0.3543	0.00218	0.3563	6.15×10^{-4}	0.3651	0.00236	0.3515	0.0967	0.1151	0.0415	0.0463
8	0.00412	0.3321	0.00477	0.3175	0.00513	0.3248	3.12×10^{-4}	0.3560	0.00116	0.3522	0.1008	0.1196	0.0276	0.0490
9	0.00145	0.3470	0.00171	0.3405	0.00188	0.3458	4.52×10^{-4}	0.3526	0.00155	0.3392	0.1362	0.1100	0.0370	0.0819
11	0.00156	0.3467	0.00170	0.3401	0.00187	0.3453	...	...	...	...	0.1119	...	0.025	...

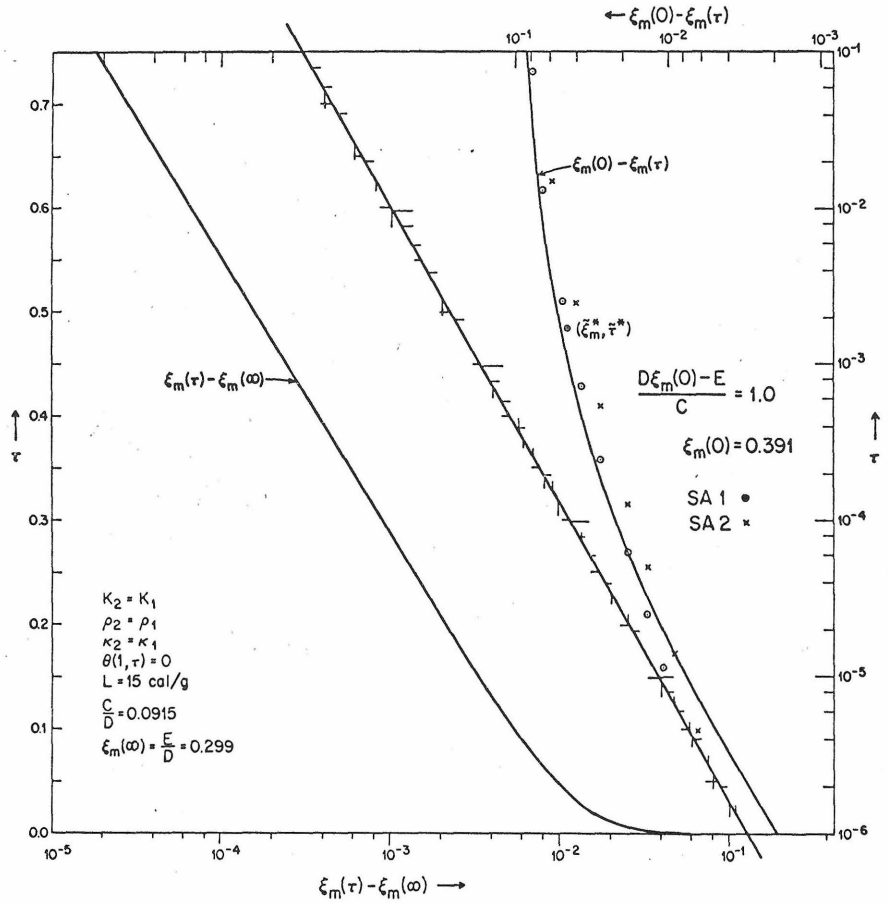

Fig. 12. Model 2. Log-log and semi-log plots showing the nature of motions of the phase boundary for model 2. See Figure 11. The only difference between models 1 and 2 is the values of the latent heat.

Nevertheless, it too will be in error as $\tau \rightarrow 0$, because implicit in the Stefan approximation is the assumption that the instantaneous temperature distribution is not influenced by the change in temperature at the phase boundary. However, for very short times the effect of the change in temperature at the phase boundary becomes large, and the neglect of this effect results in noticeable error. Nevertheless, for $\tau > 10^{-5}$, the Stefan approximation is reasonably good. For $\xi_m(0) - \xi_m(\tau) \gtrsim 0.015$, SA1 is the better approximation, never departing from the actual solution by greater than 0.005 in ξ, and remaining close to the actual solution for the latter two-thirds of the motion. The point (ξ_m^*, τ^*) is also shown, and, as was the case for model 1, the Stefan approximation remains good well beyond this point.

The long-term behavior, represented by the linear portion of the curve on the left of Figure 11, begins at nearly the same time for model 2 as for model 1; it obtains for a smaller fraction of the total displacement, however, owing to the faster motion of the phase boundary. Owing to the relatively small latent heat

in model 2, the long-term decay is controlled almost completely by the decay of the temperature distribution. In model 1 on the other hand, the latent heat was sufficient to affect the long-term behavior, as may be seen by the smaller logarithmic derivative $1/\tau_l$ as given in Table 3. For either model the agreement between τ_l and $\tilde{\tau}_l$ is satisfactory.

We have seen that the motion of the phase boundary may be quite accurately predicted for short times and for long times. However, between the time before which the boundaries of the region are not felt and the time beyond which the boundaries are completely felt is usually a period of transition between these two types of behavior. The duration in time or the length of this transition region will depend on all the parameters of the problem, and predicting the motion of the boundary in this region may be a difficulty. Nevertheless, the curves in Figures 11 and 12 in this region are smoothly varying, and one might expect to reasonably approximate the curves by continuing the Stefan approximation and then utilizing the exponential behavior for the long-term behavior.

Model 3 is identical to model 2, except that the lower boundary condition (27*b*) $\theta(1, \tau) = 0$ is replaced by

$$\left.\frac{\partial \theta}{\partial \xi}\right|_{\xi=1} = 0$$

Thus the short-term behavior is identical to that of model 2, and the only difference is in the long-term behavior.

A typical temperature curve is shown in Figure 9*b*, and, since the effect of the lower boundary is not yet apparent, this curve applies equally to either model 2 or 3. The motion of the phase boundary is not shown, as it differs from that for model 2 only for long times.

We may construct a quasi-steady-state solution for this case in the same manner as was done for the constant temperature boundary condition.

$$\tilde{\theta}_{SS}(\xi, \tau) = \begin{cases} \dfrac{D\xi_m - E}{\xi_m}\,\xi; & 0 \le \xi \le \xi_m \\ D\xi_m - E; & \xi_m \le \xi \le 1 \end{cases}$$

Insertion of $\tilde{\theta}_{SS}$ into (28) yields

$$\frac{1}{(\xi_m - E/D)}\frac{d\xi_m}{d\tau} = \frac{E}{D}\frac{1}{\left[\dfrac{C}{D} + 1 - \dfrac{1}{2}\dfrac{E}{D}\right]} \equiv \frac{1}{\tilde{\tau}_l} \quad \text{as} \quad \xi_m \to E/D$$

The relaxation time for

$$\left.\frac{\partial \theta}{\partial \xi}\right|_{\xi=1} = 0$$

is considerably larger than for the gutted problem for $\theta(1, \tau) = 0$, as can be seen by comparison with equation 44.

The approximate ($\tilde{\tau}_l$) and actual (τ_l) relaxation times for case 3 are given in Table 3. The agreement is satisfactory.

The time τ^{**} after which logarithmic behavior should certainly obtain may be estimated in a manner analogous to that used for models 1 and 2. This yields $\tau^{**} \approx [6(1 - E/D)^2]/\pi^2$. As may be seen from the theoretical and actual values for τ^{**} in Table 3, the agreement is satisfactory.

The comparisons of the results obtained by the numerical solution of the gutted problem with those obtained from elementary physical considerations show them to be in reasonable agreement, and we conclude that the essential behavior of the generalized Stefan problem for regions with matched thermal constants is well understood. It may be noted that the important parameters are the ratios C/D and $E/D = \xi_m(\infty)$. C and E are the dimensionless latent heat and zero intercept of the Clapeyron curve and may be estimated fairly well for realistic models. The parameter D is the difference between the Clapeyron slope and initial temperature gradient and is probably one of the more uncertain and critical parameters to be estimated in constructing realistic geophysical models.

Unmatched thermal constants. We now turn to cases in which the thermal conductivities of the two phases differ. Differences in thermal conductivities cause the initial and final temperature distribution to differ, and they generate a long-term transient in the temperature distribution for the whole region, as was discussed in the section on the static problem. The relevant equations for the dynamic problem are (25) and (26) in which we will neglect convective heat transport ($\nu \equiv 0$) and sources ($\sigma \equiv 0$). The initial dimensionless steady-state temperature distribution will be

$$\eta(\xi, 0) = \gamma_1 \xi \qquad 0 \leq \xi \leq \xi_m(0)$$

$$\eta(\xi, 0) = \gamma_2 \xi + \delta_2 \qquad \xi_m(0) \leq \xi \leq 1$$

where $K_2\gamma_2 = K_1\gamma_1$ and $\delta_2 \equiv \xi_m(0)\ (\gamma_1 - \gamma_2)$ by (24). (For $T_0 = (J(0, 0)/K_1)b_0$, $\gamma_1 = 1$. However, since T_0 could be chosen otherwise, we shall continue to use γ_1.)

The form of the Stefan problem for the case in which the two phases have different thermal properties is

$$\theta(\xi, \tau) = \frac{\theta_S}{(1 - \operatorname{erf} \lambda)}\left[1 + \operatorname{erf}\left(\frac{\xi - \xi_m(0)}{2\tau^{1/2}}\right)\right] \qquad \xi \leq \xi_m(\tau)$$

$$\theta(\xi, \tau) = \frac{\theta_S}{[1 + \operatorname{erf}(\lambda/\alpha^{1/2})]}\left[1 - \operatorname{erf}\left(\frac{\xi - \xi_m(0)}{2(\alpha\tau)^{1/2}}\right)\right] \qquad \xi \geq \xi_m(\tau)$$

$$\xi_m(0) - \xi_m(\tau) = 2\lambda\tau^{1/2}$$

where λ is the root of

$$N(\lambda, \alpha, K_2/K_1, 1) = \lambda\pi^{1/2}\left\{\frac{\exp(-\lambda^2)}{1 - \operatorname{erf}\lambda} + \frac{K_2 \exp[-(\lambda^2/\alpha)]}{K_1\alpha^{1/2}[1 + \operatorname{erf}(\lambda/\alpha^{1/2})]}\right\}^{-1} = \frac{\theta_S}{C}$$

The function $N(\lambda, \alpha, K_2/K_1, 1)$ is a special case of (54) and is shown in Figure 7 for the values of the arguments used in this paper. The symbol N used for this function is in honor of Franz Neumann who first presented the solution to this type of problem [*Neumann*, 1860]. With this solution we may thus construct

Stefan approximations as in the case of the gutted problem by substituting $\theta_c(\xi_m)$ for θ_s and by regarding λ as a function of ξ_m. The Stefan approximation for the case with unmatched thermal constants does not have a discontinuity in the gradient at $\xi_m(0)$; hence it does not satisfy equation 26*d*. If $K_2 = K_1$ or $\partial\eta(\xi, 0)/\partial\xi = 0$, this Stefan approximation will satisfy the field equations and boundary conditions in the same way that it did for the gutted problem.

Because of the fact that the thermal constants of the two phases differ, equations 25 and 26 are rather complicated in comparison with the gutted problem. These complications arise because the temperature has a discontinuous gradient at certain points. In the definition of $\theta(\xi, \tau) \equiv \eta(\xi, \tau) - \eta(\xi, 0)$ we have subtracted $\eta(\xi, 0)$, which has a discontinuous gradient at $\xi_m(0)$, from $\eta(\xi, \tau)$, which has a discontinuous gradient at $\xi_m(\tau)$. Hence discontinuities in $\partial\theta/\partial\xi$ will exist at $\xi_m(\tau)$ and $\xi_m(0)$. Except at these two points, $\partial\theta/\partial\xi$ will be continuous everywhere, as can be seen in Figure 13*a*. The resultant perturbation temperature distribution is thus quite different than that for the three previous cases, and the final distribution, $\theta(\xi, \infty)$, is not identically zero everywhere. The equation for $d\xi_m/d\tau$ now includes the term $[1 - (K_2/K_1)]\ [\partial\eta(\xi, 0)/\partial\xi]$, and at the initial position of the phase boundary, equation 26*d* applies. The term

$$\left(1 - \frac{K_2}{K_1}\right) \frac{\partial\eta(\xi, 0)}{\partial\xi}\bigg|_{\xi=\xi_m-(\tau)}$$

in (26*c*) is a constant and therefore does not dominate the behavior near the singularity in $d\xi_m/d\tau$. The initial behavior in all regions will therefore be like the initial behavior of the gutted problem. If $K_2 > K_1$, the term

$$\left(1 - \frac{K_2}{K_1}\right) \frac{\partial\eta(\xi, 0)}{\partial\xi}\bigg|_{\xi=\xi_m-(\tau)}$$

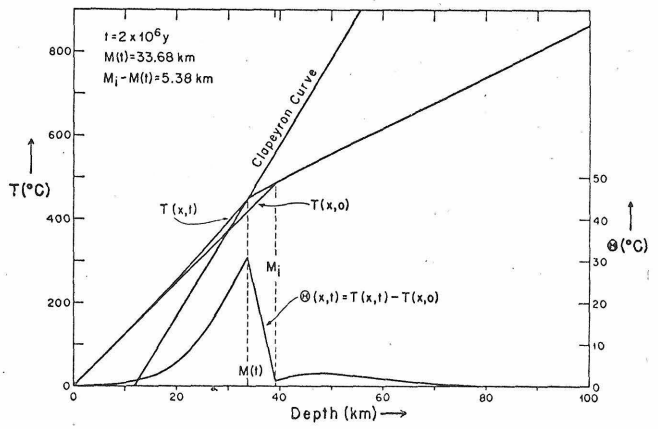

Fig. 13*a*. Model 4 and model 5 with conductivity difference ($K_2 \neq K_1$). Initial temperature and temperature after 2 × 10^6 years. The two models are indistinguishable at this time. The lower curve shows $\Theta(x, t)$ at the same time. Note the discontinuities in $\partial\Theta/\partial x$ at $x = M_i$ and $x = M(t)$.

is negative and acts like a heat source; thus it tends to decrease the magnitude of the velocity of the phase boundary. The additional term in (26*d*) has the same magnitude but is of different sign, and it acts like a sink at the boundary $\xi_m(0)$. If we attempt to extend the Stefan approximation to treat this case, the natural extension would be to replace C in equation 26*c* by

$$C + \left(\frac{K_2}{K_1} - 1\right) \frac{\partial \eta(\xi, 0)}{\partial \xi}\bigg|_{\xi=\xi_m(\tau)} \frac{[\xi_m(0) - \xi_m(\tau)]}{2\lambda^2}$$

which is analogous to SA2. We shall not use this, however, in the ensuing discussion.

We may estimate the time $\tau^\dagger$ at which the term

$$\left(\frac{K_2}{K_1} - 1\right) \frac{\partial \eta(\xi, 0)}{\partial \xi}\bigg|_{\xi=\xi_m-(0)}$$

in equation 26*d* has a significant effect on the temperature. This will certainly be the case when the flux from the Stefan approximation is equal to the jump in flux at the boundary $\xi_m(0)$:

$$-\frac{K_2}{K_1} \frac{\partial \tilde{\theta}_{SA}}{\partial \xi}\bigg|_{\xi=\xi_m(0)} = \left(\frac{K_2}{K_1} - 1\right) \frac{\partial \eta(\xi, 0)}{\partial \xi}\bigg|_{\xi=\xi_m-(0)}$$

This yields, using SA1

$$(\tau^\dagger)^{1/2} = \frac{\xi_m(0) - E/D}{q_1(\lambda, \alpha, \Delta\gamma/D)} \tag{48}$$

where

$$q_1(\lambda, \alpha, \Delta\gamma/D) = [1 + \operatorname{erf}(\lambda/\alpha^{1/2})]\pi^{1/2}\alpha^{1/2}(\Delta\gamma/D) + 2\lambda; \qquad \Delta\gamma \equiv \gamma_1 - \gamma_2$$

and λ is the root of

$$q_2(\lambda, \alpha, \Delta\gamma/D, K_2/K_1) = [D\xi_m(0) - E]/C$$

where

$$q_2(\lambda, \alpha, \Delta\gamma/D, K_2/K_1) = \frac{N(\lambda, \alpha, K_2/K_1, 1)q_1(\lambda, \alpha, \Delta\gamma/D)}{(\Delta\gamma/D)[1 + \operatorname{erf}(\lambda/\alpha^{1/2})]\pi^{1/2}\alpha^{1/2}}$$

For small enough λ we may approximate q_1 by

$$q_1(\lambda, \alpha, \Delta\gamma/D) \approx \pi^{1/2}(\Delta\gamma/D)\alpha^{1/2} + 2[1 + (\Delta\gamma/D)]\lambda - (2\Delta\gamma/3\alpha D)\lambda^3$$

For the parameters used in this paper, the error incurred in using this approximation is less than 2.5%. The function q_2 is shown in Figure 14 for values of the arguments used in this paper.

As has been seen in Figures 2 and 3, the heat due to the difference between the initial and final temperature distributions may be quite significant. Hence we may expect that the redistribution of this heat will be a major feature of the problem and will govern the motion of the phase boundary when the singularity is no longer dominant and possibly before the effect of the lower boundary becomes evident. We may estimate the time $\tau^{\dagger\dagger}$ beyond which this will be the case by equating the transport of heat away from the phase boundary for the

Stefan approximation with the effective flux source

$$-\left(1-\frac{K_2}{K_1}\right)\frac{\partial\eta(\xi,0)}{\partial\xi}\bigg|_{\xi=\xi_m-(\tau)}$$

at the phase boundary. This corresponds to the velocity of the phase boundary being zero if the temperature distribution in the neighborhood of the phase boundary is given by the Stefan approximation. Although this value of $\tau^{\dagger\dagger}$ will correspond to a value of $\xi_m(\tau^{\dagger\dagger})$ from the Stefan approximation, which will be physically realizable, we should not expect either the Stefan approximation for ξ_m or θ to be a good approximation to the actual values at this time. This criterion yields, using SA1

$$(\tau^{\dagger\dagger})^{1/2} = (K_1/K_2)(C\lambda/\Delta\gamma) \tag{49}$$

where λ is the root of

$$q_3(\lambda, \alpha, \Delta\gamma/D, K_2/K_1)$$

$$\equiv N(\lambda, K_2/K_1, \alpha, 1) + (K_1 2D/K_2\,\Delta\gamma)\lambda^2 = [D\xi_m(0) - E]/C$$

This function is shown in Figure 14.

Since the final temperature distribution and location of the phase boundary depend strongly on the lower boundary condition, numerical solutions were first obtained for two cases: constant flux (model 4) and constant temperature (model 5) at the lower boundary, which was fixed at 100-km depth. In both models $K_2 = 2K_1$.

The temperature distributions for model 4 at selected times are shown in Figure 13*b*. For extremely short times these are almost identical to those of the gutted problem. The discontinuity in

$$\frac{\partial\theta}{\partial\xi}\bigg|_{\xi=\xi_m(0)}$$

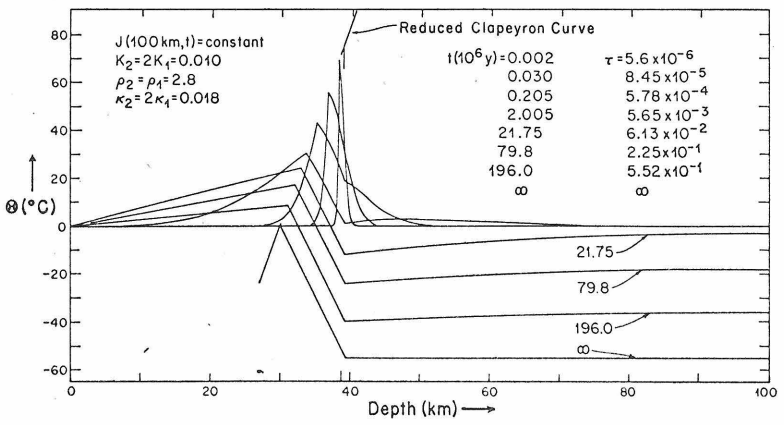

Fig. 13*b*. Model 4. Perturbation temperature at selected times for the case with constant flux at the lower boundary. The initial pulse develops similarly to that in Figure 6 but is changed later by the development of the discontinuity in $\partial\Theta/\partial x$ at $M(0) = 39$ km. Note the long-term transient and final steady state.

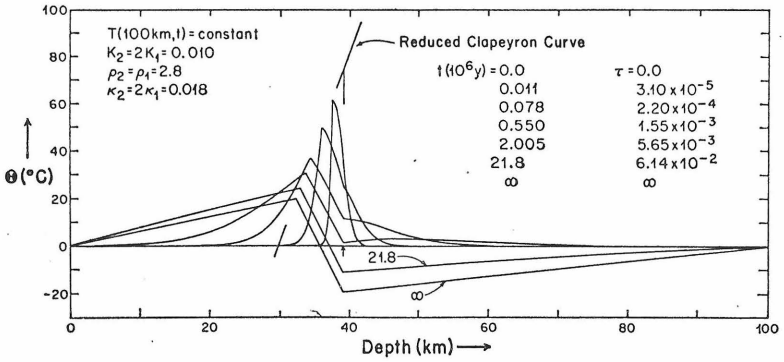

Fig. 13c. Model 5. Perturbation temperatures for the case with constant temperature at the lower boundary. Note the limited long-term transient and final steady state.

is apparent at $\tau = 6 \times 10^{-4}$ in the third temperature profile. This may be compared with the estimate for $\tau^{\dagger}$ of 3×10^{-4} in Table 3. The position of the phase boundary may also be compared. The value for $\tau^{\dagger\dagger}$ is also given in Table 3. By this time the discontinuities in the temperature distribution are well developed, and the incipient behavior of the long-term motion has begun to manifest itself. The effect of the discontinuity on the temperature may be seen in the last five temperature profiles, in which the long-term transient obviously dominates. Through profile 4 the temperature everywhere exceeds the initial steady state;

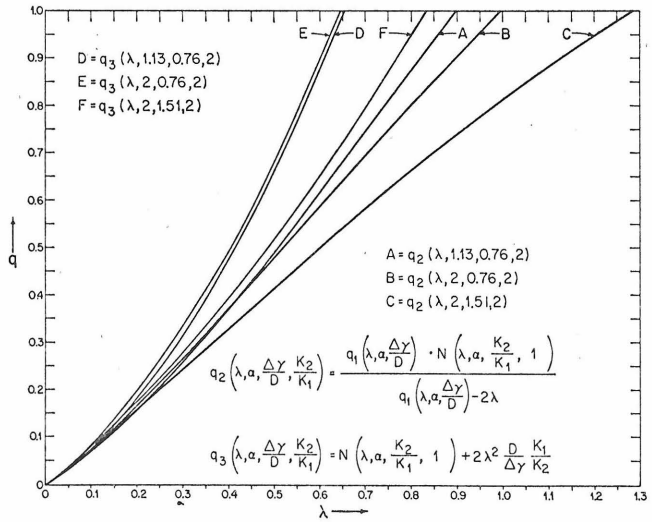

Fig. 14. Graphs of the functions q_2 and q_3 for selected values of the arguments. These functions define $(\tau\dagger)^{1/2}$ and $(\tau\dagger\dagger)^{1/2}$, $\lambda\dagger\dagger$ and $\lambda\dagger$. $\lambda\dagger\dagger$ is the root of q_3 $(\lambda\dagger\dagger, \alpha, \Delta\gamma/D, K_2/K_1) = (D\xi_m(0) - E)/C$ and $(\tau\dagger\dagger)^{1/2} = C\lambda K_1/K_2\,\Delta\gamma$. $\lambda\dagger$ is the root of q_2 $(\lambda\dagger, \alpha, \Delta\lambda/D, K_2/K_1) = (D\xi_m(0) - E)/C$ and $(\tau\dagger)^{1/2} = (\xi_m(0) - E/D)/q_1$ $(\lambda\dagger, \alpha, \Delta\lambda/D)$ (see text for q_1).

subsequent to this time ($\sim\tau^{\dagger\dagger}$) the temperature for part of the region is less than the initial state and greater than the final state.

The motion of the phase boundary for model 4 is shown in Figure 15*a*. Comparison of the numerical results shows that the motion is nearly identical with that of the gutted problem for $\tau < \tau_1^{\dagger}$. The departure after that time is apparently due to the influence of the discontinuity in

$$\left.\frac{\partial\theta}{\partial\xi}\right|_{\xi=\xi_m(0)}$$

and the dominance of the long-term transient for $\tau > \tau_1^{\dagger}$.

It should be pointed out that in models 1, 2, and 3, the Stefan approximation, where applicable, appears to be nearly an exact solution. For model 4, while the Stefan approximation appears to be a reasonable one, it is not an accurate representation for θ for sizeable displacements, as can be seen from the estimate for $\xi_m(\tau^{\dagger})$ and $\xi_m(\tau^{\dagger\dagger})$.

The long-term motion may be estimated in a manner analogous to that used

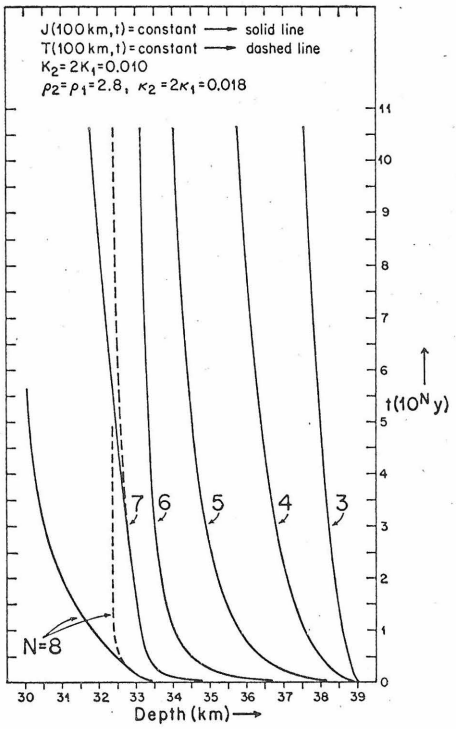

Fig. 15*a*. Models 4 and 5. The position of the phase boundary versus times, comparing the effects of constant flux or constant temperature at the lower boundary (c.f. Figure 13*b*, *c*). Note that the curves for different values of N correspond to different time scales.

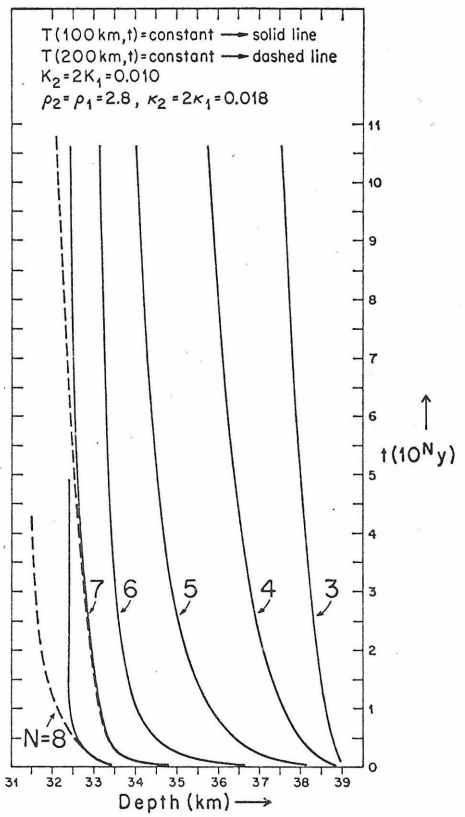

Fig. 15*b*. Models 5 and 6, illustrating the effect of the depth at which the lower boundary condition is applied. Note that the long-term motion for model 6 is intermediate to those of models 4 and 5.

in the previous cases. For a case with constant flux at the lower boundary, this yields a relaxation time

$$\tilde{\tau}_l = \frac{E}{D}\left\{\frac{C}{D} + \frac{E}{D}\left[\frac{\gamma_1}{D} + \frac{1}{2}\right]\left[1 - \frac{2\gamma_1}{\gamma_2\alpha}\right] + \frac{\gamma_1}{\gamma_2\alpha}\left[1 + \frac{\gamma_1}{D} - \frac{\gamma_2}{D}\left(1 - \frac{E}{D}\right)\right]\right\} \tag{50}$$

which is given in Table 3. As can be seen in Figure 15*a*, there is a very prominent long-term transient, as would be expected from the steady-state discussion and the magnitude of τ_l for this case.

The time τ^{**}, after which the above long-term behavior should obtain, is given by

$$\tilde{\tau}^{**} = 2(1 - E/D)^2/\alpha\pi^2 \tag{51}$$

which is analogous to equation 46. This is given in Table 3.

We now consider model 5, which is identical to model 4, except that the lower boundary condition is taken as constant temperature rather than as constant flux at the lower boundary.

The governing equations for case 5 are, of course, identical to those of case 4, except for the change in the lower boundary condition. Hence, the same criteria for the breakdown of Stefan behavior at $\tau = \tau^{\dagger}$ and $\tau = \tau^{\dagger\dagger}$ apply, and the only difference between the two cases occurs for long-term behavior governed by the lower boundary condition.

The final equilibrium position of the phase boundary for this case is given by the root of

$$(D + \gamma_1)\left(\frac{\gamma_1}{\gamma_2} - 1\right)\xi_m^2 + \left[D + \gamma_1 - \frac{\gamma_1}{\gamma_2}\eta(1, 0) - \left(\frac{\gamma_1}{\gamma_2} - 1\right)E\right]\xi_m - E = 0 \tag{52}$$

Thus for this case $\gamma_1 \neq \gamma_2$ (or $K_1 \neq K_2$), $\xi_m(\infty)$ will *not* be E/D, as in the previous cases. For this reason the Stefan approximation is not internally consistent in that $\xi_{m\,SA}$ may be less than $\xi_m(\infty)$. The formal equations of the Stefan approximation which are used for estimates of $\tau^{\dagger}$, $\tau^{\dagger\dagger}$ may be subject to more error than in the previous cases, and $\xi_{m\,SA}(\tau^{\dagger\dagger})$ may lie outside of the accessible region for ξ_m. In addition, the long-term behavior for this case may be significantly different from that of the cases where $\xi_m(\infty) = E/D$.

Construction of a quasi-steady-state temperature distribution with the correct limiting end point $\xi_m(\infty)$ yields

$$\frac{1}{(\xi_m(\tau) - \xi_m(\infty))}\frac{d\xi_m}{d\tau}$$

$$\rightarrow \frac{2\xi_m(\infty)(D + \gamma_1)\left[\frac{\gamma_1}{\gamma_2} - 1\right] - E\left[\frac{\gamma_1}{\gamma_2} - 1\right] + D + \gamma_1 - \frac{\gamma_1}{\gamma_2}\eta(1, \tau)}{\left[C + ((D+\gamma_1)\xi_m(\infty) - \frac{1}{2}E)\left(1 - \frac{\gamma_1}{\gamma_2\alpha}\right) + \frac{\gamma_1}{2\gamma_2\alpha}(D + \gamma_1 - \eta(1, 0))\right][1 - \xi_m(\infty)]\xi_m(\infty)}$$

$$= \frac{-1}{\tilde{\tau}_l} \quad \text{as} \quad \xi_m \rightarrow \xi_m(\infty) \tag{53}$$

Comparison of the actual and approximate values may be seen in Table 3.

The long-term relaxation time for this case is considerably less than that for model 4. In addition, the distance the phase boundary must move is less for this case than for model 4.

The development of the temperature distribution with time is shown in Figure 13*c*. Prior to 20×10^6 years the temperature distribution for this case is nearly identical to that for model 4 (cf. Figure 12*b*); after that time the two models diverge. Model 5 attains equilibrium fairly rapidly, in contrast to model 4 whch approaches equilibrium quite slowly.

This may also be seen in Figure 15*a*, which shows the motion of the phase boundary for both cases. The long transient for model 4 is apparent. On the other hand, in model 5, the phase boundary nearly reaches its final position before the long-term behavior becomes evident; in fact, for this case a long-term transient is essentially nonexistent in relation to the total displacement of the phase boundary. This illustrates the primary effect of the lower boundary condition on the problem. For constant temperature at the lower boundary $b(t)$, equilibrium is approached by internally redistributing the excess heat from $\xi > \xi_m$ to the region $\xi < \xi_m$, which has a heat deficit compared with the final state. In contrast, for constant flux at $b(t)$, there is no region that has a lower temperature than the final steady state; hence the excess of heat cannot be compensated for internally and must escape at the boundary $\xi = 0$, which leads to a major long-term transient.

In the preceding models the thickness of the region was 100 km and the phase boundary was originally near the center of the region. To evalute the effects of distance to the lower boundary, we have investigated model 6, in which the lower boundary is at 200 km, at which the temperature is constant.

The motion for short times will be the same as in cases 4 and 5; the only difference will be the long-term behavior and the final position of the phase boundary.

The long-term relaxation time will be given by equation 50, as it was for model 5. Note, however, that, since b_0 is different for the two models, the scale factor relating dimensionless time τ to real time t will not be the same for the two cases. As can be seen in Table 3, the relaxation time for model 6 is nearer that for model 4 (constant flux at 100 km) than that for model 5 (constant T at 100 km). The final position of the phase boundary will be intermediate between those for models 4 and 5. In the limit $b_0 \to \infty$ for the same initial steady state, the final position of the phase boundary will be E/D for either boundary condition.

The motion of the phase boundary is shown in Figure 15*b*, where it is compared with model 5. Comparison with Figure 15*a* will demonstrate that this case is intermediate between models 4 and 5.

Comparison of the effects of different boundary conditions and the depth at which they apply shows that the boundary conditions do not affect the short-term behavior; they do, however, significantly affect the long-term behavior, both in terms of the rates of movement of the phase boundary and its final position. In the consideration of a realistic geophysical problem including the thermal impedance of the material causing the pressure pulse, sedimentation and erosion

rates (particularly the latter), and isostasy, it is clear that the choice of the lower boundary condition may be primary in determining the elevation and duration of positive surface relief. The proper lower boundary condition that describes the actual geophysical conditions is not obvious to the authors.

In model 5 the pressure pulse was the maximum that could be applied without overdriving the system. To better illuminate the response when $(1/C)$ $(D\xi_m(0) - E) < 1$, model 7 was investigated. In model 7 the latent heat was taken as 30 cal/g, rather than 15 cal/g, as in model 5. Otherwise, the models are identical. The short-term behavior for this model agrees with that predicted by the Stefan approximation, as can also be seen in Table 3. As in the comparison between models 1 and 2 for the gutted problem, the greater latent heat significantly slows the phase boundary in the region of Stefan behavior. The long-term behavior is, however, little affected by the larger latent heat, as is expected, since the primary process is the redistribution of the heat of the initial temperature distribution.

All the preceding models have had the same reduced Clapeyron curve $D\xi_m - E$, which partly determined: (1) the total displacement of the phase boundary $\xi_m(0) - \xi_m(\infty)$; (2) the initial temperature at the phase boundary $D\xi_m(0) - E$; (3) the criteria τ^* and $\tau^\dagger$ for cessation of Stefan behavior; and (4) the long-term relaxation time τ_l.

As an illustration of the effect of the Clapeyron slope, model 8 was constructed such that the reduced Clapeyron slope was reduced to one-half of its value in the previous models. In order to keep $\xi_m(0)$ unchanged (for purposes of comparison with previous models), it was necessary to alter E as well. All other parameters were unchanged from model 5. The numerical and theoretical results are presented in Table 3. The agreement is as expected from previous cases. It should be noted that the short-term motion is slower than in model 5, owing to the smaller initial perturbation temperature at the phase boundary, and that the long-term transient is more prominent, owing primarily to the larger total displacement of the phase boundary for this model.

In all the models that have so far been considered, we have taken $\alpha = K_2/K_1$. Since α appears only in the field equations, whereas K_2/K_1 appears in the boundary conditions, it was considered desirable to consider a case for $\alpha \neq K_2/K_1$. This was done in model 9. A Stefan solution has been presented that approximates this model and may therefore be compared with the numerical solution. The motion of the phase boundary compared with that for model 5 is shown in Figure 16. The motion for model 9 is initially faster than that for model 5, because the smaller diffusivity of model 9 reflects a larger heat capacity ($\kappa = K/\rho c$). Thus more heat may be released into the region behind the phase boundary for the same rise in temperature as for model 5. The fact that model 9 lags behind model 5 for longer times ($t \gtrsim 7 \times 10^4$ yr) is due to the redistribution of the heat that was originally behind the phase boundary. Again this is a reflection of the greater latent heat of model 9. The approximate solutions for both short and long times are again in good agreement with the numerical results.

Convective heat transport. We have so far discussed only the most elementary cases in which we neglected convective heat transfer and the presence of heat sources. We now turn to the investigation of the effects of including convec-

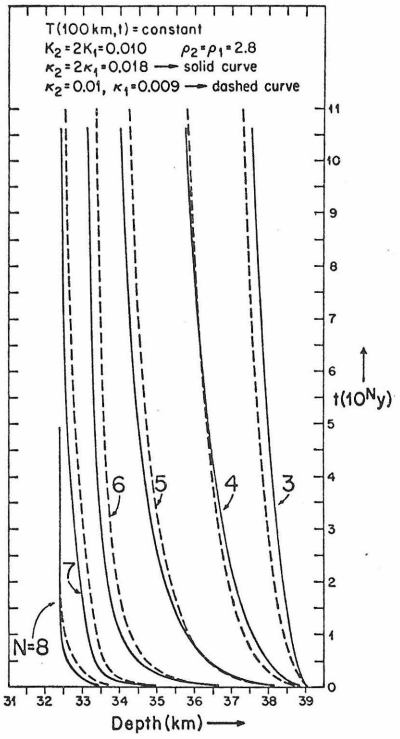

Fig. 16. Models 5 and 9. The effect of the thermal diffusivity of the lower layer on the motion of the phase boundary. Although both curves have the same endpoint, there are slight differences in the detailed motion of the phase boundary.

tive heat transfer, which is expressed by the term

$$\nu\left(\frac{\partial\theta(\xi,\tau)}{\partial\xi}+\frac{\partial\eta(\xi,0)}{\partial\xi}\right)$$

in the field equations 25 and the motion of the lower boundary $\beta(\tau)$. Thus the difference in density of the two phases will no longer be neglected, and the mass in the region $0 < \xi < \beta(\tau)$ will be conserved. In the ensuing discussion we will assume $K_2 > K_1$.

For short times less than τ^{**}, as defined in (51), the effect of the lower boundary $\beta(\tau)$ will be insignificant and we need only investigate the effect of the convective term in the field equation. Owing to the nonlinearity of the field equations with the convective term included, it is no longer possible to consider the perturbation temperature $\theta(\xi, \tau)$ separately from the initial steady state, as is indicated by the presence of the term $[\partial\eta(\xi, 0)/\partial\xi]$ in the field equations 25.

Initially the velocity of the phase boundary and the temperature gradients in the neighborhood of the phase boundary are singular, and $[\partial\theta(\xi, \tau)/\partial\xi]$ will dominate the convective term in the field equations in the neighborhood of the phase boundary. We may investigate this term by appealing once again to the Stefan approximation. A solution to the generalized Stefan problem, including convected heat, may be obtained from the form given by *Carslaw and Jaeger* [1959, p. 290]:

$$\theta_{SA}(\xi, \tau) = \frac{\theta_c(\xi_m)}{1 - \operatorname{erf}\lambda}\left[1 + \operatorname{erf}\frac{\xi - \xi_m(0)}{2\tau^{1/2}}\right]; \qquad \xi \leq \xi_m(\tau)$$

$$\theta_{SA}(\xi, \tau) = \frac{\theta_c(\xi_m)}{1 + \operatorname{erf}(\lambda\rho_1/\alpha^{1/2}\rho_2)}\left\{1 - \operatorname{erf}\left[\frac{\xi - \xi_m(0)}{2(\alpha\tau)^{1/2}} + \frac{\lambda(\rho_2 - \rho_1)}{\rho_2\alpha^{1/2}}\right]\right\} \qquad \xi \geq \xi_m(\tau)$$

$$\xi_m(0) - \xi_m(\tau) = 2\lambda(\xi_m)\tau^{1/2}$$

where λ is the root of

$$N(\lambda, \alpha, K_2/K_1, \rho_2/\rho_1) \equiv \lambda\pi^{1/2}\left\{\frac{e^{-\lambda^2}}{1 - \operatorname{erf}\lambda} + \frac{K_2}{K_1}\frac{e^{-(\lambda\rho_1/\alpha^{1/2}\rho_2)^2}}{\alpha^{1/2}[1 + \operatorname{erf}(\lambda\rho_1/\alpha^{1/2}\rho_2)]}\right\}^{-1} = \frac{\theta_c}{C}(\xi_m) \qquad (54)$$

This is an exact solution to the problem defined in (25) and (26) if (1) $\sigma_2 = \sigma_1$; (2) $[\partial\eta(\xi, 0)/\partial\xi] = 0$; (3) $\theta(\xi_m, \tau) =$ constant; and (4) the region is infinite. Owing to the initial singularity in $d\xi_m/d\tau$, condition 2 is nearly satisfied near the phase boundary for short times for all cases.

The function $N(\lambda, \alpha, K_2/K_1, \rho_2/\rho_1)$ is shown in Figure 7 and compared with $N(\lambda, \alpha, K_2/K_1, 1)$ for equivalent arguments. It is evident from the similarity of the two curves that the term $\nu(\partial\theta/\partial\xi)$ in the field equation has little effect on the velocity or position of the phase boundary for a 20% difference in density. In region 1, at a given time, the effect of convected heat does not change the functional form of the temperature distribution but only the magnitude of the perturbation, because of the change in the value of the root of $N(\lambda, \alpha, K_2/K_1, \rho_2/\rho_1)$ as compared with $N(\lambda, \alpha, K_2/K_1, 1)$. In region 2 the spatial temperature distribution will be altered owing both to the scaling due to the change in the characteristic root and to the motion of colder material toward the phase boundary. This will tend to decrease the width of the temperature peak to the right of the phase boundary and corresponds to a translation of the temperature distribution by $[2\lambda(\rho_2 - \rho_1)/\rho_2]\,\tau^{1/2}$.

As has been stated, the singularity in $[\partial\theta(\xi, \tau)]/\partial\xi$ at $\tau = 0$ makes $[\partial\eta(\xi, 0)]/\partial\xi$ or any other finite term negligible in the immediate neighborhood of the phase boundary for the initial motion. At points somewhat removed from the immediate vicinity of the phase boundary, however, the terms $[\partial\theta(\xi, \tau)]/\partial\xi$ and $[\partial\eta(\xi, 0)]/\partial\xi$ may cancel for some given points in space and time. As seen from the Stefan problem, such 'accidental' cancellations should not significantly affect the actual solution to the problem, since the effect of convective heat transport is small for the cases considered here.

At distances from the phase boundary where the temperature is little affected by the heat released at the phase boundary, $[\partial\eta(\xi, 0)]/\partial\xi$ will become the dominant term in the field equation. In the limiting case at point ξ_i, where the temperature is invariant

$$\left.\frac{D\eta(\xi, \tau)}{D\tau}\right|_{\xi=\xi_i} = 0$$

and

$$\left.\frac{[\partial\theta(\xi, \tau)]/\partial\tau}{\nu\{[\partial\eta(\xi, 0)]/\partial\xi + [\partial\theta(\xi, \tau)]/\partial\xi\}}\right|_{\xi=\xi_i} = -1$$

will apply. Thus $[\partial^2\theta(\xi, \tau)]/\partial\xi^2 = 0$ and the time dependence of the temperature is completely dominated by the convective term. This will apply at the lower boundary $\xi_l = \beta(\tau)$, if $\eta(\beta(\tau), \tau) =$ constant. If the lower boundary condition is constant flux, then

$$\frac{\partial\theta(\beta(\tau), \tau)}{\partial\xi} = \frac{\partial\eta(\beta(0), 0)}{\partial\xi} - \frac{\partial\eta(\beta(\tau), 0)}{\partial\xi}$$

If there are no sources, it follows that $[\partial\theta(\beta(\tau),\tau)]/\partial\xi = 0$; hence again the term $[\partial\eta(\xi, 0)]/\partial\xi$ completely dominates the convective term. In these cases the changes in temperature are totally due to the translation of the initial temperature distribution.

The principal effect of the motion of the lower boundary is its effect on the final equilibrium position of the phase boundary and the final temperature distribution; even this, however, is slight for geophysically reasonable models.

From the preceding discussion it can be seen that the neglect of the convective heat transport results in two effects: (1) the temperature distribution in the immediate neighborhood of the phase boundary will be altered and the motion of the phase boundary will be too slow; (2) the total movement of the phase boundary, $\xi_m(0) - \xi_m(\infty)$, will be slightly overestimated and the final temperature will be too low. The magnitude of these errors will, of course, depend on the values of the parameters used. For the geophysical situation considered in this paper, the errors appear to be unimportant, especially considering the uncertainties in the lower boundary condition and the values of the parameters.

It may be noted that, if the nonlinear terms in the field equation are neglected, but the lower boundary $\beta(\tau)$ is moved so that the matter conservation equations are satisfied, and the correct boundary conditions are applied at that point, then the system will approach the proper final equilibrium state. This approximation effectively generates, however, an anomalous transient in the temperature distribution corresponding to a heat source or sink depending on the sign of the velocity. This may be understood by referring to Figure 17*a*. In the region between $M(t)$ and $b(t)$, the nonzero value of Θ is primarily due to convected heat. If this means of heat transport is neglected, the final temperature distribution in this region will have to be attained solely by conduction, which will generate a long-term transient.

In order to show the effects discussed in the preceding paragraphs, numerical solutions were obtained. In both models 10 and 11 the parameters are identical with those of model 9. In model 10 the lower boundary $\beta(\tau)$ was moved to satisfy mass conservation in the region $0 \leq \xi \leq \beta(\tau)$, and the temperature at $\beta(\tau)$ was kept constant. The convective term $\nu\{[\partial\theta(\xi, \tau)]/\partial\xi + [\partial\eta(\xi, 0)]/\partial\xi\}$ in the field equation was *neglected*. Model 11 is identical to model 10 except that the convective heat transport is *not* neglected. The position of the phase boundary with time for each case is shown in Figure 18. It should be noted that both cases have the same final equilibrium states.

The temperature distributions in the vicinity of the phase boundary at a relatively short time are shown in Figure 17*b* for both cases. It may be seen that the phase boundary for the model including the convective term has traveled slightly

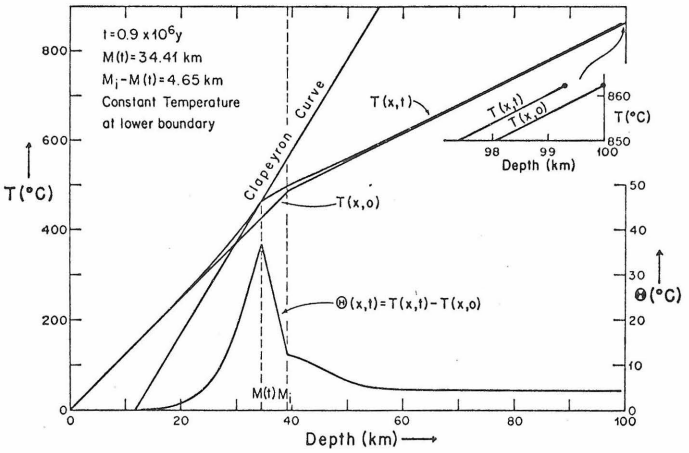

Fig. 17*a*. Model 11. Initial temperature and temperature after 0.9 m.y., showing the effect of convective heat transport. The upper detail shows the effects due to the convective heat transport. The nonzero value of Θ for depths greater than 60 km is almost entirely due to the translation of the initial steady state in this region.

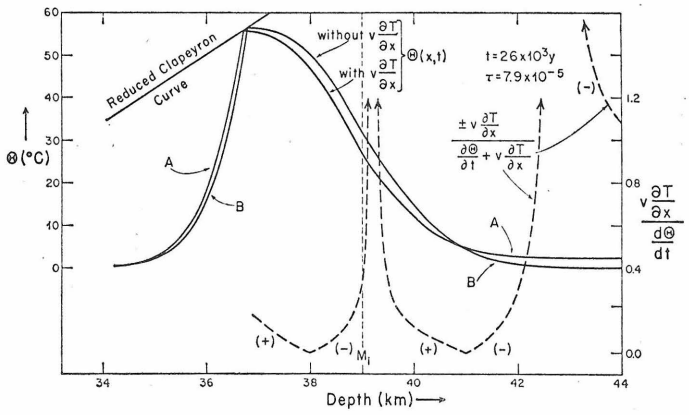

Fig. 17*b*. Curve *A* shows the temperature in the neighborhood of the phase boundary for model 11 for short times. Curve *B* is for model 10, in which convective heat has been neglected but the lower boundary moved to conserve mass. The dashed curve shows the ratio of the convective term $V\ \partial T/\partial x$ to the total time derivative of the temperature $D\Theta/Dt = \partial\theta/\partial t + V\ (\partial T/\partial x)$. This ratio is less than 0.2 near the phase boundary except for an isolated point and becomes dominant in the region approaching the lower boundary. The + and — signs correspond to branches of the dashed curve where $V\ (\partial T/\partial x)/(D\Theta/Dt)$ is positive or negative, respectively.

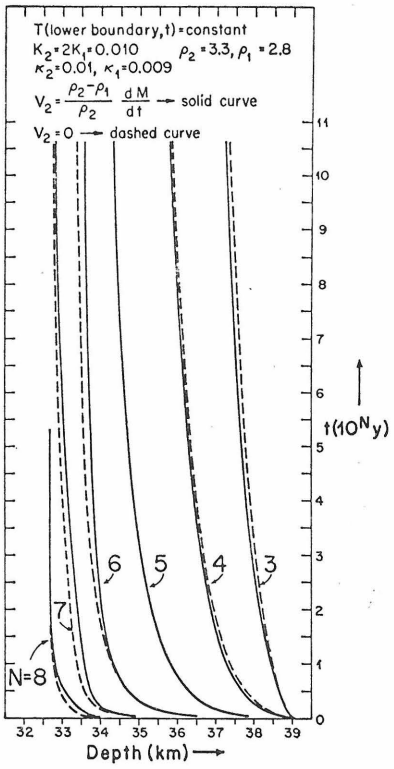

Fig. 18. Effect of convective heat on the motion of the phase boundary. In model 10 (dashed line), convective heat is neglected but mass is conserved by moving the lower boundary. In model 11 convective heat is not neglected. The difference between the two curves for long times is due to the anomalous long-term transient that results from the neglect of convective heat in model 10. In general the difference between the two curves is small.

farther than for the model neglecting the convective term. In addition, the temperature immediately behind the phase boundary is lower for the former case, owing to the motion of 'colder' material toward the phase boundary. Farther behind the phase boundary, the temperature for the case with convective heat transport is greater than for the other case. This is due to the term $\nu[\partial\eta(\xi, 0)]/\partial\xi$ and is a result of the translation of the whole region $\xi_m \leq \xi \leq \beta$ toward the phase boundary.

Also shown in Figure 17*b* is the ratio of the convective term $V\ (\partial T/\partial x)$ to the total time derivative $D\Theta/Dt = (\partial\Theta/\partial t) + V\ (\partial T/\partial x)$ for model 10. Since the velocity vanishes identically in front of the phase boundary, this ratio also vanishes. Immediately behind the phase boundary the convective term is up to twenty per cent of $D\Theta/Dt$. The singularities in the ratio at depths of 39.2 and 42.3 km are due to the vanishing of $D\Theta/Dt$ and do not have a noticeable effect on the temperatures at these points. At depths greater than 43 km the neglected convective term would account for all the temperature, as is seen by comparing the temperature for model 11 in this region. At the point $\beta(\tau)$ (which may be seen in Figure 17*a*), the ratio is -1, as required by the invariance of the temperature at the lower boundary.

Thermal blanketing and reversals. In all the preceding discussion we have assumed that the pressure pulse ΔP has no thermal impedance. As discussed in the section on static behavior, the initial effect of a thermal blanket is insignifi-

cant, and the phase boundary will rise in response to the pressure pulse and move toward the position M_f as determined for no thermal impedance. However, the upper boundary conditions must finally dominate and cause the phase boundary to move toward the true equilibrium position, which may involve a reversal of motion. The time and position at which such a reversal occurs is of deep significance, since these factors determine the depth of maximum subsidence and the time at which the motion of the surface will reverse and uplift will begin. The time and position of reversal in conjunction with erosion rates, will govern the height and duration of positive relief.

Although it is not the purpose of this paper to discuss the detailed geophysical problem, including the effects of sedimentation and erosion rates, we can point out the basic effects that will result and the characteristic constants of the motion. We will present a discussion of the more complete geophysical problem in another paper.

Let us consider a sediment layer of thickness $s = \Delta P/\rho g$ at zero temperature deposited instantaneously on the surface $x = 0$. The top of the sediments will then be at $x = -s$. The temperature distribution immediately after the deposition of the sediments will be

$$T(x, 0) = 0 \qquad -s \leq x \leq 0$$

$$T(x, 0) = \frac{J(0, 0)}{K_1} x \qquad 0 \leq x \leq M(0)$$

$$T(x, 0) = \frac{J(0, 0)}{K_2} (x - M(0)) + \frac{J(0, 0)}{K_1} M(0) \qquad M(0) \leq x \leq b(0)$$

Subsequent to deposition, the temperature of the sediments and the material beneath the sediments will rise because of the flux from beneath, which is comprised of the initial flux and the flux due to the latent heat released by the phase change. The temperature gradient in the region $0 \leq x \leq M(t)$ will therefore be decreased, which will slow the motion of the phase boundary.

For short times the effect of the thermal blanketing will be small in the region of the phase boundary, and the initial motion of the phase boundary will be essentially Stefan-like in behavior as shown in Figure 19*a*. Eventually, however, the temperature distribution in the region $-s \leq x \leq M(t)$ will become substantially different from that for Stefan behavior, owing to the effects of the boundaries, which differ from those discussed in the previous sections because of the thermal blanketing caused by the sediments between $-s \leq x \leq 0$.

We may estimate when the effects of the thermal blanketing will become significant by considering the superposition of the solution to the thermal blanketing alone superposed on the solution for Stefan behavior.

As the problem is intrinsically nonlinear, this approach is not exact. As before, however, we assume that a good approximation for ξ_m is obtained if the approximation for θ is a solution to the field equations, satisfies the initial conditions satisfies the boundary condition at ξ_m, and approximately satisfies the other boundary conditions. We will first formulate the problem exactly and then obtain approximations for θ.

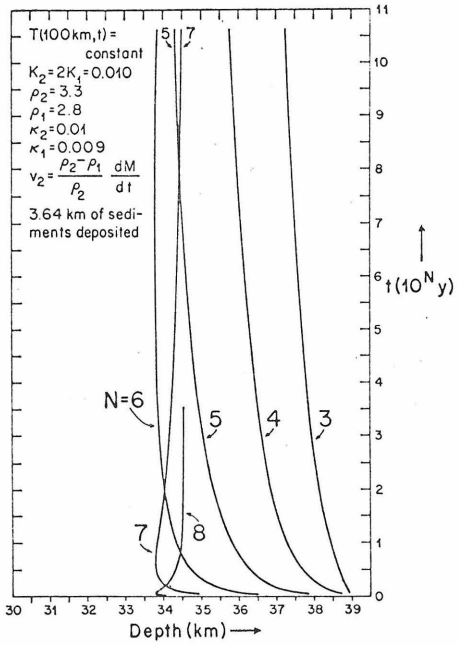

Fig. 19*a*. The motion of the phase boundary for model 13 in which sediments have been instantaneously placed on the surface at time $= 0$. The effect of the sediments is not apparent much before the motion reverses direction at 7×10^6 years, as can be seen by comparison with model 11.

In terms of the perturbation temperature θ, the problem for the thermal blanketing may conveniently be formulated by defining

$$\eta(\xi, 0) = \gamma_1 \xi \qquad \xi_s \leq \xi \leq 0; \qquad \xi_s \equiv -s/b_0$$

This extends the initial temperature distribution into the region where the sediments will be deposited such that $\partial\eta(\xi, 0)/\partial\xi$ is continuous, thus assuring that $\partial\theta(\xi, \tau)/\partial\xi$ will be continuous in the region $\xi_s \leq \xi \leq \xi_m(\tau)$ for $\tau > 0$.

The initial perturbation temperature distribution is thus

$$\begin{aligned} \theta(\xi, 0) &= -\gamma_1 \xi \qquad && \xi_s \leq \xi \leq 0 \\ \theta(\xi, 0) &= 0 \qquad && 0 \leq \xi \leq \beta(0), \quad \xi \neq \xi_m(0) \\ \theta(\xi_m(0), 0) &= \theta_c(\xi_m(0)) \end{aligned} \tag{55}$$

The boundary condition at the surface becomes $\theta(\xi_s, \tau) = -\gamma_1 \xi_s$. This initial state may be seen in Figure 19*b*.

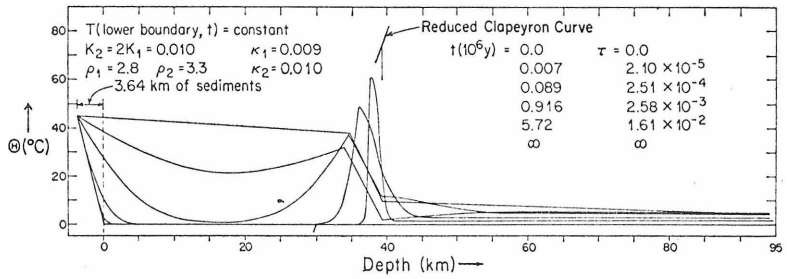

Fig. 19*b*. Perturbation temperature profiles for model 13. The sediments initially have the perturbation temperature shown to the left of $x = 0$. The phase boundary reverses its motion at $\tau = 0.0192$, just after the time of the second to last profile. The last profile shows the final steady state.

We will here consider the case where ξ_s is small relative to ξ_m. If we then neglect some of the heat initially in the sediments, i.e. $\theta(\xi, 0) = -\gamma_1\xi \cong 0$, $\xi_s < \xi \leq 0$ then

$$\begin{aligned} \theta(\xi_s, 0) &= -\gamma_1\xi_s \\ \theta(\xi, 0) &= 0 \qquad\qquad \xi_s \leq \xi \leq \beta(0), \quad \xi \neq \xi_m(0) \\ \theta(\xi_m(0), 0) &= \theta_c(\xi_m(0)) \end{aligned}$$

an approximate solution for short times will be given by [*Carslaw and Jaeger*, 1959, p. 310]

$$\tilde{\theta}_R(\xi, \tau) \equiv \tilde{\theta}_{SA}(\xi, \tau) + \tilde{\theta}_B(\xi, \tau)$$

$\tilde{\theta}_B$ is the solution for a slab of thickness $\xi_m - \xi_s$, initially at zero temperature, whose boundaries at ξ_s and ξ_m are maintained at temperatures of $-\gamma_1\xi_s$ and 0, respectively. Thus

$$\tilde{\theta}_B(\xi, \tau) = \frac{\gamma_1 s}{b_0} \sum_{n=0}^{\infty} \left\{ \operatorname{erfc}\left[\frac{(2n+1)(\xi_m - \xi_s) - \xi_m + \xi}{2\tau^{1/2}}\right] - \operatorname{erfc}\left[\frac{(2n+1)(\xi_m - \xi_s) + \xi_m - \xi}{2\tau^{1/2}}\right]\right\}$$

for $\xi_s \leq \xi \leq \xi_m(\tau)$ and

$$\tilde{\theta}_B(\xi, \tau) = 0$$

for $\xi_m(\tau) \leq \xi \leq \beta(\tau)$.

$\tilde{\theta}_B$ satisfies the initial condition $\tilde{\theta}_B = 0$ everywhere except at $\xi = \xi_s$, and $\tilde{\theta}_B(\xi_s, \tau) = -\gamma\xi_s$. Hence $\tilde{\theta}_R = \tilde{\theta}_B + \tilde{\theta}_{SA}$ satisfies the initial conditions and the boundary condition $\tilde{\theta}_R(\xi_m, \tau) = \tilde{\theta}_c(\xi_m)$. The boundary condition $\theta(\xi_s, \tau) = -\gamma_1\xi_s$ is in error by the amount $\tilde{\theta}_{SA}(\xi_s, \tau)$ and that at $\beta(\tau)$ is in error by $\tilde{\theta}_{SA}(\beta(\tau), \tau)$.

Inserting $\tilde{\theta}_R$ into the condition at the moving boundary $\xi_m(\tau)$ yields

$$-C\frac{d\xi_m}{d\tau} \approx Q(\xi_m, \lambda) \equiv \frac{1}{\pi^{1/2}\tau^{1/2}}\left\{\frac{\theta_c \exp(-\lambda^2)}{1 - \operatorname{erf}\lambda} + \frac{\gamma_1\theta_c \exp(-\lambda^2/\alpha)}{\gamma_2(1 + \operatorname{erf}\lambda/\alpha^{1/2})} + 2\gamma_1\xi_s \sum_{n=0}^{\infty} \exp\left[-\frac{(2n+1)^2(\xi_m - \xi_s)^2}{4\tau}\right]\right\} \tag{56}$$

Setting $\lambda = [\xi_m(0) - \xi_m(\tau)]/2\tau^{1/2}$ and $\theta_c = D\xi_m - E$ thus results in a first-order differential equation for $\xi_m(\tau)$. This first-order equation may be integrated numerically to obtain $\xi_m(\tau)$. The time at which the phase boundary reverses motion is defined as τ_R and for this approximation $\tilde{\tau}_R$ may be determined by the condition $-C\, d\xi_m/d\tau = Q = 0$. Since $\tilde{\tau}_R$ is obtained by a simple integration, the effectiveness of this method for estimating $\tilde{\tau}_R$ is of considerable importance.

In the above approximation, $\tilde{\tau}_R$ is a root of $Q(\xi_m, \lambda) = 0$, which defines a curve in the (ξ_m, λ) plane. Thus the intersection of a curve $\lambda(\xi_m)$ with $Q = 0$ defines $(d\xi_m/d\tau) = 0$ for the approximation of $\lambda(\xi_m)$ used. It would be useful to obtain an analytic expression for τ_R in order to gain some insight into the dependence of τ_R on the other parameters of the system. Insofar as the position of the phase

boundary as a function of time prior to reversal does not deviate greatly from the Stefan approximation, we may estimate λ by use of the characteristic equation (54) $N(\lambda, \alpha, K_2/K_1, \rho_2/\rho_1) = \theta_c(\xi_m)/C$ and $Q = 0$, resulting in an approximation of τ_R. It should be noted that this approximation is internally inconsistent.

For the case for small λ, $N \approx [\pi^{1/2}\lambda/(1 + K_2/K_1)]$, and using (35) and (56), in which only the first term in the infinite series is retained, we obtain the approximate relationship

$$\tau_R \cong \tilde{\tau}_{R_1} \equiv \frac{(\xi_m - \xi_s)^2}{4 \log [-2\gamma_1\xi_s/C(\pi)^{1/2}\lambda]} \tag{57}$$

$$\tilde{\tau}_{R_1} = \frac{\left\{\left[\dfrac{C(\pi)^{1/2}}{D[1 + (\gamma_1/\gamma_2)]}\xi_m(0) + 2(E/D)\tau_R{}^{1/2}\right] \Big/ \left(\dfrac{C(\pi)^{1/2}}{D[1 + (\gamma_1/\gamma_2)]} + 2\tau_R{}^{1/2}\right) - \xi_s\right\}^2}{4 \log \left\{\dfrac{-2\gamma_1\xi_s\left[\dfrac{C(\pi)^{1/2}}{D[1 + (\gamma_1/\gamma_2)]} + 2\tau_R{}^{1/2}\right]}{C(\pi)^{1/2}[\xi_m(0) - E/D]}\right\}} \tag{58}$$

For finite positive values of τ, we must then have $\lambda \leq -2\gamma_1\xi_s/[C(\pi)^{1/2}]$, which implies that $\theta_c \leq -\gamma_1\xi_s 2/(1 + K_2/K_1)$. For the case when $K_2 = K_1$ this simply states that the perturbation temperature at the phase boundary at the time of reversal must be less than $-\gamma_1\xi_s$, which is the perturbation temperature at the top of the sediments. The transcendental equation (58) may be solved graphically for τ_R.

Equation 58 may be too coarse an approximation, since the intersection of $Q(\xi_m, \lambda) = 0$ with $\lambda(\xi_m)$ may be very sensitive to the trajectory $\lambda(\xi_m)$. Since the determination of $(\xi_m(\tau_R), \tau_R)$ is the most subtle of the characteristics of the motion so far discussed, it appears desirable to use the set of equations most consistent with the actual problem and to integrate equation 56 directly. Nevertheless, equation 58 should not be in serious error, since it depends only logarithmically on the value of λ.

Two models that include the effects of thermal blanketing were studied, and numerical solutions were found for θ, ξ_m by solving equations 25 and 26 with the initial and boundary conditions 55. Models 12 and 13 have 3.64 km of sediments deposited on the surface, and the lower boundary condition was fixed at a depth of 95 km beneath the bottom of the sediments. Otherwise models 12 and 13 are identical to models 2 and 11, respectively.

The temperature distributions for model 13 at selected times are shown in Figure 19*b*. The time of reversal is $\tau_R = 0.019$. The temperature curves show that as the time approaches τ_R, the temperature everywhere in the region between the sediment surface and the phase boundary has risen significantly and at τ_R the temperature distribution is dominated by the effect of the sediments. Model 13 takes into account different properties of the phases and the motion of the lower boundary. Nevertheless, the essential behavior is quite similar for both models 12 and 13.

TABLE 4. Actual and Predicted Reversal Times of the Phase Boundary

Model	12	13
τ_R	0.0219	0.0192
$\xi_m(\tau_r)$	0.3175	0.3379
$\tilde{\tau}_{R_1}$	0.0278	0.0284
$\tilde{\xi}_m(\tilde{\tau}_{R_1})$	0.3117	0.3170
$\tilde{\tau}_{R_2}$	0.0162	0.0151
$\tilde{\xi}_m(\tilde{\tau}_{R_2})$	0.3022	0.3010

Estimates for τ_R were obtained from equation 58 ($\tilde{\tau}_{R_1}$), and by numerically integrating equation 56 ($\tilde{\tau}_{R_2}$) to find the point $Q = 0$. These values are given in Table 4, as are the corresponding ξ_m values from equation 34*a*. The agreement of the $\tilde{\tau}_R$ with the actual value of τ_R is quite good. For either model, $\tilde{\tau}_{R_1}$ overestimates and $\tilde{\tau}_{R_2}$ underestimates τ_R. The agreement between $\tilde{\xi}_m(\tilde{\tau}_R)$ and $\xi_m(\tau_R)$ is not quite so good, although it is satisfactory. It therefore appears that the theoretical considerations provide a good estimate for the time and position of reversal, as well as a simple functional expression for this time in terms of the initial state of the system for the case of impulsive loading.

Effects of (radioactive) heat sources. The presence of sources enters the problem in two distinct ways: (1) as a term $\alpha(\sigma_1 - \sigma_2)$ in the field equations and (2) in the determination of the initial steady state $\theta(\xi, 0)$ and the final equilibrium state.

The source terms appear explicitely as the difference $\alpha(\sigma_2 - \sigma_1)$ in the field equation in region 3 but are not present in either region 1 or 2. They appear in region 3 only because of the change in spatial concentration due to the density change across the phase boundary, and they would vanish identically if $\rho_2/K_2 = \rho_1/K_1$. This region in which the source term appears comprises only the space between the phase boundary and its initial position, and, therefore, for the initial motion the region is extremely limited. However, owing to the source term, the final equilibrium value of $\partial^2\theta/\partial\xi^2$ will be nonzero, which will result in a curvature in θ in region 3 as compared with the source-free case where $\theta(\xi, \infty)$ is linear in every region. This term thus generates a transient in θ in region 3, owing to the difference between the initial state $\theta(\xi, 0) = 0$ and the curved final state, where $[\partial^2\theta(\xi, \infty)]/\partial\xi^2 = \sigma_1 - \sigma_2$. Insofar as $\alpha(\sigma_2 - \sigma_1)$ is small, as would occur for most geophysical considerations, it is to be expected that the source terms are of little significance in the field equations.

The initial steady state enters the field equations in the term $\nu\,[\partial\eta(\xi, 0)/\partial\xi]$ for convective heat. The effect of sources in making $[\partial\eta(\xi, 0)/\partial\xi]$ a linear function of ξ rather than a constant can be no greater than the effect that the term had in the case with no sources. As pointed out earlier, this term primarily compensates for the mass transport with respect to the fixed spatial coordinates and has only a minor effect.

In the boundary conditions 26*c* and 26*d*, the terms $[\partial\eta(\xi, 0)/\partial\xi]$ appear as the break in slope of $\eta(\xi, 0)$ at the location of the phase boundary due to the

change of conductivity. The effect of these terms will be the same as in the case with no sources. Some minor differences will occur, since in the source-free case the exact magnitude of this term is a constant independent of $\xi_m(0)$. However, in the case with sources, since $\eta(\xi, 0)$ is a quadratic function, the gradient will depend on the position of the phase boundary.

In the models with no sources, the reduced Clapeyron curve $\theta_c(\xi) = \eta_c(\xi) - \eta(\xi, 0)$ was a linear function, $\theta_c(\xi) = D\xi - E$, since both $\eta_c(\xi)$ and $\eta(\xi, 0)$ were linear. When sources are present, however, $\eta(\xi, 0)$ is no longer a linear function; hence $\theta_c(\xi)$ will also be a quadratic function of ξ. This may be seen in Figure 20*a*. This figure compares the initial temperature $T(x, 0)$ and Clapeyron curve $T_c(x)$ for a model with sources (model 14), with $\hat{T}(x, 0)$ and $\hat{T}_c(x)$, for a no-source model (model 11), which is used to approximate the model with sources. The Clapeyron slopes $[dT_c(x)/dx] = d\hat{T}_c/dx \equiv G\rho_1 g$ are equal for both cases, as are the initial positions and temperature gradients at the phase boundary. Making these values coincide and utilizing equations 5 to construct the source-free model required a new value of F and $J(0, 0) \equiv J_i$ in the approximation. Thus $\hat{T}_c(0)$ is less than $T_c(0)$ and $\hat{J}(0, 0)$ is less than $J(0, 0)$. In both cases the application of a pressure pulse ΔP shifts the Clapeyron curve a distance $\Delta P/\rho g$ to the left, and the temperature at the phase boundary increases by the same amount $G\ \Delta P$ for both cases. The reduced Clapeyron curves $\Theta_c(x)$ and $\hat{\Theta}_c(x)$ after application of the pressure pulse are shown on the right of Figure 20*a*. They have the same value and slope at the initial location of the phase boundary $x = M_i$. The initial motion of the phase boundary should thus be the same for both models. Owing to its curvature, $\Theta_c(x)$ diverges from $\hat{\Theta}_c(x)$ for $x \neq M_i$, and the former intercepts the x axis at a smaller value of x. Thus, for longer times the source model will depart slightly from the other, mainly owing to the different final equilibrium position of the phase boundary.

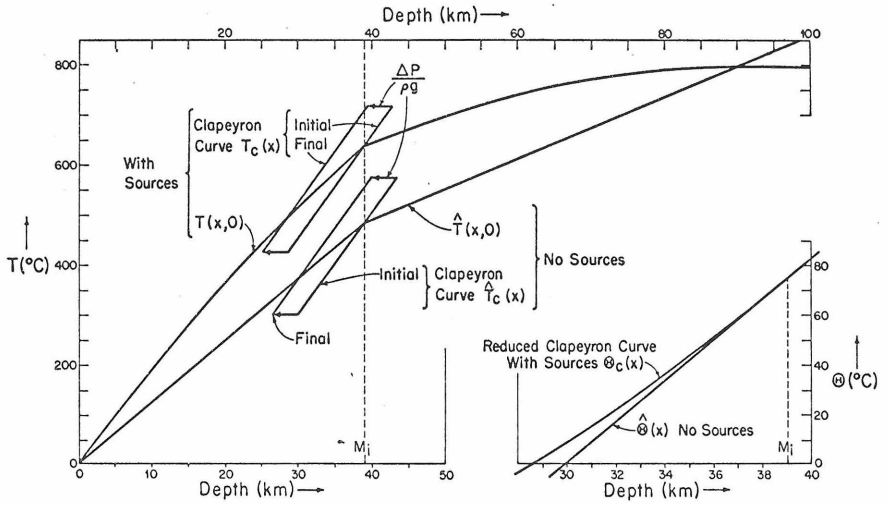

Fig. 20*a*. Initial states for a model with moderate sources and an approximation to it without sources. The shift of the Clapeyron curve is shown. The reduced Clapeyron curve for each model is at lower right. The reduced Clapeyron slopes at the initial location of the phase boundary M_i are the same for both models.

The magnitude of this difference will depend on the curvature of $\Theta(x)$, hence on the magnitude of the sources. For larger sources than those shown here, the final position of the phase boundary could be substantially different for the two models and there would be a larger long-term displacement of the phase boundary for the model with sources. The effect of the curvature per se should be quite small, and, if proper account is taken of the initial and final positions of the phase boundary, the motion of the phase boundaries for the two cases should not differ significantly.

Lastly, it should be noted that the final perturbation temperature distribution will be composed of straight-line segments except for the region between $\xi_m(0)$ and $\xi_m(\infty)$, and that only in this region will the sources directly affect the temperature distribution. Thus the dependence of the solution on the source distribution is extremely limited, and we may therefore expect to be able to represent quite adequately a model with sources by a suitable model with no sources.

In order to compare a model with sources with a 'no-source' approximation to it, a numerical solution was obtained for model 14, which has a source concentration of 3.6×10^{-14} cal/g sec in each phase. These heat sources, distributed through 100 km, are able to account for all the surface heat flux of 1.0 μcal/cm^2 sec, as may be seen in Figure 20*a*. Model 11 is a 'no-source' approximation to model 14 in the sense that both have (1) the same initial position of the phase boundary M_i; (2) the same Clapeyron slope G; (3) the same reduced Clapeyron slope at M_i; and (4) equal initial pressure pulses applied to them, and all other material properties the same. This has been achieved by adjusting the zero intercept of the Clapeyron curve F, and the initial surface heat flux $J(0, 0)$. The resultant values of the parameters are given in Table 1 and 2, and the initial states of both models may be seen in Figure 20*a*.

The motion of the phase boundary for each case is shown in Figure 20*b*. For the first half of the motion, the difference between the two cases is insignificant. Since the final position of the phase boundary is different for each model, the motion for model 14 departs slightly from that for model 11 for longer times. Nevertheless, the behavior of the model with sources is entirely predictable from the model without sources, and we conclude that the effect of sources is insignificant for such cases, except in that they partly determine the final position of the phase boundary.

Since the source concentration in model 14 was not particularly high, a numerical solution was obtained for model 15 in which the source concentration was 1.25×10^{-13} cal/g sec. These sources were distributed only in the upper 40 km of the crust, which was underlain by a layer with no sources but with thermal properties identical to those of the high-density phase. The resultant nonradiogenic heat flux was only 3% of the surface flux of 1.5 μcal/cm^2 sec. The initial state for this model is shown in Figure 21*a*.

The first curve in Figure 21*b* shows the final perturbation temperature for model 15 and illustrates the primary effects of the sources. The curve is not linear in the region between the initial position of the phase boundary M_i and the final position M_f. In addition, the discontinuities in $\partial\Theta/\partial x$ at M_i and M_f are not equal in magnitude, as they would be for a case without sources. The result is

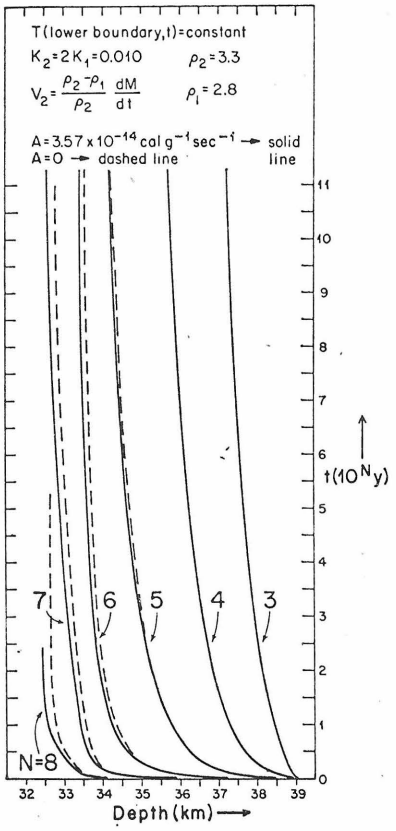

Fig. 20*b*. Motion of the phase boundary for models shown in Figure 20*a* (models 14 and 11). The difference which begins to appear at $t > 3 \times 10^5$ years is due to the different values of $M(\infty)$ for each model (cf. Θ_c in 20*a*). Apart from the difference, the two curves are almost identical.

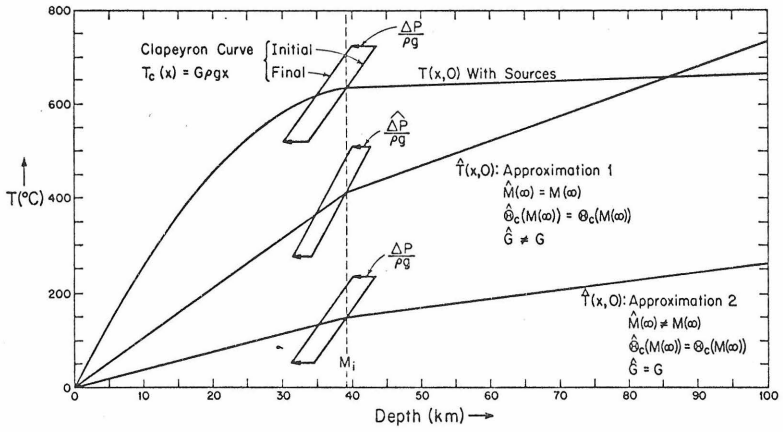

Fig. 21*a*. Initial states for a high-source model (model 15) and two no-source approximations (model 16 and 17). Model 15 has no sources below $x = 40$ km (cf. Figure 22).

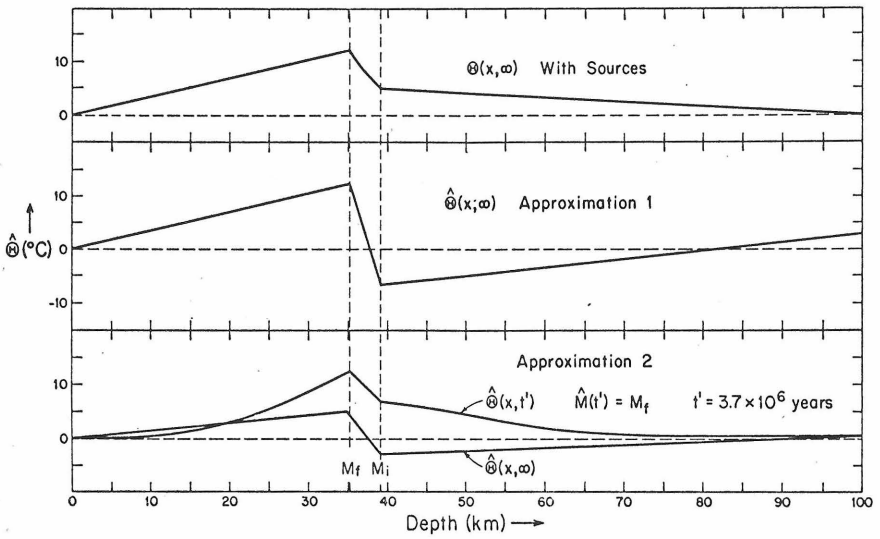

Fig. 21*b*. Final perturbation temperatures for models 15, 16, and 17. Note that $\hat{\Theta}(x, t')$ for approximation 2 comes nearest to $\hat{\Theta}(x, \infty)$ for model 15 (with sources), cf. Figure 22.

that the temperature of the final state is everywhere greater than that of the initial state. This is in marked contrast with the models without sources investigated earlier. We may expect that the result of this will be a limitation of any long-term transients in the motion. The short-term motion should remain unaffected, however, for the same reasons given for model 14.

Model 15 was approximated by models without sources in a manner analogous to the method used previously. In general, in constructing a no-source approximation, certain parameters are adjusted to make certain characteristics of the approximation coincide with those of the model being approximated. For our purpose, we wished to make the following values the same for both models: (1) the initial position of the phase boundary M_i; (2) the final position of the phase boundary M_f; (3) the initial perturbation temperature at the phase boundary $\Theta(M_i, 0)$; and (4) the final perturbation temperature at the phase boundary $\Theta(M_f, \infty)$. This was done by adjusting the following parameters in equations 5, 7, and 26*d*: (1) the initial surface flux $J(0, 0)$; (2) the zero intercept of the Clapeyron curve F; (3) the Clapeyron slope G; and (4) the pressure pulse ΔP. This resulted in model 16, or approximation 1. The initial and final states are given in Figure 21, where it may be seen that the final state differs considerably from that for model 15 in the region behind the phase boundary.

The motion of the phase boundary for each case is shown in Figure 22. Approximation 1 and the model with sources have the same final position for the phase boundary. As can be seen in Figure 21*b*, approximation 1 has a much more prominent long-term transient; hence the phase boundary approaches its final position much more slowly and lags considerably behind the phase boundary of the model with sources. The reason for this lag is that in constructing the approximation we have changed the initial temperature gradient in the vicinity

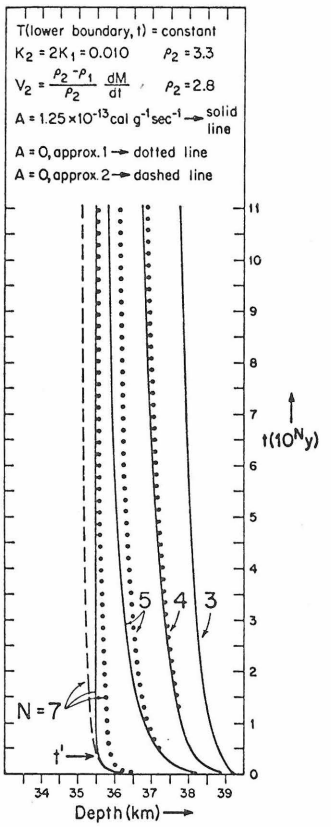

Fig. 22. Motion of the phase boundary for models 15, 16, and 17. Note that the curve for $N = 6$ has been omitted for clarity. Approximation 2 (model 17) is indistinguishable from model 15 for $t < t' = 3.7 \times 10^0$ years (cf. Figure 21).

of the phase boundary, which is obvious in Figure 21*a*. However, as was seen in the section on unmatched thermal constants, the initial temperature gradient enters the dynamic problem through the terms in $\partial\eta/\partial\xi$ in (26*c*) and (26*d*) and results in a slowing of the motion of the phase boundary, which becomes apparent for times near $\tau^\dagger$ and dominant for times near $\tau^{\dagger\dagger}$. The slower motion of model 16 is primarily due to the effect of the larger temperature gradient near the phase boundary for this source-free model in comparison to the high-source model. The appearance of this effect by relatively short times indicates that attempts to approximate the long-term motion (in particular the final position of the phase boundary) may seriously affect the short-term motion.

To better approximate the short-term motion, a second no-source approximation, model 17, was constructed in a manner similar to that used to construct model 14. The only difference in the two methods of approximation is that, whereas the Clapeyron curve of model 11 matches the slope of the reduced Clapeyron curve of model 14 at M_i, model 17 has a reduced Clapeyron slope which is intermediate to the reduced Clapeyron slope of model 15 at points M_i and M_f. $J(0, 0)$ and F were adjusted to make the reduced Clapeyron curves for this model and model 15 coincide at M_i and M_f, as determined from model 15. The Clapeyron slope, pressure pulse and initial position of the phase boundary are the same for both models; only the final positions of the phase boundary and

the curvatures of the reduced Clapeyron curves are different. As can be seen in Figure 21*a*, this approximation (approximation 2) is more similar to model 15 in the vicinity of the phase boundary than was approximation 1. Figure 22 shows that this model approximates the motion of the phase boundary extremely well over nearly the entire displacement for model 15. At $t = t'$, the approximation has reached the final position of the phase boundary for model 15, and at this point the two models have the same perturbation temperature at the phase boundary. The temperature distribution at this time may be seen in Figure 21*a*, where its similarity with the final distribution for model 15 is apparent. In contrast, the final distributions for both approximations differ considerably from that for model 15, although approximation 2 appears to be the better one.

These examples indicate that we cannot expect all the aspects of a model with sources to be represented by a no-source model. However, if no attempt is made to accurately model the long-term motion (e.g. by matching M_f), then nearly all of the motion may be accurately modeled so long as the slopes of the temperature and Clapeyron curves are reasonably matched, as was done in models 11 and 17. Thus the effects of sources on the dynamics of the short-term motion are extremely small. The main effect of sources is in the determination of the final steady state, which influences the long-term motion. The numerical results presented here are a clear verification of the conclusions about sources drawn previously from inspection of the field equations in terms of the perturbation temperature.

Time-dependent loading. In all the preceding discussions we have considered only the response to an instantaneous load causing a pressure change ΔP. We will now extend this treatment to the case where P is time dependent; we will determine the condition that obtains when constant sedimentation rates may be approximated by an impulse load, and the criteria that determine if the phase boundary will be in 'secular equilibrium.'

The effects of pressure enter the problem only through the Clapeyron curve $\mathfrak{I}_c(P) = GP - F$; hence the field equations and boundary conditions remain unchanged from those used so far, with the exception of the condition for the temperature at the phase boundary (26*e*), (27*d*). In dimensionless form this becomes

$$\theta_c(\xi_m(\tau)) = D\xi_m(\tau) - E(\tau) \tag{59}$$

where

$$E(\tau) = (F/T_0) - [GP(t)/T_0] \equiv E(0) - \varphi(\tau)$$

$P(t)$ is the time-dependent pressure applied at the surface. In all the previous cases with impulse loading, $P(t)$ has been a step function of magnitude ΔP:

$$P(t) = 0 \qquad t < 0$$

$$P(t) = \Delta P \qquad t \geq 0$$

We have shown that the generalized Stefan approximation is an accurate representation for impulsive loading for short times primarily because of the singular behavior. In addition, by comparison with the numerical solution, it appears

that this approximation yields a reasonable description even after significant motion of the phase boundary has taken place, as long as the effects of the upper boundary are not strong. These conclusions apply to any impulsive loading, however small. It therefore follows that the initial motion should always be of the Stefan form even for an infinitesimal ΔP. This suggests that more realistic models with finite loading rates may be approximated with a sequence of small impulsive loadings, even though the problem is nonlinear. We are thus led to apply a Stefan-type expression to approximate the temperature field for finite sedimentation rates and thus obtain an equation for $d\xi_m/d\tau$. Letting $\theta(\xi, \tau) = \tilde{\theta}_{SA}(\xi, \tau)$ as before, we obtain from (27*c*), and (29)

$$C\frac{d\xi_m}{d\tau} \approx -\frac{\theta_c(\xi_m)}{\pi^{1/2}\tau^{1/2}}\exp(-\lambda^2)\left[\frac{1}{1-\operatorname{erf}\lambda}+\frac{1}{1+\operatorname{erf}\lambda}\right] \tag{60}$$

where we have assumed $\rho_1 = \rho_2$, $K_1 = K_2$, $\kappa_1 = \kappa_2$ for simplicity, and $\lambda(\xi_m) = [\xi_m(0) - \xi_m(\tau)]/2\tau^{1/2}$ as before. For a sufficiently small impulsive load, λ as determined from $n(\lambda) = \theta_c/C$ is small. Therefore, for continuous loading with $P(0) = 0$, $n(\lambda)$ will be linear in λ for some time. For such a case $\theta(\xi, \tau) \approx \tilde{\theta}_{SAC}(\xi, \tau)$, where $\tilde{\theta}_{SAC}(\xi,\tau) \equiv \tilde{\theta}_{SA}(\xi, \tau)$ under the condition $\eta(\lambda) \approx (\pi^{1/2}/2)\lambda$ and $\Delta P = P(t)$. Equation 60 then becomes

$$C\frac{d\xi_m}{d\tau} \approx \frac{-2}{\pi^{1/2}}\frac{\theta_c}{\tau^{1/2}} = \frac{-2}{\pi^{1/2}}\frac{(D\xi_m - E(\tau))}{\tau^{1/2}}$$

or

$$\frac{d(\xi_m(0) - \xi_m)}{d(\tau)^{1/2}} = \frac{-4D}{C(\pi)^{1/2}}(\xi_m(0) - \xi_m) + \frac{4}{C(\pi)^{1/2}}(E(0) - E(\tau)) \tag{61}$$

The condition of secular equilibrium is defined when the left-hand side of (61) is negligible and $\xi_m \approx E(\tau)/D$. This will be the case when

$$\left|\frac{1}{[E(0) - E(\tau)]}\frac{d}{d\tau}[E(0) - E(\tau)]\right| \equiv \left|\frac{1}{\varphi}\frac{d\varphi}{d\tau}\right| \ll \frac{2D}{C(\pi)^{1/2}}\tau^{-1/2}$$

This criterion defines the conditions under which the system will respond to the loading.

Direct integration of (61) yields

$$\xi_m(0) - \xi_m(\tau) = \frac{r}{D}\exp(-r\tau^{1/2})\int_0^{\tau^{1/2}}\exp(rZ^{1/2})[E(0) - E(Z)]\,d(Z^{1/2}) \tag{62}$$

where $r \equiv 4D/C(\pi)^{1/2}$ is the natural rate constant for the system. Hence transients will decay as $\exp(-r\tau^{1/2})$, and a criterion for long times when transients will have decayed is $r\tau^{1/2} \equiv [4D/C(\pi)^{1/2}]\,\tau^{1/2} \gg 1$. If the loading rate is a linear function of time, $\varphi(\tau) = E(0) - E(\tau) = DR\tau$, where R is a constant determining the loading rate. In this case the criterion for secular equilibrium is $r\tau^{1/2} \gg 2$, and that for long times is $r\tau^{1/2} \gg 1$, which are essentially the same. This criterion is independent of the loading rate. The time over which this approximation is valid will depend on the length of time before the effects of the upper boundary become large.

For a constant loading rate as above, (62) becomes

$$\xi_m(0) - \xi_m(\tau) = R\tau + \frac{2R}{r^2} - \frac{2R}{r}\tau^{1/2} - \frac{2R}{r^2}\exp(-r\tau^{1/2}) \tag{63}$$

or equivalently

$$\xi_m(0) - \xi_m(\tau) = 2Rr\tau^{3/2}\sum_{n=0}^{\infty}\frac{(-1)^n}{(n+3)!}(r\tau^{1/2})^n$$

$$= (R\tau)2r\tau^{1/2}\left[\frac{1}{3!} - \frac{1}{4!}r\tau^{1/2} + \cdots\right]$$

The significance of the criteria for secular equilibrium and long times is apparent from these equations. In addition it may be seen that the initial velocity is proportional to $\tau^{1/2}$; hence the singular behavior that is characteristic of the Stefan problem is no longer present.

We may represent an impulsive load by requiring that the product $R\tau$ remain finite as $\tau \to 0$. The loading function is then

$$E(0) - E(\tau) = RD\tau \qquad 0 \leq \tau \leq \Delta E/RD \equiv \tau_0$$

$$E(0) - E(\tau) = \Delta E \text{ (a constant)} \qquad \tau \geq \tau_0$$

Using this in (62), we obtain

$$\xi_m(0) - \xi_m(\tau) = \frac{\Delta E}{D}\left[1 - \exp(-r\tau^{1/2})\sum_{n=0}^{\infty}\frac{2(n+1)}{(n+2)!}(r\tau_0{}^{1/2})^n\right] \tag{64}$$

for $\tau > \tau_0$. For an impulse, $\tau_0 \to 0$ and the infinite sum on the right of (64) approaches 1. Thus, the criterion for an impulsive load is that the terms other than the first in the sum may be neglected, or

$$\tfrac{2}{3}r\tau_0{}^{1/2} = \tfrac{2}{3}r(\Delta E/RD)^{1/2} \ll 1$$

Thus the time criterion for impulsive loading is independent of the loading rate, and the response to any load deposited in a time considerably less than $\tau_0 = (3/2r)^2$ will be as for an impulsive load. For the models considered here, this time corresponds to ~1 million years. In this case (64) becomes for $\tau > \tau_0$

$$\xi_m(0) - \xi_m(\tau) = \frac{\Delta E}{D}[1 - \exp(-r\tau^{1/2})] = \frac{\Delta E}{D}r\tau^{1/2}\left(1 - \frac{r\tau^{1/2}}{2} + \cdots\right)$$

and $d\xi_m/d\tau$ is initially singular and proportional to $\tau^{-1/2}$ as required for an impulse. In addition, since $\xi_m(0) - \xi_m(\infty) = \Delta E/D$, we may write the preceding equation as

$$\xi_m(\tau) - \xi_m(\infty) = (\Delta E/D)\exp(-r\tau^{1/2})$$

which agrees with (47). It should be remembered that the above results hold only when

$$[\theta_c(\xi_m)/C] = n(\lambda) \approx [(\pi)^{1/2}/2]\lambda$$

i.e., they hold only for small pulses, and not for such large pulses as we have discussed in the previous sections.

A more general result for larger λ may undoubtedly be obtained by extension of the methods given in this paper.

Numerical solutions were obtained for three models with linear pressure loading. The models (18, 19, 20) were similar to model 2 and corresponded to the gutted problem. The loading rate R was taken as 0.1, 1.0, and 10.0 in models 18, 19, and 20, respectively. These correspond to sedimentation rates of roughly 10, 100, and 1000 m/10^6 years. The motion of the phase boundary for each model is shown in Figure 23. The initial motion, as seen in Figure 23*a*, is proportional to $\tau^{3/2}$, as predicted by equation 63. The irregularities in the curves result from numerical errors due to changes in the space and time steps, which were necessary to limit the computation time. The logarithmic plot exaggerates the numerical irregularities for short times.

The motion for longer times is best seen in Figure 23*b*. Note that the time scale is different for each curve. Thus the curve for $R = 0.1$ extends up to $\tau = 1.0$ ($R\tau = 0.1$) or $t = 355 \times 10^6$ years. Long-time behavior and secular equilibrium should obtain for $\tau^{1/2} \gg 1/r \approx 0.04$. Thus, for $\tau^{1/2} \sim 0.4$ or $\tau \sim 0.1$, secular equilibrium should obtain and transients will have decayed. As can be seen, the phase boundary is in secular equilibrium after this time and follows $E(\tau)/D$ at a constant distance.

For the Stefan approximation, the lag l of the phase boundary behind $E(\tau)/D$ is

$$l = (2R/r^2)(r\tau^{1/2} - 1 + e^{-r\tau^{1/2}}) \tag{65}$$

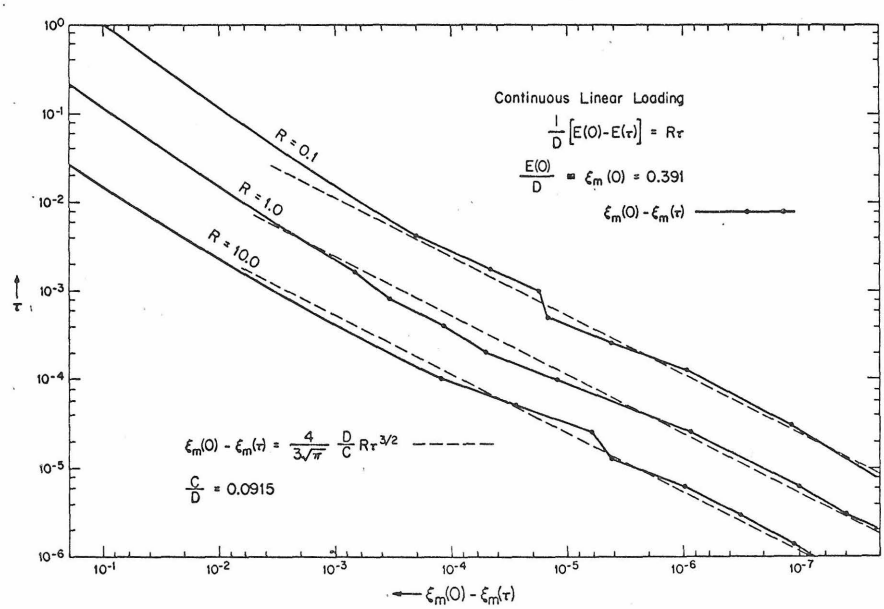

Fig. 23*a*. Motion of the phase boundary for models 18, 19, and 20, which have constant loading rates. The dashed curves show the initial motion expected from the Stefan approximation. The irregularities in the computed curves (solid lines) are due to numerical errors (see text).

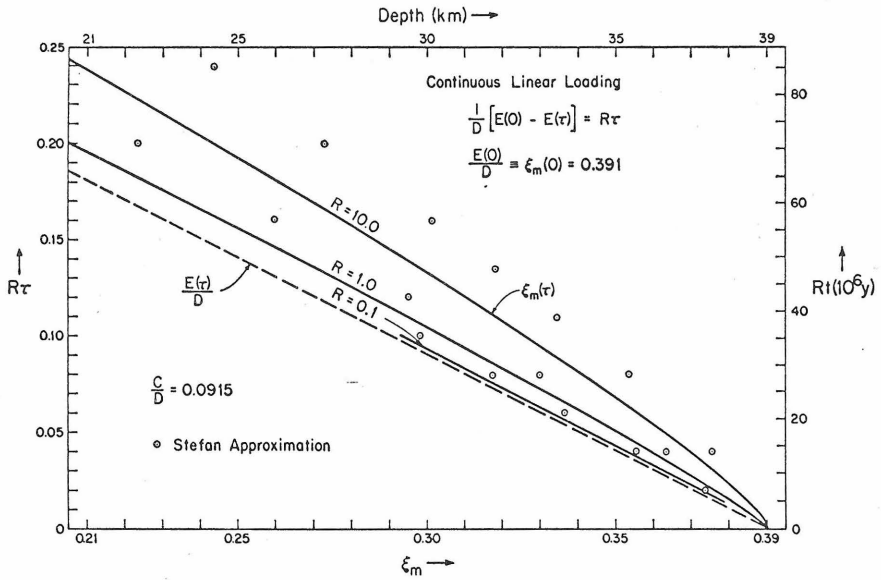

Fig. 23*b*. Linear plot of Figure 23*a* showing the motion of the phase boundary for a constant loading rate proportional to R. If secular equilibrium obtains, $\xi_m(0) - \xi_m(\tau) = R\tau$ and all continuous linear loading curves would fall on the same straight line, which is dashed. The times may be obtained from the $R\tau$ or Rt scales by dividing by R. $R = 0.1$, 1.0, and 10.0 correspond to sedimentation rates of 10, 100, and 1000 m/10^6 years, respectively. The solutions from the Stefan approximation are shown as individual points, which in each case lie above and to the right of the corresponding numerical solution. All curves lag behind $E(\tau)/D$; the Stefan approximation overestimates the actual lag.

At $\tau = 0.16$, the lag should be 0.003 in ξ or ~300 meters for $R = 0.1$. Inspection of Figure 23*b* shows that the lag remains around this value up to the time the computation was stopped when the displacement was around 10 km.

The case for $R = 1.0$ is similar. Thus the lag at $\tau \sim 0.1$ or $t \sim 35 \times 10^6$ years should be ~0.022 or 2.2 km. The actual lag is ~0.015, and the phase boundary follows $E(\tau)/D$ at this distance after this time. Similarly the lag for the case $R = 10$ at $\tau = 0.02$ is 0.055, rather than 0.08, as predicted. In both cases this is probably due to errors incurred in the linear approximation of $n(\lambda)$, which causes the Stefan approximation to overestimate the actual lag. For $\tau > 0.02$ in model 20 ($R = 10$), the lag does not increase much and the phase boundary follows $E(\tau)/D$.

The approximate solution for the position of the phase boundary without assuming secular equilibrium (equation 63) is rather good. A comparison of the computed results and those obtained from (63) are also shown in Figure 23 and indicate the accuracy of the approximation. The lag from (63) is seen to be greater than the computed lag, as mentioned before, and appears to place an upper bound on the magnitude of the lag.

The effect of the surface should become apparent for $\tau \sim \xi_m^2 \sim 0.1$ or $t \sim 35 \times 10^6$ years. The boundary condition $\theta(0, \tau) = 0$ will result in the removal of

more heat from the vicinity of the phase boundary than would be the case for an infinite medium. This in turn would tend to decrease the lag of the phase boundary behind $\xi = E(\tau)/D$. The fact that the observed lag is smaller than that predicted by (65) is undoubtedly due to the boundary effect at $\xi = 0$ in addition to the SAC approximation for the temperature field. For long times the surface effect predominates and the Stefan approximation should no longer apply.

These three models span the range of sedimentation rates that would be expected in a reasonable geophysical model, and comparison of the numerical and theoretical results indicates that it should be possible to estimate the response of most models with reasonable accuracy.

In the preceding discussion we have neglected the thermal impedance of the sediments. As discussed in the section on thermal blanketing, sediments will cause the temperature beneath them to rise, eventually stopping and reversing the motion of the phase boundary. The time at which this occurs is of paramount importance, since it signals the end of subsidence and onset of uplift, and hence also the cessation of sedimentation. Thus this will control the total amount of sediments, which in turn determine the total uplift.

As we did for impulsive loading, we approximate the temperature field by superposing the temperature due to the sediments on the temperature from the Stefan approximation. Since the thickness of the sediments, s, will in general be small compared with the depth of the phase boundary, we shall neglect it. The boundary condition of the surface is thus

$$\theta(0, \tau) \approx \theta(\xi_s, \tau) = -\gamma_1 \xi_s(\tau)$$

If s is not small in comparison with ξ_m, this case will overestimate the effect of the surface. For loading that is proportional to the time (constant sedimentation rate), the initial and boundary conditions for the temperature due to the sediments, $\tilde{\theta}_{BC}(\xi, \tau)$, are

$$\begin{aligned} \tilde{\theta}_{BC}(\xi, 0) &= 0 && 0 \leq \xi \leq \xi_m \\ \tilde{\theta}_{BC}(0, \tau) &= (\gamma_1 \rho_1 WR/\rho_s)\tau && \tau \geq 0 \\ \tilde{\theta}_{BC}(\xi_m, \tau) &= 0 && \tau \geq 0 \end{aligned}$$

where

$$W = [1 - J(0, 0)/G\rho_1 g K_1] = D(T_0/G\rho_1 g b_0).$$

ρ_s is the density of the sediments and R is the rate parameter:

$$R = \frac{1}{b_0 W} \frac{\rho_s}{\rho_1} \frac{dt}{d\tau} \frac{ds}{dt} = \frac{1}{W} \frac{\rho_s c_1 b_0}{K_1} \frac{ds}{dt}$$

We will treat ξ_m as constant in the derivation of $\tilde{\theta}_{BC}$, which is justified as long as the displacement of ξ_m is small compared with $\xi_m(0)$.

The solution to this problem is given by *Carslaw and Jaeger* [1959, p. 102]. We are concerned with the heat flux at the phase boundary, ξ_m, since it is this value that will influence the motion of the phase boundary. This is

$$\left.\frac{\partial \tilde{\theta}_{BC}}{\partial \xi}\right|_{\xi=\xi_m} = \frac{-\gamma_1 \rho_1 WR}{\rho_s} \left[\frac{\tau}{\xi_m} - \frac{\xi_m}{6} - \frac{2\xi_m}{\pi^2} \sum_{n=1}^{\infty} \frac{(-1)^n}{n^2} \exp\left(-\frac{n^2 \pi^2}{\xi_m^2} \tau\right)\right]$$

This may be added to the flux due to the Stefan approximation to determine the velocity of the phase boundary, as was done in (56).

$$-C\frac{d\xi_m}{d\tau} \approx \frac{\partial \tilde{\theta}_{\mathrm{BC}}}{d\xi}\bigg|_{\xi=\xi_m-} + \frac{\partial \tilde{\theta}_{\mathrm{SAC}}}{\partial \xi}\bigg|_{\xi=\xi_m-} - \frac{\partial \tilde{\theta}_{\mathrm{SAC}}}{\partial \xi}\bigg|_{\xi=\xi_m+}$$

This can then be integrated numerically from $\tau = 0$ to find the reversal time τ_R when $d\xi_m/d\tau = 0$. This is analogous to equation 56 for the case of impulsive loading.

Alternatively, if secular equilibrium obtains before the reversal time, then $-C(d\xi_m/d\tau) \approx RC$. But since this is proportional to the flux out of the phase boundary for the Stefan approximation, the criterion indicating the reversal of the motion may be approximated by

$$\frac{\partial \tilde{\theta}_{\mathrm{BC}}}{\partial \xi}\bigg|_{\xi=\xi_m-} + \frac{\partial \tilde{\theta}_{\mathrm{SAC}}}{\partial \xi}\bigg|_{\xi=\xi_m-} - \frac{\partial \tilde{\theta}_{\mathrm{SAC}}}{\partial \xi}\bigg|_{\xi=\xi_m+} = 0$$

or

$$\frac{\partial \tilde{\theta}_{\mathrm{BC}}}{\partial \xi}\bigg|_{\xi=\xi_m-} + RC = 0$$

Thus, at the time of reversal, the following relationship should approximately obtain:

$$\frac{C\rho_s}{\gamma_1\rho_1 W}\xi_m + \frac{\xi_m^2}{6} = \tau - \frac{2\xi_m^2}{\pi^2}\sum_{n=1}^{\infty}\frac{(-1)^n}{n^2}\exp\left(-\frac{n^2\pi^2}{\xi_m^2}\tau\right) \tag{66}$$

This may be combined with equation 63 and solved graphically for the time of reversal $\tilde{\tau}_R$. This is analogous to equation 58 for impulsive loading.

If ξ_m can be estimated, then (66) can be used alone to determine τ_R. For the parameters in models 18, 19, and 20, $\tilde{\tau}_R = 0.048$, 0.061, and 0.074 for $\xi_m = 0.25$, 0.30, and 0.35, respectively. These values correspond to times of 17, 22, and 26 million years. In each case the exponential terms have been negligible and $\tilde{\tau}_R \approx (C\rho_s/\gamma_1\rho_1 W)\xi_m + \xi_m^2/6$. If we substitute $\xi_m(\tau) = \xi_m(0) - R\tau$ in this equation, a quadratic equation for $\tilde{\tau}_R$ is obtained and the dependence on the rate R is readily seen.

Thus the reversal time depends only weakly and indirectly (through $\xi_m(\tau)$) on the sedimentation rate. It is of interest to note that it depends on the ratio C/D (since W is proportional to D).

We have not obtained numerical solutions for models including continuous sedimentation and the thermal impedance of the sediments. These will be considered in a later paper considering the more complex geophysical problem. Nevertheless, the accuracy of the above expressions for the reversal time should not be in serious error and should exhibit the dependence of $\tilde{\tau}_R$ on the parameters of the model used, if we may judge from the cases for which we have obtained numerical solutions, in particular models 12 and 13.

5. EFFECTS OF ISOSTASY

In order to consider the effect of isostasy in conjunction with a phase change, we find it convenient to consider the following model:

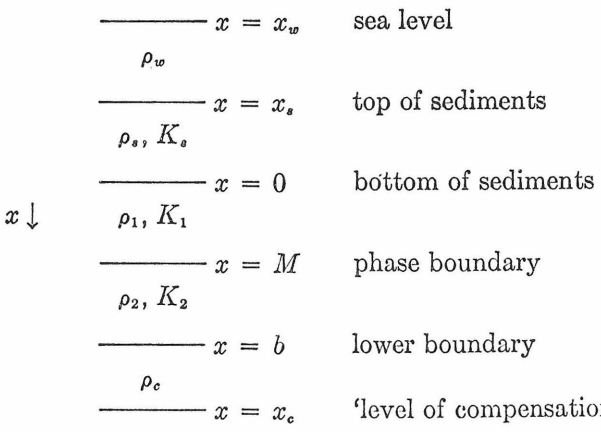

Mean sea level, x_w, is taken as a reference level, fixed with respect to the center of the earth. The depth of water is $w = x_s - x_w$; similarly, the sediment thickness is $s = -x_s$. The densities of the water and the sediments are ρ_w and ρ_s, respectively.

We shall consider isostatic equilibrium to obtain if the mass per unit area is the same after the deposition of sediments as it was before. This is equivalent to considering a crustal block floating in a denser fluid substratum.

We assume that the mass per unit area is always constant below $x = x_c$ which is fixed with respect to the center of the earth, so that $x_c - x_w$ is constant. Thus the mass per unit area above x_c will be constant if the column is in isostatic equilibrium, isostatic adjustments being made by varying the amount of matter of density ρ_c between $x = b$ and $x = x_c$ by lateral flow.

For simplicity we discuss the case with no heat sources and with constant heat flux at the lower boundary $x = b$. This is not a severe limitation, since in many cases an appropriate 'no-source approximation' can be constructed for models with sources. In addition we define

$$\rho_w(w) = \begin{cases} 1 & \text{if} \quad w \geq 0 \\ 0 & \text{if} \quad w < 0 \end{cases}$$

since $w < 0$ corresponds to the top of the sediments, x_s, being above sea level, in which case no water will be present. This allows generalization of the model to treat cases of deposition and erosion above sea level.

The initial state of the model will be specified by the initial depth of the water, w_0, the initial sediment thickness, which we take as zero, and the initial location of the phase boundary, which will be determined by the intersection of the Clapeyron curve and the temperature distribution in the earth. The location of the lower boundary b will depend on the total mass of material between $x = 0$ and $x = b$, which will be constant and on the position of the phase boundary.

If sediments of thickness s are deposited on the surface $x = 0$, the phase boundary will initially move only in response to the pressure load, but it will lag behind its equilibrium position by a distance l as discussed in the previous section. The resultant conversion of the low-density (ρ_1) phase to the high-density (ρ_2)

phase will result in the subsidence of the material in the region above the phase boundary. In addition, the entire block $x \leq b$ will subside, owing to the isostatic response to the load of the sediments. The exact magnitude of this subsidence will depend on how rapidly isostatic adjustments are made. Except where otherwise stated, we shall assume that the time scale of isostatic adjustments is much shorter than that of the response of the phase boundary; consequently, we assume that a state of isostatic equilibrium always obtains. If on the other hand the time scale for isostatic adjustment is much greater than the time for the phase boundary to respond (as may be determined from the Stefan approximation), then the effects of isostasy will not be important and may be neglected altogether.

For longer times the effect of thermal blanketing by the sediments will influence the motion of the phase boundary and may cause it to reverse the direction of its motion. For times less than the time of reversal, which can be estimated, the effect of thermal blanketing will be small, as was shown in the previous section on thermal blanketing and reversals. Thus we may discuss the response of the model to sedimentation for times less than the time of reversal by neglecting the thermal effect of the sediments altogether. We will include the effect of thermal blanketing later in the discussion.

The requirement that the mass per unit area be conserved in the regions $x \leq x_c$ and $J \leq x \leq b$, subject to $x_c - x_w$ constant, gives the following relation between the sediment thickness $s(t)$, water depth $w(t)$, and initial water depth w_0. At any given instant of time

$$Q_w w - Q_{w_0} w_0 + Q_s s = -l\rho_1[(1/\rho_1) - (1/\rho_2)] \tag{67}$$

where

$$Q_i \equiv \rho_i\left[\left(\frac{1}{\rho_i} - \frac{1}{\rho_c}\right) - \frac{1}{W}\left(\frac{1}{\rho_1} - \frac{1}{\rho_2}\right)\right]; \qquad i = s, w, w_0$$

and

$$W \equiv 1 - (J_M/K_1 G g \rho_1)$$

Since ρ_w is a function of w, to allow the treatment of cases involving uplift above sea level ($x_s < x_w$ or $w < 0$), we must distinguish between Q_w and Q_{w_0}. The lag of the phase boundary, $l(t)$ is defined as the distance of the boundary behind the position it would have if thermal equilibrium obtained at each instant of time. Equation 67 applies to a source-free model, in which case $J_M = J(0, 0)$. To treat a case when sources are present it is necessary to model the case with sources by a no-source approximation, as discussed in the section on radioactive heat sources. In this case, $J_M \approx K_1[T(M(0), 0) - T(M(t), 0)]/[M(0) - M(t)]$ and J_M is considered as a constant.

If $\rho_1 = \rho_2$, the phase change will have no effect on subsidence, and (67) reduces to the equation for isostatic adjustment alone [*Jeffreys*, 1962, p. 336]. Similarly, we can obtain the effect of the phase change alone in the absence of isostatic adjustment by letting $\rho_c \to \infty$ in (67). It should be noted that, when $Q_s = 0$, equation 67 is independent of s and the sediment thickness is indeterminate.

The nature of the subsidence can best be seen by differentiating (67):

$$dw/ds = -(Q_s/Q_w) - (\rho_1/Q_w)[(1/\rho_1) - (1/\rho_2)]\, dl/ds \qquad (68)$$

At a given instant of time a negative value of dw/ds corresponds to a basin being filled as a result of sedimentation or, conversely, a decrease in elevation as a result of denudation. If $dw/ds = 0$, the subsidence rate will be exactly equal to the sedimentation rate and the water depth will remain the same even though sediments are deposited. If $dw/ds > 0$, the water depth will increase with sedimentation. For this case then, if the rate of sedimentation increased with the water depth, initial sedimentation would cause subsidence, which would result in even more rapid sedimentation and subsidence. Hence we shall regard the case $dw/ds > 0$ as dynamically unstable. The two previous cases we shall regard as dynamically stable ($dw/ds < 0$) and neutrally stable ($dw/ds = 0$), respectively.

Assuming $Q_w > 0$, a given model will be dynamically unstable if

$$Q_s + \rho_1[(1/\rho_1) - (1/\rho_2)](dl/ds) < 0$$

As can be seen from the definition of Q_s, this term will be negative for $(1/W)$ $[(1/\rho_1) - (1/\rho_2)] > (1/\rho_s - 1/\rho_c)$, which will be the case for sufficiently small $W\ J_M/(K_1\ G g \rho_1)$ or sufficiently close to 1.0. This condition can be attained for values of the parameters that are not outside the range of probability. (For example, for model 11, $Q_s = -0.012$ if $\rho_s = 2.4$ and $\rho_c = 3.5$.) In this case the value of dl/ds becomes critical in determining the sign of dw/ds, and hence the dynamic stability of the system. Systems that exhibit dynamic instability at one time may become stable at later times, and conversely. This is due to the time dependence of $l(t)$.

It should also be noted that the possibility of instability is not due solely to the presence of the phase change, since instability would result if $\rho_s > \rho_c$ with no phase change. The phase change does, however, permit instability to occur for $\rho_s < \rho_c$, as would generally be expected in a geophysical model. The instabilities discussed here appear to have been overlooked by previous workers.

If we consider the case of a constant sedimentation (or denudation) rate, then we can evaluate dl/ds for the Stefan approximation (SAC) from (65):

$$\frac{dl}{ds} \approx \frac{\rho_s L(1 - W)}{4J_M W^2} \left(\frac{\pi K_1}{\rho_1 c_1}\right)^{1/2} t^{-1/2} \left\{1 - \exp\left[-\frac{4J_M W}{\rho_1 L(1 - W)} \left(\frac{\rho_1 c_1}{\pi K_1}\right)^{1/2} t^{1/2}\right]\right\}$$

Values for dw/ds for models 11 and 17, taking $\rho_s = 2.4$, $\rho_w = 1.0$, and $\rho_c = 3.5$ are given in Table 5. These models are no-source approximations to models 14 and 15, respectively.

As can be seen, the lag of the phase boundary prevents model 11 from being unstable. Examination of Figure 23*b* reveals, however, that the Stefan approximation overestimates the lag by about a factor of 2. If we had used the value of the lag from the numerical solution rather than from the Stefan approximation, the model would have shown the instability, as may be seen by substituting in (67) directly. Thus the possibility of accumulating thick deposits of sediments in relatively shallow water exists for models similar to model 14.

The values of dw/ds in Table 5 should be contrasted with the value $dw/ds = -0.44$ for the case with isostasy alone and with no phase change effect. Thus the phase change has a noticeable effect on model 17, even though this model may

TABLE 5. Effect of Phase Change with Isostasy on Subsidence Due to Sedimentation

Time, 10^6 yr	dw/ds, Model 11	dw/ds, Model 17
0.2	−0.41	−0.37
1.0	−0.29	−0.32
5.0	−0.16	−0.27
10.0	−0.13	−0.26
15.0	−0.090	−0.26
20.0	−0.075	−0.26
30.0	−0.057	−0.26
50.0	−0.040	−0.26
All times (no phase change)	−0.44	−0.44

be considered conservative in terms of the magnitude of Q_s (since W is relatively large). The effect of the phase change in model 11 is very marked, as would be expected, owing to the negative value of Q_s.

If we consider a basin subject to sedimentation as long as the surface is below sea level, sedimentation will stop when either (1) the basin fills up or (2) the motion of the phase boundary reverses, owing to thermal blanketing, eventually causing the surface to be elevated above sea level. The maximum thickness of sediments that could be deposited in the basin will be attained if (1) occurs, i.e. if the basin fills completely before the phase boundary reverses; hence this maximum thickness is given by setting $w = 0$ in (67). For neutrally stable or unstable cases, this may result in a root for s that is negative and does not constitute a real physical solution. Since the time at which the phase boundary reverses motion has been estimated in the previous section, one can roughly determine whether or not this maximum thickness will be attained for a given sedimentation rate. If (2) occurs first, sediment thickness may be estimated from the sedimentation rate and the reversal time. The exact thickness will depend on the amount deposited after reversal.

After the reversal of the phase boundary, the effect of thermal blanketing will dominate the motion. Hence, since the thermal blanketing effects of the surface were completely neglected, equation 67 will no longer apply. Instead the elevation $(-w)$ will be given by

$$Q_w w - Q_{w_0} w_0 + Q_s' s = -l\rho_1[(1/\rho_1) - (1/\rho_2)] \tag{69}$$

where Q_w and Q_{w_0} are as defined in (67) and l is the lag (or lead) of the phase boundary from the position it would have if thermal equilibrium including the effects of the sediments obtained at each instant of time. This is the same definition as before; however the thermal blanketing effects are now to be included.

$$Q_s' = Q_s + (K_1\rho_1/K_s)(1/Y)[(1/\rho_1) - (1/\rho_2)]$$

where $Y \equiv (Gg\rho_1 K_1/J_s) - (J_M/J_s)$ and where J_s/K_s is the average temperature gradient in the sediments. If there are no heat sources in the sediments, $J_s =$

$J(0, 0)$. The problem of sedimentation in a basin may now be approached by considering the possible sequences of events. The maximum sediment thickness that can be accumulated in a basin will occur if the basin completely fills up before the thermal blanketing causes the phase boundary to reverse its motion. This thickness may be found by setting $w = 0$ in equation 67. The time necessary for the deposition of this thickness of sediments can then be obtained from the sedimentation rate. If this time is greater than the reversal time of the phase boundary, then the reversal of the boundary, resulting in uplift, may cause the surface to rise above sea level before the above-mentioned maximum sediment thickness has been attained. In this event the sediment thickness may be estimated from the sedimentation rate and the reversal time. In either event, once the sediment thickness is known, the maximum final elevation can be determined from (69) by setting $l = 0$, which is equivalent to assuming that the final steady-state thermal equilibrium has been attained. This maximum elevation would be attained only under the exceptional circumstance of no erosion and then only after a time sufficiently long for the region $x_s \leq x \leq b$ to approach thermal equilibrium. For a region ~100 km thick, this would be of the order of 10^8 years. Since the Stefan approximation certainly does not apply after the reversal of motion of the phase boundary, we will not attempt to estimate the uplift in the event of erosion. It should be noted, however, that, owing to isostatic compensation and the effect of the phase change (through the term dw/ds discussed above), the erosion of a given thickness of sediment will not cause a decrease in elevation of the same amount but rather less.

In Table 6 are the maximum sediment thicknesses calculated from equation 67 with $w = 0$ and the final elevations calculated from equation 69 for various values of the lag of the phase boundary for several cases. All of the cases employ the physical parameters used in model 15 (to which model 17 is the appropriate no-source approximation), but with various values for the surface heat flux (J_s) and sediment conductivity (K_s). In all cases J_M, the heat flux in the vicinity of the phase boundary, and all other relevant parameters are identical to those in model 17 (or 15). This may be considered a fairly conservative model, since, as shown in Table 5, the value of dw/ds is not especially small. If the ratio $J_M/K_1Gg\rho_1$ were greater, as would be the case if more heat originated below the phase boundary, i..e for $x > M$, then the sediment thickness and final elevation could be substantially greater. This would also be the case for denser sediments, a less dense substratum, or a greater density change with the phase change than considered here.

The first six cases are for marine deposition and later emergence above sea level. The last case, on the other hand, treats the rapid erosion to a reference level (taken arbitrarily at sea level) of a surface initially 1 km above that reference level. Since there is no water present, the ratio of the change in elevation to the sediments removed (dw/ds) is less than would be the case for a marine environment.

For all cases for the values of l given in Table 6, model 11 is unstable; i.e., the only limit to the sediment thickness is the time of reversal of the phase boundary. Since this has been previously shown to be ~20 million years, the

TABLE 6. Possible Sediment Thickness and Final Elevation Assuming No Erosion for Models (including phase change and isostasy)

J_s Average Flux in Sediments, μ cal/cm²/sec	K_s Conductivity of Sediments, cal/cm/sec/°C	w_0 Initial Water Depth, km	l Lag of Phase Boundary, km	s† Maximum Thickness of Sediments, km	$-w$ Maximum Final Elevation, km
1.0	0.005	3	0	12.6	2.3
			2	10.6	1.6
			4	8.6	1.0
1.2	0.005	3	0	12.6	2.7
			2	10.6	2.0
			4	8.6	1.3
1.2	0.0035	3	0	12.6	3.9
			2	10.6	3.0
			4	8.6	2.1
1.5	0.005	3	0	12.6	3.4
			2	10.6	2.6
			4	8.6	1.7
		5	0	21.0	5.7
			2	19.0	4.8
			4	17.0	4.0
1.5	0.0035	3	0	12.6	4.9
			2	10.6	3.8
			4	8.6	2.7
1.5	0.005	−1*	0	−6.5	−1.7*
			−1	−5.5	−1.3*
			−2	−4.5	−0.92*
			−3	−3.5	−0.50*

* Surface initially above sea level, subsequently eroded to sea level. Weight of water neglected.
† $\rho_s = 2.4$; $\rho_c = 3.5$.

sediment thickness will be just the amount that can be deposited in that time, and it will be independent of the initial water depth.

Thus, there seems to be little difficulty in accounting for thick sections of sediments that were deposited in relatively shallow water, so long as the deposition was sufficiently rapid. The long-term evolution of the surface after uplift will depend on the erosion of the surface above sea level and may be subject to an extension of the simple analysis as presented in this paper.

The possibility of a small value of dw/ds would indicate that rapid erosion rates may not substantially reduce the elevation of the eroded surface.

6. SUMMARY

The dynamic response of a phase boundary to sudden changes in pressure has been investigated by considering a one-dimensional model of two layers separated by a phase change. The problem was formulated in terms of a dimensionless perturbation temperature by subtracting the initial steady temperature distribution. In this form the simplest case, neglecting radioactive heat sources, convective heat transport, and the difference in thermal properties of the two phases, may be approximated by a simple generalization of Neumann's solution to the problem of freezing at a constant temperature. Comparison of the approximate solution with exact numerical solution revealed that the approximation very accurately described both the initial motion of the phase boundary and the temperature distribution. More complex models considering the differences in thermal properties of the two phases may also be accurately described by the approximate solution up to a time that may be determined from the approximation. In all cases, the initial motion is completely determined from (1) the ratio of the latent heat of the phase change to the difference between the Clapeyron slope and the earth's temperature gradient and (2) the product of the Clapeyron slope and the applied pressure divided by the latent heat.

The motion of the phase boundary for long times may also be accurately described from simple considerations based on the over-all geometry of the model. In addition to (1) above, the motion then depends most critically on the location of, and the boundary conditions at, the lower boundary. Since for most geophysical models the effects of the lower boundary will probably dominate the behavior for long times, the choice of this boundary condition is extremely important and is probably the most severe limitation of a one-dimensional model that attempts to describe the complete geophysical problem.

The effect of convective heat transport, which is partly estimable from the approximate solution, has been shown to be small for many geophysical cases by direct comparison of numerical solutions. Thus neglect of the convective term in the field equations is probably justified, considering the implicit limitations of a one-dimensional model and the uncertainties in the parameters.

Radioactive heat sources were shown to enter the problem only in the region through which the phase boundary actually moved. In addition, comparisons of numerical solutions indicated that the effect of sources per se on the dynamics of the motion is small. Thus a model with sources can be adequately approximated by a model without sources to which all the previous conclusions apply.

The effect of thermal blanketing by sediments has also been considered. The approximate time at which the blanketing would cause the phase boundary to reverse its motion may be determined from an analytic expression or by the integration of a first-order linear differential equation. Since the time at which reversal occurs signals the start of uplift, this criterion is especially important.

The approximate solution for impulsive loads was extended to the case of continuous sedimentation at a constant rate, and the accuracy verified by comparison with numerical solutions for sedimentation rates ranging from ~10 meters/10^6 years to ~1000 meters/10^6 years. It was shown that a condition of secular equilibrium would eventually obtain, where the phase boundary would follow

the applied load, and criteria were presented to determine when such a situation would obtain. In addition, the criterion determining when a continuous load would appear as an impulsive one was determined and shown to be independent of the loading rate. Similarly, the time at which the phase boundary would reverse its motion was shown to have only weak dependence on the loading rate, and an explicit expression for this time was given.

The effect of a phase change in conjunction with isostatic compensation on subsidence due to sedimentation was shown to be major. For a proper choice of reasonable parameters, the thickness of sediments that can be deposited in a basin is limited primarily by the time at which the phase boundary reverses motion, and *not* the initial depth of water. For a phase change at a depth of ~40 km, this time is ~20 million years; thus for a wide variety of cases, where the basin is not filled before reversal the sediment thickness depends almost exclusively on the sedimentation rate. The final elevation after uplift and attainment of thermal equilibrium can be substantial; the actual elevation will depend, however, on erosion rates after uplift, which have not been studied here. The proper study of the problem including erosion will depend strongly on the actual long-term behavior. Since this behavior will be dominated by the boundary conditions at depth, the problem of the proper choice for this condition must be resolved for further progress with a one-dimensional model.

The existence of reasonably accurate analytic approximations to the actual solution permits the dependence of the solution on the various parameters to be readily seen. This allows various geophysical models to be considered without the need of obtaining numerical solutions for each one. In addition, certain characteristics of the solution may be identified (e.g. long- or short-term motion), or certain aspects of the model may be characterized in terms of their effect on the solution (e.g. slow or rapid sedimentation). The problem may be separated into rather distinct physical processes with characteristic time constants. The characteristic times are determined from the initial state of the model. Insofar as the characteristic times of the various processes are distinct, the separate modes of the motion are then subject to an a priori analysis. When the characteristic times overlap, the motion may be more complicated. This allows the determination of the conditions under which the motion of a phase change will be an important geophysical process. Once this is done, the problem of whether such conditions actually exist may be treated separately.

APPENDIX 1

The gutted problem is formulated for $\theta(\xi, \tau)$, $\xi_m(\tau)$:

$$\partial\theta/\partial\tau = \partial^2\theta/\partial\xi^2, \qquad 0 \leq \xi < \xi_m, \quad \xi_m < \xi \leq 1, \quad \tau > 0 \tag{A1}$$

$$\theta(0, \tau) = \theta(1, \tau) = 0, \qquad \tau \geq 0 \tag{A2}$$

$$\left.\frac{\partial\theta}{\partial\xi}\right|_{\xi=\xi_m^+(\tau)} - \left.\frac{\partial\theta}{\partial\xi}\right|_{\xi=\xi_m^-(\tau)} = C\frac{d\xi_m}{d\tau} \tag{A3}$$

$$\theta(\xi_m(\tau), \tau) = D\xi_m(\tau) - E, \qquad \tau \geq 0 \tag{A4}$$

$$\theta(\xi, 0) = 0, \qquad \xi \neq \xi_m(0); \qquad \theta(\xi_m(0), 0) = D\xi_m(0) - E \tag{A5}$$

$$C, D, E \text{ constants}, \quad 0 < E < D, \quad 0 < \xi_m(0) < 1, \qquad C \geq D\xi_m(0) - E \tag{A6}$$

We will show that these equations determine the initial motion of the phase boundary, that the phase boundary is bounded by the equilibrium position and the initial position, that the temperature to the right of the phase boundary always lies beneath the Clapeyron curve, and that the sign of $\partial^2\theta/\partial\xi^2$ immediately to the right of the phase boundary is determined.

Multiplying (A1) by θ and integrating

$$\int_0^{\xi_m} \frac{\partial}{\partial\xi}\left(\theta\frac{\partial\theta}{\partial\xi}\right) d\xi + \int_{\xi_m}^1 \frac{\partial}{\partial\xi}\left(\theta\frac{\partial\theta}{\partial\xi}\right) d\xi$$
$$= \int_0^{\xi_m}\left[\left(\frac{\partial\theta}{\partial\xi}\right)^2 + \frac{1}{2}\frac{\partial}{\partial\tau}(\theta^2)\right] d\xi + \int_{\xi_m}^1\left[\left(\frac{\partial\theta}{\partial\xi}\right)^2 + \frac{1}{2}\frac{\partial}{\partial\tau}(\theta^2)\right] d\xi$$

Carrying out the integration on the left and substituting (A2), (A4), and (A5)

$$(D\xi_m(\tau) - E)\left(-C\frac{d\xi_m}{d\tau}\right)$$
$$= \int_0^{\xi_m}\left[\left(\frac{\partial\theta}{\partial\xi}\right)^2 + \frac{1}{2}\frac{\partial}{\partial\tau}(\theta^2)\right] d\xi + \int_{\xi_m}^1\left[\left(\frac{\partial\theta}{\partial\xi}\right)^2 + \frac{1}{2}\frac{\partial}{\partial\tau}(\theta^2)\right] d\xi$$

Integrating with respect to τ and using (A5), which implies

$$\int_0^1 \theta^2(\xi, 0)\, d\xi = 0$$

we obtain

$$\int_0^\tau [D\xi_m(\tau) - E]\left[-C\frac{d\xi_m}{d\tau}\right] d\tau$$
$$= \int_0^\tau\left[\int_0^{\xi_m}\left(\frac{\partial\theta}{\partial\xi}\right)^2 d\xi + \int_{\xi_m}^1\left(\frac{\partial\theta}{\partial\xi}\right)^2 d\xi\right] d\tau + \frac{1}{2}\int_0^1 \theta^2(\xi, \tau)\, d\xi$$

This is strictly positive, since the terms on the right are positive and vanish only if θ and $\partial\theta/\partial\xi$ vanish identically on the whole interval. If the integration is carried out on the left

$$C[(D/2)(\xi_m(0) + \xi_m(\tau)) - E][\xi_m(0) - \xi_m(\tau)] > 0$$

By reductio ad absurdum $D\xi_m(0) - E > 0$ implies $\xi_m(0) - \xi_m(\tau) > 0$ and $D\xi_m(0) - E < 0$ implies $\xi_m(0) - \xi_m(\tau) < 0$. Thus the phase boundary is constrained to lie on only one side of its initial position, and the sign $(d\xi_m/d\tau)|_{\tau=0+}$ is determined.

By applying the maximum-minimum principle, we now show that $\xi_m(\tau)$ never crosses $\xi = E/D$, which is the only equilibrium position for the phase boundary. This principle states that, if $\partial^2\theta/\partial\xi^2 = \partial\theta/\partial\tau$ on a region in space R with boundary B, that both the maximum and minimum of θ on R for $\tau_1 \geq \tau \geq 0$, where τ is some arbitrary time, will be attained for either $\xi\epsilon B$, $\tau_1 \geq \tau > 0$ or $\xi\epsilon R$, $\tau = 0$.

Hence, the extrema must lie on the boundaries

$$\xi = 0, \quad \xi = \xi_m(\tau), \quad \tau > 0 \quad \text{or} \quad 0 \leq \xi \leq \xi_m(0), \quad \tau = 0 \quad \text{in region 1}$$

or

$$\xi = \xi_m(\tau), \quad \xi = 1, \quad \tau > 0 \quad \text{or} \quad \xi_m(0) \leq \xi \leq 1, \quad \tau = 0 \quad \text{in region 2}$$

If the zero of the Clapeyron curve has not been crossed, $\xi_m(\tau) \geq E/D$. Use of the minimum principle then shows $\theta(\xi, \tau) \geq 0$. If ξ_m approaches E/D from the right, then $d\xi_m/d\tau < 0$. We now show that $d\xi_m/d\tau$ either goes to zero or reverses sign, if $\xi_m = E/D$.

$$\left.\frac{\partial\theta}{\partial\xi}\right|_{\xi_m = E/D^+} = \lim_{\epsilon \to 0}\left[\frac{\theta[(E/D) + \epsilon, \tau] - \theta[(E/D), \tau]}{\epsilon}\right] \geq 0$$

and similarly

$$\left.\frac{\partial\theta}{\partial\xi}\right|_{\xi_m = E/D^-} \leq 0$$

Hence, from (A3)

$$\left.\frac{d\xi_m(\tau)}{d\tau}\right|_{\xi_m = E/D^+} \geq 0$$

at the boundary, whereas it is negative when approaching the boundary; hence, $\xi = E/D$ is never crossed and $\xi_m(\tau) \geq E/D$.

We now show that the Clapeyron curve is never exceeded in region 2. Consider the function $\theta'(\xi, \tau) = \theta(\xi, \tau) - (D\xi - E)$ in region 2. Since obviously $\partial^2\theta/\partial\xi^2 = \partial\theta'/\partial\tau$, we may apply the maximum principle. Since

$$\begin{aligned} \theta'(\xi, 0) &= -(D\xi - E) < 0 && \xi_m(0) < \xi \leq 1 \\ \theta'(1, \tau) &= -(D - E) < 0 && \tau > 0 \\ \theta'(\xi_m(\tau), \tau) &= 0 && \tau \geq 0 \end{aligned}$$

then $\theta'(\xi, \tau) \leq 0$ or $\theta(\xi, \tau) \leq D\xi - E$. Thus the temperature to the right of the phase boundary always lies beneath the Clapeyron curve. In addition, if $\xi_m(\tau) < \xi_m(0)$, applying the maximum principle to θ shows that $\theta(\xi, \tau) < \theta(\xi_m(0), 0) = D\xi_m(0) - E$.

We now exhibit a relationship that determines the sign of $\partial^2\theta/\partial\xi^2$ at the phase boundary. This or an analogous relationship may be useful in providing insight to other problems of this type.

Since $\theta(\xi_m, \tau) = D\xi_m - E$, we obtain by the chain rule

$$D\frac{d\xi_m}{d\tau} = \left.\frac{\partial\theta}{\partial\xi}\right|_{\xi=\xi_m}\frac{d\xi_m}{d\tau} + \left.\frac{\partial\theta}{\partial\tau}\right|_{\xi=\xi_m} = \left.\frac{\partial\theta}{\partial\xi}\right|_{\xi=\xi_m}\frac{d\xi_m}{d\tau} + \left.\frac{\partial^2\theta}{\partial\xi^2}\right|_{\xi=\xi_m}.$$

Hence

$$\left.\frac{\partial^2\theta}{\partial\xi^2}\right|_{\xi=\xi_m} = \left[D - \left.\frac{\partial\theta}{\partial\xi}\right|_{\xi=\xi_m}\right]\frac{d\xi_m}{d\tau}$$

To the right of the phase boundary, θ is bounded by the Clapeyron curve; hence

$$D - \frac{\partial \theta}{\partial \xi}\bigg|_{\xi=\xi_m+} \geq 0$$

Therefore

$$\frac{\partial^2 \theta}{\partial \xi^2}\bigg|_{\xi=\xi_m+} \Big/ \frac{d\xi_m}{d\tau} \geq 0$$

Thus, if $d\xi_m/d\tau \leq 0$, then

$$\frac{\partial^2 \theta}{\partial \xi^2}\bigg|_{\xi=\xi_m+} \leq 0$$

and the shape of the temperature curve to the right of the phase boundary is always convex upward. In addition, from consideration of the initial conditions (A5), for a short enough time, say $\tau < \tau_1$,

$$\frac{\partial \theta}{\partial \xi}\bigg|_{\xi=\xi_m-} > D; \qquad \text{hence } \frac{\partial^2 \theta}{\partial \xi^2}\bigg|_{\xi=\xi_m-} \Big/ \frac{d\xi_m}{d\tau} < 0 \quad \text{for} \quad \tau < \tau_1$$

Thus, the initial shape of the temperature curve near the phase boundary is determined.

APPENDIX 2

For numerical solution, the derivatives in equations 25, 26, and 27 were replaced by standard finite difference approximations [*Forsythe and Wasow*, 1964]. The field equation $\partial\theta/\partial\tau = \partial^2\theta/\partial\xi^2$ was replaced by the implicit difference equation

$$\frac{\theta(\xi, \tau + k) - \theta(\xi, \tau)}{k} = \frac{\theta(\xi - h, \tau + k) - 2\theta(\xi, \tau + k) + \theta(\xi + h, \tau + k)}{h^2} \tag{A7}$$

where h and k are the space and time increments, respectively. This may be written, with $\mu = k/h^2$, as

$$\theta(\xi, \tau) = -\mu\theta(\xi - h, \tau + k) + (1 + 2\mu)\theta(\xi, \tau + k) - \mu\theta(\xi + h, \tau + k) \tag{A8}$$

which may be regarded as a system of simultaneous linear equations for the values of $\theta(\xi, \tau + k)$ at the net points $\xi = ih$, $i = 0, 1, 2, \cdots$. If the number of equations is finite and suitable boundary conditions are applied at the end points of the region, the above system can be solved for $\theta(\xi, \tau + k)$ in terms of $\theta(\xi, \tau)$ at the net points.

The advantage of such an implicit method is that it is stable for all values of μ; that is, it obeys the same maximum-minimum principle as does the original differential equation [*Forsythe and Wasow*, 1964, p. 102].

The above method can be applied in each of the regions $0 \leq \xi \leq \xi_m$ and $\xi_m \leq \xi \leq 1$, provided $\xi_m(\tau + k)$, and hence $\theta(\xi_m(\tau + k), t + k)$ are known. If $\xi = m_1 h$ and $\xi = m_2 h$ are the net points immediately to the left and right of the

phase boundary, and $h_1 \equiv \xi_m - m_1 h$, $h_2 \equiv m_2 h - \xi_m$, the boundary condition 27c becomes

$$\xi_m(\tau + k) - \xi_m(\tau) = \frac{k}{C}\left[\frac{\theta(m_2 h, \tau') - \theta(\xi_m, \tau')}{h_2} - \frac{\theta(\xi_m, \tau') - \theta(m_1 h, \tau')}{h_1}\right] \quad \text{(A9)}$$

where τ' may be τ or $\tau + k$. $\theta(\xi_m, \tau')$ is given by the Clapeyron curve, once $\xi_m(\tau')$ is known.

The method of solution used was: knowing $\theta(\xi, \tau)$, $\xi_m(\tau)$,

(1) $\xi_m(\tau + k)$ was calculated from (9) by letting $\tau' = \tau$. Hence, $\theta(\xi_m, \tau + k)$ was calculated.
(2) The system of equations (A8) was solved for the net points $i = 1, \cdots, m_1$ and $i = m_2 \cdots, n$ where $(n + 1)\ h = 1$, by Gauss' elimination method.
(3) $\xi_m(\tau + k)$ was recalculated from (A9), using $\tau' = \tau + k$.
(4) Using this new value of $\xi_m(\tau + k)$, steps 2 and 3 were repeated.
(5) If two successive determinations of $\xi_m(\tau + k)$ were within a certain limit of one another, the iterative process was stopped and the whole process was repeated for the next time step.

The equation A9 gives the velocity of the phase boundary at a given time; the average velocity over a time step was used to calculate the movement of the phase boundary:

$$\xi_m(\tau + k) - \xi_m(\tau) = \tfrac{1}{2}k\left[\frac{d\xi_m}{d\tau}\bigg|_{\tau=\tau} + \frac{d\xi_m}{d\tau}\bigg|_{\tau=\tau+k}\right]$$

In addition, since the velocity of the phase boundary is singular at $\tau = 0$, it was assumed in analogy with the classical Stefan problem that $d\xi_m/d\tau$ was proportional to $\tau^{-1/2}$ for short times. Thus $\xi_m(k) - \xi_m(0)$ could be calculated from $(d\xi_m/d\tau)|_{\tau=k}$. (For problems in which the singular behavior is of paramount importance a change of variable to $\sqrt{\tau}$ may be desirable). In order to check this assumption, the integral form of the boundary condition

$$-C\frac{d\xi_m}{d\tau} = \frac{d}{d\tau}\int_0^1 \theta\, d\xi + \frac{\partial\theta}{\partial\xi}\bigg|_{\xi=0} - \frac{\partial\theta}{\partial\xi}\bigg|_{\xi=1}$$

was used in the computer program, performing the integral numerically by the trapezoidal rule. In this way the displacement of the phase boundary is determined directly for each time step rather than the velocity. Thus it was found, using this form of the boundary condition:

$$\frac{\xi_m(2k) - \xi_m(0)}{\xi_m(k) - \xi_m(0)} = 1.44$$

Using the differential form including the assumption on $d\xi_m/d\tau$ gave a ratio slightly closer to $2^{1/2} = 1.414$, which was the expected value. Considering the inherent difficulties in treating such a singularity numerically, the results were considered acceptable.

The singularity in velocity at $\tau = 0$ also made it desirable to use an extremely fine space net and small time steps. The retention of such a fine net, however, would have required a prohibitively long execution time for the solution to proceed to large enough values of τ. Therefore, provisions were made in the program both for making the space net coarser and for varying the time step. The space net was made coarser at times chosen so that θ would be sufficiently smooth to be relatively unaffected by the change. The time step k was doubled whenever $|\xi_m(\tau + k) - \xi_m(\tau)|$ was less than a predetermined minimum. A maximum step was set, though, beyond which k was not increased. Comparisons in trial cases showed no significant differences between cases where the maximum k resulted in $\mu = 3.2$ or where μ reached 102.4. In the solutions used in this paper, μ varies from 0.1 initially to a final value of 51.2.

Comparisons of trial solutions with different net spacings and time steps indicated: (1) refinement of the space net caused the phase boundary to move faster, especially for small τ; and (2) a smaller time step caused the phase boundary to move more slowly, especially for small τ. The maximum difference between any two trial solutions for the location of the phase boundary at a given time was 300 meters, and this difference appeared during the first 15% of the 9 km of total movement of the phase boundary, the difference decreasing slowly during the last 85%.

Thus, the finite net spacing and time steps seem to cause errors of opposite sign that are significant only during the initial phases of the solution. These errors may be attributed primarily to the singularity in velocity at time $\tau = 0$. The solutions presented in this paper have all been performed with the same net spacing and initial time steps; comparisons among them should therefore be subject to relatively little error.

Acknowledgments. We wish to acknowledge helpful discussions with M. Lees who suggested the method of numerical solution in appendix 2 and some of the mathematical results in appendix 1. Some of the initial investigations of the steady-state aspects were done by A. Ramo. We wish to thank C. Chase for his careful efforts in the calculation and tabulation of the special functions used in this work.

This work was supported by the National Science Foundation.

REFERENCES

Carslaw, H. S., and J. C. Jaeger, *Conduction of Heat in Solids,* 510 pp., Oxford University Press, 1959.

Forsythe, G. E., and W. R. Wasow, *Finite Difference Methods for Partial Differential Equations,* 444 pp., John Wiley & Sons, 1964.

Jeffreys, Harold, *The Earth, Its Origin, History and Physical Constitution,* 438 pp., Cambridge University Press, 1962.

Kennedy, G. C., The origin of continents, mountain ranges, and ocean basins, *Am. Scientist, 47,* 491, 1959.

Lovering, J. F., The nature of the Mohorovicic discontinuity, *Trans. Am. Geophys. Union, 39,* 947–955, 1958.

MacDonald, G. J. F., and N. F. Ness, Stability of phase transitions within the earth, *J. Geophys. Research, 65,* 2173–2190, 1960.

Neumann, Franz, Lecture (mentioned in Riemann-Weber: *Die partiellen Differentialgleichungen der mathematischen Physik*, vol. 2, p. 121, 5th edition, 1912), 1860.

Ringwood, A. E., and D. H. Green, Experimental investigations bearing on the nature of the Mohorovicic discontinuity, *Nature, 201,* 566–567, Feb. 8, 1964.

Wetherill, G. W. Steady-state calculations bearing on geological implications of a phase-transition Mohorovicic discontinuity, *J. Geophys. Research, 66,* 2983–2993, 1961.

(Manuscript received May 8, 1967; revised July 12, 1967.)

CHAPTER II

RESPONSE OF PHASE BOUNDARIES IN THE UPPER MANTLE TO SEDIMENTATION AND EROSION

The possible geologic consequences of shallow phase changes in the mantle have been noted and qualitatively discussed by Lovering (1958) and Kennedy (1959) and others. The geologically most interesting consequences are subsidence accompanying sedimentation because of the conversion of a low density phase to higher density owing to the increase in pressure from the overlying sediments, and the subsequent uplift of the sediments as a result of the rise in temperature at depth caused by the thermal blanketing effect of the sediments. Thus this mechanism is a candidate for explaining thick sediment sections deposited in relatively shallow water, and the subsequent uplift of the sediments above sea level.

In order to consider the question of whether the phase change mechanism is an important geologic process, one must have quantitative information about the behavior of a phase change model; and in view of the diversity of geologic conditions, one actually needs a quantitative understanding of the problem general enough to be applied to a number of different cases, and specific enough to give details of the behavior of the model to an accuracy comparable to that obtained from the geologic record. We will give a solution that meets these criteria, thus allowing the behavior of phase changes models to be easily understood and computed. Such phase change models are then a suitable means for exploring geologic phenomena, allowing one to delimit the various phenomena that can be explained by such a model, even though a phase change model might not be the correct one.

The problem of a moving phase boundary which is of interest in this problem is a type of Stefan problem, in which the location of the phase boundary must be determined together with the solution

of the partial differential equation of heat transfer. The formal problem is complicated by the nonlinearity of the boundary condition at the phase boundary, and the presence of convective heat transfer and of heat sources. Since an analytic solution has not been found, MacDonald and Ness (1960), van de Lindt (1967), and Joyner (1967) obtained numerical solutions of several specific models. MacDonald and Ness did not include the effects of isostasy, which is of paramount importance. Thus they were not able to explain very great thicknesses of sediments from their calculations. Van de Lindt (1967) did include isostasy in his numerical calculations based on MacDonald and Ness's models; however, possible errors in his work have been pointed out by O'Connell (1968). Nevertheless, these solutions are certainly suggestive in showing that a phase change mechanism with isostasy could in certain cases account for the deposition of great thicknesses of sediments and their subsequent uplift as was suggested by Wetherill (1961) on the basis of steady state models, who also pointed out some errors in the paper of MacDonald and Ness. Nonetheless, the numerical solutions still leave many questions unanswered, and more importantly, they do not provide sufficient understanding of the problem, so that the geologic consequences of phase changes can be discussed in a simple manner separate from the technical difficulties inherent in the solution of the mathematical model or from the various shortcomings of the model itself. This is especially important in view of the uncertainty of both the values of the physical parameters and the choice of proper

boundary conditions. It is important in this problem to know if the behavior of a particular model is inherent in the phase change mechanism or is only a numerical peculiarity of that one model.

O'Connell and Wasserburg (1967) (hereafter referred to as OW, which is reproduced as Chapter I of this thesis) have obtained an analytic approximation to the solution of this problem that overcomes the difficulties associated with numerical solution. This approximation defines characteristic time constants which allow the identification of different time domains during which the motion of the phase boundary exhibits a certain type of behavior. It is also shown that convected heat and radioactive heat sources have only a small effect on the problem, and may be safely neglected. The analytic expressions describing the motion of the phase boundary that one obtains from the approximation are in fact quite simple, and depend primarily on the difference in slope of the Clapeyron curve and the earth's temperature curve at the phase boundary divided by the latent heat of the phase change. For long times the expressions also depend on the distance of the phase boundary from the surface, and the position at which the lower boundary condition is applied, as well as the boundary condition itself.

Since the rationale and justification of the analytic approximations have been dealt with at length in our previous paper, we shall not go into them here. The object of this paper is to collect the analytical expressions relevant to phase changes in the mantle, present them in usable form, extend the approximations, and compare the results of the approximations with the numerical results of another worker (Joyner, 1967). In doing these things,

we hope to demonstrate the usefulness and simplicity of the approximations we have developed, and to indicate how they allow the geologic problem to be attacked in both a quantitative and qualitative manner.

In order to provide a conceptual framework for our discussion, we shall first qualitatively describe the history of a sedimentary basin underlain by a phase change. The basin has an initial depth w_0, is full of water, and is subject to sedimentation. After some sediments are deposited, the original surface will subside owing to isostatic response to the load of the sediments. This will proceed at a rate characterized by the isostatic response time. Owing to this subsidence, the reduction in the depth of the water will be less than the thickness of sediments deposited.

In addition to the isostatic response, the phase boundary will also respond to the load from the sediments. The depth of the phase boundary is determined by the pressure and temperature distribution in the earth. Changes in either of these can change the equilibrium position of the phase boundary. Sediments deposited on the surface will increase the pressure at depth; we assume that the surface pressure is transmitted perfectly to the depth of the phase boundary and is not supported by the strength of the overlying material. This causes the phase boundary to move and low density material to change to a denser phase. The conversion of a low density, high entropy phase to a high density, low entropy phase will result in the liberation of heat at the phase boundary. The removal of this extra heat will govern the rate of movement of the phase boundary.

The reduction in volume from the change in phase will cause the original surface to subside. This subsidence will be in addition to that from isostasy, and will have the same effect. The total subsidence will be the sum of the subsidence from the two mechanisms.

The latent heat released at the phase boundary will result in a transient temperature field associated with the moving phase boundary. Initially, after the start of sedimentation, this transient temperature perturbation will be largely confined to the immediate vicinity of the phase boundary. We shall call the short time or initial response of the phase boundary that movement of the phase boundary during the period when the temperature perturbation from the latent heat is substantially unaffected either by the thermal boundary conditions arising from the presence of the surface or by thermal boundary conditions specified at depth in the earth. This is illustrated in Figure 1.

In contrast to the short time response defined above, we shall call long term response that movement of the phase boundary during the period when the temperature field near the phase boundary is predominantly determined by the temperature distribution of the entire region under consideration, which in turn depends on the boundary conditions at the surface and at depth and on the distribution of thermal conductivity with depth. This is also illustrated in Figure 1.

Owing to the subsidence of the surface and the different thermal conductivities of the two phases, the movement of the phase boundary may result in a temperature distribution which differs

FIGURE 1

Temperature field for different regimes of behavior. During short time behavior, the temperature near the phase boundary $M(t)$ is not influenced by either boundary or by the sediments on the surface. During blanketed response, the temperature field near $M(t)$ is noticeably influenced by the thermal blanketing of the sediments. During long time response, the temperature field in the whole region between the surface and the lower boundary is primarily influenced by the boundary conditions at the boundaries. Also shown is a representative illustration of the history of a sedimentary basin subsiding as it is filled with sediments. The sediments will probably be eroded after they emerge above sea level. (Note: temperature effects exaggerated in Figure.)

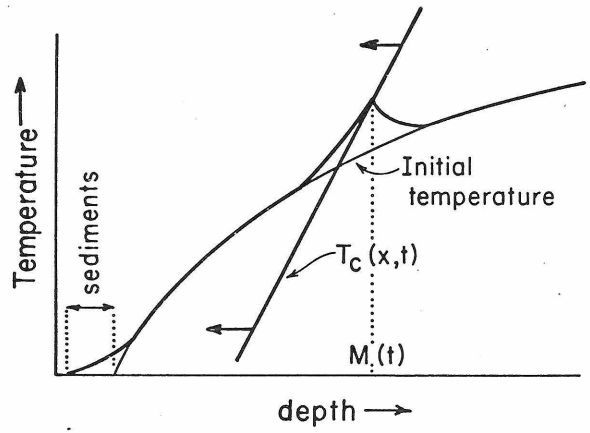

Short time behavior

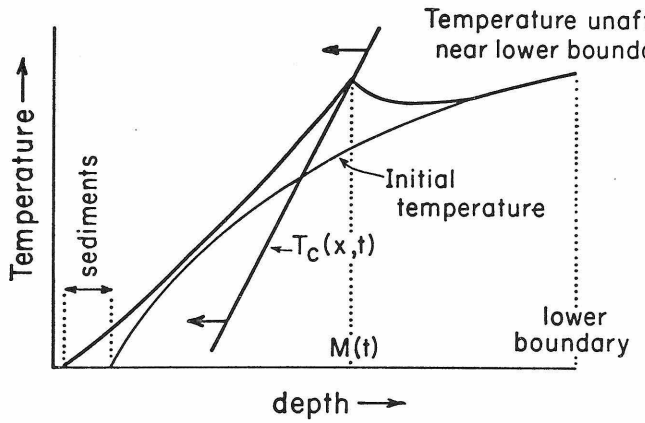

Blanketed response

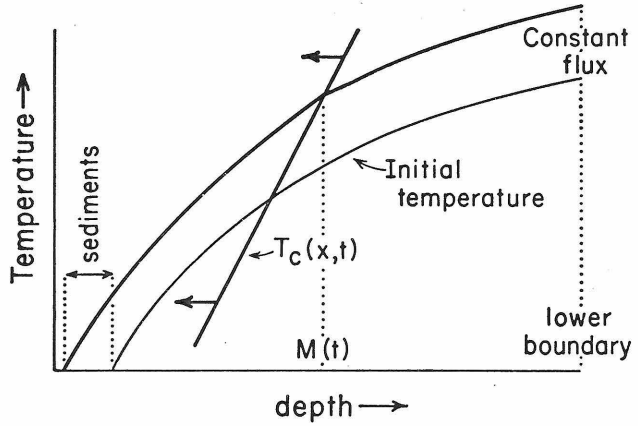

Long time response

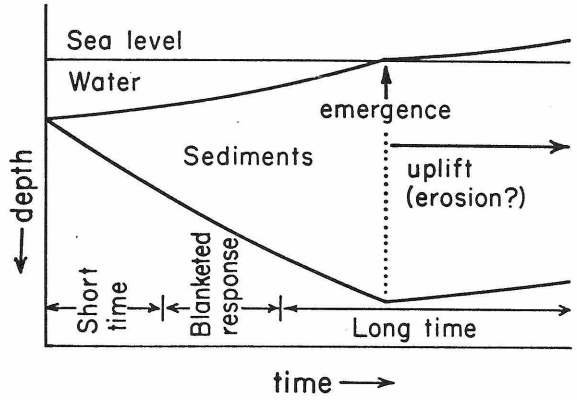

FIGURE 1

from the initial temperature distribution over the entire region in consideration which may extend to considerable depths in the earth. For our analysis, this region is limited by a lower boundary. The position of this boundary, and the boundary condition specified at it, will influence the temperature field of the whole region above it, and can significantly influence the motion of the phase boundary.

Thus as sedimentation proceeds, the phase boundary will first exhibit short time behavior. Eventually, the thermal effects of the boundaries will begin to predominate, and the motion of the phase boundary will enter the regime of long term behavior.

During the period of short term response, the thermal effect of the sediments on the surface will be negligible. When the thermal effects of the sediments do finally reach the phase boundary, they will affect its motion by favoring the conversion of the low entropy, high density phase to the higher entropy, lower density phase. This effect is just opposite to that from the pressure loading from the sediments, and will tend to retard or reverse the upward motion of the phase boundary due to the pressure loading.

We shall call blanketed response the movement of the phase boundary when it is substantially affected by the blanketing effect of the sediments. Note that this differs from long term response since the latter includes the effects of both surface and the lower boundary. This is illustrated in Figure 1.

In summary then, as sedimentation proceeds in the basin, the rate of subsidence due to the phase change will decrease as the period of initial response gives way to that of blanketed response.

Consequently the water depth will decrease more rapidly. Eventually the basin will fill up completely with sediments. Owing to the subsidence due to both the phase change and isostasy, the basin will contain a thickness of sediments considerably greater than the initial water depth. Presumably, sedimentation will stop when the basin fills up. With the cessation of sedimentation, the changing pressure responsible for the upward motion of the phase boundary will cease. The effect of thermal blanketing will continue for some time, however, since thermal equilibrium will not be immediately attained. Thus the response of the phase boundary will be dominated by the thermal blanketing, and it will move downward, away from the surface. This will change dense material to less dense, and will cause the surface to be uplifted above sea level. As the sediments are uplifted they will presumably be eroded. This will cause a decrease in pressure, and will force the phase boundary to move even deeper, uplifting the sediments in response to erosion. Thus just as subsidence from sedimentation allows a basin to exist even after sediments thicker than the initial water depth had been deposited, so emergence occasioned by erosion can maintain elevations above sea level even though considerable thicknesses are eroded away.

Model for Analytic Description

We now turn to a quantitative treatment of the problem. The basic model used to represent the crust and upper mantle, including the effects of a phase change and isostasy, is that introduced before (OW, p. 396).

		$x = x_w$	sea level
			$w \equiv x_s - x_w$
water	ρ_w	$x = x_s$	top of sediments
			$s \equiv - x_s$
sediment	ρ_s, K_s	$x = 0$	bottom of sediments
low-density phase	ρ_1, K_1	$x = M$	phase boundary
high-density phase	ρ_2, K_2	$x = b$	thermal lower boundary
asthenosphere	ρ_c	$x = x_c$	level of isostatic compensation

The origin of the coordinate system $x = 0$ is fixed in the upper crust at the original sedimentation surface. Mean sea level, x_w, the top of the sediments x_s, the position of the phase boundary M, the bottom of the denser phase b, and the level at which isostatic compensation takes place x_c, are all expressed relative to the origin in the upper crust. The water density ρ_w is equal to 1 if $w > 0$ and is equal 0 if $w < 0$, to take into account the fact that no water will be present when the surface is above sea level.

This is thus a model of a sedimentary basin with water of depth $w = x_s - x_w$ with sediments of thickness $s = - x_s$. We consider the basin to be in isostatic equilibrium when the mass per unit area is the same after the deposition of sediments as it

was before. Our reference level is mean sea level, which is fixed with respect to the level of isostatic compensation. Thus $x_c - x_w$ is constant. In addition the mass between $x = b$ and $x = 0$ is conserved, although the volume may change owing to the motion of the phase boundary.

We shall assume that the phase boundary is a plane separating the two phases. Thus we do not permit the nucleation of a phase away from the phase boundary or the presence of a mixed phase region.

In order to treat the motion of the phase boundary M, we shall neglect the presence of radioactive heat sources. This has been previously justified (OW, pp. 347, 384-390). Thus the temperature near the phase boundary is similar to that shown in Figure 2, except that the initial temperature curve near the phase boundary is taken as linear with slope $\partial T(x, 0)/\partial x = J_M/K_1$ where J_M is the original heat flux at the phase boundary and K_1 is the thermal conductivity of the low density phase which was originally present in this region.

If there were no thermal transients associated with the movement of the phase boundary, it would be at the intersection of the Clapeyron curve and initial temperature distribution, M_e, as shown in Figure 2. Because of the latent heat of the phase change, there will be a thermal transient due to the release of latent heat at the phase boundary, and $M(t)$, the position of the phase boundary, will actually lag a distance $\ell(t)$ behind M_e. Since

FIGURE 2

Temperature field near moving phase boundary. $M_e(t)$ is defined as the intersection of the Clapeyron curve $T_c(x, t)$ and the initial temperature curve $T(x, 0)$. The phase boundary $M(t)$ will lag a distance $\ell(t)$ behind $M_e(t)$ because of transient thermal effects due to the release of the latent heat of the phase change. The thermal effect of sediments on the surface is also indicated.

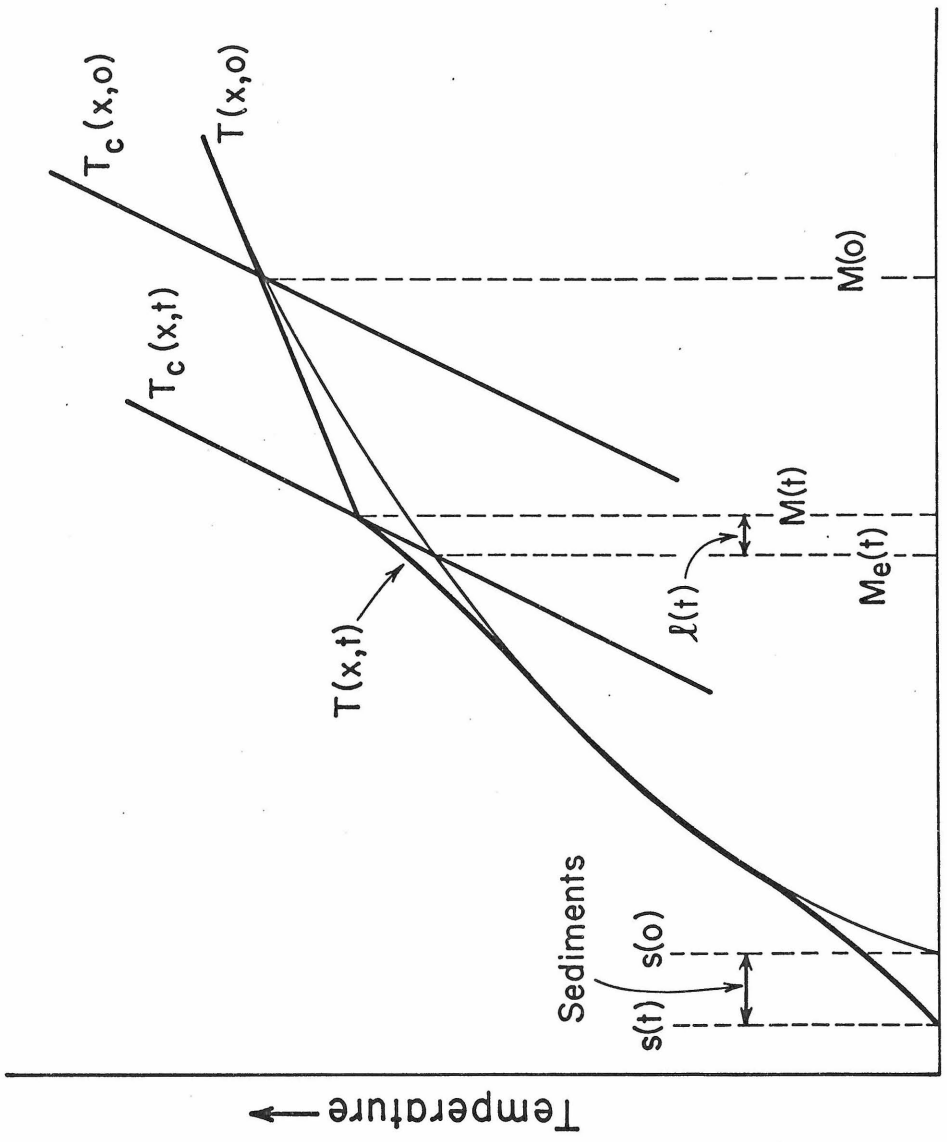
Temperature
Depth
Sediments
s(t)
s(o)
T(x,t)
T_c(x,t)
T_c(x,o)
T(x,o)
ℓ(t)
M_e(t)
M(t)
M(o)

FIGURE 2

we can compute M_e at any time from a knowledge of the pressure and initial state of the model, we can write $M(t) = M_e(t) + \ell(t)$ in which case all the information about the dynamic response of the phase boundary is contained in the lag, $\ell(t)$. For our model, neglecting heat sources,

$$M(0) - M_e(t) = \frac{G[P_0(t) - P_0(0)]}{[G\rho_1 g - J_M/K_1]}$$

where the Clapeyron slope is $\frac{\partial T_c}{\partial P} = G$ and $P_0(t)$ is the pressure at the surface.

We thus obtain the following basic relation for an isostatic model between water depth w, initial water depth w_0, sediment thickness s, and the lag of the phase boundary ℓ,

$$Q_w w - Q_{w_0} w_0 + Q_s s = -\ell\rho_1 \left(\frac{1}{\rho_1} - \frac{1}{\rho_2}\right) \tag{1}$$

where Q_i are constants defined by the initial conditions of the model:

$$Q_i \equiv \rho_i\left[\frac{1}{\rho_i} - \frac{1}{\rho_c} - \frac{1}{W}\left(\frac{1}{\rho_1} - \frac{1}{\rho_2}\right)\right]; \quad i = s, w, w_0 \tag{2}$$

and

$$W \equiv 1 - \frac{J_M}{K_1 G\rho_1 g} \equiv 1 - \frac{\partial T(x,0)}{\partial x}\bigg|_{x=M} \Big/ \frac{\partial T_c(x)}{\partial x}\bigg|_{x=M} \tag{3}$$

This relationship has been given and discussed previously (OW, p. 398), and it was noted that the model may be unstable in the sense that an increase in sediment thickness could result in an increase in water depth. This remarkable effect is an example of the magnitude and possible importance of this mechanism and had not previously been recognized, and will be discussed more fully later.

When sedimentation starts at some rate in water of depth w_0, the original surface will subside owing to both the isostatic effect and the movement of the phase boundary. Insofar as the time scale of the sedimentation process we are considering is longer than the characteristic time for isostatic response, we can consider the model to be in isostatic equilibrium at all times, in which case Equation (1) applies. Thus at any time we can compute the water depth w, knowing the sediment thickness s, and the lag of the phase boundary ℓ.

On the other hand, if the isostatic response time is long compared to the time scale we are considering, we must include the effect of imperfect isostatic adjustment. This could be done, but since the time scale with which we shall be concerned in this problem is of the order of millions of years, and the characteristic time for isostatic processes is of the order of tens of thousands of years (McConnell, 1965), our assumption of instantaneous isostatic response should suffice for most cases. The limiting case with no isostasy corresponds to letting $\rho_c \to \infty$ in (1). The non-isostatic response can thus be readily compared with the isostatic case. This also gives an estimation of the effect of imperfect isostasy without going to the trouble of obtaining an explicit solution.

On the basis of this model, knowing the lag $\ell(t)$, allows us to describe a basin in which sediments are being deposited. Eventually the basin will completely fill with sediments and sedimentation will stop. Throughout the whole period during which the basin is filling up, Equation (1) will apply, so long as the lag is correct, and the various regimes of motion mentioned before are considered in its calculation. The basin will be full, of course, when $w = 0$. The sediment thickness s given by Equation (1) when $w = 0$ is the thickness of sediments that can accumulate in the basin.

Before explicitly calculating the exact value of the lag, we can obtain certain characteristics of the model. By setting $\ell = 0$ and $w = 0$ in Equation (1) and solving for s, we obtain the maximum sediment thickness that can be deposited in the basin. This will be a strict upper bound to the thickness, which would be attained only if there were no thermal effects associated with the motion of the phase boundary. The equation for this maximum thickness is then:

$$s_{max} = \frac{Q_{w_0}}{Q_s} w_0 \tag{4}$$

For an unstable model Q_s is negative and Equation (4) is meaningless, since it may give a non-positive value for s_{max}. The definition of any conditions for instability (OW, p. 399) come from considering the incremental change in water depth w, with sedimentation by differentiating Equation (1):

$$\frac{dw}{ds} = - \frac{Q_s}{Q_w} - \frac{\rho_1}{Q_w} \left(\frac{1}{\rho_1} - \frac{1}{\rho_2}\right) \frac{d\ell}{ds} \tag{5}$$

At a given instant of time $\frac{dw}{ds} < 0$ corresponds to a basin being filled as a result of sedimentation, and the model is considered as dynamically stable. If, on the other hand, $\frac{dw}{ds} > 0$ the basin will become deeper as sedimentation proceeds, and we consider the model as dynamically unstable in this instance. If $Q_w > 0$ (note that $Q_w > Q_s$), this will be the case if

$$Q_s + \left(1 - \frac{\rho_1}{\rho_2}\right) \frac{d\ell}{ds} < 0 \qquad (6)$$

From Equation (2), Q_s will be negative if the ratio of the slopes $J_M/K_1 G\rho_1 g$ is sufficiently near 1, i.e., if W is small enough. Thus Q_s can be negative when the slopes of the Clapeyron curve and temperature curve are nearly the same at the phase boundary. Although for typical models $d\ell/ds$ is positive, a large negative value of Q_s could cause the model to be unstable by overwhelming the term in $d\ell/ds$ in (6).

If Q_s is positive for a given model, the appearance of dynamic instability is precluded if $d\ell/ds$ is positive. A model satisfying this is termed stable. If Q_s is negative we cannot know if the model will exhibit instability until we know $d\ell/ds$. Nevertheless, since the possibility of instability exists, we shall term such a model unstable. Examples of stable and unstable behavior are shown in Figure 3.

For some cases with a varying sedimentation rate, $\frac{d\ell}{ds} \equiv \frac{d\ell}{dt} \Big/ \frac{ds}{dt}$ may be negative or undefined. In such cases, the above treatment of dynamic instability may not apply, and new

FIGURE 3

Comparison of stable and unstable behavior. For a stable model, the water depth always decreases as sediments are deposited, and the basin fills up. For an unstable model, there may be times of dynamic instability when the water depth increases as sediments are deposited. Thermal blanketing eventually causes the behavior to become dynamically stable again so that the basin does eventually fill up.

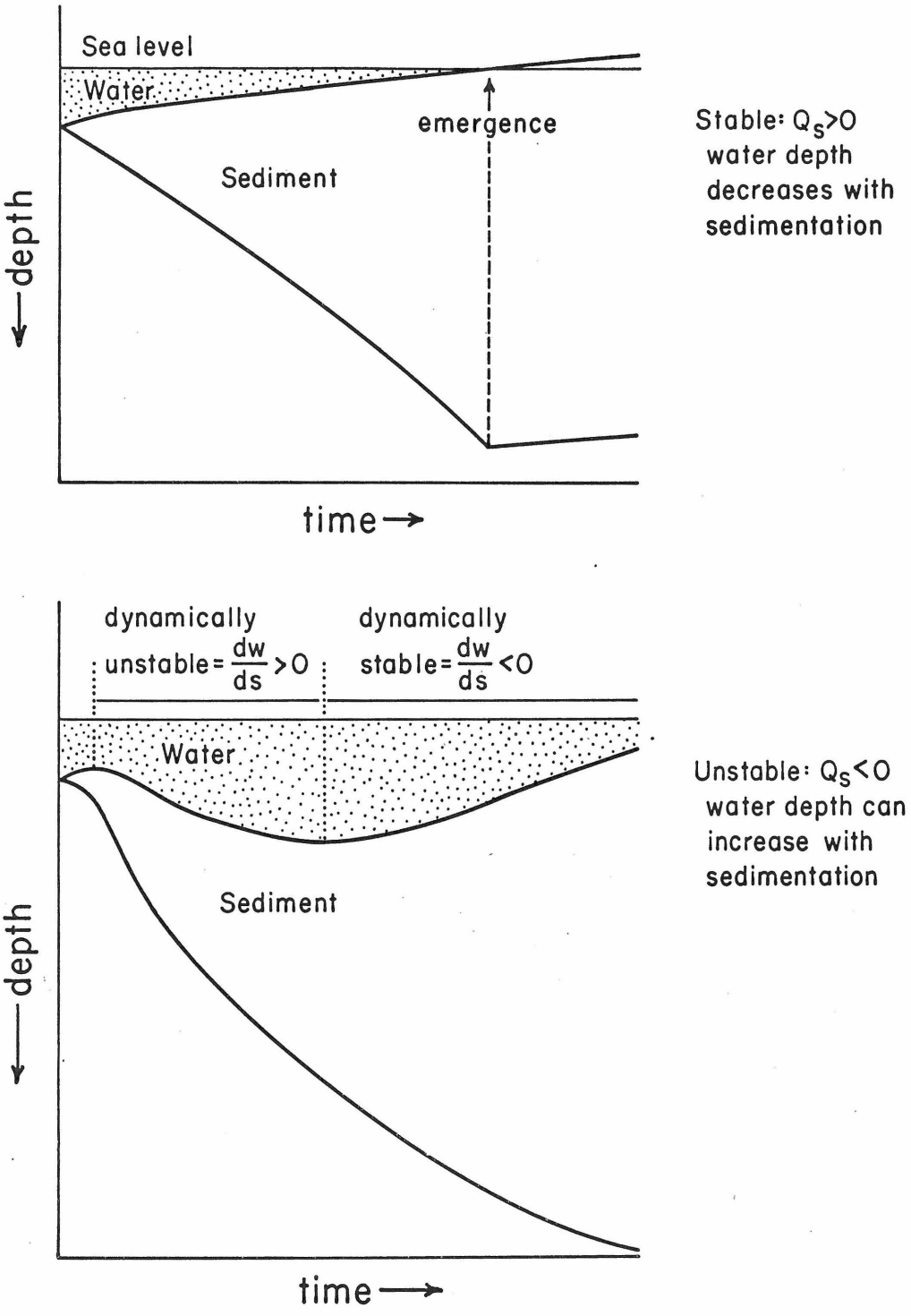
Sea level
Water
emergence
Sediment
depth
time
Stable: $Q_s>0$ water depth decreases with sedimentation
dynamically unstable = $\frac{dw}{ds}>0$
dynamically stable = $\frac{dw}{ds}<0$
Water
Sediment
depth
time
Unstable: $Q_s<0$ water depth can increase with sedimentation

FIGURE 3

criteria may have to be found based upon more detailed knowledge of $d\ell/ds$. For models with a constant sedimentation rate, our criteria suffice.

Thus Equation (4) is valid only for stable models. For unstable models there is no absolute maximum to the sediment thickness. Only consideration of the value of the lag can indicate the thickness of sediments that the basin can accept before filling up.

We shall present expressions for the lag $\ell(t)$ for the various regimes of motion defined previously. The basis of and justification for the analytical expressions for the value of the lag have been treated at length in our previous paper (OW). Since different expressions apply for different regimes of the motion we shall present the criteria for distinguishing these regimes and the proper expressions for the lag during each regime. In addition we shall extend some of our previous work to treat the problem of thermal blanketing for longer times.

The analytic results we shall present recommend themselves through their simplicity and the insight they give into the fundamental characteristics of the problem. Moreover, they are accurate enough to allow one to investigate the problem without resorting to more sophisticated methods, including numerical solutions for each specific model. All of our approximations derive ultimately from approximating the temperature field and then formally deriving the motion of the phase boundary. These approximate solutions have been compared with numerical solutions of the exact equations for many cases in our previous paper with

excellent agreement. Thus our analytic results may be regarded either as approximate solutions formally derived from the equations governing the problem or as an empirical scheme for interpolating between the numerical solutions which have been obtained.

Short Time or Initial Response

The initial behavior of the phase boundary is obtained from the Stefan approximation (SAC) presented in our previous paper. Implicit in this approximation is the assumption that the phase boundary is in an infinite medium; consequently, we shall use this solution only until the time when the finite nature of the medium becomes important.

The change in temperature from the initial state is

$$\Theta(x,t) = \frac{\Theta_c(M)}{1 - \operatorname{erf}\lambda}\left[1 + \operatorname{erf}\left(\frac{x - M(0)}{2(\kappa_1 t)^{1/2}}\right)\right] ; \quad x \le M(t)$$

$$\Theta(x,t) = \frac{\Theta_c(M)}{1 + \operatorname{erf}(\lambda/\sqrt{\alpha'})}\left[1 - \operatorname{erf}\left(\frac{x - M(0)}{2(\alpha'\kappa_1 t)^{1/2}}\right)\right] ; \quad x \ge M(t) \tag{7}$$

where

$$\alpha' \equiv \frac{K_2\rho_2 c_2}{K_1\rho_1 c_1}$$

$$\Theta_c(x) \equiv \left(G\rho_1 g - \frac{J_M}{K_1}\right)\left[x - M_e(t)\right]$$

and λ is defined by $M(0) - M(t) = 2\lambda(\varkappa_1 t)^{1/2}$

For this approximation, the motion of the phase boundary is described by the differential equation:

$$\frac{d}{d(\varkappa_1 t)^{1/2}}[M(0) - M(t)] = -\mu[M(0)-M(t)]+\frac{\mu}{W}\frac{\rho_s}{\rho_1}s(t) \qquad (8)$$

where the constant

$$\mu \equiv \frac{2}{\sqrt{\pi}} \frac{G\rho_1 gWc_1}{L}[1 + (\alpha')^{1/2}]$$

is the fundamental rate constant for the response of the phase boundary, and has the dimension of inverse length. Equations (7) and (8) contain the effect of convected heat arising from the density change across the moving phase boundary (Appendix 1). This effect was not included in our previous paper (OW, p. 391).

Integrating (8) yields

$$M(0) - M(t) = \frac{\mu}{W}\frac{\rho_s}{\rho_1} e^{-\mu(\varkappa_1 t)^{1/2}} \int_0^{(\varkappa_1 t)^{1/2}} e^{\mu(\varkappa_1 z)^{1/2}} s(z)d(\varkappa_1 z)^{1/2} \qquad (9)$$

We can define certain characteristics of the solution in terms of the characteristic rate constant μ even without knowing the form of the sedimentation function $s(t)$. The condition of secular equilibrium is defined as that obtaining when

$$\frac{1}{s(t)} \frac{ds(t)}{dt} << \frac{1}{2} \mu \left(\frac{\kappa_1}{t}\right)^{1/2} \tag{10}$$

This will be the case when the left-hand side of (8) is negligible and

$$M(0) - M(t) \approx \frac{\rho_s}{\rho_1} \frac{s(t)}{W}$$

This condition essentially says that the lag will be small compared to the total displacement of the phase boundary.

From (9) we see that transients will decay as $\exp(-\mu(\kappa_1 t)^{1/2})$. Thus a criterion for times long enough so that transients will have decayed is $\mu(\kappa_1 t)^{1/2} >> 1$. Details in sedimentation will no longer be important or resolvable after a time satisfying this criterion.

Similarly, the model with continuous loading will behave similarly to an impulsively loaded model if the load is applied over a time satisfying

$$\frac{2}{3} \mu (\kappa_1 t)^{1/2} << 1$$

This criterion is independent of the loading rate. The phase boundary is unable to respond to changes in the sedimentation rate which occur in a time satisfying this criterion. Rather the phase boundary will respond as if a constant average load had been applied

during this time. In a sense, this criterion defines the "resolution" of the response of the phase boundary to rapid changes in sediment thickness.

We shall consider only the case where the sediment thickness is a linear function of time, i. e. the case of a constant sedimentation rate. We emphasize that this is only for convenience, since (10) holds for any sedimentation s(t). Integrating (9) for s(t) = kt where k is constant, we obtain for the lag $\ell(t)$, where

$$\ell(t) \equiv M(t) - M_e(t) = \frac{1}{W} \frac{\rho_s}{\rho_1} s(t) - [M(0) - M(t)]$$

$$\ell(t) = \frac{2}{W} \frac{\rho_s}{\rho_1} \frac{k}{\varkappa_1 \mu^2} [\mu(\varkappa_1 t)^{1/2} - 1 + e^{-\mu(\varkappa_1 t)^{1/2}}] \tag{11}$$

This then, used in (1), permits the calculation of the configuration of the sedimentary basin so long as the assumptions used in constructing approximation SAC remain valid.

Knowing $\ell(t)$ we can evaluate the criterion (6) for the dynamic stability of the model. From (11)

$$\frac{d\ell}{ds} = \frac{d\ell}{dt} \Big/ \frac{ds}{dt} = \frac{1}{k} \frac{d\ell}{dt} = \frac{\rho_s}{\rho_1 \mu W (\varkappa_1 t)^{1/2}} [1 - e^{-\mu(\varkappa_1 t)^{1/2}}]$$

so that (6) becomes

$$1 - \frac{\rho_s}{\rho_c} - \frac{\rho_s}{W}\left(\frac{1}{\rho_1} - \frac{1}{\rho_2}\right)\left[1 - \frac{1}{\mu(\varkappa_1 t)^{1/2}}\left(1 - e^{-\mu(\varkappa_1 t)^{1/2}}\right)\right] < 0$$

Taking the limit $t \to 0$, we see that a model will be initially dynamically unstable only if $\rho_s > \rho_c$; this is the same criterion one would obtain if there were no phase change, but only isostasy, namely, that the sediments be denser than the material at the level of isostatic compensation. Thus a phase change cannot contribute to dynamic instability at the onset of sedimentation.

We should note that the criterion for dynamic instability at time $t = 0$, namely $\rho_s > \rho_c$, rests upon the assumption of instantaneous attainment of isostatic equilibrium. This criterion would be different if we had considered the time dependence of isostatic adjustment. This, however, does not affect our conclusion that a phase change does not contribute to dynamic instability at the very onset of sedimentation.

In the context of approximation SAC, however, an unstable model will be dynamically unstable by a time satisfying

$$\mu(\varkappa_1 t)^{1/2} \geq \frac{\rho_s}{W}\left(\frac{1}{\rho_1} - \frac{1}{\rho_2}\right)\frac{1}{(-Q_s)} \qquad (12)$$

Remember that Q_s is negative for an unstable model. Thus the value of the time satisfying (12) will tell us whether dynamic instability can occur during the period when approximation SAC is valid, as well as give an indication of the degree of dynamic

instability that will occur. We note that (12) is independent of the sedimentation rate.

End of Short Term Behavior

Since the Stefan approximation is based upon a solution in an infinite medium, it will become invalid when the boundaries of the region, at $x = 0$ and $x = b$, begin to substantially affect the temperature field near the phase boundary. The influence of the surface on the phase boundary will be important by a time satisfying

$$\varkappa_1 t \geq \frac{(M + s)^2}{\pi} \tag{13a}$$

and the influence of the lower boundary will be important by a time satisfying

$$\varkappa_2 t \geq \frac{(b - M)^2}{\pi} \tag{13b}$$

Short term behavior will end when either boundary becomes important, i. e. when either of these criteria is satisfied. See Appendix 2 for the derivation of this.

After this time, we should not expect the Stefan approximation to hold up. Nevertheless, experience has shown that the Stefan approximation can often be used as a means of extrapolation for a while beyond this time if necessary.

Long Term Response

For times after the Stefan approximation has broken down, we appeal to a quasi-steady state approximation (QSSA). This has been given in our previous paper for the case where the loading was impulsive (OW, pp. 354, 365, 372). The solution for the continuous case is a straightforward extension of the impulsive case (Appendix 3). The QSSA should be valid when both boundaries affect the phase boundary. The effect of the surface will be felt for times satisfying

$$\varkappa_1 t \geq \frac{(M + s)^2}{\pi} \tag{14a}$$

and the effect of the lower boundary will be felt when

$$\varkappa_2 t \geq \frac{(b - M)^2}{\pi} \tag{14b}$$

Thus when both of these criteria are satisfied, long term behavior should prevail. In general this will occur at a time greater than the time given by (13) for the breakdown of the Stefan approximation, and there will be a transition period during which neither approximation is applicable. Nevertheless, our experience has shown that either one or the other approximation will usually serve as a reasonable means of extrapolating the behavior of the model during this period. This will be discussed later.

The differential equation of motion for the QSSA is (Appendix 3)

$$\frac{d}{d(\varkappa_1 t)}\,[M(0) - M(t)] = -\omega[M(0) - M(t)]$$

$$+ \frac{G\rho_s g c_1}{H}\left[\frac{s(t)}{d} + \left(\frac{d}{2} + \frac{c_2}{c_1}d'\right)\frac{1}{\varkappa_1}\frac{ds}{dt}\right] \tag{15}$$

where

$$\omega \equiv \frac{G\rho_1 g W c_1}{Hd}$$

$$H \equiv L + \frac{1}{2}c_1 G\rho_1 g W d + c_2 d'\left(G\rho_1 g - \frac{\rho_1 J_M}{\rho_2 K_2}\right)$$

and d and d' are constants: d is the average value of M(t) + s(t) and d' is the average value of b - M(t). The sediment thickness s(t) is an arbitrary function of time.

Integrating (15) gives

$$M(t_0) - M(t) = \frac{G\rho_s g c_1}{H} e^{-\omega\varkappa_1 t} \int_{\varkappa_1 t_0}^{\varkappa_1 t} e^{\omega\varkappa_1 z}\left[\frac{s(z)}{d}\right.$$

$$\left. + \left(\frac{d}{2} + \frac{c_2}{c_1}d'\right)\frac{1}{\varkappa_1}\frac{ds}{dz}\right] d(\varkappa_1 z) \tag{16}$$

As in the Stefan approximation, a criterion for times long enough so that transients have decayed is that $\omega \kappa_1 t \gg 1$. Since the QSSA will not be valid for short times, one should employ it only after the time given by (14), say t_0. Thus the solution QSSA should be matched with solution SAC at time t_0 when the transition is made from one solution to the other.

When the sediment thickness is a linear function of time, $s = kt$, we obtain for the lag of the phase boundary, with the lower limit of integration $t_0 = 0$

$$\ell(t) = \frac{G\rho_s g c_1}{H} \frac{k}{\kappa_1} \left[\frac{1}{d\omega^2} - \frac{1}{\omega} \left(\frac{d}{2} + \frac{c_2}{c_1} d' \right) \right] \left[1 - e^{-\omega \kappa_1 t} \right] \qquad (17)$$

Comparison of (17) and (11) reveals that for short times the lag eventually grows as $t^{1/2}$, whereas for long times the lag approaches a limiting value. Of course, when thermal blanketing is included in the solution, it will cause the lag to grow with time in some other manner.

Blanketed Response

By the time that the boundary effects become important, necessitating use of the QSSA, the thermal blanketing from the sediments, which is also a boundary effect, should be making itself felt. This is included in the solution for the motion of the phase boundary by considering the superposition of the temperature field due to the blanketing on that from the latent heat released by the

phase boundary (Appendix 4). We consider here only the case with a constant sedimentation rate.

A criterion for the time by which thermal blanketing would certainly dominate the motion of the phase boundary (OW, p. 66) is

$$\varkappa_1 t = \frac{LK_1\rho_s d}{c_1 J_M \rho_1 W} + \frac{d^2}{6}\left[1 + \frac{12}{\pi^2}\sum_{n=1}^{\infty}\frac{(-1)^n}{n^2} e^{-\frac{n^2\pi^2\varkappa_1 t}{d^2}}\right] \qquad (18)$$

Here $d \equiv \text{ave}[M(t) + s(t)]$ may be obtained from (11) or (17) or else just estimated. For many cases the exponential terms will be negligible, which simplifies matters. Note that (18) does not contain the sedimentation rate explicitly; it enters only through d, and thus its influence is limited.

In our previous paper, we said that the time given by (18) would signal the reversal of the motion of the phase boundary. This is not correct. Rather it will signal the end of the more rapid response of the phase boundary and the start of the retardation of the motion of the phase boundary due to the thermal blanketing. This will not in general result in the reversal of the motion of the phase boundary as was stated before (OW, p. 395).

If the phase boundary is nearer the surface than the lower boundary, blanketed response will be manifested before long term response, since the latter presupposes the influence of both the upper and lower boundaries. In this event, use of the short term approximation including thermal blanketing (SACTB) is indicated

up to the onset of long term behavior, where approximation QSSA with thermal blanketing (QSSATB) will be appropriate.

If the phase boundary is nearer the lower boundary than the surface, on the other hand, use of approximation SAC might be followed directly by use of QSSA and then QSSATB. These considerations depend on the values for the three criteria for: 1) the end of short time response, 2) the onset of blanketed response, and 3) the onset of long term response. These may occur in any sequence, except that (1) must precede (3). These possibilities, combined with other considerations are shown in Figure 4 and will be discussed more fully later.

Short Term Blanketed Response

The expression for the lag of the phase boundary, including the effect of thermal blanketing, is for the Stefan approximation (SACTB):

$$\ell(t) = \frac{2\rho_s k}{W\rho_1 \kappa_1 \mu^2}\psi(t) + \frac{3\sqrt{\pi}\, a_1}{\mu^3}\left[\frac{\mu^3}{6}(\kappa_1 t)^{3/2} - \frac{\mu^2 \kappa_1 t}{2} + \psi(t)\right] \tag{19a}$$

$$+ \frac{\sqrt{\pi}\, a_2}{2\mu}\psi(t) - \frac{\sqrt{\pi}\, a_3}{2}\sum_{n=1}^{\infty}\Phi_n(t)$$

where

$$\Phi_n(t) \equiv h_n \left\{ \frac{\mu}{2\nu_n} \left[e^{-\mu(\varkappa_1 t)^{1/2}} - e^{-\nu_n \varkappa_1 t} \right] - \frac{\mu^2}{2\nu_n^{3/2}} \left[\varepsilon\left(\frac{\mu}{2\nu_n^{1/2}} \right) e^{-\mu(\varkappa_1 t)^{1/2}} \right.\right.$$

$$\left.\left. - \varepsilon\left(\frac{\mu}{2\nu_n^{1/2}} - (\nu_n \varkappa_1 t)^{1/2} \right) e^{-\nu_n \varkappa_1 t} \right] \right\} \tag{19b}$$

$$\varepsilon(x) \equiv \frac{\sqrt{\pi}}{2} e^{x^2} \operatorname{erfc}(x)$$

$$\psi(t) \equiv \mu(\varkappa_1 t)^{1/2} - 1 + e^{-\mu(\varkappa_1 t)^{1/2}}$$

and

$$\nu_n \equiv \frac{n^2 \pi^2}{d^2} + \frac{k^2}{4\varkappa_1^2}$$

$$a_1 \equiv \frac{J_s k^2 \exp(dk/2\varkappa_1)}{2K_s \varkappa_1^2 \sinh(dk/2\varkappa_1) G\rho_1 g W}$$

$$a_2 \equiv \frac{J_s k \exp(dk/2\varkappa_1)}{2K_s \varkappa_1 \sinh(dk/2\varkappa_1) G\rho_1 g W} \left[\frac{2\varkappa_1}{k} - \frac{d}{\tanh(dk/2\varkappa_1)} \right] \tag{20}$$

$$a_3 \equiv \frac{2J_s k \pi^2 \exp(dk/2\varkappa_1)}{K_s \varkappa_1 d^3 G\rho_1 g W}$$

$$h_n \equiv \frac{(-1)^n n^2}{\left(\frac{n^2\pi^2}{d^2} + \frac{k^2}{4\varkappa_1^2}\right)^2}$$

When $\left(\frac{dk}{2\varkappa_1}\right)^2 \ll 1$ the above constants become approximately

$$\nu_n = \frac{n^2\pi^2}{d^2}$$

$$a_1 = \frac{J_s k}{K_s \varkappa_1 d G \rho_1 g W}$$

$$a_2 = -\frac{J_s k d}{6 K_s \varkappa_1 G \rho_1 g W} \qquad (21)$$

$$a_3 = \frac{2\pi^2 J_s k}{K_s \varkappa_1 d^3 G \rho_1 g W}$$

$$h_n = \frac{(-1)^n d^4}{n^2 \pi^4}$$

These approximations, which apply when the sedimentation rate is small, may considerably simplify the computation of $\ell(t)$. Also note that the terms in the infinite sum become small rapidly as t

increases; in fact, the sum is usually negligible by the time that thermal blanketing must be included in the determination of the lag.

Long Term Blanketed Response

Similarly, the quasi-steady state approximation with thermal blanketing (QSSATB) gives

$$\ell(t) = \frac{G\rho_s g c_1}{H} \frac{k}{\kappa_1} \left[\frac{1}{d\omega^2} - \frac{1}{\omega} \left(\frac{d}{2} + \frac{c_2}{c_1} d' \right) \right] (1 - e^{-\omega \kappa_1 t}) + \frac{a_1 d}{\omega} (\omega \kappa_1 t - 1 + e^{-\omega \kappa_1 t}) + a_2 d (1 - e^{-\omega \kappa_1 t}) - d\omega a_3 \sum_{n=1}^{\infty} \frac{h_n}{(\omega - \nu_n)} (e^{-\nu_n \kappa_1 t} - e^{-\omega \kappa_1 t}) \tag{22}$$

The constants a_1, a_2, a_3, h and ν_n are given by (20) or (21) as before. In this case, too, the infinite sum usually becomes small by the time thermal blanketing must be included.

The time at which a basin completely fills with sediment and uplift and erosion begin will depend on several factors, most important being the rate of sedimentation and the initial water depth. When the basin becomes completely full, at time t_f say, the sediment thickness will be

$$s(t_f) = \left[Q_{w_0} w_0 - \ell(t_f) \left(1 - \frac{\rho_1}{\rho_2} \right) \right] \frac{1}{Q_s} \tag{23}$$

This we obtained by setting $w = 0$ in (1). The proper expression to use for $\ell(t)$ will, of course, depend on which regime of motion the phase boundary is in when the basin fills. In any event (23) is a transcendental equation in time which may be solved graphically or by trial and error for the time t_f when the basin fills. In the event of multiple roots of (23), t_f should be taken as the smallest root.

When the basin is full, sedimentation should stop. At this time, the model will not be in thermal equilibrium, and the phase boundary will still have to move to reach its final equilibrium position. With the cessation of sedimentation, the driving force for the upward motion of the phase boundary will stop. The effect of thermal blanketing will persist for some time, however. This will tend to move the phase boundary deeper, which will cause the surface to emerge above sea level. If there is no erosion, i.e., $s(t) = s(t_f)$ for $t \geqq t_f$, the equilibrium value of the lag is

$$\ell(t \to \infty) = \frac{J_s}{K_s G \rho_1 g W} s \tag{24}$$

The final elevation will be given by using (24) in (1), where $-w$ is the elevation above sea level

$$-w = \left[Q_s s - Q_{w_0} w_0 + \frac{J_s s}{K_s G \rho_1 g W} \left(1 - \frac{\rho_1}{\rho_2}\right) \right] \frac{1}{Q_w} \tag{25}$$

Since the surface is above sea level, ρ_w must be taken as equal to zero in calculating Q_w. The elevation given by (25) is the maximum elevation that can be attained from the uplift due to the thermal blanketing effect. This elevation will be attained only if there is no erosion and only after final thermal equilibrium has been reached.

Since the phase boundary will ultimately enter the period of long term motion, the approach of the phase boundary to its final position given by (24), will ultimately be described by the quasi-steady state approximation. If sedimentation stops after long term motion has started, the motion of the phase boundary will be described by

$$\ell(t) - \ell(\infty) = [\ell(t_f) - \ell(\infty)]\, e^{-\omega \varkappa_1 (t - t_f)} \tag{26}$$

where t_f and $\ell(\infty)$ are given by (23) and (24). Similarly, the elevation after t_f will be

$$-w = \frac{1}{Q_w}\left[Q_s s - Q_{w_0} w_0 + \frac{J_s s}{K_s G \rho_1 g W}\left(1 - \frac{\rho_1}{\rho_2}\right)\right]\left[1 - e^{-\omega \varkappa_1 (t - t_f)}\right] \tag{27}$$

Thus final equilibrium will be approached at a rate determined by the long term response constant ω. Expressions (26) and (27) neglect the effect due to thermal transients generated by the change in the sedimentation rate, at time t_f, which enter through the

QSSATB approximation. These effects will be proportional to the sedimentation rate, and should die out as $\exp(-\varkappa_1(t - t_f)/d^2)$, where $d = \text{ave}[M(t) + s(t)]$ as before. A solution including these effects will be given later.

If the basin finally is filled at a time t_f such that $\omega\varkappa_1 t_f \gg 1$ and $\pi^2\varkappa_1 t_f/d^2 \gg 1$, then the exponential terms in (22) will be small, and (23) can be solved directly for the sediment thickness at time t_f, insofar as the QSSATB applies. This gives, with $s(t_f) = kt_f$,

$$\ell(t_f) = \frac{J_s\, s(t_f)}{K_s G\rho_1 g W} + \frac{d}{G\rho_1 g W}\ \frac{k}{\varkappa_1}\left[\frac{H}{c_1 W}\left(\frac{\rho_s}{\rho_1} + \frac{J_s}{K_s G\rho_1 g}\right)\right. \tag{28}$$

$$\left. + \frac{G\rho_s g}{2}\left(d + 2\frac{c_2}{c_1}d'\right) - \frac{J_s d}{6K_s}\right]$$

which allows (23) to be solved

$$s(t_f) = \frac{Q_{w_0} w_0 - \left(1 - \frac{\rho_1}{\rho_2}\right)\frac{kd}{G\rho_1 g W \varkappa_1}\left[\frac{H}{c_1 W}\left(\frac{\rho_s}{\rho_1} + \frac{J_s}{K_s G\rho_1 g}\right) + \frac{G\rho_s g}{2}\left(d + 2\frac{c_2}{c_1}d'\right) - \frac{J_s d}{6K_s}\right]}{Q_s + \left(1 - \frac{\rho_1}{\rho_2}\right)\frac{J_s}{K_s G\rho_1 g W}} \tag{29}$$

Even where this expression may be inexact, as for example if $\omega\varkappa_1 t_f \sim 1$, it indicates the effects of the different parameters. For example, a slower sedimentation rate (smaller k) will permit a

a greater thickness of sediments, so long as long term behavior obtains when the basin finally fills completely.

Considerations in Modeling a Basin

With the analytic expressions we have presented for the lag of the phase boundary, we are now able to quantitatively treat the problem of sedimentation in a basin underlain by a phase boundary. Before actually doing so though, it is useful to consider the possible relations between the various regimes of motion and any other times or events defined by the analytic scheme we have introduced. In addition, we shall outline a possible schedule for attacking the problem, pointing out conclusions that may be drawn at various stages, which provide insight into the particular model being treated.

Presumably, the initial state of the model is known, as well as the sedimentation rate. The first thing to do is to evaluate the constants W and Q_i given by (3) and (2). A small value of W indicates that the phase change may be very responsive to loading, since $M(0) - M_e(t) \propto 1/W$. And the determination of the sign of Q_s will reveal if the model is absolutely stable or not.

If Q_s is positive and the model is absolutely stable, then the maximum sediment thickness can be calculated from (4). From the sedimentation rate, the time needed to attain this thickness can then be calculated. This time should first be compared with the time for the end of short-term response (13) and the time for the onset of long-term response (14). In these two equations, M(0)

may be used as a first approximation for $M(t) + s(t)$ or for $M(t)$ (in the term $b - M(t)$. This comparison will indicate in which time domain the basin will fill up.

If the basin should fill well before the end of short-term behavior, we need not be concerned with the other regimes of motion. If secular equilibrium obtains (as determined from (10)) before the basin is filled, then the sediment thickness when the basin is filled may be quite near the maximum thickness. If the basin should fill before secular equilibrium, on the other hand, the actual sediment thickness may be considerably less than the maximum. These cases are shown as case 1a in Figure 4.

The end of short-term response depends on the effect of the boundary nearest the phase boundary. If this boundary is the surface, then thermal blanketing effects may become important before the end of short-term behavior, necessitating use of the approximation SACTB (19). Thus if the basin should fill near the end of short-term response, this time should be compared with the time, given (18), by which thermal blanketing effects will be large. Then, if indicated, the final sediment thickness can be determined using (19) for the lag. This case is shown as case 1b in Figure 4.

If the boundary nearest the phase boundary is the lower boundary, then short-term response will end before thermal blanketing is important. Thus for this case, in contrast to the previous case, the effect of thermal blanketing need not be considered if the basin is filled during short-term response. This case is shown as case 2a in Figure 4.

FIGURE 4

Effect of different types of behavior on the sediment thickness. During short term response, the attainment of secular equilibrium allows the maximum sediment thickness to be approached more nearly (cases 1ai and 1aii). The end of short term response decreases the sediment thickness that fills the basin (cases 1ai and 2a). The onset of blanketed response markedly reduces the sediment thickness that fills the basin (cases 1b and 2b). Note that the start of blanketed response can occur during either short time or long time behavior. (The maximum sediment thickness is that attained when the lag of the phase boundary $\ell(t) = 0.$)

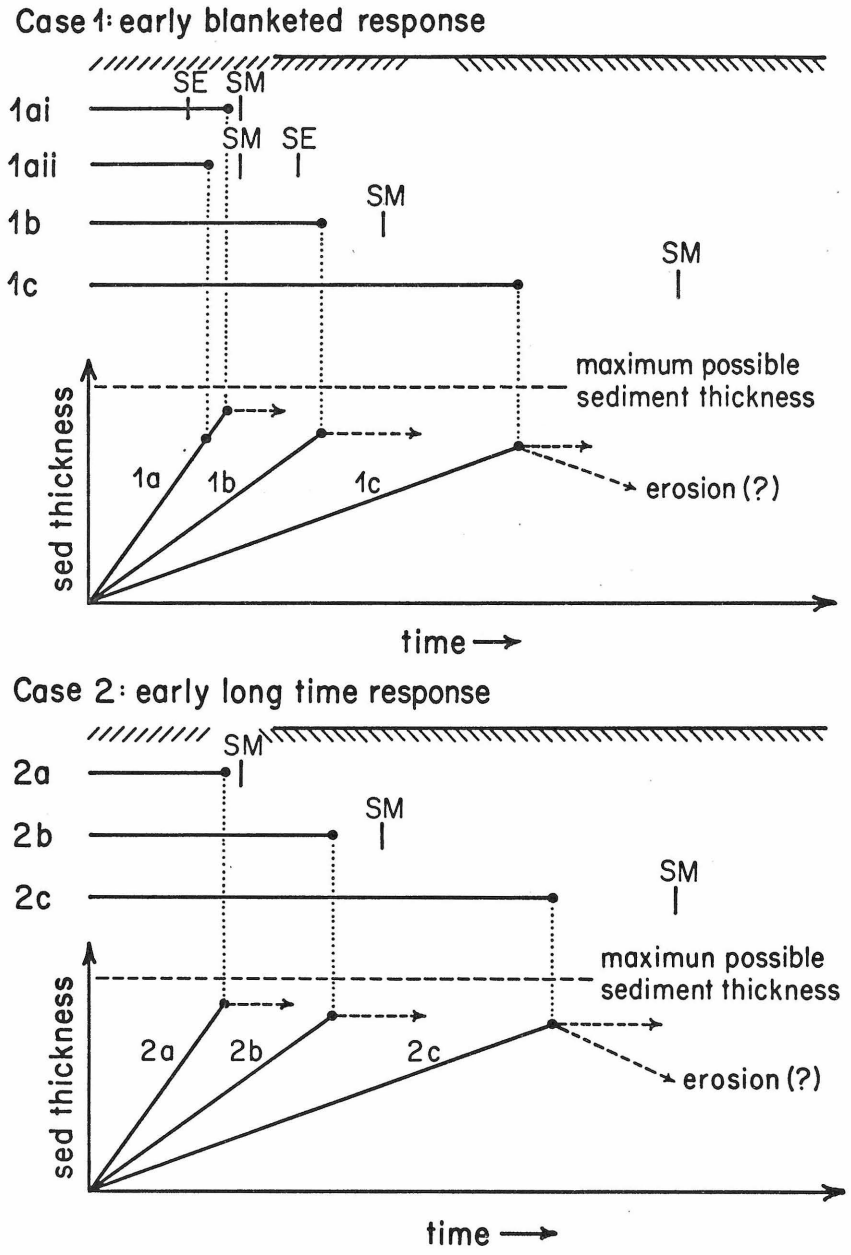
Case 1: early blanketed response
SE
SM
1ai
SM
SE
1aii
SM
1b
SM
1c
maximum possible
sediment thickness
sed thickness
1a
1b
1c
erosion (?)
time
Case 2: early long time response
SM
2a
SM
2b
SM
2c
maximun possible
sediment thickness
sed thickness
2a
2b
2c
erosion (?)
time
Short time response
Long term response
Blanketed response
SE
Time for secular equilibrium
SM
Time for maximum sediment thickness

FIGURE 4

If the time for attaining s_{max} falls in the domain of long-term behavior, then it may not be possible to apply such general reasoning as used above, and the lag must be computed and (23) solved as a transcendental equation. The exception to this is when it takes a very long time for the basin to fill, such that $\omega \varkappa_1 t_f >> 1$. In this case (28) applies, and the final sediment thickness is given by (29). The final sediment thickness will then be considerably less than s_{max}. This case is shown as cases 1c and 2c in Figure 4.

If a model is unstable, it is not possible to calculate a maximum sediment thickness. In such cases, the time for dynamic instability to appear, from (12) should be compared with the time for the end of short-term behavior (13) and the time by which thermal blanketing is important (18). If the model is dynamically unstable during short-term response and before blanketed response, then the water depth will probably not decrease much, if any, during this time. Once blanketed response begins, of course, the water depth will decrease, and eventually the basin will fill. During the whole time, though, equation 1 will apply, with the lag determined from the appropriate formula. If the sedimentation is such that the basin only filled after a long time such that $\omega \varkappa_1 t >> 1$, (23) and (29) will apply, in which the effect of a negative Q_s on the final sediment thickness may be seen. In such a case (26) and (27) will govern uplift if there is no erosion. In (27) a negative Q_s by itself tends to reduce the final elevation, but is played off

against Q_w (which becomes less as Q_s does, but not as fast) and the term in $J_s/K_s G \rho_1 g W$. It is this latter term which actually dominates, since W must be small to make Q_s negative, and $J_s/K_s G \rho_1 g$ should be greater than 1. Thus an unstable model will allow a comparatively thick section of sediments to be deposited, and will in turn tend to uplift the surface to an elevation comparatively high, relative to a similar but stable model.

During the transition period from short-term to long-term response, there are, unfortunately, no hard and fast rules to indicate which expression to use for the lag. The end of short-term response depends on the distance of the boundary nearest the phase boundary; the beginning of long-term response depends on the distance to the boundary farthest from the phase boundary. If the phase boundary is roughly equidistant between the upper and lower boundaries the transition period will be short and should present little difficulty. If the phase boundary is nearer the surface, use of SACTB will take into account the effect of the surface, and thus this approximation may be the best to use during the transition period. If the phase boundary is nearer the lower boundary, then use of QSSA might be best, since it does take into account the effects of the lower boundary. In any event, short-term and long-term solutions may be compared during the transition period; if they differ little then either may be used. If they differ significantly, then it is probably best to adhere to the rules given above.

The two solutions for the motion of the phase boundary including thermal blanketing, SACTB (19) and QSSATB (22) are both correct from $t = 0$, insofar as the solutions without thermal blanketing are also correct. For short times, though, the infinite sums in the solutions do not converge rapidly, thus causing the evaluation of the solution to be tedious. Since the effect of thermal blanketing is small for such short times the corresponding solutions without thermal blanketing may be used with no significant error. However, by the time given by (18), thermal blanketing should be very important; Hence it should be included in the solution some time before this. At any time, the effect of thermal blanketing can be determined by comparing the various terms in the expressions for the lag, (19) and (22).

We may note here that errors incurred in using the wrong approximation during a period of time will be important only in relation to the length of the period compared to the total length of time that we are considering. Thus error incurred during a 10 million year transition period will be relatively small if we are considering the configuration of the basin 150 million years after the start of sedimentation. In fact, even the error incurred in using QSSA rather than SAC during short term response of 20 million years will probably be small.

Comparison with Numerical Results

In our previous paper (OW), we compared the continuous Stefan approximation (SAC) with numerical solutions of the exact equations governing the problem, with excellent agreement, thus

verifying the general validity of the approximation. In addition we similarly showed that the QSSA governed the long-term behavior, and that the effect of thermal blanketing could be superimposed on the solution for the effect of the moving phase boundary.

As a further, and independent, test of our approximate solutions, we shall now compare them with results obtained by another worker (Joyner, 1967) who used a numerical scheme to solve the exact equations. This comparison also allows us to draw general conclusions about the behavior of the models investigated, based on the general understanding gained from the analytical solutions.

The models of Joyner's we have chosen for comparison are models 2, 4 and 5c. The parameters for the models, in our notation, are given in Table 1. The gradient at the phase boundary, J_M/K_1, is taken as that for the initial state of the model at $M(0)$. The change in gradient with depth, due to heat sources, has no significant effect for the range of motion of the phase boundary encountered in these models. Similarly the average gradient in the sediments was taken as that given by the original surface heat flux.

Rather than specifying a constant latent heat for the phase change, as we have, Joyner specified a constant entropy change ΔS. We have taken the latent heat as $T(M(0), 0)\,\Delta S$. The change in latent heat with the position of the phase boundary has no significant effect on these models.

TABLE 1 MODEL PARAMETERS

		MODEL		
		2	4	5c
K_s	joule/cm sec ^oC	0.017	0.025	0.021
K_1		0.025	0.025	0.025
K_2		0.033	0.033	0.033
ρ_s	g/cm^3	2.5	2.7	2.6
ρ_1		2.9	2.9	2.9
ρ_2		3.4	3.4	3.4
ρ_c		3.4	3.4	3.4
c_s	joule/g ^oC	0.85	0.85	0.85
c_1		1.1	1.1	1.1
c_2		1.1	1.1	1.1
G	^oC/kbar	141.0	141.0	66.0
L	joule/g	31.8	31.8	67.9
J_M	erg/cm^2 sec	28.6	28.6	28.6
J_s		45.7	45.7	45.7
d	km	41	41	41
d'	km	19	19	19

For cases such that the gradient at the phase boundary and the latent heat change significantly with the motion of the phase boundary, adjustments can be made in these parameters as the phase boundary moves, or else an average value may be used. For the models considered here, however, this was not necessary.

The derived constants and times for the three models are given in Table 2. We shall discuss each model in turn, but a few characteristics common to all three models are worth mention here.

All the models have a phase boundary at around 40 km depth, while the lower boundary is at 60 km. The lower boundary condition is that of constant heat flux at 60 km. A consequence of this geometry is that the effects of the lower boundary will be felt roughly four times earlier than the effect of the surface. Thus there will be a prominent transition period between short-term and long-term behavior. In accord with our previous discussion, it will probably be best to use the QSSA during most of this period since the lower boundary is nearer to the phase boundary. We shall, however, compare both short-term and long-term solutions during this period.

The density of the lowest layer, that in which isostatic compensation takes place, is equal to the density of the denser phase. Consequently, the isostatic effect is maximized in that a denser substratum would result in smaller isostatic effect. This does not affect the motion of the phase boundary; it only affects the elevation of the surface.

TABLE 2. Derived Model Parameters

	Model		
	2	4	5c
κ_1 cm^2/sec	0.00784	0.00784	0.00784
κ_2	0.00882	0.00882	0.00882
W	0.715	0.715	0.391
Q_S	0.0873	0.0139	-0.102
Q_W	0.635	0.635	0.576
μ $(km)^{-1}$	2.51	2.51	0.30
$1/\mu^2\kappa_1$ y	6407	6407	447,909
$\frac{M(0)^2}{\kappa_1\pi}$ 10^6 y	21.6	21.6	21.6
$\frac{(b-M(0))^2}{\kappa_2\pi}$ 10^6 y	4.13	4.13	4.13
ω $(cm)^{-2}$	5.65×10^{-14}	5.65×10^{-14}	4.18×10^{-14}
H joule/g	1360	1360	470.8
$1/\omega\kappa_1$ 10^6 y	71.6	71.6	96.84

The first model we consider is Joyner's model 2a. This is a model of a sedimentary basin 1.5 km deep being filled at a rate of 200 meters per 10^6 years. From Table 2 we see that the value of W (0.715) is not particularly small compared to 1.0, and that the phase change is not as responsive as it might be if W were smaller. The model is stable.

We shall first compare the four approximations and their relation with the various regimes of motion. Figure 5 shows the lag $\ell(t)$ for all four solutions; SAC, SACTB, QSSA, QSSATB from time $t = 0$ to 50 million years, as well as the end of a short-term response (13), the start of long-term response (14) and the time by which thermal blanketing dominates (18). Also shown is $M(0) - M_e(t)$, which is the value the lag would have if the phase boundary didn't move at all. This, then, is an absolute upper bound for the lag. Comparing SAC and QSSA with their thermal blanket extensions clearly shows the effect of thermal blanketing for longer times. Note that by the time given by (18), thermal blanketing clearly is important, and it should be included in the solution well before this time.

The insert in the upper left-hand corner of Figure 5 is a plot at an expanded vertical scale which better shows the relationship of the solutions for short times. Note that at the end of short time response (4 m. y.) all the solutions are virtually identical. During the transition period, the QSSATB solution is most likely the best, since it takes the lower boundary condition into account as was discussed above. After the start of long term behavior

FIGURE 5

Lag of the phase boundary for different solutions of Joyner's model 2a. For short times (see insert in upper left), the solutions differ only slightly. Note the divergence of the solutions with thermal blanketing (SACTB and QSSATB) from the solutions without thermal blanketing (SAC and QSSA) by the time that thermal blanketing is dominant (14×10^6 y). For short times, SAC is the proper solution. During the transition interval between short and long time behavior ($4 - 22 \times 10^6$ y), QSSATB is probably the best solution since it takes into account the effect of the lower boundary, which SACTB doesn't. For long times, QSSATB is the proper solution.

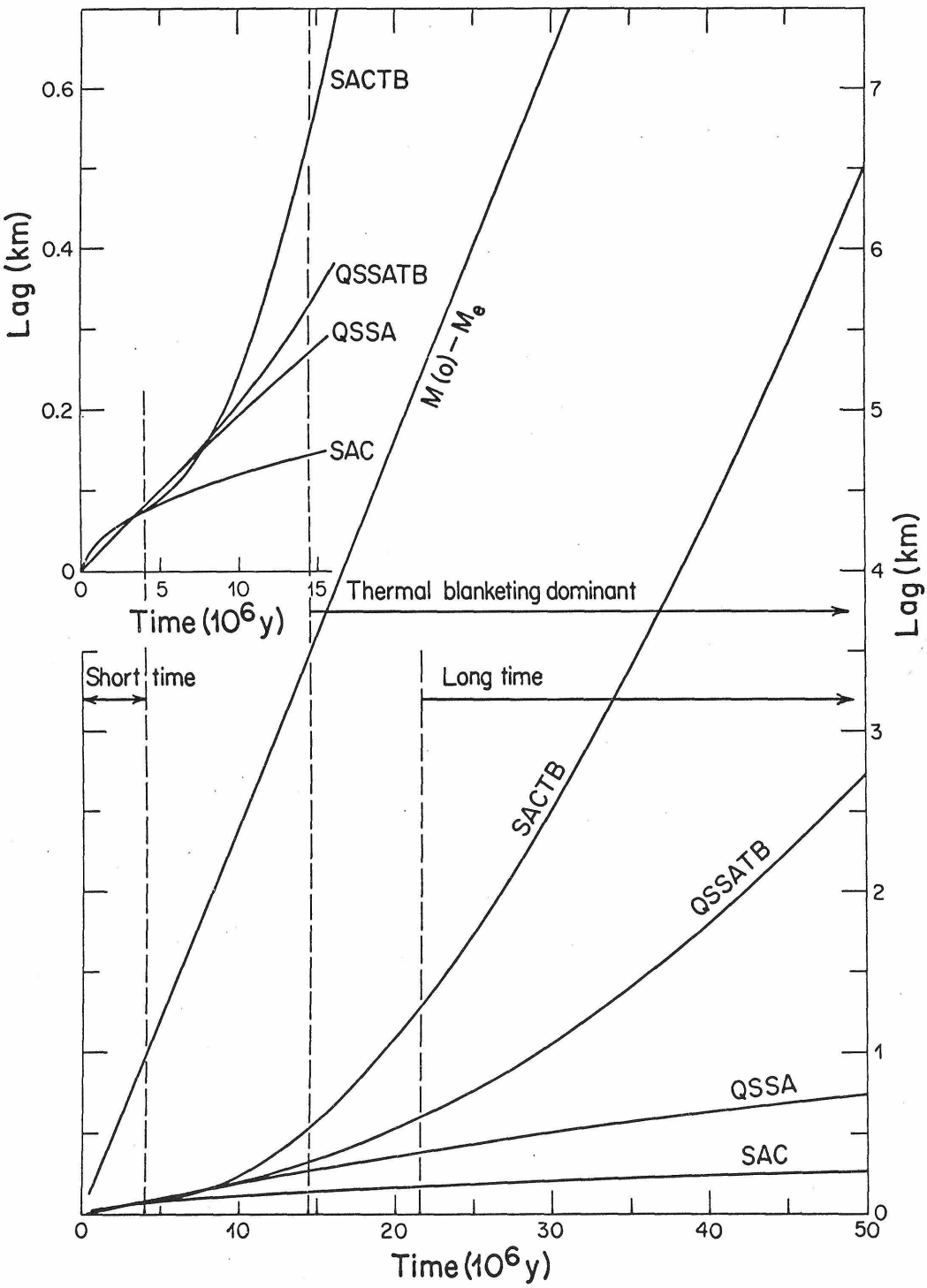
Lag (km)
0.6
0.4
0.2
0
SACTB
QSSATB
QSSA
SAC
M(o) − Me
0
5
10
15
Time (10^6 y)
Thermal blanketing dominant
Short time
Long time
SACTB
QSSATB
QSSA
SAC
0
10
20
30
40
50
Time (10^6 y)
7
6
5
4
3
2
1
0
Lag (km)

FIGURE 5

(22 m. y.), of course, it clearly is the best solution. Owing to the excellent agreement between the SACTB and QSSATB solutions at short times, the QSSATB solution could be used from time $t = 0$ with no noticeable error, in the value of the lag. The temperature field could be in error however.

Because of the way we have defined the lag $\ell(t)$ a large error in its value may still result in a proportionally smaller error in the value of the motion of the phase boundary $M(0) - M(t)$. Thus at 20 m. y., values of the lag from the solutions QSSATB and SACTB differ by a factor of two; in terms of the total motion of the phase boundary the two solutions differ by only $\sim 15\%$.

Figure 6 shows a copy of Joyner's Figure 5, showing his results for model 2a with the analytic solutions QSSATB and SACTB added. As mentioned above, the QSSATB solution is the more accurate; the results of the SACTB solution were added to illustrate that it differs only slightly from solution QSSATB in this plot, in spite of the fact that the values of the lag for the two solutions differ significantly.

The open circles in Figure 6 are Joyner's numerical results for this model. The irregularities in the numerical solution arise from the fact that sediments were deposited in units of 1 km thick slabs rather than continuously. Thus in this model, one km of sediments was placed instantaneously on the surface every 5 million years. This type of deposition produces irregularities in the curve showing the surface of the sediments which may

FIGURE 6

Results for Joyner's model 2a. Solutions QSSATB (solid line) and SACTB (dashed line) compared with Joyner's numerical solution (dotted line). The time at which the surface emerged above sea level is indicated for each solution. The numerical solution probably overestimates the time of emergence (see text). Solution QSSATB is the proper solution; the results for solution SACTB were included to show that it is not in gross error even though it is beyond its regime of applicability.

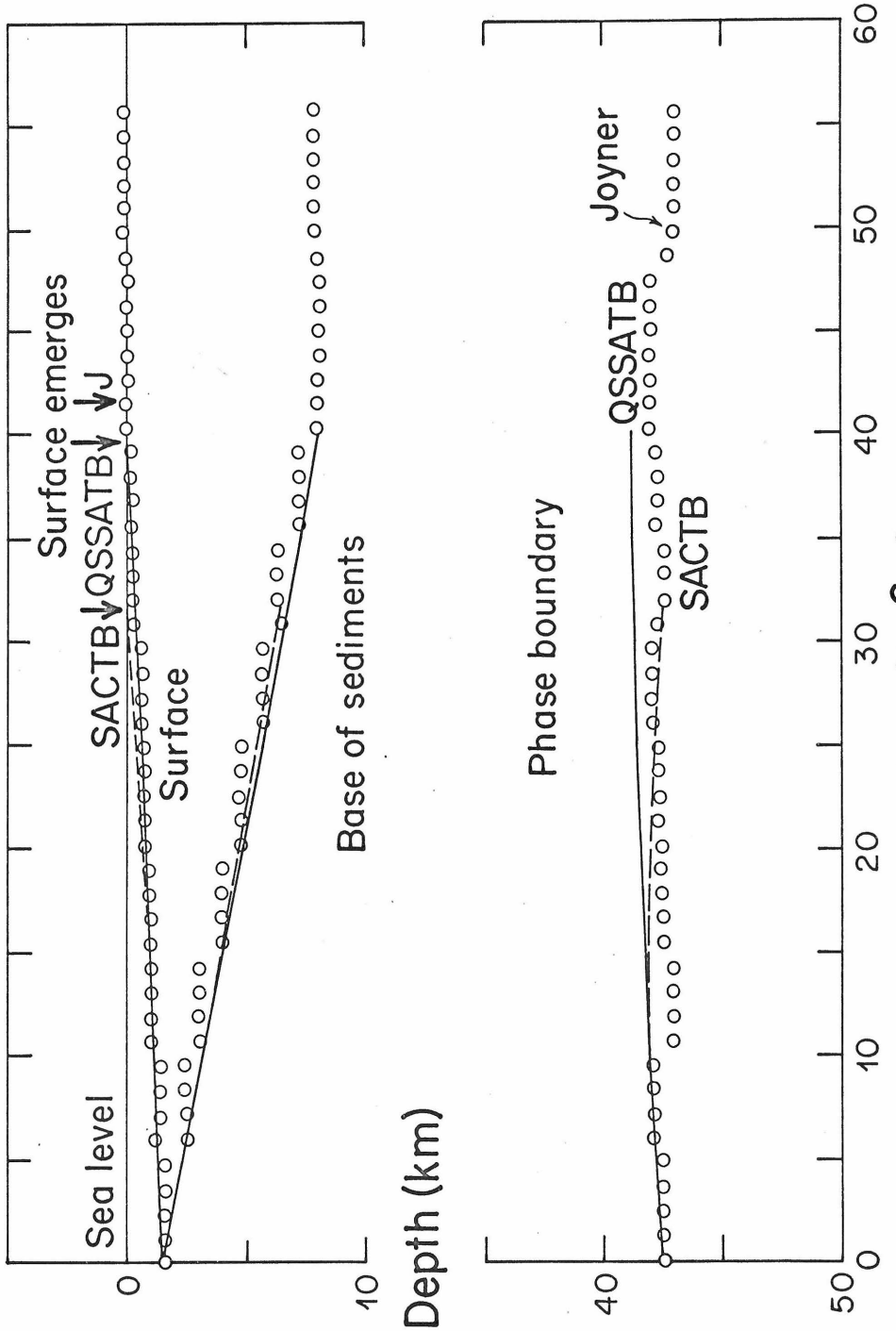
Surface emerges
SACTB
QSSATB
J
Sea level
Surface
Base of sediments
Depth (km)
0
10
Phase boundary
QSSATB
Joyner
SACTB
40
50
0
10
20
30
40
50
60
Time (10⁶ y)

FIGURE 6

cause the surface to emerge above sea level at a time considerably different from the time of emergence had deposition been continuous. Thus the time of emergence from the numerical solution may easily be in error by ± 5 million years for this model.

The agreement between the two solutions QSSATB and SACTB shown in Figure 6 is remarkably good considering the different values of the lag from the two solutions for times greater than $\sim$ 10 million years. The agreement is so good because we have isolated the only unknown, the response of the phase boundary, in the term containing the lag. Everything else, the isostatic response and $M(0) - M_e(t)$ can be calculated exactly. Since the subsidence depends on all three of these factors, an error in the lag does not cause an error of the same relative magnitude in the subsidence. Thus we expect that the errors that arise from our approximate solutions for the lag will not seriously affect any solutions for the history of a sedimentary basin.

With the irregularities in the numerically computed curve taken into account, the agreement of Joyner's numerical solution with our solution is remarkably good. In fact, it would require a numerical solution considerably more refined than Joyner's to reveal errors in the approximate solution. In view of the approximations inherent in a one-dimensional model, and the uncertainties in the appropriate parameters, a more accurate solution is probably not justified. Thus the approximate analytic solutions we have presented are to be preferred over numerical solutions, because of the analytic form of the former, which provides

considerable insight into the problem and a much more basic understanding of the process. Of course, even the relative simplicity of the analytic solution recommends its use, since it reduces the computational effort from the level of a large computer to the level of a slide rule.

Joyner's models 2b through 2f are variations of model 2a, with different sedimentation rates and initial water depth. The parameters for these models, the times of emergence of the surface, the final sediment thickness and the ratios of final thickness to initial water depth for the numerical and analytic solutions are given in Table 3. The agreement is again excellent. Again, in view of the irregularities in the numerical solution, we should regard the final thicknesses obtained numerically as accurate to only ± 1 km.

The fact that the final sediment thickness increases as the sedimentation rate does is undoubtedly due to the effect of thermal blanketing, which increases with time. Thus the models with a slower sedimentation rate spend more time in the regime of blanketed response, which tends to reduce the final sediment thickness. Similarly, the models of a shallower basin, 2d, 2e, 2f, attain a relatively greater final sediment thickness since they fill in a shorter time, again reducing the effect of thermal blanketing.

Since model 2a barely gets into long-term response, we shall also consider Joyner's model 4, for which sedimentation continues for 200 million years. Thus this model should exhibit long-term response for most of its history. Model 4 has denser sediments of higher thermal conductivity than model 2a. Thus, the

TABLE 3. Sediment Thickness Attained in Basin for Models 2a-2f

Model	2a	2b	2c	2d	2c	2f
initial depth (km)	1.5	1.5	1.5	0.5	0.5	0.5
sedimentation rate ($m/10^6 y$)	200	500	1000	200	500	1000
sediment thickness (km) to fill basin	7.93	8.92	9.25	3.05	3.24	3.09
duration of deposition (m. y.)	39.6	17.8	9.25	15.2	6.47	3.09
ratio between sediment thickness and initial depth	5.3	5.9	6.2	6.1	6.5	6.2
sediment thickness Joyner	8	9	10	4	4	4
maximum possible thickness	10.9	10.9	10.9	3.64	3.64	3.64
solution used	QSSATB	QSSATB	QSSATB	QSSATB	SACTB	SAC

isostatic response should be greater, and the effect of thermal blanketing less than for model 2a.

The comparison between the numerical solution and the QSSATB solution is shown in Figure 7. The agreement, especially for the position of the phase boundary, is extremely good. The times for the emergence of the surface, however, differ by 50 million years, which is fairly large. In view of the irregularities in the numerical solution, and the excellent agreement for the position of the phase boundary, the emergence time for QSSATB solution is probably more accurate. Note that for the numerical solution, the surface emerged just after a slab of sediments had been deposited. Had deposition been continuous, emergence would have been sooner. Thus the discrepancy is not surprising, especially when one considers that in the numerical solution, sediments are deposited in units of 1 km thickness in a basin less than 0.5 km deep.

In an attempt to obtain thick sediment sections in a basin only 0.5 km deep, Joyner designed model 5c, which has a relatively small Clapeyron slope. In doing this, he inadvertently designed an unstable model, which allows us to compare our solution with a numerical solution of this type of model. For model 5c a value of $W = 0.391$, which is not very small, compared to 1.0, nevertheless results in a value of $Q_s = -0.102$. Thus the model is unstable, and should exhibit dynamic instability by a time,

FIGURE 7

Results of Joyner's model 4, comparing solution QSSATB (solid line) and Joyner's numerical solution (dotted line). The agreement for the position of the phase boundary is excellent. The discrepancy between the emergence times is most probably due to the discontinuous sedimentation in the numerical solution as discussed in the text.

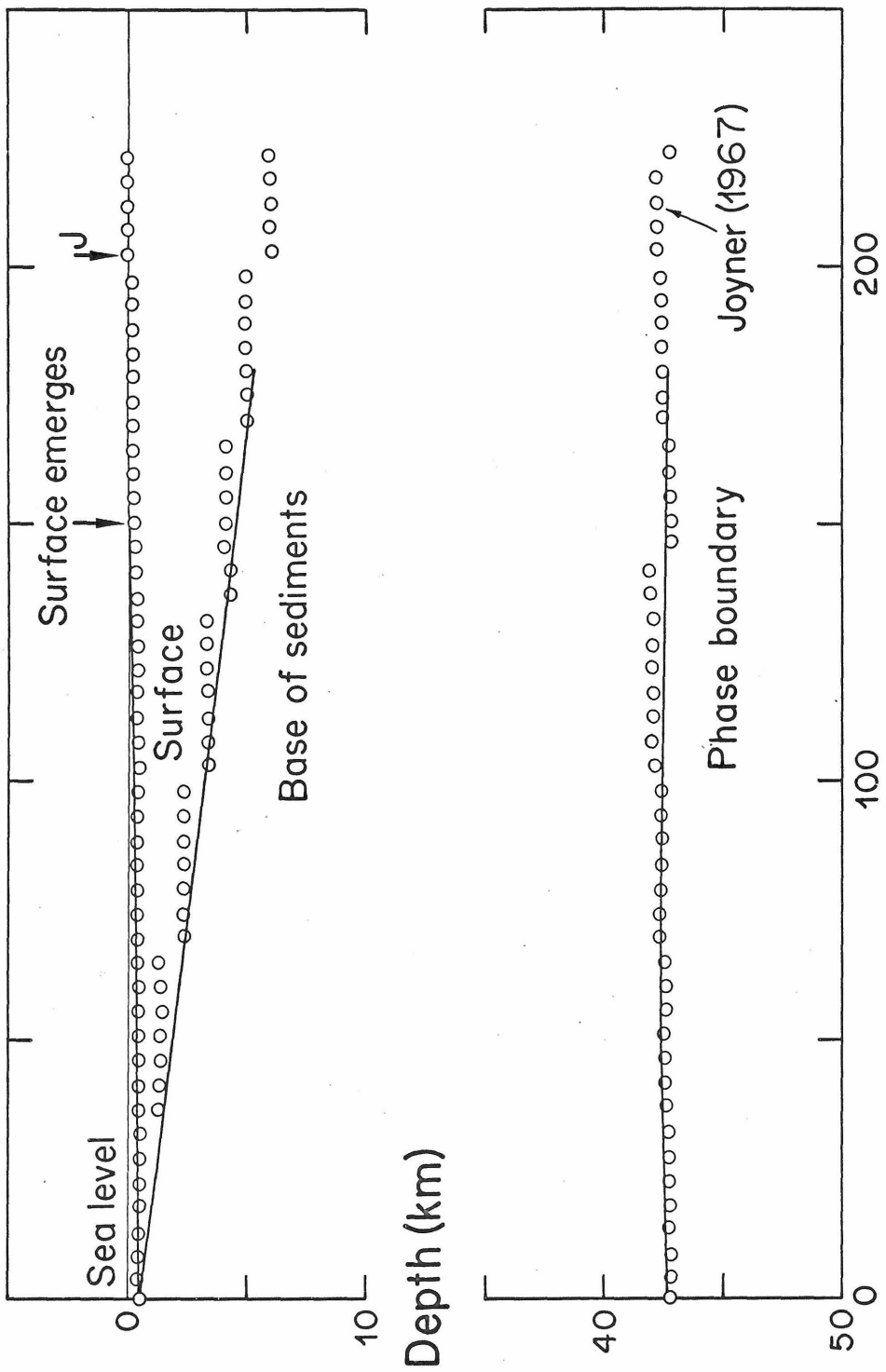
Sea level
Surface emerges
J
Surface
Base of sediments
Depth (km)
0
10
40
50
Phase boundary
Joyner (1967)
0
100
200
Time (10^6 y)

FIGURE 7

given by (12), of 5 million years. Since thermal blanketing should be dominant by a time of 30 million years (18), the model should exhibit dynamic instability for some time between 5 and 30 million years.

Figure 8 shows the numerical results for model 5c, taken from Joyner's Figure 8. Also shown is the solution QSSATB, which differs only insignificantly from solution SACTB for short times. The agreement between the two solutions is remarkably good, with the QSSATB solution appearing as a smoothed version of the numerical solution.

The instability of the model was manifested in the numerical solution by an increase in water depth when the first sediment slab was deposited at 33 million years. The responsiveness of the phase boundary is shown by its rapid movement upward when the slab was deposited. The SACTB solution showed dynamic instability around 5 million years; the effect of thermal blanketing, however, caused the model to be dynamically stable by 10 million years, but only barely. Thus during the first 40 million years of deposition, while 1.2 km of sediments were put in the basin, the water depth decreased by only around 50 meters. After this time, the thermal blanketing, which became dominant at around 30 million years, starts to dominate, and the water depth decreases more rapidly, becoming zero by around 100 million years. Thus the unstable nature of this model caused the water depth to remain essentially constant during the initial 40 million years of deposition. Had the sedimentation rate been greater, a considerable

FIGURE 8

Results for Joyner's model 5c, which is unstable. For the numerical solution (dotted line) the water depth increased when the first 1 km slab of sediments was deposited. For solution QSSATB (solid line), the water depth remains nearly constant for the first 40 million years of sedimentation, even though 1.2 km of sediments were deposited. In spite of the irregularity of the numerical solution, the agreement of the two solutions is excellent.

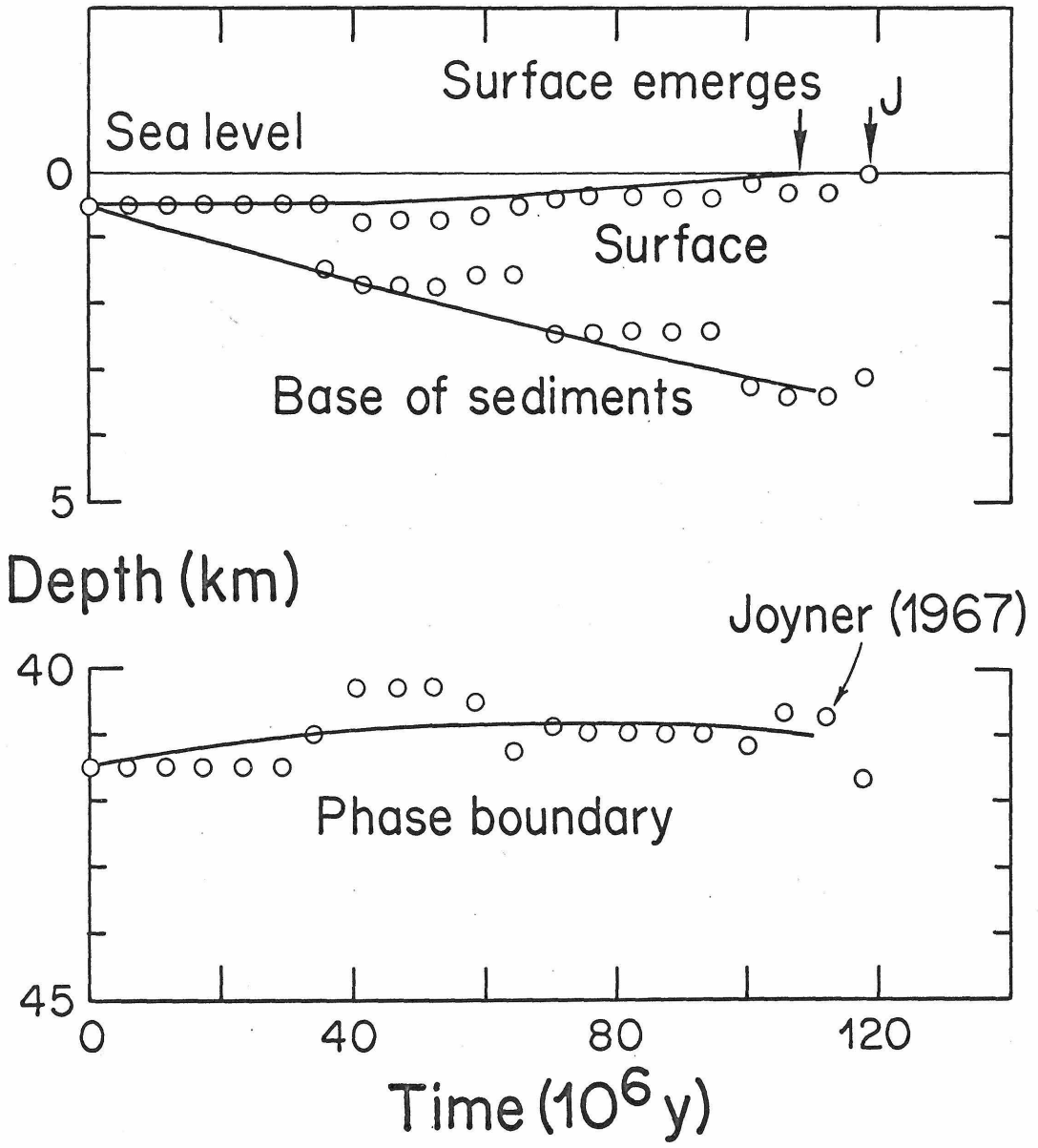
Surface emerges
J
Sea level
0
Surface
Base of sediments
5
Depth (km)
Joyner (1967)
40
Phase boundary
45
0
40
80
120
Time (10^6 y)

FIGURE 8

greater sediment thickness could have been accommodated in the basin, since more could have been deposited during the time that the water depth did not decrease significantly.

Deposition and Erosion

We have so far applied our solution only to cases of deposition. The examples we have just given have demonstrated the accuracy and utility of the solutions, so that we feel secure in now extending the QSSATB solution to cases involving several cycles of erosion and deposition.

As before, we combine the solutions for the heat flux at the phase boundary from the QSSA solution which the heat flux due to the thermal blanketing of the sediments, and then solve the resulting differential equation for the motion of the phase boundary (cf. Appendix 4). We shall treat first the case of a succession of constant erosion or deposition rates. During a time interval $t_i \leq t \leq t_{i+1}$ sediments of density ρ_s^i and conductivity K_s^i are deposited (or eroded) at a constant rate $\frac{ds}{dt} = k_i$. Thus the sediment thickness is at any time

$$(30) \qquad S = k_i t + j_i; \qquad t_i \leq t \leq t_{i+1}, \qquad i = 0, 1, \ldots$$

$$k_i \text{ - constant}; \qquad j_{i+1} = (k_i - k_{i+1}) t_i + j_i$$

We assume that the time intervals are known, i.e. the t_i are given, as is j_0 and the k_i. The times t_i between periods of erosion and deposition (or deposition or erosion at different rates) will presumably occur when the water depth w reaches some certain value, such as zero, or else when some other variable (such as sediment thickness) reaches a certain value. In this case the times t_i may be found successively by following the solution from time t_0.

The flux at the phase boundary resulting from thermal blanketing is found in a manner exactly analogous to that used for the QSSATB solution, except that the more complex variations of temperature at the surface was taken into account. This necessitated neglecting the motion of the phase boundary and surface of sedimentation relative to the region of phase 1. When only one cycle of deposition occurs, the solution will reduce to the QSSATB solution with constants defined by (21). This should not be a serious restriction on the accuracy of the solution for most geophysical cases. In any event the accuracy can be checked by comparing the QSSATB solutions using constants given by (20) with the solution using constants given by (21) for any one period of deposition or erosion.

The solution so obtained for the position of the phase boundary at time t such that $t_m \leq t \leq t_{m+1}$ is then

$$M(0)-M(t)=\frac{Ggc_1}{H}\left\{e^{-\omega\varkappa_1 t}\left[\sum_{i=0}^{m-1}\frac{\rho_s^{\,i}}{\omega}\left(\Lambda_i(t_{i+1})-\Lambda_i(t_i)-\frac{\rho_s^{\,m}}{\omega}\Lambda_m(t_m)\right)\right]\right.$$

$$\left.+\frac{\rho_s^{\,m}}{\omega}\left[\frac{k_m t+j_m}{d}-\frac{k_m}{\varkappa_1}\left(\frac{1}{\omega d}-\left(\frac{d}{2}+\frac{c_2}{c_1}d'\right)\right)\right]\right\}+\frac{c_1 J_s}{H}\left\{e^{-\omega\varkappa_1 t}\left[\sum_{i=1}^{m-1}\left(\Pi_i(t_{i+1})\right.\right.\right.$$

$$\left.\left.\left.-\Pi_i(t_i)\right)-\Pi_m(t_m)\right]-\frac{k_m t+j_m}{K_s^{\,m}\,d\omega}+\frac{k_m}{K_s^{\,m}\,\varkappa_1\omega}\left(\frac{1}{\omega d}+\frac{d}{6}\right)\right.$$

$$\left.+\frac{2}{d}\sum_{n=1}^{\infty}\frac{(-1)^n\,\Omega_n^{\,m}}{(\omega-\nu_n)}\,e^{-\nu_n\varkappa_1 t}\right\} \tag{31}$$

where

$$\Lambda_i(z)\equiv e^{\omega\varkappa_1 z}\left[\frac{k_i z}{d}-\frac{k_i}{\varkappa_1}\left(\frac{1}{\omega d}-\left(\frac{d}{2}+\frac{c_2}{c_1}d'\right)\right)+\frac{j_i}{d}\right]$$

$$\Pi_i(z)\equiv e^{\omega\varkappa_1 z}\left[\frac{k_i}{K_s^{\,i}\,\varkappa_1\omega}\left(\frac{1}{\omega d}+\frac{d}{6}\right)-\frac{k_i z+j_i}{K_s^{\,i}\,d\omega}\right]$$

$$+\frac{2}{d}\sum_{n=1}^{\infty}\frac{(-1)^n}{(\omega-\nu_n)}\,\Omega_n^{\,i}\,e^{(\omega-\nu_n)\varkappa_1 z} \tag{32}$$

$$\Omega_n^{\,i}\equiv\sum_{p=1}^{i-1}\left[\Delta_n^{\,p}(t_{p+1})-\Delta_n^{\,p}(t_p)\right]-\Delta_n^{\,i}(t_i)$$

$$\Delta_n^{\,p}(z) \equiv \frac{1}{K_s^{\,p}}\left(k_p z + j_p - \frac{k_p}{\nu_n \varkappa_1}\right) e^{-\nu_n \varkappa_1 z}$$

and

$$\nu_n \equiv \frac{n^2 \pi^2}{d^2} \qquad \text{as before in (21).}$$

In (31) and (32) the notation is the same as in the QSSATB solution and is given in (15) and (21). Note also that z is a dummy variable in (32).

In order to model a basin where sedimentation started at time t_0 with rate k_0, one would evaluate (1), using the definition of $\ell(t)$ and (31). If erosion occurred when the surface of the sediments was above sea level, one would take t_1 as the time when $w = 0$. Thus k_1 would be negative, since it would correspond to erosion. This method can be continued, of course, through any number of cycles of deposition and erosion.

As a final numerical check, we shall compare Joyner's numerical solution for model 5c with the solution given by (31).

Joyner carried his solution to 450 million years, which extended into the second period of erosion for the model. The results of the two solutions are shown in Figure 9 which is based on Joyner's Figure 8.

Comparison of Figure 8 and Figure 9 reveals the difference between solution QSSATB and that given by (31). For solution QSSATB the surface emerged after 108 million years, whereas for solution given by (31) the surface emerged after 98 million years. This difference is well within the uncertainty of Joyner's numerical scheme, so that we may regard as insignificant the errors introduced by use of (31) rather than QSSATB.

In Joyner's solution, the erosion rate was taken as proportional to the height of the surface above sea level. This is not within the capability of our solution as given by (31) which assumes a constant erosion rate. For purposes of comparison, we used a constant erosion rate of 15 meters/million years, which is very near the average erosion rate of Joyner's solution. It is also just half of the sedimentation rate, which is constant in both the numerical solution and our analytic solution (31).

As can be seen in Figure 9, the general agreement between the numerical solution and the analytic solution is very good; what differences there are can be easily explained and are minor. The first difference is the previously mentioned time of emergence of the surface of the sediments above sea level. As mentioned before,

FIGURE 9

Results for Joyner's model 5c for longer times than Figure 8. During two cycles of deposition and uplift and erosion, the analytic approximation from equation (31) agrees excellently with the numerical solution. The differences that do exist are due to the different erosion laws of the two solutions (see text) and the discontinuous sedimentation in the numerical solution.

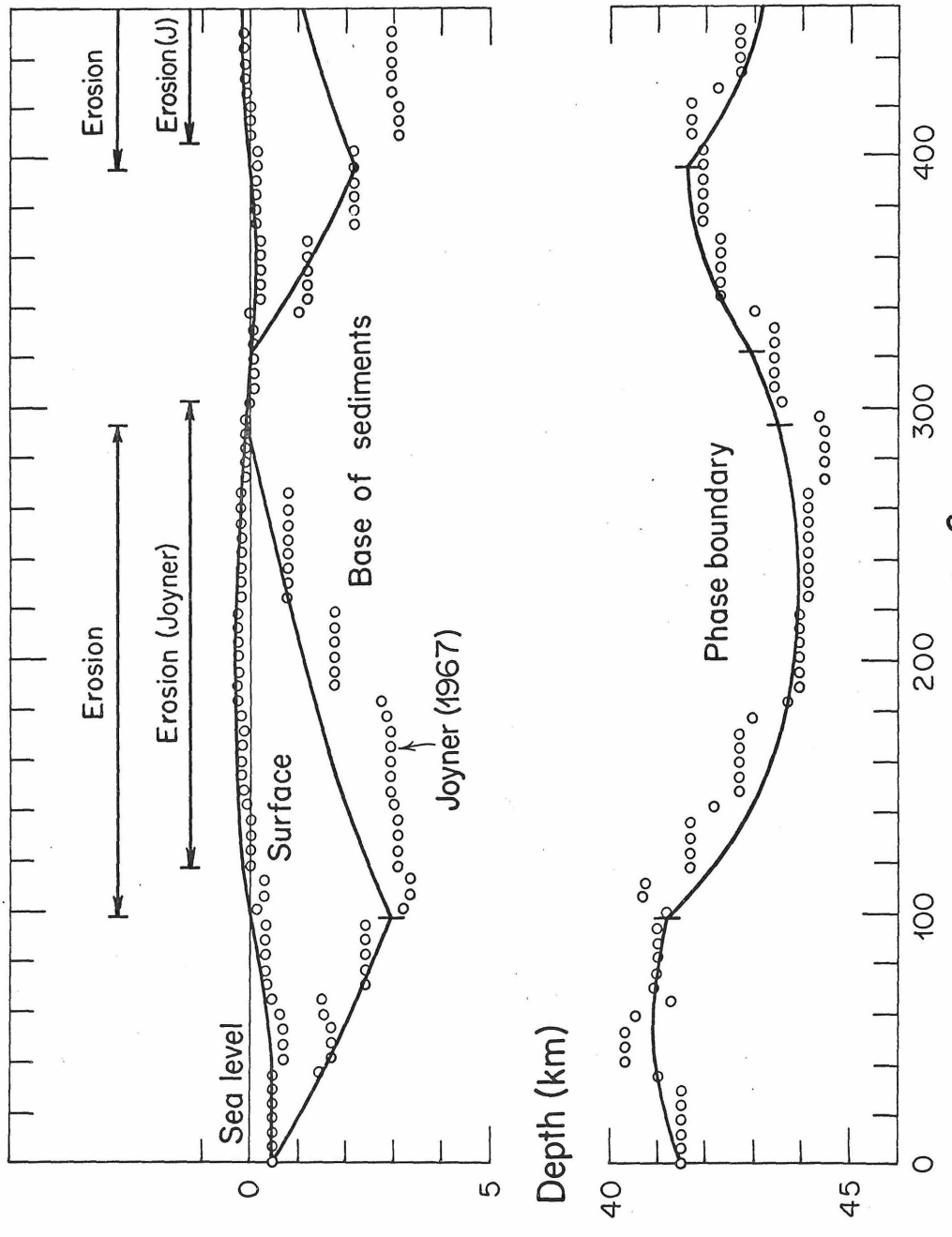
Erosion
Erosion (J)
Erosion
Erosion (Joyner)
Sea level
Surface
Base of sediments
Joyner (1967)
Depth (km)
0
5
40
45
Phase boundary
0
100
200
300
400
Time (10^6 y)

FIGURE 9

the numerical scheme Joyner used, in which sediments are deposited as one km-thick slabs, could easily result in a time of emergence that was considerably in error. This is especially obvious when one notices the roughness of the numerical solution, as evidenced by the dotted curves in Figure 9.

The second difference is during the first cycle of erosion, and is most noticeable in the curve showing the base of the sediments. This arises from the different erosion laws of the two solutions. In the numerical solution, since the erosion rate is proportional to elevation, the sediment thickness is reduced less rapidly right after emergence, when the elevation is small. When the elevation is at its maximum, at around 200 million years, the erosion rate is the greatest, and the numerical solution rejoins the analytic solution which has a constant erosion rate. The fact that the two solutions agree so well, in spite of the different erosion laws, would indicate that the type of erosion law may not be of paramount importance.

The differences between the two solutions during the second cycle of deposition and erosion may be attributed to the same reasons discussed above that accounted for the differences during the first cycle. The most noticeable difference is the sediment thickness after $\sim$400 million years. As before, the numerical scheme has probably permitted a greater thickness of sediments to be deposited than would have been the case had deposition been continuous. Examination of the curve showing the motion of the surface supports this conclusion.

At the end of the first cycle of erosion, all the sediments had been removed while the surface was still above sea level. It is not clear whether or not Joyner permitted the basement rock to be eroded in his solution when this occurred. In the analytic solution shown in Figure 9, the basement rock was not eroded; it does not differ substantially from a similar solution in which the basement rock was eroded, so that the uncertainty on this point does not affect any of our conclusions. This effect probably results from the fact that when $w > 0$, water is present, whereas if $w < 0$, water is not present. This gives rise to asymmetry expressed in the fact that ρ_w is a function of w in equation (1).

The existence of a second cycle of sedimentation and erosion for model 5c raises the question of just how many such cycles could occur. We should note that van de Lindt (1967) also observed more than one cycle in some of his models and also the erosion of basement rock. To investigate this question, the solution for model 5c was carried out to 1000 million years. The movement of the surface and base of the sediments is shown in Figure 10. The third and fourth cycles are exactly the same as the second cycle, at least within the accuracy of ~ 1 part in 10^4 to which the solution was computed. It is clear that the solution is periodic after the first cycle, and that subsequent cycles would appear the same as the second, third, and fourth.

During each cycle of 234 million years, 2.21 km of sediments are deposited while the water depth never exceeds 120 meters.

FIGURE 10

Analytic solution of model 5c of Figure 9 extended to 10^9 years showing the existence of undamped oscillations after the first cycle of deposition and erosion. During the 80 million year deposition phase of each cycle, 2.21 km of sediments are deposited in water that never exceeds 120 meters' depth. During the erosion of these 2.21 km of sediments, a surface elevation of up to 164 meters is maintained. In this solution, deposition occurs at a constant rate when the surface is below sea level, and erosion occurs at a constant rate when the surface is above sea level.

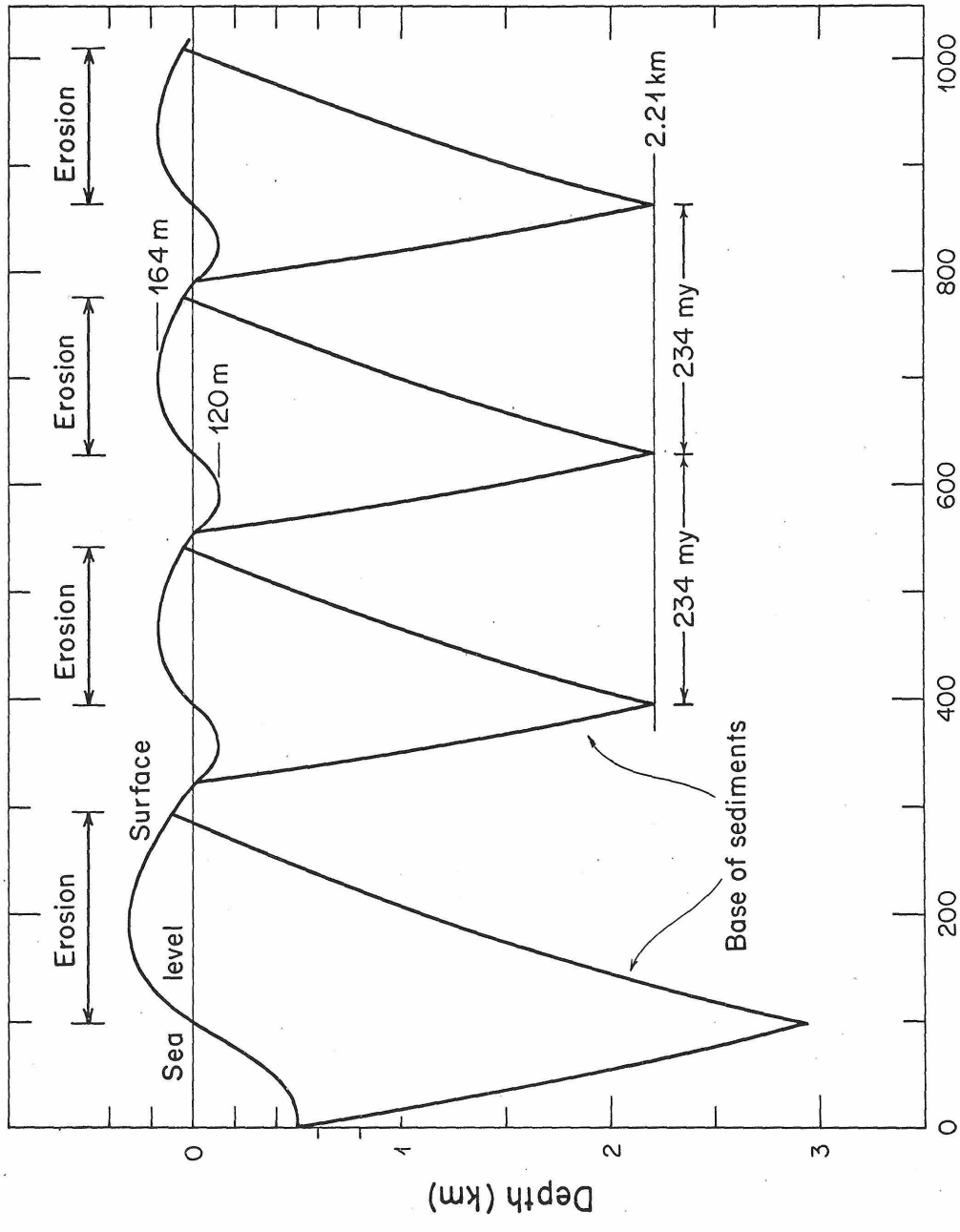
Erosion
Erosion
Erosion
Erosion
Surface
Sea level
164 m
120 m
2.21 km
234 my
234 my
Base of sediments
Depth (km)
Time (10^6 y)
0
1
2
3
0
200
400
600
800
1000

FIGURE 10

The resulting ratio of sediment thickness to water depth of 18.4 exceeds by far the value of 6 for the first cycle, and is a striking illustration of the amount of subsidence that this mechanism can cause.

Oscillatory Solutions

The fact that oscillations can occur is important for the geologic consequences of a phase change model. If the mechanism permitted only one cycle, some means would have to be found to account for the presence of an initial basin. This basin could only be filled once, unless an outside mechanism would again create a new basin.

An oscillatory process, on the other hand, periodically creates a new basin, allowing the whole cycle of deposition, uplift, and erosion to be repeated again and again. If the period of a cycle is a few hundred million years, as for model 5c, only a few cycles can account for a significant period of geologic time. Thus it is worthwhile to further investigate the possibilities of oscillatory solutions.

For models with a constant sedimentation or erosion rate, the solution given by (31) can be used to calculate the history of any such model. A few variations of model 5c were solved, and it was found that when the density of the lowest layer, ρ_c, was raised from 3.4 to 3.7 (changing Q_s from -0.102 to -0.048), the oscillations were damped so that only the first two cycles were

significant. This occurred even though the model was still unstable, since Q_s was less than zero. Other models indicated that the existence of oscillations was not dependent primarily on the erosion rate.

To investigate the problem of oscillations in more detail, we shall use a model for which the sedimentation rate is a linear function of water depth, and the erosion rate is the same linear function of erosion. We shall also neglect the functional dependence of the water density ρ_w on the value of w, so that all the parameters in the model will be the same during both deposition and erosion.

The differential equation of motion for the phase boundary is

$$\frac{d}{d(\kappa_1 t)}[M(0)-M(t)] = -\omega[M(0)-M(t)] + \frac{G\rho_s g c_1}{H}\left[\frac{s(t)}{d}+\left(\frac{d}{2}+\frac{c_2}{c_1}d'\right)\frac{1}{\kappa_1}\frac{ds}{dt}\right]$$
$$+\frac{c_1}{H}\frac{2\pi^2\kappa_1}{d^3}\sum_{n=1}^{\infty}(-1)^n n^2 e^{-\frac{\kappa_1 n^2\pi^2 t}{d^2}}\int_0^t e^{\frac{\kappa_1 n^2\pi^2 z}{d^2}}\frac{J_s}{K_s}s(z)dz \qquad (33)$$

Using the relation

$$M(0) - M(t) = M(0) - M_e(t) - \ell(t) = \frac{\rho_s}{\rho_1 W}s(t) - \ell(t) \qquad (34)$$

and Equation (1), we obtain the following equation:

$$\frac{Q_w}{(1 - \frac{\rho_1}{\rho_2})} \frac{dw}{dt} = \left[\frac{G\rho_s g c_1 \kappa_1}{H} \left(\frac{d}{2} + \frac{c_2}{c_1} d'\right) - \frac{1 - \rho_s/\rho_c}{1 - \rho_1/\rho_2} \right] \frac{ds}{dt} - \frac{G\rho_1 g c_1 \kappa_1 W Q_s}{Hd(1 - \rho_1/\rho_2)} s$$

$$- \frac{\omega \kappa_1 Q_w}{1 - \rho_1/\rho_2} w + \frac{\omega \kappa_1 Q_{w_0}}{1 - \rho_1/\rho_2} w_0 \qquad (35)$$

$$+ \frac{2\pi^2 \kappa_1^2 c_1 J_s}{d^3 H K_s} \sum_{n=1}^{\infty} (-1)^n n^2 e^{-\frac{\kappa_1 n^2 \pi^2}{d^2} t} \int_0^t e^{\frac{\kappa_1 n^2 \pi^2 z}{d^2}} s(z)\, dz$$

Since we are looking for oscillatory solutions, we assume

$$w(t) = C_1 e^{i\gamma t} \qquad (36)$$

where γ is the frequency of the oscillation and is constant. Using our sedimentation and erosion law

$$\frac{ds}{dt} = \beta w$$

we have

$$s(t) = \frac{\beta}{i\gamma} C_1 e^{i\gamma t} + B_0 \qquad (37)$$

Plugging (36) and (37) into (35), and letting $\gamma = 0$, we obtain for long times such that $e^{-\frac{\kappa_1 \pi^2 t}{d^2}} << 1$,

$$Q_{w_0} w_0 = Q_s B_0 + (1 - \frac{\rho_1}{\rho_2}) \frac{J_s B_0}{K_s G \rho_1 g W}$$

This is just (1) with $w = 0$, with (24) for $\ell(t)$ and B_0 for s. Thus for zero frequency, the solution reduces to the steady state case as it should. In addition, it says that the solution will oscillate around this steady state solution.

For non-zero frequency, we obtain

$$a_1' \gamma^2 = a_2' i\gamma + a_3' + a_4' \sum_{n=1}^{\infty} \frac{(-1)^n n^2}{\kappa_1 \nu_n + i\gamma} [1 - e^{-(\kappa_1 \nu_n + i\gamma)t}] \quad (38)$$

where a_1', a_2', a_3', and a_4' are constants, $\nu_n \equiv \frac{n^2 \pi^2}{d^2}$ and $i \equiv \sqrt{-1}$ again. Neglecting the exponential terms leads us to a solution for times after all initial transients have decayed. It is just this solution that we seek, since it will reveal the existence of persistent oscillations if they exist. Thus for times long enough so that the exponential in the sum is small, we neglect it, in which case we can evaluate the sum. Thus

$$\sum_{n=1}^{\infty} \frac{(-1)^n n^2}{\kappa_1 \nu_n + i\gamma} = \frac{d^2}{\kappa_1 \pi^2} \; I\left(\frac{i\gamma d^2}{\kappa_1 \pi^2}\right)$$

where we define

$$I(z) \equiv \sum_{n=1}^{\infty} \frac{(-1)^n n^2}{n^2 + z} = \frac{-\pi\sqrt{z}}{2 \sinh(\pi\sqrt{z})}$$

In terms of a dimensionless frequency

$$\sigma \equiv \frac{d^2}{\kappa_1} \gamma \tag{39}$$

Equation (38) reduces to

$$A_1 \sigma^2 - A_2 i\sigma - A_3 = \frac{\sqrt{i\sigma}}{2 \sinh\sqrt{i\sigma}}$$

where

$$A_1 \equiv \frac{Q_w H K_s \kappa_1}{(1 - \frac{\rho_1}{\rho_2}) 2c_1 J_s \beta d^3}$$

$$A_2 \equiv \frac{G g \rho_1 K_s}{2 J_s} \left[\frac{\kappa_1 W Q_w}{d^2 \beta (1 - \frac{\rho_1}{\rho_2})} - \frac{\rho_s}{\rho_1} \left(\frac{1}{2} + \frac{c_2}{c_1} \frac{d'}{d}\right) \right] + \frac{H K_s (1 - \frac{\rho_s}{\rho_c})}{2 d c_1 J_s (1 - \frac{\rho_1}{\rho_2})}$$

$$A_3 \equiv \frac{G g \rho_1 K_s W Q_s}{2 J_s (1 - \frac{\rho_1}{\rho_2})} \tag{41}$$

Separating σ into real and imaginary parts

$$\sigma = u + iv \ ;$$

where u and v are both real, allows us to separate (40) into two equations:

$$A_1(u^2 - v^2) + A_2 v - A_3 = \frac{z \sinh z \cos y + y \cosh z \sinh y}{2[\sinh^2 z \cos^2 y + \cosh^2 z \sin^2 y]} \tag{42}$$

$$2A_1 uv - A_2 u = \frac{y \sinh z \cos y - z \cosh z \sin y}{2[\sinh^2 z \cos^2 y + \cosh^2 z \sin^2 y]} \tag{43}$$

where

$$z \equiv r \cos \phi \qquad y \equiv r \sin \phi$$

$$r \equiv (u^2 + v^2)^{1/4} \qquad \phi \equiv \frac{1}{2} \tan^{-1} (-\frac{u}{v})$$

$$0 \leq \theta \leq \frac{\pi}{4}, \ v \leq 0 \qquad \frac{\pi}{4} \leq \theta \leq \frac{\pi}{2}, \ v \geq 0$$

$$u \geq 0$$

The right-hand side of (42) is shown in Figure 11; the right-hand side of (43) is shown in Figure 12.

The values of u and v that simultaneously satisfy (42) and (43) will then give the frequency and damping (or growth rate) of a stable oscillatory solution of (33), if such a solution exists. Thus the solution for the water depth w is

$$w(t) = C_1 \exp(i u \frac{\kappa_1}{d^2} t - v \frac{\kappa_1}{d^2} t)$$

from (36). We consider only the root $u \geq 0$, since (42) and (43) are symmetric in $\pm u$, if θ is allowed negative values for negative u. In contrast, v may be either positive or negative; if v is positive, the oscillations are damped; if v is negative, the amplitude of the oscillations grows exponentially.

Let us examine the conditions for the existence of roots for a few special cases.

i) undamped oscillations, i.e. $v = 0$. In this case, the left-hand side of (42) is

$$A_1 u^2 - A_3$$

which is a parabola, concave upward, that intersects the vertical axis at $-A_3$. Thus a solution to (42) with $v = 0$ will exist for $A_3 \geq -\frac{1}{2}$ (cf. Figure 11).

However, (43) must be satisfied at the same time. The left-hand side of (43) becomes $-A_2 u$, which is a straight line of

FIGURE 11

Function for determining frequency of oscillatory solution for model with deposition or erosion rate proportional to water depth or elevation. Frequency equals $\varkappa_1/d^2\ (u + iv)$, and u and v satisfy $A_1(u^2 - v^2) + A_2 v - A_3 =$ function illustrated, as well as satisfy equation of Figure 12.

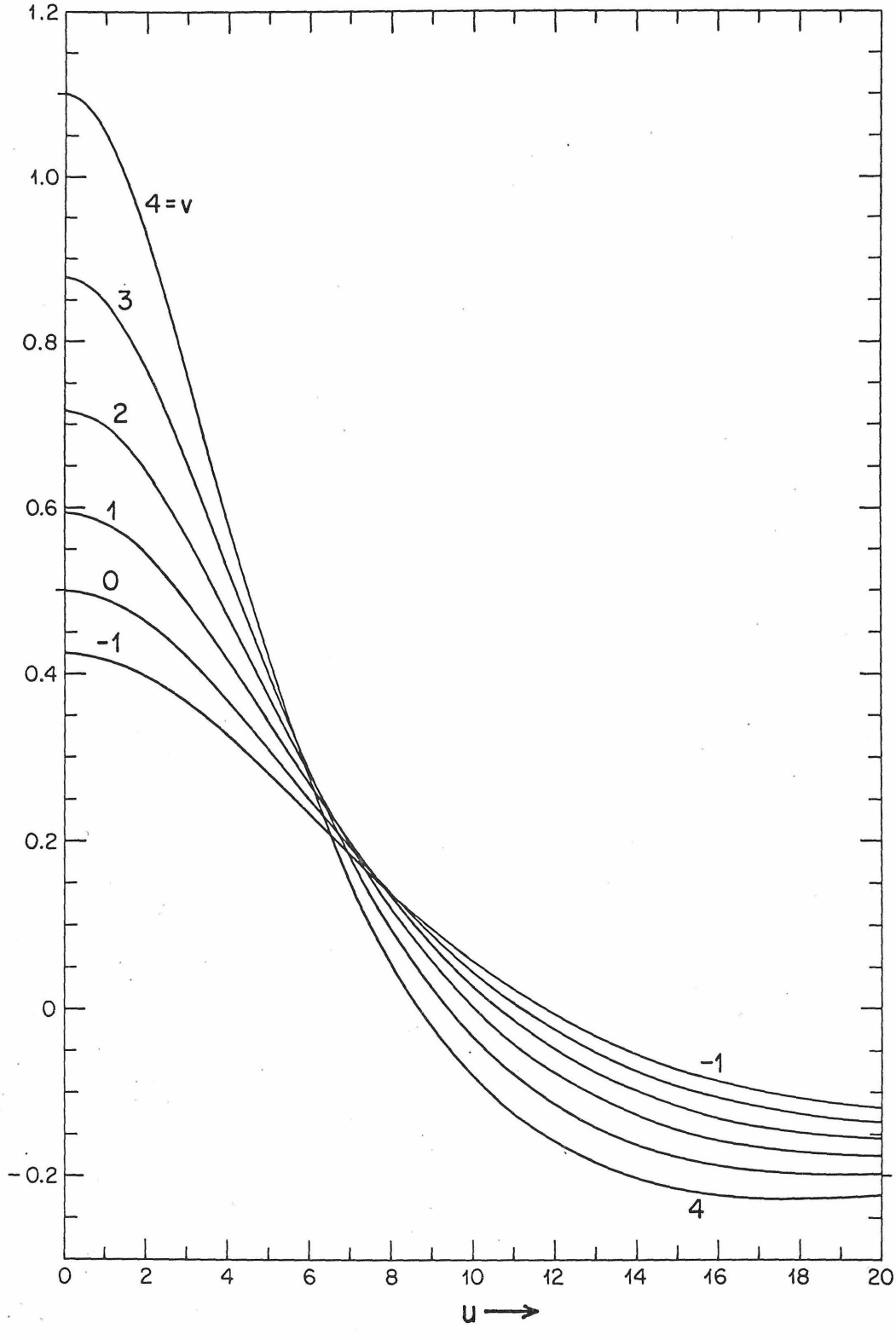

FIGURE 11

FIGURE 12

Analogous to Figure 11. Roots u and v must satisfy $2A_1 uv - A_2 u$ = function illustrated, as well as satisfy equation of Figure 11.

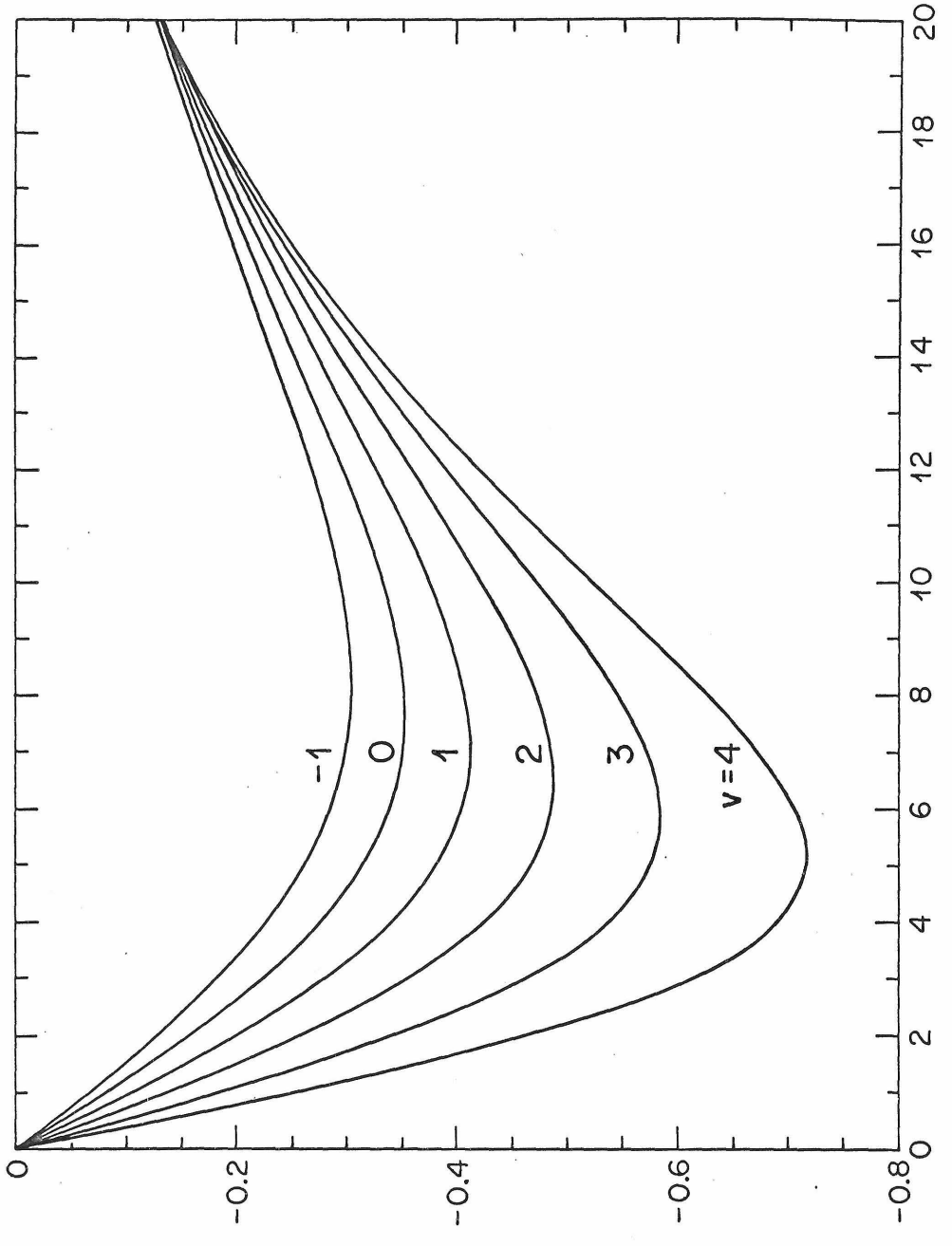

FIGURE 12

slope $-A_2$ which passes through the origin. Thus (43) can have a root for u, with $v = 0$, only if $A_2 \leq -\frac{1}{12}$. However, this root will not in general be the same as the root for (42). A solution will occur only for special cases such that (42) and (43) can be satisfied simultaneously with $v = 0$. We may conclude then that an undamped oscillatory solution will in general occur only for special cases.

ii) non-oscillatory solution, i.e. $u = 0$. In this case, (42) becomes

$$-A_1 v^2 + A_2 v - A_3 = -A_1 (v - \frac{A_2}{2A_1})^2 - (A_3 + \frac{A_2^2}{4A_1}) = \frac{\sqrt{v}}{2 \sin \sqrt{v}} \qquad (44)$$

If $v < 0$, the right-hand side becomes

$$\frac{\sqrt{-v}}{2\sinh \sqrt{-v}}$$

where $-v$ is positive. This function is shown in Figure 13.

The left-hand side of (44) is a parabola, convex upward, with a maximum of $-(A_3 + A_2^2/2A_1)$ at $v = A_2/2A_1$. Examination of Figure 13 indicates that there will always be a root of (44) near $v = \pi^2$, where the parabola will intercept the branch coming from $-\infty$. This root does not interest us, however, since we have assumed that the time was such that the exponential terms in (38) may be neglected, viz. $\exp(-\frac{\kappa_1 \pi^2 t}{d^2}) << 1$. A solution with $v = \pi^2$

FIGURE 13

Function given in Figure 11 plotted as a function of v with $u = 0$. If $v > 0$, the solution decays exponentially, if $v < 0$, the solution grows exponentially. The root v (with $u = 0$) must satisfy $-A_1 v^2 + A_2 v - A_3 = \sqrt{v}/2 \sin \sqrt{v}$ which is function shown. Roots from the branch that approaches $-\infty$ at $v = \pi^2$ decay so rapidly as to be unimportant. A growing solution with $v < 0$ will exist if $-A_3 > 1/2$.

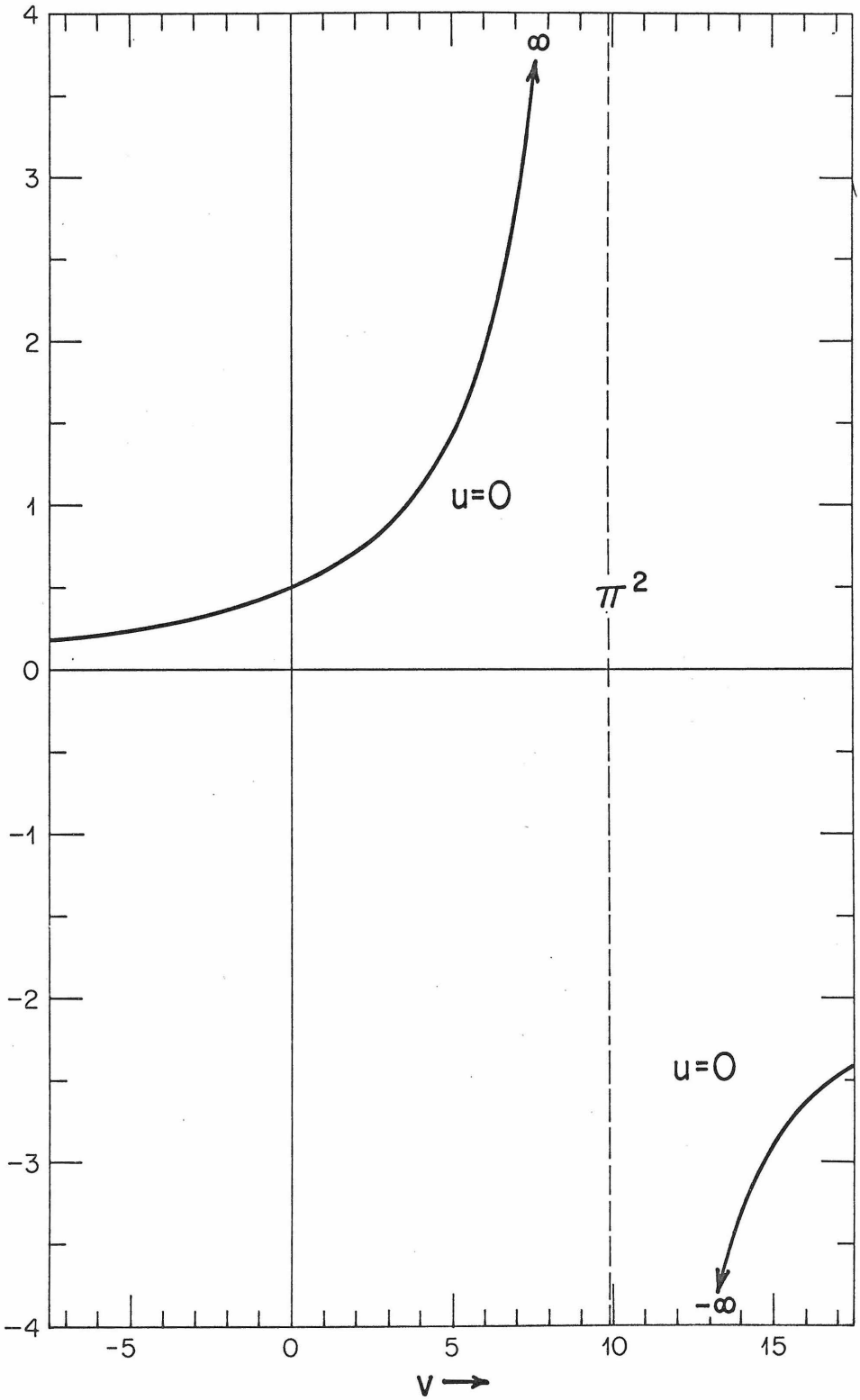

FIGURE 13

would be proportional to $\exp(-\frac{\kappa_1 \pi^2 t}{d^2})$ and would thus be small by this time.

There will be a negative root of (44) if $-A_3 > 1/2$, as well as a positive root. The negative root, however, will give rise to a solution that will grow exponentially, and hence will dominate. Two positive roots could exist only if $-A_3 < 1/2$, $A_2 > 1/2$, and $-(A_3 + A_2^2/4A_1) > 1/2$, which in turn requires $A_1 < 0$. However, $A_1 > 0$ if $Q_w > 0$ (cf. (41)), thus two positive roots are not possible, unless $Q_w < 0$, which is unlikely.

For $u = 0$, (43) is always satisfied identically, thus the above mentioned roots of (44) are solutions.

From these two limiting cases, then, we conclude i) that a purely oscillatory solution is a special case and will not occur in general and ii) if $A_3 < -1/2$, a solution will exist that grows exponentially. From (41), the condition for an exponentially growing solution is

$$Q_s < \frac{J_s}{K_s G g \rho_1 W} (1 - \frac{\rho_1}{\rho_2})$$

In general, roots u and v of (42) and (43) will have to be found by solving the equations, which must be done by trial and error or some other such process.

As an example, we present the roots for model 5c, which we have previously solved for the case when sedimentation and

erosion rates were constant. The roots we now present will give the frequency and decay (or growth) constants for an oscillatory solution which will exist for times considerably after $d^2/\pi^2\kappa_1 \approx 7$ million years. Thus the oscillatory behavior should prevail by 20 or 30 million years after the start of sedimentation.

The dimensionless frequency constants u and v are given in Table 4, along with the period of the oscillations (time for one complete cycle of deposition and erosion) and the e-folding time of the growth or decay of the oscillations (time for solution to decay to 1/e of its former amplitude, or to grow to e times its former amplitude). These all are given for several sedimentation rate constants, and for cases with water present or absent at all times. The asymmetric case, where water is present during deposition but absent during erosion, will probably lie between these two cases.

Since our solution doesn't fix the amplitude of the oscillations, but only the frequency, we do not know the absolute sedimentation rates. However, for an average water depth of 100 meters, the average sedimentation and erosion rates would range from 10 to 50 m per million years for our values of β(0.1 to 0.5 (m. y.)$^{-1}$).

The mean value of the sediment thickness is $B_0 = 2.8$ km, from (37); thus the sediment thickness will oscillate around this value. If more than 5.6 km of sediments are eroded during any period of erosion, the basement rock will be exposed to erosion. At an erosion rate of 50 m/million years, this would require 112 million years of erosion or a period of 224 million years for one whole cycle. This is of the same order as the periods given in

TABLE 4

Frequencies of Oscillatory Solutions for Model 5c

	water absent: $\rho_w = 0$						water present: $\rho_w = 1$				
β $(10^6$ years$)^{-1}$	0.1	0.2	0.25	0.3	0.4	0.5	0.1	0.2	0.3	0.4	0.5
u	1.22	1.72	1.91	2.07	2.35	2.59	1.61	2.21	2.63	2.96	3.23
v	0.196	0.059	-0.004	-0.065	-0.178	-0.283	0.094	-0.119	-0.304	-0.467	-0.614
* period $(10^6$y)	351	249	224	206	182	165	266	194	163	144	132
† folding time $(10^6$y)	347	1,149	16,600	1,053	382	241	725	572	224	146	111

* period $\equiv \frac{2\pi d^2}{u\varkappa_1} = \frac{428}{u}$ million years .

† folding time $\equiv \frac{d^2}{|v|\varkappa_1} = \frac{68.1}{|v|}$ million years, $v > 0$ means oscillations decay, $v < 0$ means oscillations grow.

Table 4; thus the erosion of all the sediments and the exposure of basement rock is clearly within the realm of possibility.

The most striking fact revealed in Table 4 is the number of exponentially growing solutions. The most rapidly growing of these will increase in amplitude by a factor of e in 111 million years or in less than one period (132 million years); in less than two periods the amplitude of oscillation will increase by a factor of ten. The sedimentation rate will also increase by a factor of ten; thus the deposition and erosion of a considerable thickness of sediments should be a feature of this model. The basement rock will eventually be exposed and eroded as well.

Even for the decaying solutions, the rate of decay is slow enough that a few cycles of significant amplitude could occur. In fact, some solutions grow or decay so slowly as to be essentially stable. Thus we may expect solutions with oscillations for a considerable range of sedimentation rate constants for model 5c, and models with a sedimentation rate constant β greater than $\sim 0.5(\text{m. y.})^{-1}$ should exhibit rapidly growing oscillations. Models with sedimentation constants much less than $\sim 0.1(\text{m. y.})^{-1}$ should have oscillations that damp out so rapidly that they should exhibit only one or two cycles of appreciable amplitude.

Before discussing the implications of these oscillatory solutions further, we should determine whether model 5c is a fairly representative realistic model, or is it an unusual model with little applicability to geologic conditions. The main thing that distinguishes model 5c from other models devised by Joyner or other workers, is the value of W (0.391) that results in the model's

instability. This value is smaller than that for most other models investigated, which arises from the fact that the temperature gradient at the phase boundary (11.4°C/km) is 0.61 times the Clapeyron slope (18.7°C/km). Yet neither of these gradients is unrealistic; in fact, the Clapeyron slope would have been even less (14.2°C/km) had the value of G (50°C/kbar) (Clark, 1966) for the reaction albite → jadeite + quartz been used. This would have resulted in a model even more unstable than model 5c. Thus we conclude that models similar to model 5c might reasonably be expected to represent actual geologic situations, and that the phenomenon of repeated oscillations exhibited by such models may very well be important geologically and are worthy of further investigation.

In order to start the first cycle of erosion or deposition, either an initial basin or initial elevation must exist. For a model with growing oscillations, this initial state need not be very far from equilibrium, for the successive cycles will grow in amplitude. Each cycle will obliterate the record of the preceding cycle, since it will erode away more than was deposited during the preceding cycle.

For a model with decaying oscillations, on the other hand, the first cycle will be the largest, hence the initial impetus that starts the process must be considerable. Each cycle, however, will leave its record, since a cycle will not erode all of the sediments deposited during the previous cycle.

For any oscillatory solution, the ratio of sediment thickness deposited to the maximum water depth can be considerable, since the period of the oscillation, and hence the time available for

deposition, is independent of the water depth. Thus if the period is 200 million years, and the average water depth is 100 m, then for $\beta = 0.3\ (\text{m. y.})^{-1}$, 3 km of sediments will be deposited, while the maximum water depth will be 157 m. The ratio of sediment thickness to water depth will be 19.1. In fact, this ratio is independent of the water depth, and is approximately equal to $\beta T/\pi$ where T is the period of the oscillation. The value of 19.1 obtained above may be contrasted with the value of 3.0 for this ratio if there were no phase change, but only isostasy.

The existence of oscillations, and even the presence of uplift after deposition, associated with phase change models are both cases of a system "overshooting" when it moves to equilibrium. This arises for phase change model because, while the pressure of the sediments is transmitted to the phase boundary at the speed of sound (several km/sec), the thermal effect of the sediments is only transmitted with a velocity characterized by κ_1/d, which is of the order of 10^{-14} km/sec. The resultant phase lag between the two effects at the phase boundary causes the phase boundary to move toward a "false" equilibrium position; false because it is determined by the thermal effect from a previous configuration of sediments, and the pressure effect from the present configuration. Anything that tends to increase or speed up the thermal effect at the phase boundary will tend to reduce the phase lag between pressure and temperature effects, and hence the period of any oscillations. Thus a more rapid sedimentation rate, by causing a more rapid change of surface thermal conditions, tends to reduce the period of oscillation. This is seen in Table 4. A lower value of thermal conductivity for the sediments, a shallower phase

boundary, a higher surface heat flux or a higher value of κ_1 would have the same effect. In this manner, the effect of most parameters can be predicted and understood.

Limitations and Extensions of Model Results

The analytic, approximate solutions we have presented have been shown to be quite accurate for the general type of models considered. In addition they have allowed us to understand the problem well enough to confidently predict the effects of different parameters of a model. How restricted are our solutions as a result of implicit assumptions in the model? We shall discuss several points.

The fact that the model is one-dimensional is clearly a simplification. Yet if we are concerned with shallow phase changes not much deeper than the Mohorovicic discontinuity, and with areas more than $\sim$ 100 km in extent, the one-dimensional model is probably quite good. For deeper phase changes, or more limited regions, the one-dimensional model exaggerates the effects associated with the phase boundary. Nevertheless, the effects should be of the same type, only reduced in amplitude somewhat.

The proper boundary condition to apply at the base of the model, indeed even the depth which one should take for the base, is not known, although it is of great importance for the long term behavior of the model (OW, p. 337, 372). We have constructed the QSSA approximation for the case with constant heat flux prescribed at the base of the model. In this case the depth of the lower boundary enters primarily through d' in the values for H and in

the differential equation (15). A deeper lower boundary results in a smaller value of ω in (15), and hence a slower long term response.

The proper quasi-steady state approximation can be easily derived for the case with constant temperature at the lower boundary, although we shall not do it here. In general, a model with constant temperature at the lower boundary will respond faster for long times than a similar model with a constant flux boundary condition.

The quasi-steady state approximation lends itself easily to other boundary conditions as well. For example, a time dependent temperature could be prescribed at the lower boundary. This might be a suitable model of a phase change in the lithosphere above a convection cell that is not in a steady state, e. g. it may be starting to overturn or else moving under the region of the phase change. Such a model could be used to investigate the movement of western North America over the East Pacific rise, for instance.

In our models we have assumed that the phase boundary is a plane of separation between two phases, and that no mixed phase region exists. Phase transitions in the earth, though, are most probably characterized by transition regions of mixed phase. These regions may be several kilometers thick, so that we must re-examine our assumption of a plane phase boundary.

For very short times, the width of the temperature disturbance will be narrow (cf. Figure 1); if the width is of the same order as a transition zone or less, the assumption of a plane phase boundary will probably not be very good. For longer times, however,

when the temperature disturbance is considerably wider than the transition region, the finite width of the phase boundary should have only a limited effect, since it will, in fact, be narrow compared with width of the temperature disturbance. Thus our assumption should be reasonably good. This is so because the diffusion of latent heat away from the phase boundary will be controlled by the transport of heat over the whole region of the temperature disturbance, and thus will not be strongly dependent on details near the phase boundary.

We may note that the width of the temperature disturbance has been given for the Stefan approximation (OW, p. 351). The width for the solution SAC is exactly analogous to this, and this width may be compared with the width of a transition region. This will allow one to determine when the assumption of a plane phase boundary is justified for short times.

For long times the behavior of a model is described by the solution QSSA, which is obtained by integrating the change in temperature over the whole region of interest. The resultant solution should be affected little if any by the presence of a transition region, since the movement of the phase boundary is governed by the escape of heat at the boundaries and the change in the overall shape of the temperature disturbance. In fact, one could easily construct a quasi-steady state approximation for a whole series of phase transition regions, such as a series of metamorphic reactions in sediment section, underlain by even more phase changes.

Therefore the quasi-steady state approximation is not particularly restricted by our assumption of a plane phase boundary.

Since the solutions based on this approximation are applicable for all but short times, the conclusions we have drawn from our model should be little affected by the assumption of a planar phase boundary. In particular, the existence of oscillatory solutions like those we have demonstrated, should not depend on this assumption.

We have been assuming that the level at which isostatic compensation takes place is deeper than the phase boundary. This has led to the operation of both isostasy and the phase change in promoting subsidence. If the phase change were beneath the level of isostatic compensation, it would be insulated from pressure changes at the surface by the fluid-like layer in which flow takes place to achieve isostatic compensation. Such a deep phase change, then, would play no role in the processes we have been considering. Thus in considering the geologic problem of subsidence and uplift, interest will have to be restricted to those phase changes that occur in the uppermost mantle and crust above the level of isostatic compensation.

The solutions we have presented are still of value in studying phase changes below the level of isostatic compensation. For example, how rapidly a phase change responds to a change in pressure due to a change in the earth's rotation rate can be readily determined from the SAC solution. And, of course, the general type of problem associated with a moving phase boundary arises in many other contexts and disciplines. The general techniques we have used in constructing our solutions may well be applicable in some of these other cases.

Broader Considerations

It is not our purpose in this paper to explore the geological complexities of the phase change mechanism. That would entail a detailed study of the possible phase changes in the upper mantle and crust, a study of the crust and mantle structure of many areas to see if any phase changes can be correlated with known structure, and a study of the geologic record of regions where it is thought that a phase change mechanism might have played a role. All of these are the subjects of a different type of study than we have been doing, and are best left to another work. We shall, nonetheless, offer a few brief comments on some of these aspects of the problem, in perhaps a speculative vein.

One most likely candidate for a phase change is still a basalt-eclogite transition, since it has a substantial change in density, and might well be expected to occur in the uppermost mantle or crust. The transition would probably be spread out over a considerable interval thus would not be a sharply defined feature. Such a phase change could be a local feature, and would not necessarily coincide with the Mohorovicic discontinuity. It would be found in areas with sufficient basaltic material at some depth. A likely source of this basalt is either basaltic magmas which have come up from depth, or else the oceanic crust, which had been skimmed off the top of a tectonic plate as it descended into the mantle. This would be the same process as that which presumably skims the oceanic sediments off the plate and piles them up into a continental margin; the 5 km. oceanic crust, being too light to descend into the mantle with the

100 km. thick slab of lithosphere beneath it, would also pile up, but beneath the sediments. This then could be a starting point for a cycle of erosion, submergence, deposition and uplift.

A "phase change" that should not be overlooked is the series of reactions of mineral assemblages to different metamorphic facies or grades. These reactions occur at the borders of stability fields in pressure-temperature space, and thus are the same general type of phase change as a basalt-eclogite transition. The important fact about these reactions is that they can be expected to occur in thick sediment sections, as the lower sediments are buried to a considerable depth. Thus a thick section of sediments that has accumulated in a basin has a built-in phase change. The transition zone is the whole sediment pile, and the density change is the integrated density change over the whole section. There would seem to be no difficulty in treating this type of model with a quasi-steady state approximation.

Another phase change that could be readily treated by a quasi-steady state transition is the serpentinization of peridotite. The role of this in causing uplift could then be quantitatively determined, for such regions as the Colorado Plateau. For this case a model with a changing temperature at depth could be constructed to investigate the effect of heat sources associated with the East Pacific rise moving under the phase change.

The role of phase changes in promoting subsidence has received more attention in the literature than the role of phase changes in promoting emergence during erosion. Yet the phase change mechanism is more effective in the latter process, since it takes place above sea level, and the effective density of the

sediments is not reduced by the buoyant effect of the water. Thus the role of phase changes in maintaining positive elevations above sea level while kilometers of sediments and basement rock are removed by erosion is certainly worthy of more investigation.

In taking erosion and sedimentation laws based on elevation relative to sea level, we have been implicitly assuming that there was a source of sediments when the surface was below sea level, and a convenient sink of sediments when the elevation was positive. This assumption would be easily satisfied at a continental margin. For an inland basin, on the other hand, while a source of sediments is readily available, there might not be available a location to accept a large volume of eroded sediments when the sediments were uplifted. Thus care should be used in accepting sea level as the boundary between erosion and deposition. A case in point is that of a mountain range being eroded adjacent to a basin being filled, such as may be found in the basin and range province. The important parameter for erosion and deposition is the relative relief between the mountains and the basin. A model of this situation may then require the solution of two models simultaneously, and the erosion-sedimentation rates would depend on the solutions of both models.

We finally note that the temperature effects associated with a moving phase boundary may be important. First, the latent heat associated with a moving phase boundary may be an important local source (or sink) of heat. Second, the maintenance of the temperature of the phase boundary at the Clapeyron temperature may cause significant temperature changes over a large region, especially for long times (cf. Figure 1). Third, the change in the distribution of

thermal conductivity due to the movement of a boundary between two phases with different conductivities might also result in significant temperature changes over a substantial region as thermal equilibrium is reestablished.

Any of these temperature effects could result in partial melting in regions where the temperature was near or on the melting curve. In addition they could cause regions to follow a path in temperature-pressure space which might be well removed from the path representing thermal equilibrium, which might result in the formation of new mineral assemblages, thus resulting in more phase boundaries.

We have presented approximate analytic solutions for the history of a sedimentary basin (or eroding elevation) underlain by a phase change and which is isostatically compensated. These solutions are in closed form, and can be evaluated without recourse to high speed computers. The solutions are accurate, especially in view of the uncertainties of the appropriate parameters that should be used in modelling a basin on the earth. The analytic form of these solutions, and their simplicity allows the effect of the parameters of a model to be readily seen. Thus the behavior of models that are variations of a model that has been solved can be confidently predicted.

In addition, certain characteristics of a model permit a classification of its behavior. Thus, for example, criteria for both long and short term behavior, which are distinct, allow one to consider the behavior of a model in a general sense, and permit

discussion of models in terms of these general characteristics. There are also criteria which establish generic types of models, such as stable or unstable. Models of one type all share certain important characteristics, which allows one to discuss the behavior and consequences of a sedimentary basin in terms of these general classes of models, rather than on the basis of individual cases. In essence, one might say that the solutions we have presented permit the creation of a vocabulary for discussing the behavior of models without dealing in particulars of any single model.

This vocabulary then allows one to discuss the geological problem in a precise and quantitative manner. Thus, whether or not phase changes actually are an important feature of sedimentary basins, a framework for discussing and investigating the question has been established. With this framework, the roles of phase changes in subsidence and uplift in the earth's history can be investigated in an orderly way.

Thus, the existence of practicable solutions allows one to predict the consequences of any model; in this way models can be tested, and either discarded or accepted. The conditions on a model for it to be acceptable can be evaluated, and the likelihood of these conditions being fulfilled can be treated as a question apart from the behavior of a model.

APPENDIX 1

The equations governing the motion of the phase boundary may be written

$$\frac{\partial T}{\partial t} = \varkappa_1 \frac{\partial^2 T}{\partial x^2} + \frac{A_1}{\rho_1 c_1} ; \qquad 0 \leq x \leq M(t)$$

$$\frac{\partial T}{\partial t} + V \frac{\partial T}{\partial x} = \varkappa_2 \frac{\partial^2 T}{\partial x^2} + \frac{A_2}{\rho_2 c_2} ; \quad M(t) \leq x \leq b(t)$$

$$K_1 \frac{\partial T}{\partial x}\bigg|_{M^-} - K_2 \frac{\partial T}{\partial x}\bigg|_{M^+} = - L\rho_1 \frac{dM}{dt}$$

$$V = (1 - \frac{\rho_1}{\rho_2}) \frac{dM}{dt} ;$$

$$b(0) - b(t) = (1 - \frac{\rho_1}{\rho_2}) [M(0) - M(t)]$$

The coordinate system is fixed in the region of phase 1; if $\rho_2 \neq \rho_1$, the region of phase 2 will move with velocity V with respect to the coordinate system as the phase boundary moves. The presence of the convective term in the field equations is due to this motion, and because it is a nonlinear term, it may complicate the solution.

The term is easily removed if it is borne in mind that the two regions are indeed separate, and that solutions in the two regions need only match at the phase boundary M(t). Thus there is no need to use the same coordinate system for both regions; rather two coordinate systems, fixed in each region may be used, as long as the boundary condition at M(t) takes this into account. In this way any convective term in the field equations can be eliminated.

Thus if we let

$$z = x, \quad 0 \leq x \leq M(t)$$

$$z = M(t) + \frac{\rho_2}{\rho_1}(x - M(t)), \quad M(t) \leq x \leq b(t)$$

the governing equations become

$$\frac{\partial T}{\partial t} = \varkappa_1 \frac{\partial^2 T}{\partial z^2} + \frac{A_1}{\rho_1 c_1}; \quad 0 \leq z \leq M(t)$$

$$\frac{\partial T}{\partial t} = \frac{\rho_2^2}{\rho_1^2} \varkappa_2 \frac{\partial^2 T}{\partial z^2} + \frac{A_2}{\rho_2 c_2}; \quad M(t) \leq z \leq M(0) + \frac{\rho_2}{\rho_1}[b(0) - M(0)]$$

$$K_1 \frac{\partial T}{\partial z}\bigg|_{M^-} - \frac{\rho_2}{\rho_1} K_2 \frac{\partial T}{\partial z}\bigg|_{M^+} = -L\rho_1 \frac{dM}{dt}$$

and the lower boundary $x = b(t)$ maps into $z = M(0) + \frac{\rho_2}{\rho_1}[b(0) - M(0)]$ which is constant. Thus all translation of region 2 has been eliminated from the equations. This coordinate transformation directly gives the solution for the simple Stefan problems with a change in volume. (Carslaw and Jaeger, (1959) p. 290) from the solution with no change in volume.

APPENDIX 2

We obtain the criterion for the cessation of Stefan type behavior by comparing analogous solutions for a half space and a slab. Since the Stefan approximation (SAC) applies for a half space, we determine the time when the finite extent of the region becomes important.

Consider the gradient at $x = 0$ for a half space $x > 0$ with $T(0,t) = 1$, $T(x,0) = 0$:

$$\left.\frac{\partial T}{\partial x}\right|_{x=0} = -\frac{1}{(\pi \varkappa t)^{1/2}}$$

For a slab $0 \leq x \leq d$, with the same conditions and $T(d,t)$ $T(d,\ t) = 0$

$$\left.\frac{\partial T}{\partial x}\right|_{x=0} = -\frac{1}{(\pi \varkappa t)^{1/2}}\left[1 + 2\sum_{n=1}^{\infty} e^{-\frac{n^2 d^2}{\varkappa t}}\right]$$

The two solutions will diverge when the terms in the sum become large; we take as our criterion for the cessation of Stefan behavior

$$\varkappa t \geq \frac{d^2}{\pi}$$

at which the first term in the sum is 0.043.

APPENDIX 3

The derivation of the quasi-steady state approximation (QSSA) for the case of continuous loading is basically an extension of that given for impulsive loading in our previous paper (OW, p. 354, 372), although there are some minor differences. We shall derive the equations for the motion of the phase boundary in dimensionless notation; the reader should refer to our previous paper (OW, p. 330) for an explanation of the notation.

Using the integral form of the boundary condition at the phase boundary (OW, p. 348) and using material coordinates rather than spatial coordinates (Appendix 1) we have

$$-C\frac{d\xi_m}{d\tau} = \frac{\partial\eta}{\partial\xi}\bigg|_{\xi_s} - \frac{K_2\rho_2}{K_1\rho_1}\frac{\partial\eta}{\partial\xi}\bigg|_1 + \int_{\xi_s}^{\xi_m}\frac{\partial\eta}{\partial\tau}\,d\xi + \frac{c_2}{c_1}\int_{\xi_m}^{1}\frac{\partial\eta}{\partial\tau}\,d\xi$$

We take for the quasi-steady state temperature distribution for the case with constant flux at $\xi = 1$

$$\eta(\xi,\tau) = \frac{B\xi_m - E(\tau) - \gamma_1\xi_s}{\xi_m - \xi_s}(\xi - \xi_s) + \gamma_1\xi_s \;;\; \xi_s \le \xi \le \xi_m$$

$$\eta(\xi,\tau) = B\xi_m - E(\tau) + \gamma_2(\xi - \xi_m) \;;\quad \xi_m \le \xi \le 1$$

where $B \equiv \frac{G\rho_1 g b_0}{T_0}$ and $\gamma_2 = \frac{K_1 \rho_1}{K_2 \rho_2} \gamma_1$

Now, regarding ξ_s as constant with regard to partial differentiation by time, we obtain

$$\left[C + \frac{D\delta}{2} + \frac{c_2}{c_1} \epsilon (B - \gamma_2)\right] \frac{d\xi_m}{d\tau}$$

$$\approx - \frac{D}{\delta} \xi_m + \frac{E(\tau)}{\delta} + \left(\frac{\delta}{2} + \frac{c_2}{c_1} \epsilon\right) \frac{dE}{d\tau}$$

where δ is a constant equal to an average value of $\xi_m - \xi_s$ and ϵ is a constant equal to an average value of $1 - \xi_m$. This approximation includes the effect of convective heat transport, since we have used material coordinates.

APPENDIX 4

The inclusion of the effect of thermal blanketing is done as in our previous paper (OW, p. 379, 395). We shall superimpose the temperature field due to the movement of the phase boundary and the field from the blanketing effect of the sediments. The heat flux at the phase boundary from both temperature fields is set proportional to the velocity of the phase boundary to obtain a differential equation for the motion of the phase boundary.

The temperature field from the thermal blanket is the solution of:

$$\frac{\partial \theta_{BC}}{d\tau} = \frac{\partial^2 \theta_{BC}}{\partial \xi^2} \; ; \quad \xi_s \leq \xi \leq \xi_m$$

$$\theta_{BC}(\xi_s, \tau) = \frac{J_s}{K_s} \frac{K_1}{J_M} \gamma_1 \xi_s(\tau); \quad \theta_{BC}(\xi_m, \tau) = 0$$

$$\frac{d\xi_s}{d\tau} \approx -U \; ; \quad \frac{d\xi_m}{d\tau} \approx -U \; ; \quad \xi_m - \xi_s \approx \delta$$

δ, U constants

J_s is the average heat flux in the sediments, which have conductivity K_s. This is the same as the temperature field used before (OW, p. 395) except that it partially takes into account the

movement of both the surface ξ_s and the phase boundary, and the conductivity of the sediments.

Using Laplace transforms (cf. Carslaw and Jaeger, 1959, p. 388) we obtain

$$\left.\frac{\partial\theta_{BC}}{\partial\xi}\right|_{\xi_m} = -\frac{J_s K_1 \gamma_1}{K_s J_M} e^{\frac{1}{2}U\delta}\left[\frac{(\frac{1}{2}U\tau + 1/U)}{\sinh(\frac{1}{2}U\delta)} - \frac{1}{2}\delta\frac{\cosh(\frac{1}{2}U\delta)}{\sinh^2(\frac{1}{2}U\delta)}\right.$$

$$\left. - \frac{2\pi^2}{\delta^3}\sum_{n=1}^{\infty}\frac{(-1)^n n^2}{(\frac{\pi^2 n^2}{\delta^2} + \frac{U^2}{4})^2} e^{-(\frac{\pi^2 n^2}{\delta^2} + \frac{U^2}{4})\tau}\right] \equiv \Gamma\frac{b_0}{T_0}$$

where, in dimensional units

$$\Gamma \equiv -\frac{J_s}{K_s \kappa_1}\frac{ds}{dt} e^{\frac{d}{\kappa_1}\frac{ds}{dt}}\left[\frac{\frac{1}{2}t\frac{ds}{dt} + \frac{\kappa_1}{ds/dt}}{\sinh(\frac{1}{2}\frac{d}{\kappa_1}\frac{ds}{dt})} - d\frac{\cosh(\frac{1}{2}\frac{d}{\kappa_1}\frac{ds}{dt})}{\sinh^2(\frac{1}{2}\frac{d}{\kappa_1}\frac{ds}{dt})}\right.$$

$$\left. - \frac{2\pi^2}{d^3}\sum_{n=1}^{\infty}\frac{(-1)^n n^2}{[\frac{\pi^2 n^2}{d^2} + \frac{(ds/dt)^2}{4\kappa_1^2}]^2}\exp\left[-(\frac{n^2\pi^2}{d^2} + \frac{(ds/dt)^2}{4\kappa_1^2})\kappa_1 t\right]\right] \qquad \text{(A1)}$$

In the limit neglecting the movement of the surface and the phase boundary ($U \to 0$), we get the result of our previous paper (OW, p. 395) and

$$\Gamma = -\frac{J_s \frac{ds}{dt}}{K_s \varkappa_1}\left[\frac{\varkappa_1 t}{d} - \frac{d}{6} - \frac{2d}{\pi^2}\sum_{n=1}^{\infty}\frac{(-1)^n}{\varkappa^2}\exp\left(-\frac{\pi^2 n^2}{d^2}\varkappa_1 t\right)\right] \qquad (A2)$$

This expression is considerably simpler than (A1), and is sufficiently accurate where $\frac{1}{2}\frac{d}{\varkappa_1}\frac{ds}{dt} \lesssim 0.1$. A further simplification comes if the infinite sum on the right of (A1) and (A2) can be neglected. This often is the case by the time that thermal blanketing must be included in the solution for the lag $\ell(t)$.

To include the effect of thermal blanketing in the Stefan approximation (SAC) we must include a term

$$\frac{2c_1(\varkappa_1 t)^{1/2}}{L}\Gamma$$

on the right hand side of (7). For the quasi-steady state approximation (QSSA), we must add a term $\Gamma/(\frac{H}{c_1})$ to the right hand side of (15). In either case the resulting differential equation is still directly integrable. For the SAC, a term

$$e^{-(\varkappa_1 t)^{1/2}}\int_0^{(\varkappa_1 t)^{1/2}} e^{(\varkappa_1 z)^{1/2}}\frac{2\,c_1(\varkappa_1 z)^{1/2}}{L}\Gamma\, d(\varkappa_1 z)^{1/2}$$

should be added to the right hand side of (9). For the QSSA a term

$$e^{-\omega \varkappa_1 t} \int_0^{\varkappa_1 t} e^{\omega \varkappa_1 z} \frac{c_1 \Gamma}{H} \, d(\varkappa_1 z)$$

should be added to the right hand side of (16).

REFERENCES (Chapter II)

Carslaw, H.S., and J.C. Jaeger, Conduction of Heat in Solids, 2nd ed., Oxford University Press, 1959.

Clark, S.P., Jr., Ed., Handbook of Physical Constants, revised edition, Geol. Soc. Am. Memoir 97, 1966.

Joyner, W.B., Basalt-eclogite transition as a cause for subsidence and uplift, J. Geophys. Res., 72, 4977 - 4998, 1967.

Kennedy, G.C., The origin of continents, mountain ranges and ocean basins, Am. Scientist, 47, 491, 1958.

Lovering, J.F., The nature of the Mohorovicic discontinuity, Trans. Am. Geophys. Union, 39, 947-955, 1958.

MacDonald, G.J.F., and N.F. Ness, Stability of phase transitions within the earth, J. Geophys. Res., 65, 2173-2190, 1960.

McConnell, R.K., Jr., Isostatic adjustment in a layered earth, J. Geophys. Res., 70, 5171 - 5188, 1965.

O'Connell, R.J., Critique of the paper by W.J. van de Lindt, 'Movement of the Mohorovicic discontinuity under isostatic conditions,' J. Geophys. Res, 73, 6604 - 6607, 1968.

O'Connell, R.J., and G.J. Wasserbutg, Dynamics of the motion of a phase change boundary to changes in pressure, Rev. Geophys., 5, 329 - 410, 1967.

van de Lindt, W.J., Movement of the Mohorovicic discontinuity under isostatic conditions, J. Geophys. Res., 72, 1289 - 1297, 1967.

Wetherill, G.W., Steady state calculations bearing on geological implications of a phase-transition Mohorovicic discontinuity, J. Geophys. Res., 66, 2983 - 2993, 1961.

PART 2

PLEISTOCENE GLACIATION AND THE VICOSITY OF THE LOWER MANTLE

CHAPTER I

DEGLACIATION AND THE EARTH'S SECULAR ACCELERATION

The secular angular deceleration of the earth has been observed from growth rings on Devonian corals, observations of eclipses in antiquity and astronomical observations over the last few hundred years (1). This deceleration (increase in the length of day, l. o. d.) is interpreted as primarily due to the effect of lunar tidal friction, which transfers angular momentum from the earth to the Moon. From observations of the longitude of the Moon, the Sun and Mercury over the last few hundred years, as well as from the effect of tidal torques on artificial satellites, one can calculate the variation in the rotation of the earth due to the tidal torques responsible for the acceleration of the Moon. Over this same period of time, though, short term non-tidal variations in the observed l. o. d. are so great as to swamp the tidal effect, which precludes a direct comparison of the tidal deceleration with that actually observed. However, records of the locations of eclipses in antiquity do permit one to calculate the actual change in l. o. d. over the last 2000 or 3000 years. Comparison of this observed variation, with that expected from tidal torques reveals that the earth has not slowed down as much as would be expected from a constant tidal friction over the last few thousand years, i.e. there is an apparent non-tidal angular acceleration of the earth. One likely cause of this would be a decrease in the earth's moment of inertia.

We shall here investigate the effect of the isostatic compensation of the earth to the melting of the Pleistocene ice sheets and the consequent rise in sea level. It will be seen that this effect can completely account for the non-tidal acceleration if the isostatic relaxation time has certain values. Since this relaxation time is at

present not known, one can attribute the acceleration to this effect and in turn infer the relaxation time. Under this assumption, the rheological properties of the mantle may be estimated from the relaxation times given by this method and from studies of uplift of formerly glaciated regions.

I have expanded the areal extent of the Pleistocene ice sheets (2) into surface spherical harmonies, and treated the ice as a uniform surface mass distribution. The total change in the surface distribution of mass upon melting was then determined using the ocean function to include the rise in sea level. (See following chapter)

The first effect upon melting would be an increase in the moment of inertia of the earth as mass is transferred from the polar regions to the more equatorially situated oceans. Isostatic compensation of the load would then result in the flow of subcrustal material from under the oceans to beneath the formerly glaciated regions, which would decrease the moment of inertia. After complete compensation, of course, the net effect will be a slightly greater moment of inertia than before the ice melted, because rock under the oceans would have been replaced by an equal mass of water, which, being less dense, would have a greater moment of inertia since its center of mass would be farther from the earth's center than that of the rock was. I shall neglect this vertical mass redistribution, and treat the mass redistribution as a change in a surface mass distribution. This should introduce no significant errors.

To calculate the magnitude of the effect of deglaciation on the moment of inertia, the time history of the melting was taken to be proportional to the rise in sea level over the last 18,000 years. Figure 1 shows three sea level curves that I have used. In view of the uncertainty about changes in sea level in the past, these should be regarded only as possible curves; the dependence of the conclusions I draw on details of the melting curves will be discussed later.

The rate of isostatic response to a surface load was taken to be proportional to the uncompensated load, i.e. it is exponential with a relaxation time τ which follows from the behavior of a viscous sphere. The spherical harmonic components of different degrees which characterize a given surface deformation will in general exhibit a different relaxation time for each degree.

The moment of inertia of a surface mass distribution $\underline{s}$ on a sphere of radius $\underline{a}$, where

$$s = \sum_{\ell=0}^{\infty} \sum_{m=0}^{\ell} \bar{P}_\ell^m(\cos\theta) \left[C_\ell^m \cos m\lambda + S_\ell^m \sin m\lambda\right]$$

is, if C_0^0 vanishes

$$I = -\frac{8\pi}{3\sqrt{5}} a^4 C_2^0$$

where θ is colatitude, λ is longitude, and the Legendre functions $\bar{P}_\ell^m(\cos\theta)$ are normalized so that the mean square of a spherical harmonic is unity.

FIGURE 1

Rise of sea level over the last 18, 000 years used in calculation of the change in Earth's moment of inertia. The circles show Shepard and Curray's (3) proposed eustatic curve and the crosses the lower limit of curves measured on the east coast of the U.S. as reported by Shepard and Curray (3).

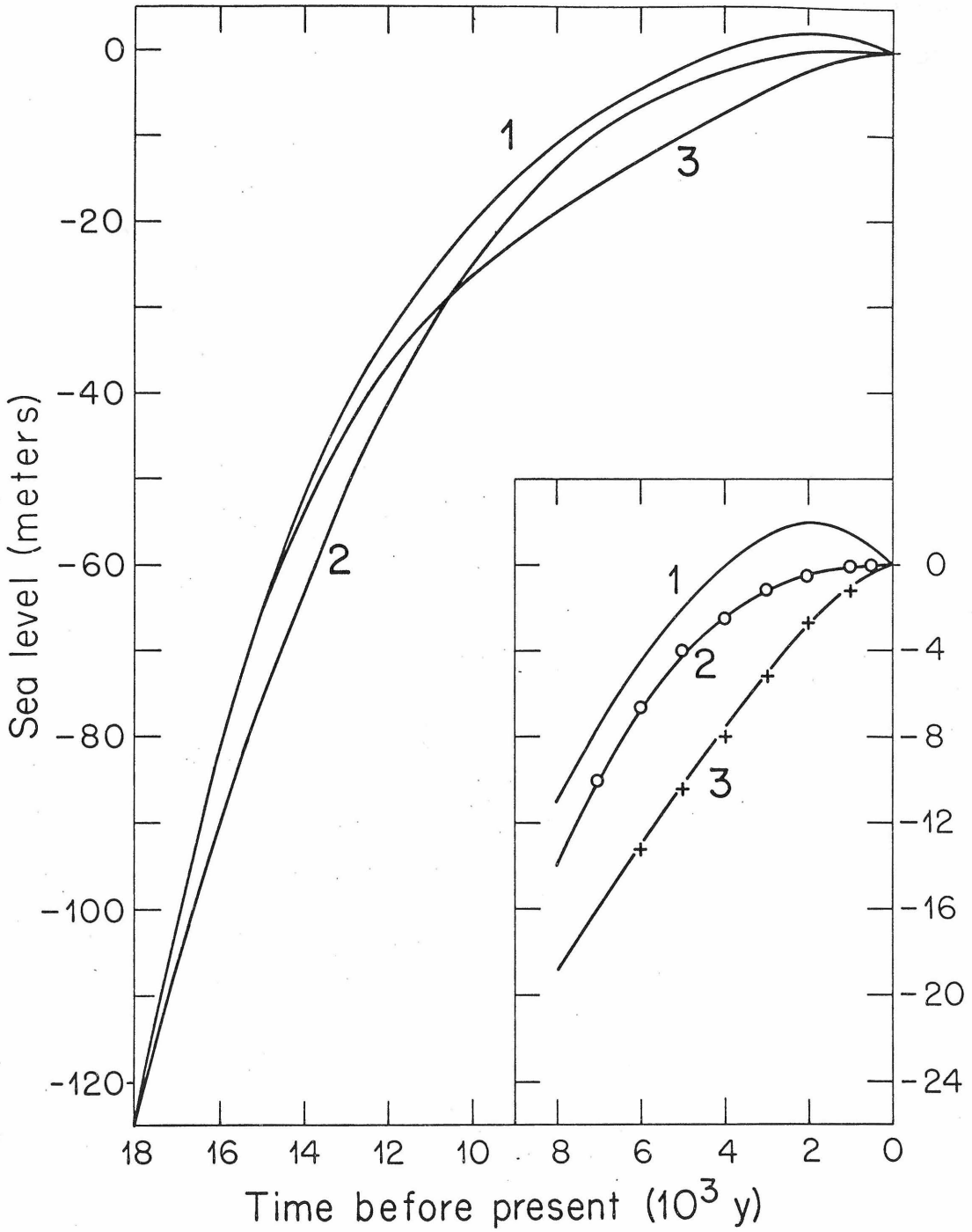
0
-20
-40
-60
-80
-100
-120
Sea level (meters)
1
2
3
18
16
14
12
10
8
6
4
2
0
Time before present (10^3 y)
0
-4
-8
-12
-16
-20
-24

FIGURE 1

The second degree component of the surface load from the ice and water alone is $\sigma_1(t)$ and is a function of time proportional to the rise in sea level. As mentioned above, we regard the mass redistribution due to isostatic compensation as a surface load as well; thus the second degree component of the total surface load $\sigma(t;\tau)$ will be a function of time and the relaxation time τ. The exponential nature of isostatic adjustment then gives

$$\frac{d}{dt}\ \sigma\ =\ -\ \frac{1}{\tau}\sigma\ +\ \frac{d}{dt}\ \sigma_1$$

which can be integrated directly:

$$\sigma(t;\tau)\ =\ \sigma_1(t)\ -\ \frac{1}{\tau}\, e^{-t/\tau} \int_0^t e^{\xi/\tau}\, \sigma_1(\xi)\, d\xi$$

The integral can be evaluated since we know $\sigma_1(t)$ from the rise of sea level.

The moment of inertia of this surface load can be written

$$I' = \frac{8\pi}{3\sqrt{5}}\ a^4\ C_2{}^{0*}\ y(t;\tau)$$

where C_2^{0*} is the coefficient from the ice load $\sigma_1(t)$ at the present, i.e. the surface load from the complete melting of the ice sheets and the rise of sea level to its present stand. The dimensionless function $y(t;\tau)$ is proportional to the $\ell = 2$, $m = 0$ coefficient of the expansion of $\sigma(t;\tau)$ and contains all the information on the time history of the melting and the nature of the isostatic response.

Thus, after subtracting out the change in angular velocity due to tidal friction, conservation of angular momentum of the earth requires

$$\frac{d}{dt}\left[(I + I')\,\omega\right] = 0$$

where I is the polar moment of inertia of the earth and ω is the angular velocity of the earth. Since I' is small in comparison with I, this yields

$$\left.\frac{d}{dt}\,y(t;\tau)\right|_{t=t_0} \approx -\frac{3/5}{8\pi a^4}\,\frac{I}{C_2^{0*}}\,\frac{\dot{\omega}}{\omega}$$

where $\dot{\omega}$ is the observed angular acceleration at time t_0. This equation can of course be integrated to relate the average value of $y(t;\tau)$ over a time interval to the average value of $\dot{\omega}$ over

the same interval. It is this value that is appropriate for comparison with $\dot{\omega}$ inferred from ancient eclipse data, whereas the value of $\frac{d}{dt} y(t; \tau)$ at the present time should be compared with present astromonical values of $\dot{\omega}$. If we knew the relaxation time τ, we could calculate the expected acceleration for a given history of sea level.

The relaxation time for an $\ell = 2$, $m = 0$ spherical harmonic deformation of the earth has been previously inferred from the magnitude of the non-hydrostatic bulge of the earth, which is assumed to be anomalous and due to incomplete adjustment to the decelerating rotation of the earth (4). This assumption is now suspect, however, since the ellipticity of the equator is as great as the non-hydrostatic bulge; the fact that the C_2^0 coefficient in the geopotential is larger than the C_2^2 coefficient is merely due to the choice of coordinate axes (5). To see this, we will, following McKenzie (4), compare the approximate energy represented by the various terms in the geopotential, using

$$E_\ell^m \propto [(C_\ell^m)^2 + (S_\ell^m)^2] (\ell - 1)(2\ell + 1)$$

where $S_\ell^0 = 0$. Taking for the non-hydrostatic coefficients of the geopotential (6)

$$C_2^0 = -4.7 \times 10^{-6}; \quad C_2^2 = 2.42 \times 10^{-6};$$

$$S_2^2 = -1.36 \times 10^{-6}; \quad C_2^1 = S_2^1 = 0$$

we thus get $E_2^0 \propto 110 \times 10^{-12}$ and $E_2^2 \propto 38.5 \times 10^{-12}$. It was this difference that led McKenzie to conclude that the non-hydrostatic bulge was anomalously large. That this is merely a consequence of the coordinate system he used can be seen by transforming to a new system, which we will designate by primes, with the $\theta' = 0$ pole aligned with the axis of the smallest moment of inertia of the earth and $\lambda' = 0$ aligned with the present pole. The harmonic coefficients of the geopotential in this system will also be represented by primes. The addition theorem for spherical harmonics (7) then yields

$$(C_2^{0'})^2 = \frac{3}{4}[(C_2^2)^2 + (S_2^2)^2] + \frac{1}{4}(C_2^0)^2 - \frac{\sqrt{3}}{2} C_2^0 [(C_2^2)^2 + (S_2^2)^2]^{1/2}$$

Since $\sum_{m=0}^{\ell} [(C_\ell^m)^2 + (S_\ell^m)^2]$ is independent of the coordinate system (7) we can obtain $(C_2^{2'})^2 + (S_2^{2'})^2$. Thus,

$E_2^{0'} \propto 113 \times 10^{-12}$ and $E_2^{2'} \propto 36.0 \times 10^{-12}$.

The difference between the energies is the same as before, but now $E_2^{0'}$ is associated with the ellipticity of the equator while $E_2^{2'}$ is associated with the bulge. Thus the energy associated with the departure from hydrostaticity is the same for either term, and we must then conclude that the nonhydrostatic bulge is no more anomalous than the ellipticity of the equator. In view of this result it does not seem justified to associate the non-hydrostatic bulge with the deceleration of the earth's rotation.

Thus, having no other estimate of the relaxation time τ, we can assume that the observed non-tidal acceleration is due entirely to the melting of the ice sheets. On this basis we can then infer a value of τ, if one exists, that will satisfy equation (1) using the measured acceleration and an assumed sea level curve.

Figure 2 shows the left hand side of equation (1) at the present and averaged over the last 2000 and 3000 years, plotted against the relaxation time. The right hand side of equation (1) is represented by the shaded regions. The stippled area uses Munk and MacDonald's (1) range of values for the angular acceleration, which is based on Fotheringham's study of ancient eclipses. The hachured area is based on more recent data using Newton's values for the angular acceleration based on his analysis of tidal torques through their effect on artificial satellites and on Curott's study of

FIGURE 2

Plot of equation (1) versus the relaxation time for the three sea level curves in Figure 1. Solid line: calculated acceleration at present; long dashes: calculated acceleration averaged over last 2000 years; short dashes: acceleration averaged over last 3000 years. The intersections of the dashed lines with the shaded regions define acceptable values for the relaxation time for an $\ell = 2$ deformation of the earth. As can be seen, the relaxation time is either around 2000 years or 100,000 years.

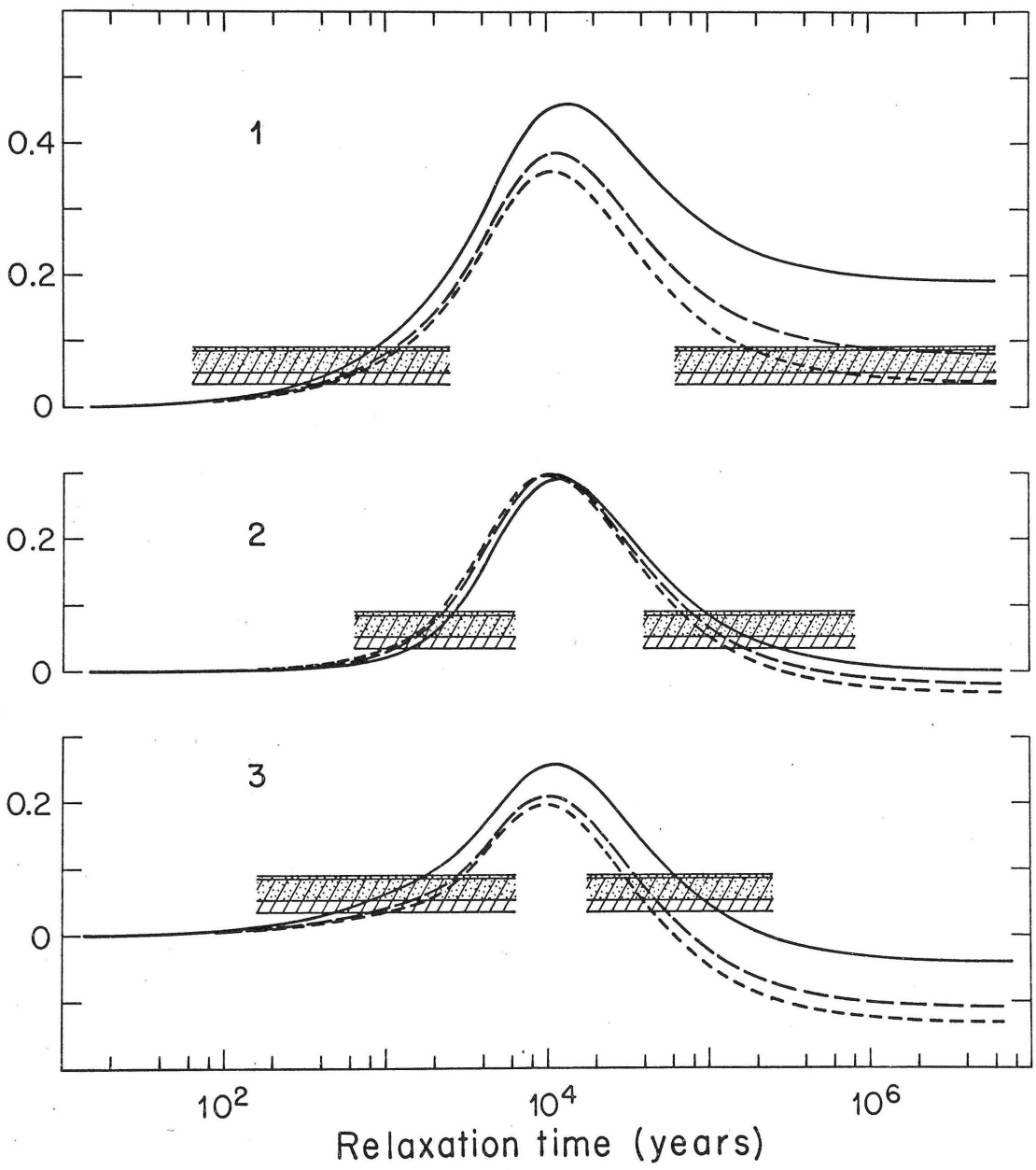

FIGURE 2

ancient eclipses (8). In both regions the effect of a range of C_2^{0*} corresponding to a rise in sea level of 100 to 125 meters over the last 18,000 years has been included.

The first thing to notice is that the effect of isostatic compensation to the melting of the ice sheets could have a very large effect on the acceleration of earth. In fact, if τ were $\sim 10^4$ years (which is the characteristic time scale for the melting of the ice sheets) the magnitude of the effect could be up to ten times greater than the observed non-tidal acceleration, which would then be greater than the tidal deceleration, but of the opposite sign.

The first set of curves corresponds to the sea level curve with a stand 2 meters above the present sea level 2000 years ago. A possible value for the relaxation time is around 800 years. If this is correct for the earth, the non-tidal acceleration should have increased by 50% over the last 3000 years. The other possible root for this sea level curve is greater than a few hundred thousand years. In this case the non-tidal acceleration would have increased roughly by a factor of 4 over the last 3000 years and the present non-tidal acceleration would nearly cancel the present tidal deceleration.

Similarly for the other sea level curves, there are two roots: either around 2000 years or near 100,000 years, and in every case except $\tau \sim 2000$ y. for the second set of curves, the non-tidal acceleration should have increased over the last 3000 years. Dicke (9) finds evidence for a <u>decrease</u> in the non-tidal acceleration from

3000 to 2000 years before the present. However, since such a trend is not apparent in Curott's more comprehensive study, it does not seem possible to unequivocally exclude possible combinations of sea level curves and relaxation times solely on this basis.

The values we have obtained as possible relaxation times removes some of the dependence of the calculated relaxation times on details in the sea level curve. If the relaxation time is short, we are mainly seeing the effect of sea level changes over the last few thousand years, since effects prior to that will have already decayed. If the relaxation time is long, we are seeing the total change in sea level, and any small irregularities in sea level will be "averaged out". These conclusions derive from the fact that either calculated relaxation time is significantly different from the characteristic time scale of the melting, which is $\sim$ 10,000 years. Of course changes in sea level during the period over which we calculate the change in ω have a large effect, as can be seen in Figure 2. Nevertheless, the separation of possible relaxation times into two possible ranges which are quite distinct, appears to be a firm conclusion that one can draw from this calculation.

We should note that if the relaxation time is of the order of 100,000 years, the earth may still be responding to changes in sea level that might have occurred prior to 18,000 years ago. The calculated value for the relaxation time of 100,000 years thus rests upon the assumption that the ice sheets persisted, except for variations over a time scale less than 100,000 years, for the 100,000

years or so preceding the onset of the melting 18,000 years ago. If this assumption is not satisfied, the calculated relaxation time will be somewhat less, which will in turn weaken the dependence of the calculation on the ice history 100,000 years ago.

McConnell (10) has used another argument to deduce the relaxation time of an $\ell = 2$ deformation. He assumes that the present non-hydrostatic bulge is a result of deglaciation. From the magnitude of the bulge, and the non-tidal acceleration he calculates a relaxation time of $\sim 3 \times 10^5$ years. However, his assumption that the bulge is due to deglaciation is suspect because, as shown above, the bulge is not anomalously large, and thus there is no need to explain it by some other mechanism, such as deglaciation or the secular deceleration of the earth. In addition his assumption that the present bulge is a remnant of deglaciation implies directly that the isostatic disequilibrium from deglaciation is still substantial, which implicitly implies that the relaxation time is sufficiently long that the disequilibrium would not yet have had time to decay. In addition, the magnitude of C_2^0 calculated from the actual configuration of the ice (see following chapter) is too small by a factor of three to explain the non hydrostatic bulge, i.e. that the isostatic disequilibrium following deglaciation could account for only 1/3 of the present bulge, even if the earth had not relaxed at all following the melting of the ice sheets. Thus our values for the relaxation time of an $\ell = 2$ deformation are to be preferred for these reasons.

We should note that McKenzie (4, 11) has also discussed this problem, and shown that if the relaxation time is $\sim$7000 years that only $\sim$ 5% of the present bulge could be due to deglaciation. He also suggests that the non-tidal acceleration is due to isostatic response following deglaciation.

REFERENCES (Chapter I)

1. J. W. Wells, Nature 197, 948 (1963), W.H. Munk and G. J. F. MacDonald, The Rotation of the Earth (Cambridge, 1960), W.H. Munk, in The Earth-Moon System, B.G. Marsden and A.G.W. Cameron, Ed. (Plenum, New York, 1966).

2. W.L. Donn, W.R. Farrand and M. Ewing, Jour. Geol. 70, 206 (1962).

3. F.P. Shepard and J.R. Curray, Progress in Oceanography, 4 M. Sears, Ed. (Pergamon, New York, 1967).

4. D.P. McKenzie, J. Geophys. Res. 71, 3995 (1966); W.H. Munk and G.J.F. MacDonald, op. cit.

5. P. Goldreich, and A. Toomre, J. Geophys. Res., in press (1969).

6. W.M. Kaula, J. Geophys. Res. 71, 5303 (1966).

7. W.M. Kaula, Rev. Geophys. 5, 83 (1967).

8. R. Newton, Geophys. J. Roy. Astron. Soc. 14, 505 (1968); D.R. Curott, Astron. J. 71, 264 (1966).

9. R.H. Dicke, in The Earth-Moon System, B.G. Marsden and A.G.W. Cameron, Ed. (Plenum, New York, 1966).

10. R.K. McConnell, Jr., J. Geophys. Res., 73, 7089 (1968).

11. D.P. McKenzie, Geophys. J. Roy. Astron. Soc. 14, 297 (1967).

CHAPTER II

CORRELATION OF PLEISTOCENE ICE SHEETS WITH THE PRESENT GEOPOTENTIAL

In the previous chapter we have seen that the relaxation time for a degree two deformation of the earth is either $\sim$ 2000 years or $\sim$ 100,000 years. The argument that was used to obtain these times, however, was incapable of discriminating between them. The consequences of these two relaxation times are distinctly different. If the proper choice is $\sim$ 2000 years, the long wavelength components of the deformation will have decayed by a factor of $\sim$ 1000 since the ice melted, and thus would be hardly detectable today. If the proper choice is $\sim$ 100,000 years, the long wavelength components will have decayed by only a few percent, and might well be still observable.

The change in the earth's moment of inertia discussed in the previous chapter may be alternatively expressed as a change in the degree two, order zero component of the earth's gravitational field. (McKenzie, 1967). This leads us to inquire if any evidence of the isostatic anomalies resulting from deglaciation can be found in the other coefficients of the geopotential. Since deformations characterized by different wavelengths or degrees will decay at different rates, we shall focus attention on the components of the geopotential of lowest degree, since these are most likely to have a relaxation time similar to the degree two relaxation time. In particular, the degree $\ell = 2$, order $m = 2$ components will have the same relaxation time as the moment of inertia; thus if the relaxation time for an $\ell = 2$ deformation is long, the coefficients of the geopotential corresponding to $\ell = 2$, $m = 2$ should still contain the anomalies from deglaciation.

This investigation should also answer the question of whether the non-hydrostatic bulge is a result of deglaciation, as suggested by

Wang (1966), and assumed by McConnell (1968) in his calculation of the viscosity of the lower mantle.

In order to detect any effects of deglaciation on the geopotential, we will first expand the mass redistribution upon melting as a series of surface spherical harmonics. The gravitational potential from this mass redistribution will then be compared with a spherical harmonic representation of the geopotential. This will be done by correlating the two potentials at a fixed radius, and then inquiring into the significance of the calculated correlation coefficient.

Harmonic Expansion of Ice Distribution

The distribution of Pleistocene ice sheets which existed less than 30,000 years ago has been taken from Donn et. al. (1962), who also give the thickness and ice volume of each ice sheet. In addition, the extent of South America glaciation was taken from Flint (1957). The distribution of ice in the northern hemisphere is shown in Figure 1. In order to obtain the harmonic coefficients of the mass of the ice, each ice sheet was first expanded separately as a function equal to one where the ice was present and zero everywhere else (Appendix 1). For this purpose, the ice sheets were assumed to be bounded by lines of latitude and longitude, which are shown as dotted lines in Figure 1. The expansion was carried out to degree 12. The coefficients of each ice sheet expansion were then multiplied by the average thickness assumed for the ice sheet, and the coefficients for all the ice sheets were combined to give an

FIGURE 1

Distribution of Pleistocene ice sheets that existed less than 30,000 years before present. The areas expanded into spherical harmonics are shown by the dotted lines.

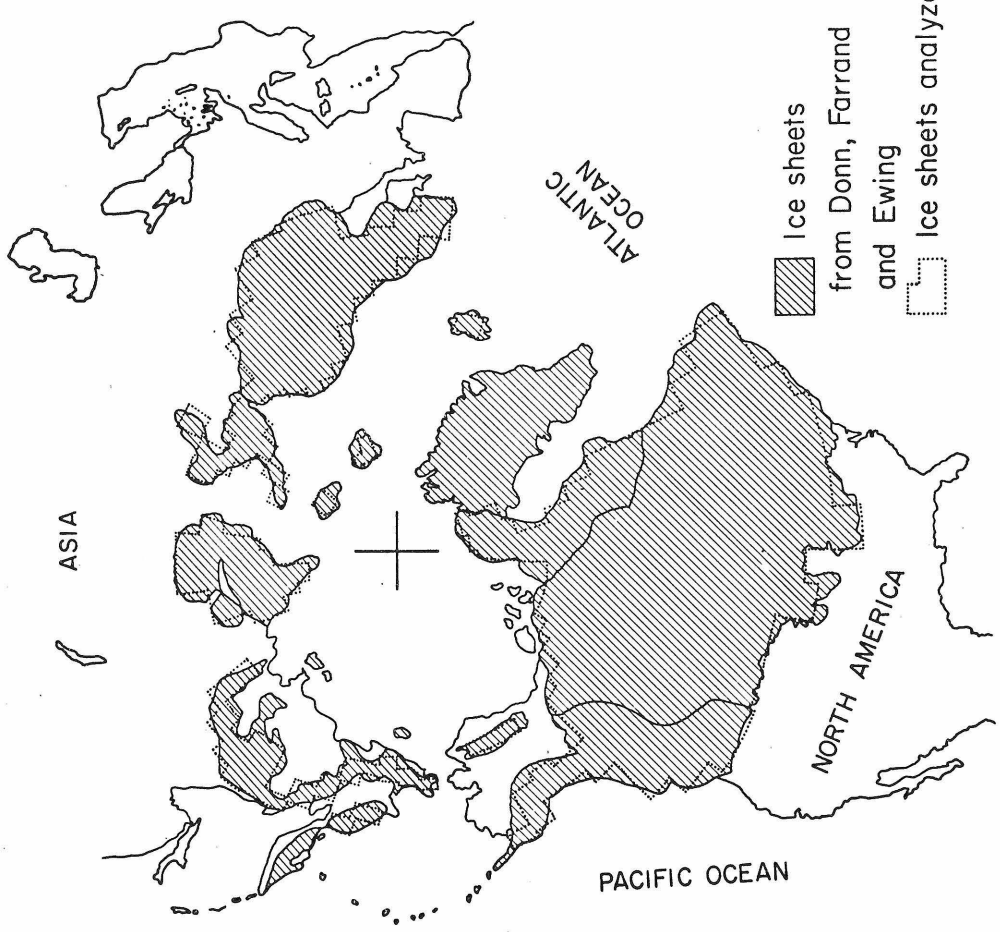
ASIA
ATLANTIC OCEAN
NORTH AMERICA
PACIFIC OCEAN
Ice sheets from Donn, Farrand and Ewing
Ice sheets analyzed

FIGURE 1

expansion of the world ice thickness. The coefficients for the mass was obtained by multiplying the thickness by the ice density (0.9174 g/cm^3). The areas, and thicknesses of the ice sheets which were analyzed are given in Table 1.

The areas of the ice sheets analyzed was 16% less than the areas of the ice sheets as given by Donn et. al. (1962). This difference should partially compensate for the fact that the outer margins of the ice sheets were thinner than the average, and that they also would have been the first to disappear. Thus the area actually analyzed corresponded to the thicker, more central portions of the ice sheets, and thus are probably better for our purpose than an expansion that included the margins of the ice sheets as well. The thicknesses taken for the smaller ice sheets are probably too large; they are so small in area, though, that this doesn't have any effect on our conclusions, as will be seen.

In order to obtain the total change in mass distribution upon melting of the ice sheets, the mass change from the rise in sea level was obtained using the coefficients of the ocean function given by Lee and Kaula (1967); the mass of the ice was assumed transferred uniformly to the oceans upon deglaciation. The resulting rise in sea level was 85 meters. Thus, if anything, we have underestimated the mass redistribution. The effect of a larger rise in sea level can be found just by scaling the harmonic coefficients we have obtained.

In order to determine the effect that our lack of knowledge of the details of the ice distribution might have on our study, two different harmonic analyses of the ice distribution were used. The

Table 1. Areas and Average Thicknesses of Ice Sheets

Ice Sheet	Area (10^6 km^2)	Thickness (m)
Laurentide	10.97	2500
Cordillera	1.88	1100
Brooks Range	0.14	1000
Fennoscandia	3.04	1770
Iceland	0.05	600
Spitzbergen	0.03	1000
Siberian Islands	0.04	1000
Urals	0.52	1000
North Central Siberia	1.12	1570
East Siberia	1.15	1000
Kamchatka	0.12	1000
South America	0.27	1000

first is as described above, and consists of the ice sheets shown in Figure 1 and listed in Table 1. This will be called ice analysis 1. The second, called ice analysis 2, consists of only the Laurentide, Cordillera, Fennoscandia and Ural ice sheets. These ice sheets account for $\sim$ 85% of the glaciated area, and will probably account for most of the world wide effects associated with deglaciation. By comparing the results of the two ice analyses, we will be able to assess the importance of the smaller ice sheets, or details of the larger ice sheets and the effect of our approximating the borders of the ice sheets by lines of latitude and longitude. It will be seen that the two ice analyses give nearly the same results; thus our conclusions will not rest upon details in the ice distribution we have used.

Earth's Gravitational Field

We shall use the notation and conventions used by Kaula (1963). The earth's gravitational potential is given by

$$V = \frac{KM}{r}\left\{1 + \sum_{\ell=2}^{\infty} \left(\frac{a}{r}\right)^{\ell} \bar{P}_{\ell}^{m}(\cos\theta)\left[C_{\ell}^{m}\cos m\lambda + S_{\ell}^{m}\sin m\lambda\right]\right\}$$

where θ is colatitude, λ is longitude, r is the radial coordinate, a is the radius of the earth, K is the gravitational constant and M is the mass of the earth. The fully normalized Legendre functions satisfy

$$\int_0^{2\pi}\int_0^{\pi}\left[\bar{P}_\ell^m(\cos\theta)\begin{Bmatrix}\cos m\lambda\\ \sin m\lambda\end{Bmatrix}\right]^2 \sin\theta\, d\theta\, d\lambda = 4\pi$$

The spherical harmonic coefficients of the geopotential C_ℓ^m and S_ℓ^m represent the departure of the field from spherical symmetry. By far the largest of these is C_2^0 which represents the hydrostatic bulge of the earth due to its rotation. Since we will be interested in the non hydrostatic field, we shall subtract the value of C_2^0 for a truly hydrostatic earth, H_2^0, (Jeffreys, 1963) from the observed value of C_2^0. A similar correction will be made to C_4^0.

The values for the harmonic coefficients of the geopotential we shall use are from Kaula (1966). The values we shall use primarily are those of Kaula, obtained by combining values for the coefficients obtained from orbiting satellites with information from terrestrial gravimetry. These values are given in Table 8 of Kaula's paper.

For purposes of comparison, to determine the effect of our choice of a particular set of coefficients for the geopotential, we shall also use Gaposhkin's values for the coefficients, given as solution G8 in Table 5 of Kaula's paper. These coefficients were determined from satellite data alone. We shall see that the results we obtain are the same for either set of coefficients for the geopotential.

Comparison of Ice Potential and Geopotential

We first compare the relative magnitudes of the geopotential and ice potential in order to see if the latter is actually large enough to noticeably affect the geopotential. A measure of the magnitude of the different degrees of a function is the degree variance or power spectrum σ_ℓ, where

$$\sigma_\ell^2 = \sum_{m=0}^{\ell} \left[(C_\ell^m)^2 + (S_\ell^m)^2 \right]$$

This is independent of the coordinate system used, although the individual coefficients C_ℓ^m and S_ℓ^m are not (Kaula, 1967).

The degree variances for the ice potentials from both analyses 1 and 2, and the degree variances for three different determinations of the geopotential are shown in Figure 2. The ice potential is smaller than the geopotential by a factor of 3 for $\ell = 2$, is comparable to the geopotential for $\ell = 7$ and $\ell = 8$, and falls off relative to the geopotential for higher degrees. The hump in the curve for the ice potentials around $\ell = 7$ is a reflection of the average size of the ice sheets and ocean basins, since $\ell = 7$ corresponds to a function with a characteristic wavelength of $\sim$ 5000 km. (The wavelength λ of a function of spherical harmonic degree ℓ on a sphere of radius a may be taken as $\lambda = 2\pi a/[\ell(\ell + 1)]^{1/2}$.)

The degree variances for the three determinations of the geopotential agree among themselves very well for degrees 2, 3 and

FIGURE 2

Degree variances or power spectra for the potential from the redistribution of mass due to deglaciation, and for three determinations of the geopotential. The geopotential spectrum A & S is from the solution by Anderle and Smith as reported by Kaula (1967b). Note that the ice potential is of a magnitude comparable to the geopotential.

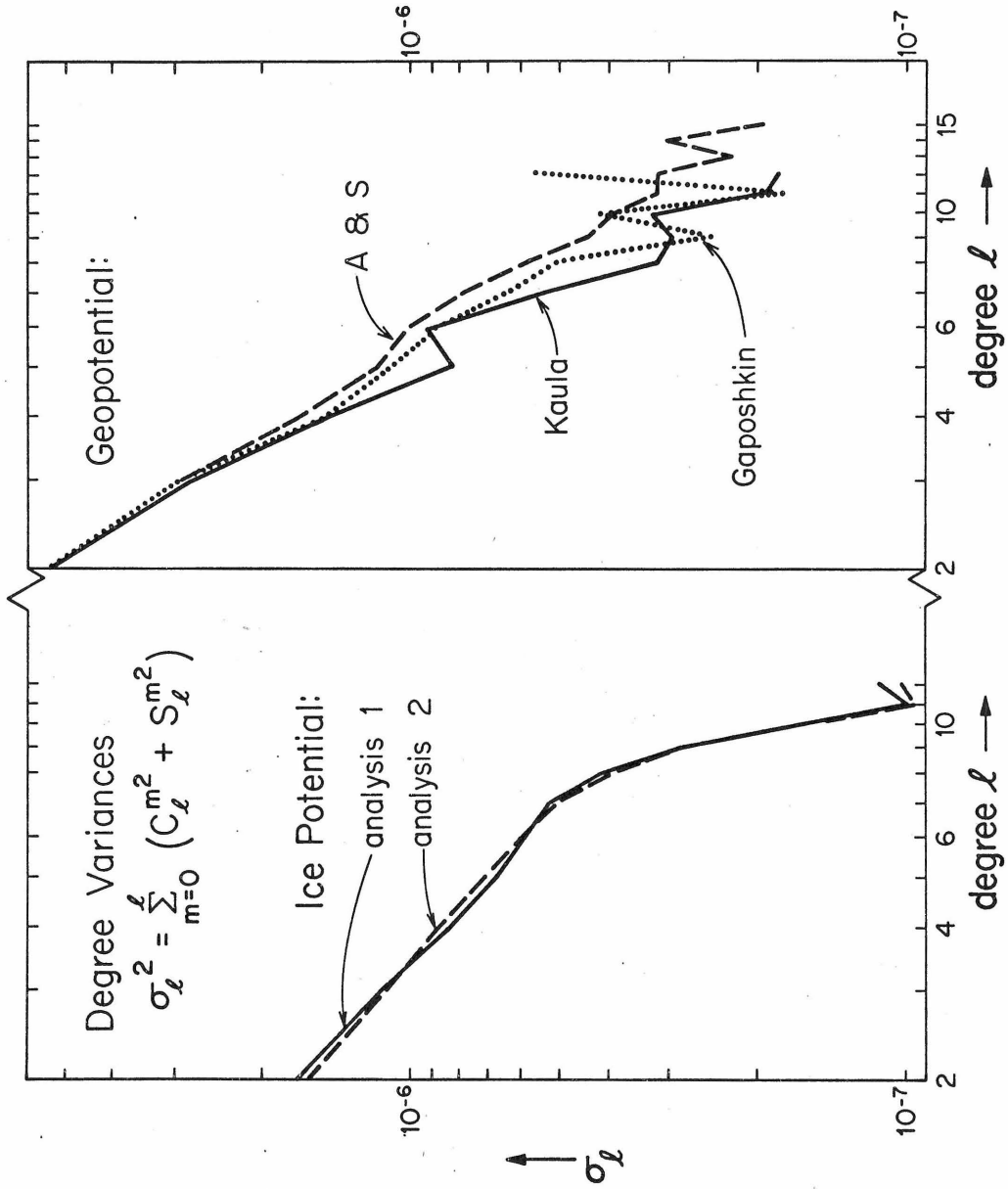
Degree Variances
$\sigma_\ell^2 = \sum_{m=0}^{\ell} (C_\ell^{m2} + S_\ell^{m2})$
Ice Potential:
analysis 1
analysis 2
Geopotential:
A & S
Kaula
Gaposhkin
σ_ℓ
10^{-6}
10^{-7}
degree ℓ
2
4
6
10
15

FIGURE 2

4. The kink in Kaula's curve at $\ell = 5$ and 6 probably arises from his use of terrestrial gravimetric data. The differences in the curves for higher degrees reflects the difficulties in accurately determining the smaller, higher degree coefficients.

Although the ice potential is up to three times smaller than the geopotential for degrees 2, 3 and 4, it is probably large enough to be detected in the present geopotential if it hasn't decayed substantially since deglaciation. For higher degrees uncertainties in the coefficients of the geopotential may make detection of the effects of the ice difficult to see, although for degrees 7 and 8 the ice potential is large enough to have a substantial effect on the geopotential. Thus it is worthwhile to attempt to detect a remnant of the effect of deglaciation in the present geopotential, since it may be large enough to be seen.

Correlation of Two Functions on a Sphere

As a measure of the relationship between the present geopotential and the ice potential we shall calculate a correlation coefficient for the two potentials evaluated at the earth's surface. The ice potential evaluated at the surface is taken as

$$U(\theta, \lambda) = \frac{KM}{a} \sum_{\ell=2}^{\infty} \sum_{m=0}^{\ell} \bar{P}_\ell^m(\cos\theta) \left[A_\ell^m \cos m\lambda + B_\ell^m \sin m\lambda\right] \quad (1)$$

where A_ℓ^m and B_ℓ^m are the coefficients of the potential obtained from the spherical harmonic expansion of the ice.

The non hydrostatic geopotential at the surface is

$$V(\theta,\lambda) = \frac{KM}{a} \sum_{\ell=2}^{\infty} \sum_{m=0}^{\ell} \bar{P}_\ell^m(\cos\theta) \left[C_\ell^m \cos m\lambda + S_\ell^m \sin m\lambda\right] \quad (2)$$

The correlation coefficient ρ is just the normalized covariance of the two functions over the sphere (Lee, 1960, p. 220; Kaula, 1967)

$$\rho = \frac{\int_0^{2\pi} \int_0^{\pi} U(\theta,\lambda)\, V(\theta,\lambda) \sin\theta \, d\theta \, d\lambda}{\left\{ \int_0^{2\pi} \int_0^{\pi} [U(\theta,\lambda)]^2 \sin\theta \, d\theta \, d\lambda \int_0^{2\pi} \int_0^{\pi} [V(\theta,\lambda)]^2 \sin\theta \, d\theta \, d\lambda \right\}^{1/2}} \quad (3)$$

or, using (1) and (2)

$$\rho = \frac{\sum_{\ell=2}^{\infty} \sum_{m=0}^{\ell} \left(A_\ell^m C_\ell^m + B_\ell^m S_\ell^m\right)}{\left\{ \sum_{\ell=2}^{\infty} \sum_{m=0}^{\ell} \left[(A_\ell^m)^2 + (B_\ell^m)^2\right] \sum_{\ell=2}^{\infty} \sum_{m=0}^{\ell} \left[(C_\ell^m)^2 + (S_\ell^m)^2\right] \right\}^{1/2}} \quad (4)$$

By the Cauchy-Schwarz inequality $\rho^2 \geq 1$. (Apostol, 1957, pp. 6, 244), and it can be shown that $\rho^2 = 1.0$ if and only if the two functions are linearly related (Apostol, 1957, p. 20). A value of ρ such that $\rho^2 < 1$ is a measure of the linear dependence of one function on the other; if $\rho = 0$ the two functions are considered linearly independent.

The correlation coefficient defined in (3) and (4) is exactly analogous to the correlation coefficient as used in statistics (Cramer, 1946, p. 265; Lee, 1960, p. 220) which is defined for random variables ξ, η as

$$\rho = \frac{E[(\xi - \bar{\xi})(\eta - \bar{\eta})]}{\left\{ E[(\xi - \bar{\xi})^2] \, E[(\eta - \bar{\eta})^2] \right\}^{1/2}} \tag{5}$$

where $\bar{\xi}$ and $\bar{\eta}$ are the respective population means and $E[f(\xi)]$ is the mathematical expectation of the random variable $f(\xi)$ (Cramer, 1946, p. 170). Thus we may regard U and V as random variables which have been mapped into the random variables A_ℓ^m, B_ℓ^m and C_ℓ^m, S_ℓ^m. (The double indices and double sum associated with these coefficients may be eliminated by a change to a single index if desired.) Since our choice of coordinate system was arbitrary, we could have chosen it so that all the coefficients had the opposite sign but same magnitude as they actually have with our present choice. Thus we conclude that the population means of A_ℓ^m, B_ℓ^m and C_ℓ^m, S_ℓ^m are zero. Thus (5) is equivalent to (4), and ρ may be regarded as the correlation coefficient of the two random variables represented by A_ℓ^m, B_ℓ^m and C_ℓ^m, S_ℓ^m.

On the basis of this analogy, we may use standard statistical techniques to determine the significance of any value of the correlation coefficient that we may obtain from correlating the ice potential and geopotential. That this is of considerable importance is easily seen.

The correlation coefficient is a measure of the linear dependence of two random variables ξ and η, i.e. it is a measure of the tendency of the variables to lie on a straight line in a ξ, η plot. In evaluating the correlation coefficient we actually deal with a limited sample x_i, y_i of the populations ξ, η; and the value we obtain for the sample correlation coefficient will have a significance that depends on the sample size. For example, if we sample each population only two times, we obtain the pairs (x_1, y_1) and (x_2, y_2). If we calculate a correlation coefficient from these we obtain ± 1.0. The only significance of this is that it confirms that a straight line can be drawn through any two points. It says nothing about the linear dependence of the two populations ξ and η.

If we designate the correlation coefficient calculated from a sample x_i, y_i as r, we see that the value of r may differ from the population correlation coefficient ρ. In fact, for small samples they may differ considerably. Thus we will need some standard by which we can assess the significance of the sample correlation coefficient r. (In the remainder of this chapter we shall use Greek letters for population characteristics or variables; the corresponding Roman letters will designate the corresponding sample characteristics or variables. Thus ξ, η, ρ refer to the population, x, y and r to the sample of the population.)

A more complete measure of the linear dependence of two random variables may be obtained by linear regression. The linear regression line

$$g(\xi) = \alpha + \beta\xi$$

minimizes $[\eta - g(\xi)]^2$ when

$$\beta = \beta_{21} \equiv \frac{\mu_{11}}{\mu_{20}} = \rho \frac{\sigma_2}{\sigma_1} \quad \text{and} \quad \alpha = \bar{\eta} - \beta_{21}\bar{\xi}$$

where

$$\mu_{ij} \equiv E[(\xi - \bar{\xi})^i (\eta - \bar{\eta})^i]$$

$$\sigma_1^2 \equiv \mu_{20} \equiv E[(\xi - \bar{\xi})^2]$$

$$\sigma_2^2 \equiv \mu_{02} \equiv E[(\eta - \bar{\eta})^2]$$

β_{21} is called the regression coefficient of η on ξ.

The corresponding sample characteristics for a sample of size n are

$$b = b_{21} \equiv \frac{m_{11}}{m_{20}} = r \frac{s_2}{s_1} \; ; \quad a = \bar{y} - b_{21}\bar{x}$$

$$m_{11} \equiv \frac{1}{n} \sum_i (x_i - \bar{x})(y_i - \bar{y})$$

$$s_1^2 \equiv m_{20} \equiv \frac{1}{n} \sum_i (x_i - \bar{x})^2$$

$$s_2^2 \equiv m_{02} \equiv \frac{1}{n} \sum_i (y_i - \bar{y})^2$$

$$r \equiv \frac{m_{11}}{s_1 s_2}$$

This is just a "least squares" straight line through the points (x_i, y_i). We shall use this means to try to determine the relation between the geopotential and the ice potential.

Significance of Calculated Correlation and Regression Parameters

In order to determine the significance of the sample correlation coefficient r and the regression coefficient b_{21} we shall answer the question: If actually $\rho = 0$, what is the probability of having obtained the value of r that we did? Thus we shall test the null hypothesis that the population correlation coefficient ρ is actually zero.

If $\rho = 0$ and the sample variable y_i of size n comes from a normal population, then the variable

$$t = r\left(\frac{n-2}{1-r^2}\right)^{1/2} \tag{6}$$

is distributed in Student's distribution with $n - 2$ degrees of freedom (Cramer, 1946).

If ρ is not zero, the maximum likelihood estimate of the regression coefficient β is b_{21} (cf. Cramer, 1946, p. 548 for a fuller discussion of the assumptions implicit in this result). Further, the variable

$$\frac{s_1}{s_2}\left(\frac{n-2}{1-r^2}\right)^{1/2}(b_{21}-\beta) \equiv \frac{(b_{21}-\beta)}{\sigma^*} \qquad (7)$$

has Student's distribution with $n - 2$ degrees of freedom. Thus if it appears that we must reject the null hypothesis that $\rho = 0$, we can place probabilistic bounds on the regression coefficient β.

Therefore our tests of significance will be:

i) to compare the computed value of the correlation coefficient r with a value that we would obtain with a certain probability had the coefficients of the geopotential been normally distributed.

ii) if we conclude that the ice potential and geopotential are correlated, to establish limits for the population regression coefficient β by establishing with what probability we would have obtained the regression coefficient b_{21} that we did had the coefficients of both potentials been normally distributed with linearly related mean values.

Linear Regression of Coefficients of Geopotential and Ice Potential

Figure 3 shows the coefficients of the geopotential plotted against the coefficients of the ice potential, i.e. C_ℓ^m vs. A_ℓ^m

FIGURE 3

Plot of harmonic coefficients of the ice potential vs. the geopotential. The linear regression line (least square fit) is dashed. Its slope is determined primarily by the coefficient C_2^0, which also causes the calculated correlation coefficient to be spuriously large.

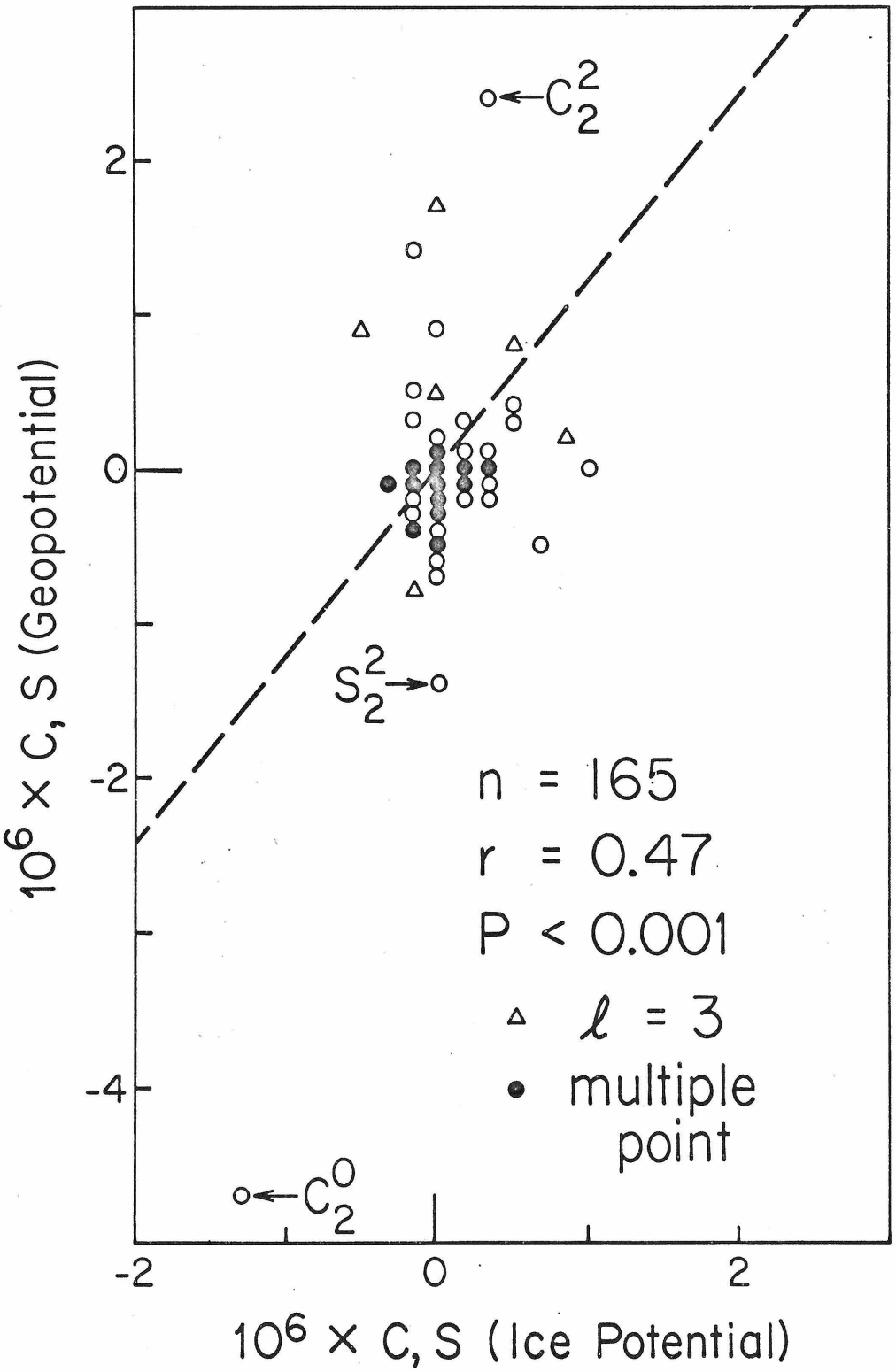
C_2^2
S_2^2
C_2^0
n = 165
r = 0.47
P < 0.001
ℓ = 3
multiple point
2
0
-2
-4
-2
0
2
$10^6 \times$ C, S (Geopotential)
$10^6 \times$ C, S (Ice Potential)

FIGURE 3

and S_ℓ^m vs. B_ℓ^m, for $\ell = 2$ to $\ell = 12$. The points for $\ell = 2$ and $\ell = 3$ are indicated.

First note that the value of C_2^0 for the geopotential is three times as great as the value A_2^0 for the ice potential. Thus the non hydrostatic bulge is too large to be explained as a result of deglaciation, as was mentioned in Chapter I.

The calculated correlation coefficient is $r = 0.47$, which is significant on the 0.001 level, i.e. the probability of obtaining this value for r is 0.001 with normally distributed coefficients. Before we conclude that there really is a correlation between the geopotential and ice potential, we should notice that the correlation coefficient is heavily dependent on the larger coefficients, and is in fact dominated by the coefficient C_2^0. That this could happen is made clear by remembering that r measures the goodness of fit of a least squares straight line through the points. Thus it will be controlled by the squares of distance of the points from the center of mass of the points. This is apparent in Figure 3, where the regression line (dashed line) is seen to be controlled by C_2^0.

We should, however, expect a correlation between C_2^0 for the geopotential and A_2^0 for the ice potential. C_2^0 should be negative because the non hydrostatic bulge exists. This in turn is merely an expression of the fact that the earth is rotating around the axis of its greatest moment of inertia. A large negative value for A_2^0 should exist because the ice sheets were located at high latitudes and the oceans are more equatorially situated than the continents. Thus there should be a correlation between C_2^0 and

A_2^0, but not a causal one. Therefore, not to bias the correlation, we should omit the coefficient C_2^0 from our correlation.

Figure 4 is similar to Figure 3, but with the point for C_2^0 omitted. The large effect of this one point is apparent. With it absent, the correlation coefficient has dropped to 0.10, which has a probability of 19% of being obtained with random coefficients. Thus on this basis it appears that there is no overall correlation between the geopotential and the ice potential for spherical harmonic degrees through $\ell = 12$.

Because anomalies of different degree or wavelength can decay at different rates, we should not actually combine the coefficients of different degrees in one correlation unless we know, or expressly assume, that the anomalies have not changed significantly in their relative magnitudes since deglaciation. Thus the correlation from Figure 4 is subject to this assumption.

To separate the coefficients of different degrees, we will correlate the coefficients of each degree separately to obtain the degree correlation coefficients, r_ℓ, and degree regression slopes b_ℓ. These are given in Table 2 for degrees 2 through 12. The parameters for $\ell = 2$ are given both with and without C_2^0 included. The parameter t is that from Equation (6), and P is the probability of having obtained that value of t with normally distributed variables. Thus, the smaller P is,the greater the likelihood that a correlation exists.

The parameter σ^* is that defined in (7). The dispersion of the regression slope Δb is

FIGURE 4

Same as Figure 3, but with the coefficient C_2^0 omitted. The slope of the regression line is much smaller, and neither it nor the value of the correlation coefficient, r, is significant.

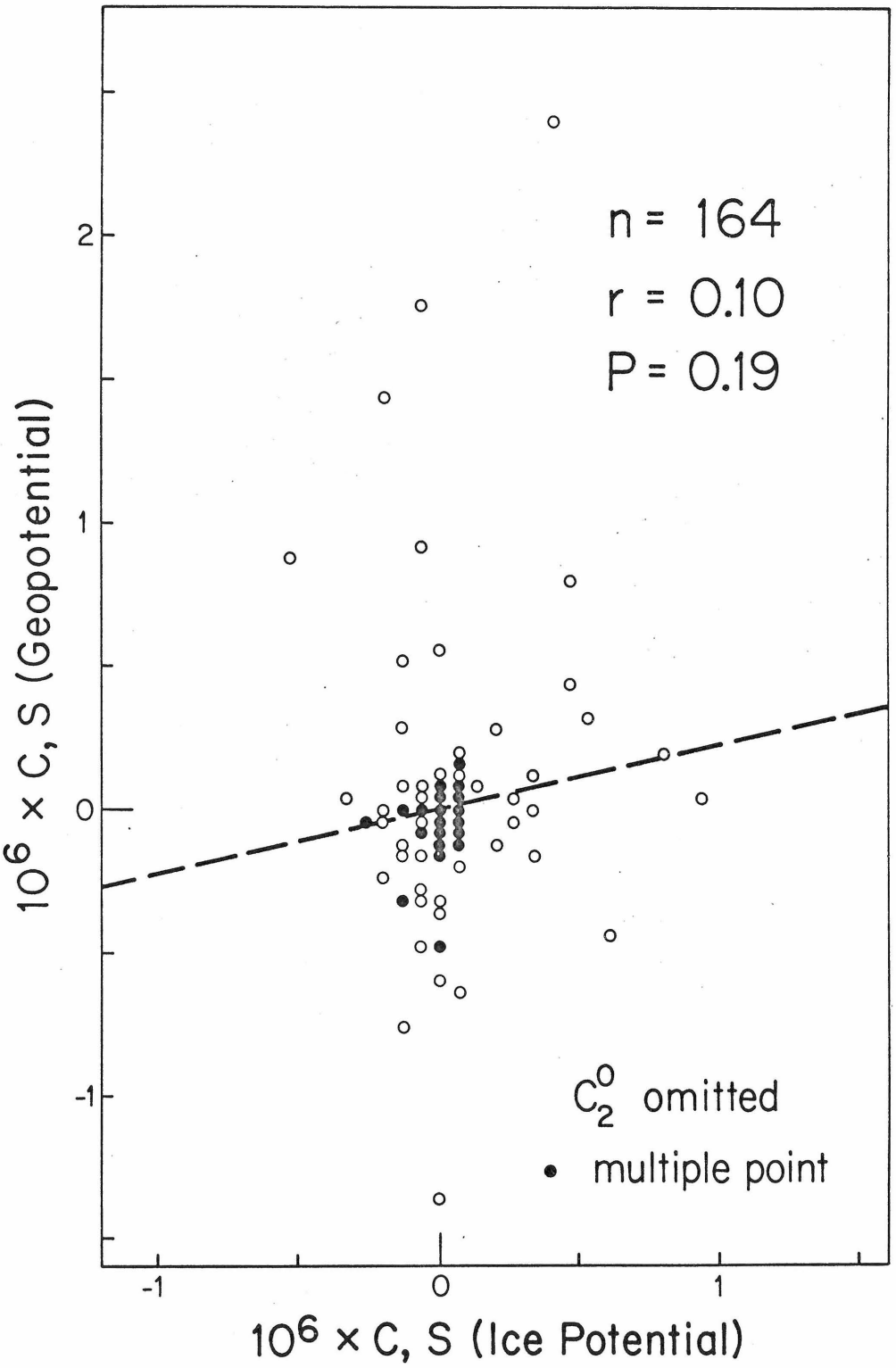
n = 164
r = 0.10
P = 0.19
C_2^0 omitted
• multiple point
10^6 x C, S (Geopotential)
10^6 x C, S (Ice Potential)
2
1
0
-1
-1
0
1

FIGURE 4

TABLE 2. Degree Regression Characteristics

ℓ	r_ℓ	t	P(%)	b_ℓ	σ^*	$\Delta b(10\%)$	n
*2	0.81	2.41	10	2.59	1.07	2.52	5
†2	0.35	0.64	60	1.00	1.56	4.55	4
3	-0.10	-0.21	>60	-0.24	1.11	2.24	7
4	-0.11	-0.28	>60	-0.19	0.67	1.27	9
5	0.54	1.89	10	0.66	0.35	0.64	11
6	-0.00	-0.01	>60	-0.01	0.48	0.86	13
7	0.39	1.52	20	0.40	0.26	0.46	15
8	0.05	0.19	>60	0.04	0.20	0.35	17
9	0.20	0.83	50	0.20	0.24	0.42	19
10	0.32	1.48	20	0.68	0.46	0.80	21
11	0.18	0.82	50	0.34	0.42	0.72	23
12	0.22	1.10	30	0.36	0.32	0.55	25

* with C_2^0 included

† without C_2^0

$$\Delta b = \sigma^* t_P$$

where t_P is the value of Student's t distribution for a probability P with $n - 2$ degrees of freedom. Thus, if a correlation exists, the population regression slope has a probability of P of differing more than Δb from the calculated sample regression slope b_ℓ, if the dependent variable is normally distributed with a mean that is a linear function of the independent variable. Thus the true regression slope has a 90% probability of lying within Δb of b_ℓ. Note that $b_\ell = 0$ means that there is no correlation between the two potentials.

The degree correlation coefficients are also shown in Figure 5. As discussed above, we should dismiss the correlation that includes the coefficient C_2^0. Thus the correlation coefficients r_ℓ for $\ell = 2$, 3 and 4 are all very small. For $\ell = 5$, r_ℓ is fairly large, and would have been obtained with a probability between 5 and 10% with random coefficients. But since we calculate 11 coefficients r_ℓ, we might well expect to have one that has only a 10% probability of occurring. Thus we need not ascribe any significance to the coefficient r_ℓ for $\ell = 5$.

In fact, it is interesting to notice that the probabilities P in Table 2 are distributed as one might expect they might be if they had been picked randomly from a population with a uniform distribution between 0 and 100.

The conclusions we draw from the regression slopes b_ℓ and the dispersion of the regression slopes Δb are similar to those from the correlation coefficients. Again, out of eleven cases, there is one case where Δb is less than b_ℓ. If there were no

FIGURE 5

Correlation coefficient for each degree separately (dashed line) and for all degrees from 2 through ℓ together. No value of the degree correlation is significant, and the sawtooth shape is most likely accidental. Note the dominance of the effect of the lower degree coefficients in the cumulative correlation coefficient (solid lines), and the large effect of including the coefficient C_2^0 in the correlation. Its inclusion causes a spurious high correlation.

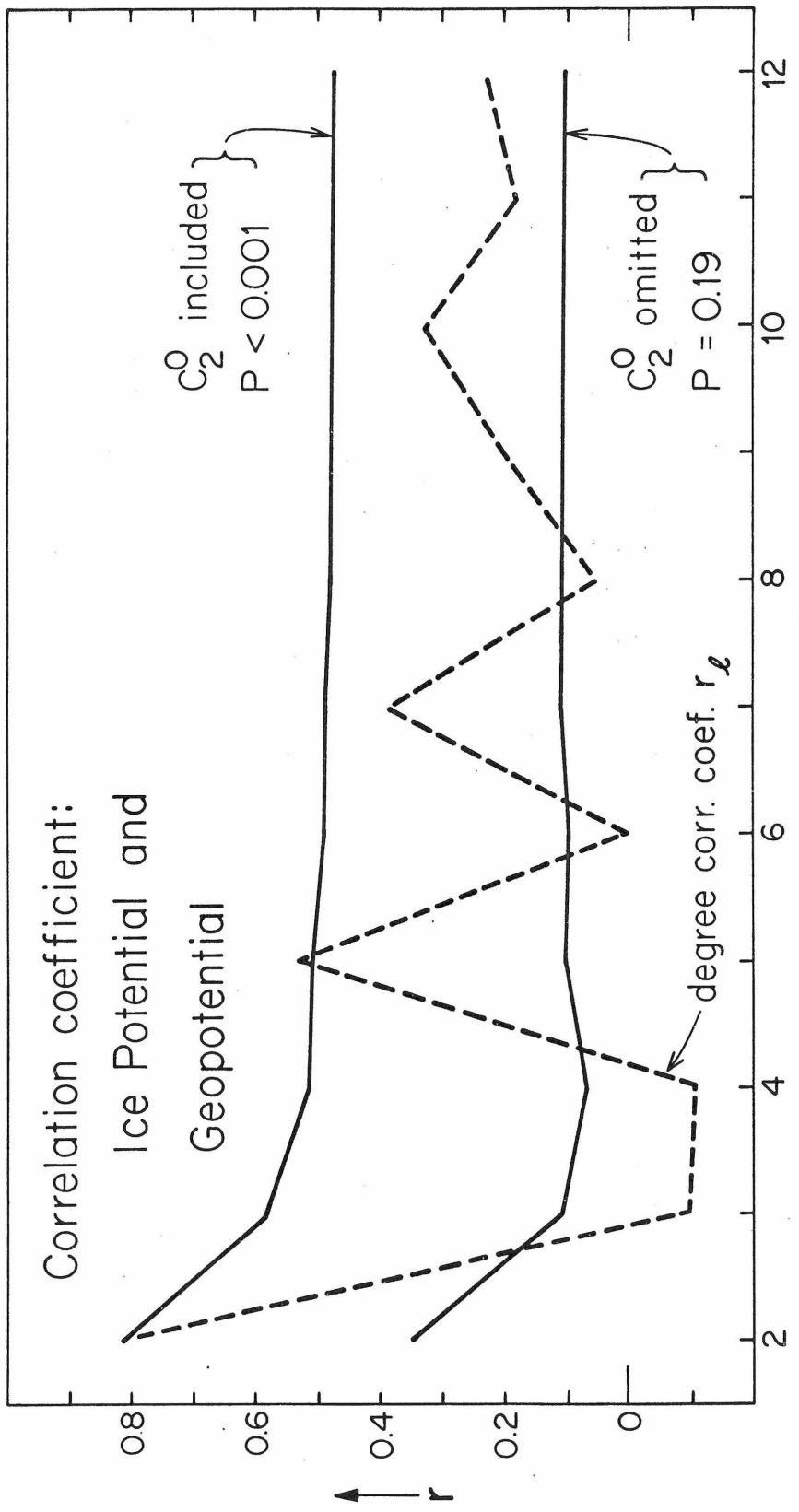
Correlation coefficient:
Ice Potential and
Geopotential
C_2^0 included
P < 0.001
C_2^0 omitted
P = 0.19
degree corr. coef. r_ℓ
r
0.8
0.6
0.4
0.2
0
2
4
6
8
10
12
degree ℓ

FIGURE 5

correlation, (hence the population regression slope $\beta = 0$) then Δb would be greater than b_ℓ with a probability of 10%. That this occurs for one case out of eleven is entirely expected and consistent with the absence of any correlation.

Therefore, on the basis of the degree correlation coefficients and degree regression slopes, we conclude that there is no correlation between the geopotential and ice potential that we have used.

Having made this conclusion we return to Figure 5 for an illustration of the perils of correlation. The solid lines are the correlation coefficients for coefficients from $\ell = 2$ through the indicated value of ℓ. The upper curve is for the correlation including the coefficient C_2^0; the lower curve is for the correlation omitting C_2^0. Thus the values of r for $\ell = 12$ from these two curves are the correlations shown in Figures 3 and 4. We shall call the variable designated by these curves the cumulative correlation coefficient.

Owing to the greater magnitudes of the coefficients for lower degrees (cf. Figure 2), the cumulative correlation coefficient is dominated by the coefficients for lower degrees. Thus the effect of just one large coefficient C_2^0 results in a seemingly significant correlation, one that would have occurred with a probability of $< 0.1\%$ had the coefficients been random. And the omission of just this one coefficient drastically changes the significance of the calculated correlation coefficient. Thus, a plot of the coefficients like Figures 3 and 4 is useful for discovering whether there are any coefficients that might dominate the correlation.

Even with C_2^0 omitted, the lower degrees still dominate the cumulative correlation coefficient, even though the higher

degrees represent many more coefficients. Thus the cumulative correlation coefficient may be highly misleading as an indicator of the degree of correlation between two functions.

As an illustration that our conclusion that the geopotential and ice potential are uncorrelated does not depend on the details of the ice distribution, we compare the results for our two different analyses of the ice distribution. Ice analysis 1 contains the effect of all the ice sheets shown in Figure 1; ice analysis 2 contains only the four large North American and European ice sheets. The degree correlation coefficients for the geopotential with each ice analysis are shown in Figure 6. The degree regression slopes are shown in Figure 7. As can be seen, the curves for the two analyses are nearly identical, and either ice analysis would lead to the same conclusion that we have drawn.

Similarly we compare the results with two different solutions for the geopotential, one by Kaula and one by Gaposhkin, as given by Kaula (1966) as mentioned before. Figure 8 contains the comparison, and again we see that our conclusions would be the same had we used Gaposhkin's geopotential rather than Kaula's.

Conclusions

The spherical harmonic analysis of the change in mass distribution upon the melting of the most recent Pleistocene ice sheets has shown that the non-hydrostatic bulge of the earth is three times too large to be explained as a result of deglaciation as was suggested by Wang (1966).

FIGURE 6

Comparison of correlation of geopotential with either ice analysis. The results are the same with either, hence our results are not sensitive to details of the ice distribution in Figure 1.

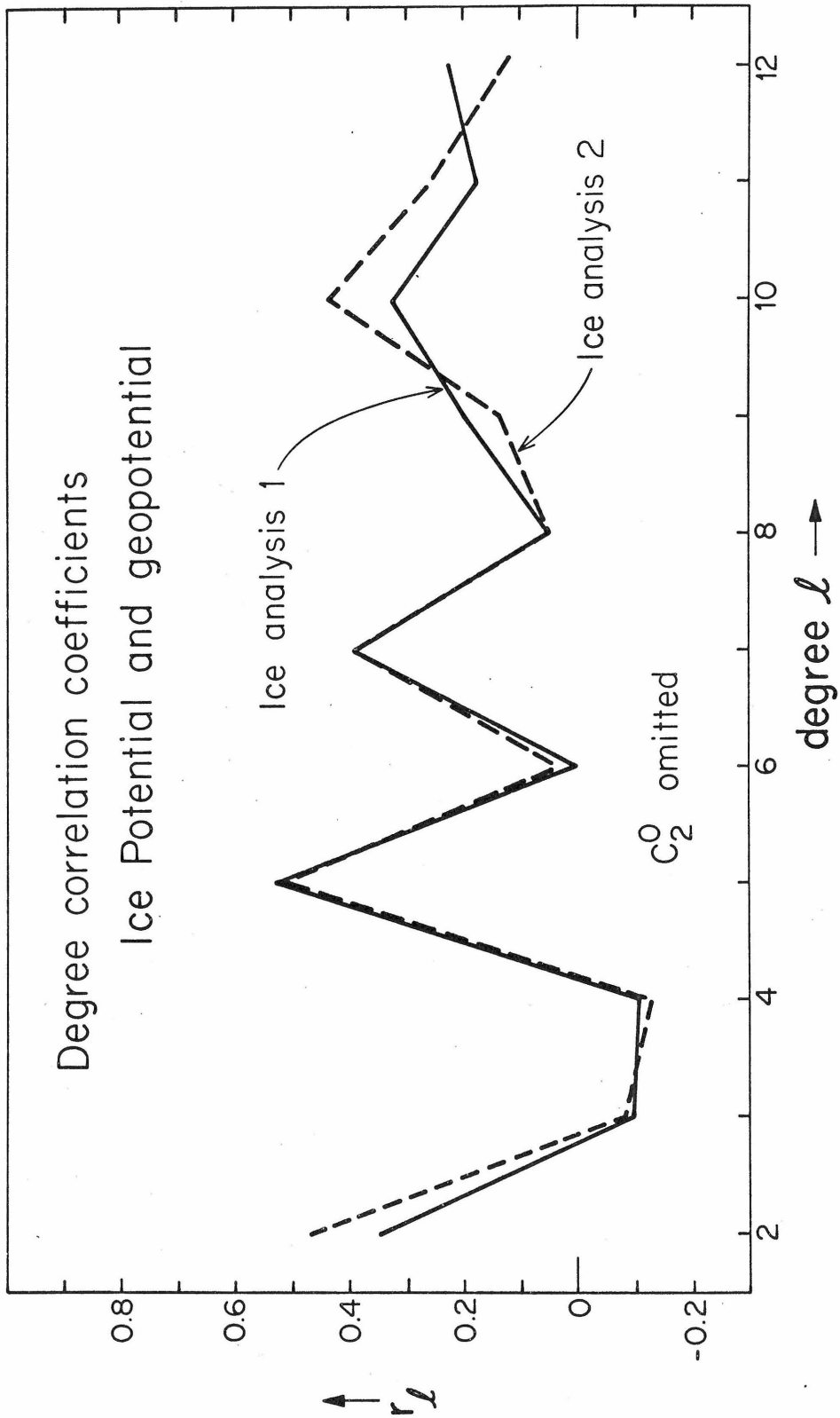
Degree correlation coefficients
Ice Potential and geopotential
Ice analysis 1
Ice analysis 2
C_2^0 omitted
r_ℓ
degree ℓ
0.8
0.6
0.4
0.2
0
-0.2
2
4
6
8
10
12

FIGURE 6

FIGURE 7

Analogous to Figure 6, but showing slope of degree regression lines.

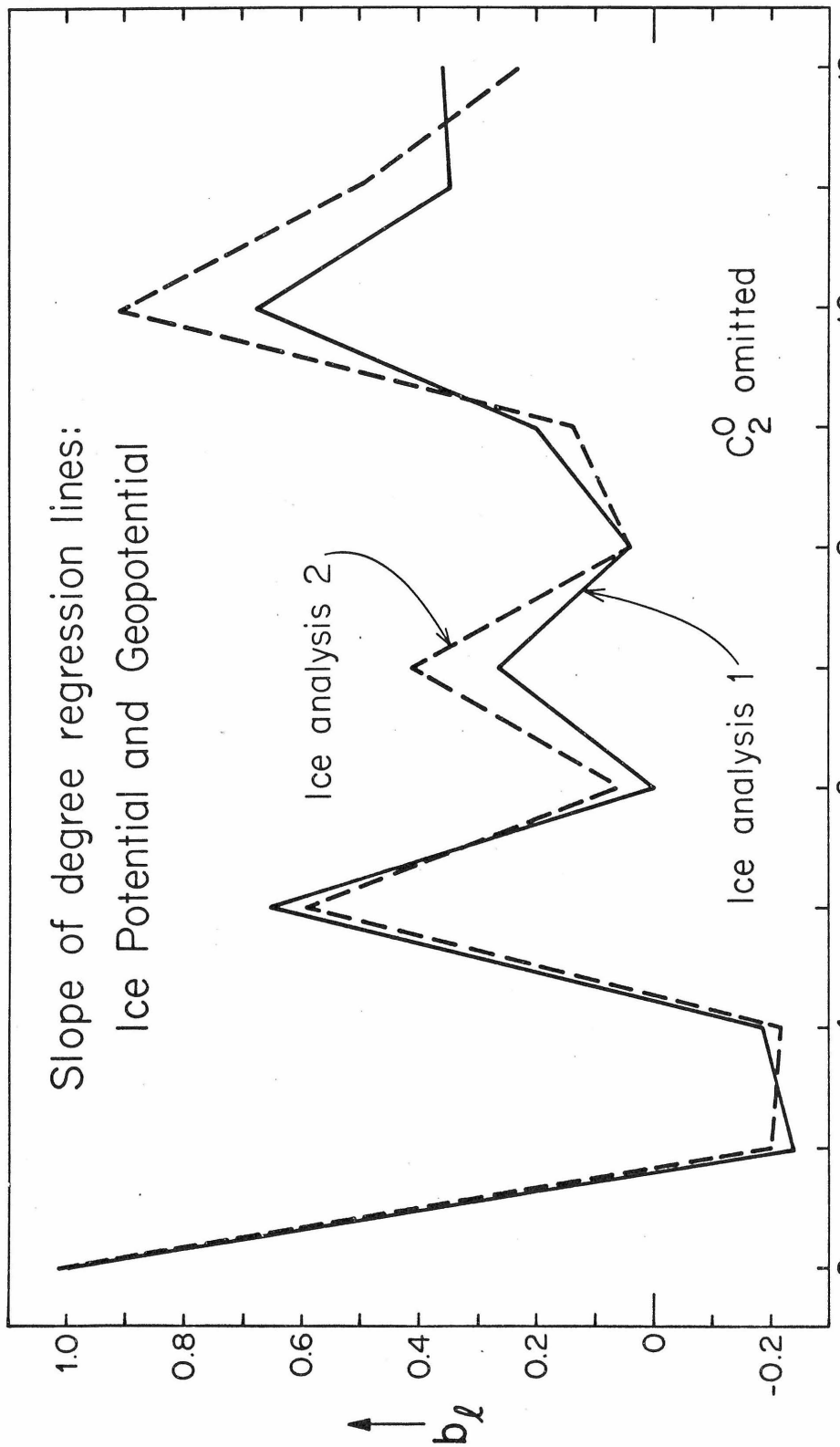
Slope of degree regression lines:
Ice Potential and Geopotential
Ice analysis 2
Ice analysis 1
C_2^0 omitted
b_ℓ
degree ℓ
1.0
0.8
0.6
0.4
0.2
0
-0.2
2
4
6
8
10
12

FIGURE 7

FIGURE 8

Comparison of correlation of ice potential with either of two solutions for the geopotential. The agreement indicates that our conclusions are not dependent on our choice of a particular solution for the geopotential.

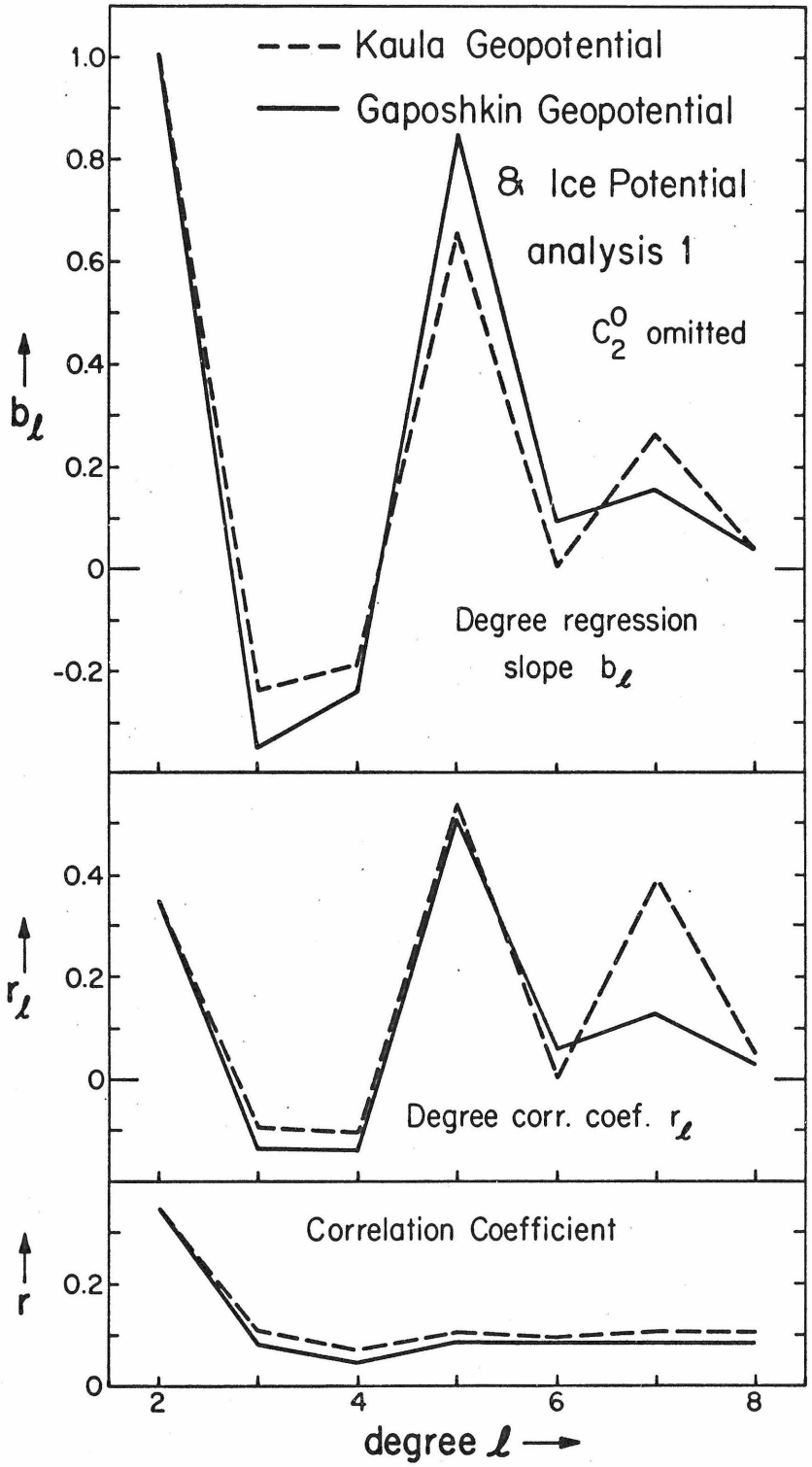
Kaula Geopotential
Gaposhkin Geopotential
& Ice Potential
analysis 1
C_2^0 omitted
Degree regression
slope b_ℓ
Degree corr. coef. r_ℓ
Correlation Coefficient
b_ℓ
r_ℓ
r
1.0
0.8
0.6
0.4
0.2
0
-0.2
2
4
6
8
degree ℓ →

FIGURE 8

A comparison of the power spectra or degree variances of the potential from deglaciation and the geopotential indicates that the effects of deglaciation were large enough to have significantly affected the geopotential. Nevertheless a correlation of the two potentials for degrees 2 through 12 indicates that there is no noticeable correlation at the present time. Moreover, the correlation coefficients for degrees 3 and 4 are particularly low. Since anomalies of these degrees would decay similarly to those of degree two, we conclude that any low degree anomalies resulting from deglaciation have already decayed substantially. This would indicate that the relaxation times for deformations of degrees 2, 3 and 4 are less than 10,000 to 20,000 years. In addition, the relaxation times for degrees 5 through 9 are most probably of the same order, though a hint of a small positive correlation for these degrees indicates that the relaxation time may increase slightly as the degree does.

Thus, if we must choose between the two possible values for the relaxation time for $\ell = 2$ as given in Chapter I, we conclude that the relaxation time is $\sim$ 2000 years.

APPENDIX 1

The spherical harmonic representation of a function $f(\theta,\lambda)$, where θ is colatitude and λ is longitude, on the surface of a sphere is

$$f(\theta,\lambda) = \sum_{\ell=0}^{\infty} \sum_{m=0}^{\ell} \bar{P}_\ell^{\,m}(\cos\theta)\,[C_\ell^{\,m}\cos m\lambda + S_\ell^{\,m}\sin m\lambda]$$

The fully normalized Legendre functions $\bar{P}_\ell^{\,m}(\sin\theta)$ are as defined by Kaula (1967) such that

$$\int_0^{2\pi}\int_0^{\pi} [\bar{P}_\ell^{\,m}(\cos\theta)\left\{\begin{matrix}\cos m\lambda\\ \sin m\lambda\end{matrix}\right\}]^2 \sin\theta\, d\theta\, d\lambda = 4\pi$$

The coefficients of the expansion are obtained from

$$C_\ell^{\,m} = \frac{1}{4\pi}\int_0^{2\pi}\int_0^{\pi} f(\theta,\lambda)\bar{P}_\ell^{\,m}(\cos\theta)\cos m\lambda\,\sin\theta\, d\theta\, d\lambda$$

$$S_\ell^{\,m} = \frac{1}{4\pi}\int_0^{2\pi}\int_0^{\pi} f(\theta,\lambda)\bar{P}_\ell^{\,m}(\cos\theta)\cos m\lambda\,\sin\theta\, d\theta\, d\lambda$$

For our analysis of the ice distribution we may use

$$f(\theta,\lambda) = 1, \qquad \theta_1 \le \theta \le \theta_2, \qquad \lambda_1 \le \lambda \le \lambda_2$$

$$f(\theta,\lambda) = 0 \quad \text{otherwise}$$

Thus

$$C_\ell^m = \frac{1}{2\pi m} \sin\frac{m}{2}(\lambda_2 - \lambda_1)\cos\frac{m}{2}(\lambda_2 - \lambda_1) \int_{\theta_1}^{\theta_2} \bar{P}_\ell^m(\cos\theta)\sin\theta\, d\theta$$

$$S_\ell^m = \tan\frac{m}{2}(\lambda_2 - \lambda_1)\, C_\ell^m$$

To evaluate this we had to do the integral of the associated Legendre functions. This was done analytically by writing the Legendre functions as

$$\bar{P}_\ell^m(\cos\theta) = \sum_{n=0}^{\infty} [A_n \sin n\theta + B_n \cos n\theta] \qquad \text{(A1)}$$

This representation lends itself readily to integration and differentiation of the Legendre functions. Since I have not found it given in the literature, I shall outline its derivation here.

First, recursion relations were found for A_n and B_n by inserting A1 directly in Legendre's equation. However, this did not determine the first terms, and hence the normalization.

The lead terms of the series, indeed the whole series, was then found by expanding the generating equation for the associated Legendre functions:

$$\frac{(2m)!\,(-1)^m}{2^m\, m!}\ \sin^m\theta\,(1 - 2h\cos\theta + h^2)^{-m-1/2}$$

$$= \sum_{\ell=m}^{\infty} h^{\ell-m}\, P_\ell^{\,m}(\cos\theta)$$

For this, $\sin\theta$ and $\cos\theta$ were written in terms of $e^{i\theta}$, and

$$(1 - 2h\cos\theta + h^2)^{-m-1/2} = (1 - he^{i\theta})^{-m-1/2}(1 - he^{-i\theta})^{-m-1/2}$$

was used, and each binomial was expanded into a series in powers of h. Coefficients of the same powers of h were equated, and the θ dependence was retained in coefficients of the form $e^{in\theta}$. The exponentials were then recombined into sines and cosines of integral multiples of θ.

Although this yielded the complete series for (A1), it was more practicable to evaluate only the first term, and then generate the remainder of the series with the recurrence relations.

The general formula was checked by comparing the formulas for $P_\ell^{\,m}(\cos\theta)$ for $\ell = 0$ to $\ell = 4$ and $m = 0$ to $m = 4$ with the formulas given in standard references. $\bar{P}_\ell^{\,m}(\cos\theta)$ was then obtained by using the appropriate normalization factor (Kaula, 1967).

References, Chapter II

Apostol, T. M., Mathematical Analysis, Addison-Wesley, Reading, Mass., 1957.

Cramer, H., Mathematical Methods of Statistics, Princeton University Press, Princeton, 1946.

Flint, R. F., Glacial and Pleistocene Geology, John Wiley, New York, 1957.

Jeffreys, H., On the hydrostatic theory of the figure of the earth, Geophys. J. Roy. Astron. Soc., 8, 196-202, 1963.

Kaula, W. M., Determination of the earth's gravitational field, Rev. Geophys., 1, 507-551, 1963.

Kaula, W. M., Tests and combination of satellite determinations of the gravity field with gravimetry, Jour. Geophys. Res., 71, 5303-5314, 1966.

Kaula, W. M., Theory of statistical analysis of data distributed over a sphere, Rev. Geophys., 5, 83-107, 1967a.

Kaula, W. M., Geophysical implications of satellite determinations of the earth's gravitational field, Space Science Rev., 7, 769-794, 1967b.

Lee, Y. W., Statistical Theory of Communication, John Wiley, New York, 1960.

Lee, W. H. K., and W. M. Kaula, A spherical harmonic analysis of the earth's topography, Jour. Geophys. Res., 72, 753-758, 1967.

McKenzie, D. P., The viscosity of the mantle, Geophys. J. Roy. Astron. Soc., 14, 297-305, 1967.

Wang, C. Y., Earth's zonal deformations, J. Geophys. Res., 71, 1713-1720, 1966.

CHAPTER III

VISCOSITY OF THE LOWER MANTLE

By attributing the non-tidal acceleration of the earth's rotation to the isostatic adjustment following deglaciation and the rise in sea level, we calculated in Chapter I that the relaxation time of the earth for a deformation of spherical harmonic degree $\ell = 2$ was either $\sim$ 2000 years or $\sim$ 100,000 years. In Chapter II a correlation of the geopotential with the potential that would have existed following deglaciation indicated that there was no observable remnant of the low degree components of the potential from deglaciation, as there should have been if the relaxation time were $\sim$ 100,000 years. We therefore concluded that the relaxation time of the earth for degree $\ell = 2$ is $\sim$ 2000 years. What can we infer about the rheological properties of the mantle from this?

We shall interpret the relaxation times of the earth in terms of a Newtonian viscosity of the mantle. We shall not justify the use of Newtonian viscosity here; this has been discussed by Gordon (1965), McKenzie (1966, 1967a) among others. In view of the dearth of data on the relaxation times, we can hardly discriminate between Newtonian and non-Newtonian behavior of the mantle at this stage.

The viscosity structure of the upper few hundred kilometers of the mantle has been worked out by McConnell (1965), using data from ancient shorelines which were upwarped by the isostatic adjustment following the deglaciation of Fennoscandia. He was unable to deduce the viscosity of the lower mantle with any certainty however, because of the limited areal extent of his data (McConnell, 1968).

The deformation from the Fennoscandia ice sheet was primarily of degree $\ell \sim 20$. In order to depend much on the viscosity of

the lower mantle, a deformation must have a wavelength of the order of twice the mantle thickness. (The wavelength of a deformation of degree ℓ is taken as $\lambda = 2\pi a/[\ell(\ell+1)]^{1/2}$, where a is the radius of the earth.) Thus deformations of degree less than ~ 6 will depend more on the lower mantle. The degree most dependent on the lower mantle is $\ell = 2$; thus our value of the relaxation time for a degree $\ell = 2$ deformation, used with McConnell's data for higher degrees should allow us to deduce the viscosity of the lower mantle.

McConnell (1965) used a plane layered half space as a model; for the shorter wavelengths with which he was concerned, this was most probably adequate. For long wavelengths, and in particular for $\ell = 2$, the effect of sphericity and the earth's fluid core are probably large. Thus we shall use a spherical model.

Model of Viscous Earth and Method of Solution

Our model viscous earth consists of concentric layers, each with uniform viscosity and density, which we assume are incompressible. In each layer the Navier-Stokes equation is satisfied. At the boundaries between layers the velocity and stress are continuous. The core of the earth is considered an inviscid fluid, and the normal stress is continuous at the mantle core boundary. At the surface of the earth, either of two boundary conditions may be applied; either the tangential traction vanishes (a free surface) or the tangential velocity vanishes (no slip surface). Since the earth does have a rigid lithosphere the no slip condition at the surface is probably the more proper one, although the movements associated with plate tectonics could conceivably accommodate some slip.

The Navier Stokes equation for an incompressible fluid was solved in each layer, in which viscosity and density were uniform. Since we are concerned only with the departure of the earth from hydrostaticity, the equation was solved in a non-rotating frame; the inertia terms were neglected since they were negligible; and the body forces resulting from the gravity perturbations from the displacement from sphericity of boundaries between layers of different density were included in the equation . (The results reported in Anderson and O'Connell (1967) did not include these body forces.) A solution was sought in the form of the product of a function of radius alone and a spherical vector harmonic (cf. McKenzie (1966), eq. 29). This separated the equation into a separate equation for each degree; furthermore each equation reduced to a second order ordinary differential equation for the functions that depended only on the radius for each degree. These were transformed into a first order inhomogeneous vector differential equation, in which the vector had as components radial velocity, radial stress, tangential velocity and tangential stress. This is the same form obtained by Takeuchi and Hasegawa (1965), except for the presence of body force terms. With a change of variable from r to $\log r$ the equation was integrable, allowing the construction of a fundamental matrix (Coddington and Levinson, 1955); this matrix, when inverted, in turn permitted the construction of a propagator matrix (Gilbert and Backus, 1966). This is a matrix $P(r, r_0)$ such that a solution of the differential equation is $\underline{f}(r) = P(r, r_0)\,\underline{f}(r_0)$ where r_0 is constant.

A solution for the relaxation time τ_ℓ for a given degree ℓ was obtained by assuming that the surface of the earth was deformed

as a spherical harmonic. The deformation was assumed to decay exponentially in time with relaxation time τ_ℓ. Thus the radial velocity was related through τ_ℓ to the radial displacement which was proportional to the radial stress at the undeformed boundary. Using the propagator matrix from the core boundary to the surface with the boundary conditions gave a quadratic equation for τ_ℓ, in which the coefficients were elements of the propagator matrix.

Since the body force field could not be known until the velocity solution was, it was first set equal zero and a solution obtained. This solution was then used to evaluate the body force field, and a new solution found. This process was iterated until it converged on a solution.

Model Solutions

We first present an illustration of the effect of a fluid core, and the density distribution of the mantle, on the relaxation time for low degrees. Figure 1 shows the relaxation time vs. degree for four different models of the earth. The first is a uniform sphere, with no core. The second has a liquid core of the same density as the mantle. The third has a liquid core with a density greater than that of the mantle. The density jump at the core-mantle boundary is the same as for the earth. The fourth model is a realistic model of the earth with a uniform viscosity mantle, but with a five layer density distribution in the mantle similar to Bullen's model A' (Bullen and Haddon, 1967). The large effect these different features have on the relaxation time for $\ell = 2$ is apparent, and points up the inadequacy of a planar model for low degrees.

FIGURE 1

Relaxation time spectrum for spherical earth models with increasing degrees of a realistic density structure. All four models have a uniform mantle viscosity. The introduction of a core with the same density as the mantle decreases τ_2. The inclusion of a density jump at the core mantle boundary (case 3) increase τ_2, as does the inclusion of an increase of density with depth in the mantle (case 4). The latter model is a realistic model of the earth with a uniform mantle viscosity. Note that $\tau_\ell \propto$ viscosity; thus the relaxation times can be found for any value of the viscosity by appropriate scaling.

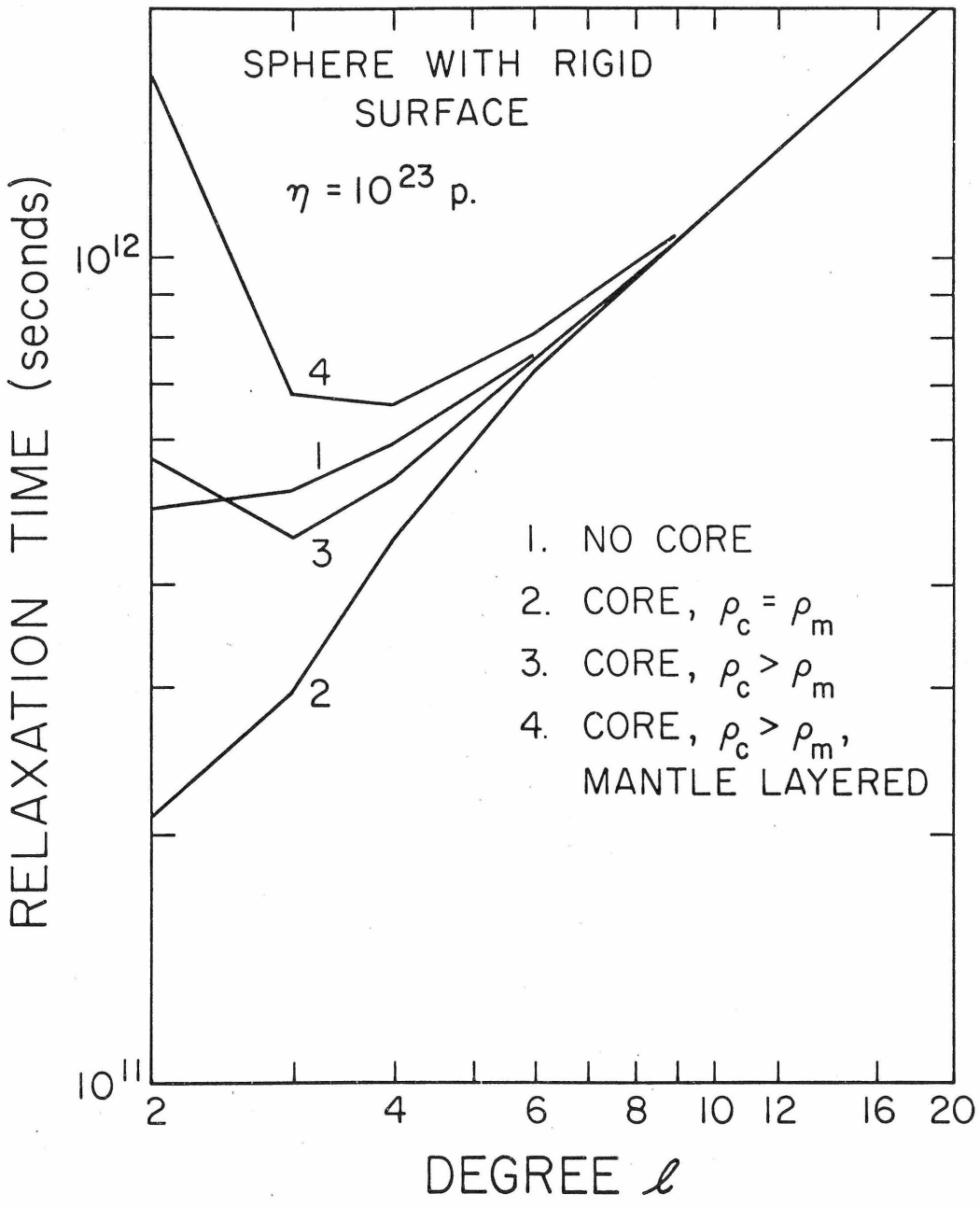
SPHERE WITH RIGID SURFACE
$\eta = 10^{23}$ p.
RELAXATION TIME (seconds)
10^{12}
10^{11}
2
4
6
8
10
12
16
20
DEGREE ℓ
1. NO CORE
2. CORE, $\rho_c = \rho_m$
3. CORE, $\rho_c > \rho_m$
4. CORE, $\rho_c > \rho_m$, MANTLE LAYERED

FIGURE 1

It is interesting to note that the relaxation times increase as more density variation is included in the model. This is probably because the body forces arising from the displacement of a region with a density gradient couple the motion of one part of the mantle to that of another. Thus the relaxation of the surface to an equilibrium position is coupled with the relaxation of the core-mantle boundary through the gravity field associated with the deformation of the surface.

Since the effects from the presence of a core and density structure in the earth are large, we now compare the solutions for a spherical model and flat earth model with the same viscosity structure. The spherical model has a realistic density variation, while the half space model has uniform density. The viscosity model is model 62-12 of McConnell (1965), which gave the best fit to the data from the uplifted shore lines in Fennoscandia. The model is shown as a solid line in Figure 2. This model has a low viscosity channel at a depth of $\sim$ 400 km, with a rising viscosity at greater depths.

The relaxation time curve, calculated for the realistic spherical model, is shown in Figure 3, together with the data from the shore lines. The flat earth solution, which is not shown, fit the data points very well, and gave a τ value for $\ell = 2$ of 3800 years. The spherical model exhibits a longer relaxation time at low degrees than the flat earth model. Presumably this is because of gravitational coupling. If one wished to fit the shore line data, the viscosity of the lower mantle would have to be lower than shown in Figure 2. If one were to fit a relaxation time for $\ell = 2$ of $\sim$ 2000 years, as suggested by the two previous chapters, the lower mantle

FIGURE 2

Viscosity models used in calculations. The solid line is McConnell's (1965) model 62-12, which best fit data from the uplift of Fennoscandia. Model a demonstrates the effect of the viscosity between 400 and 1200 km. on τ_{20}. Models b and c show that a high viscosity lower mantle will increase τ_2 even with a large region of lower viscosity in the upper mantle.

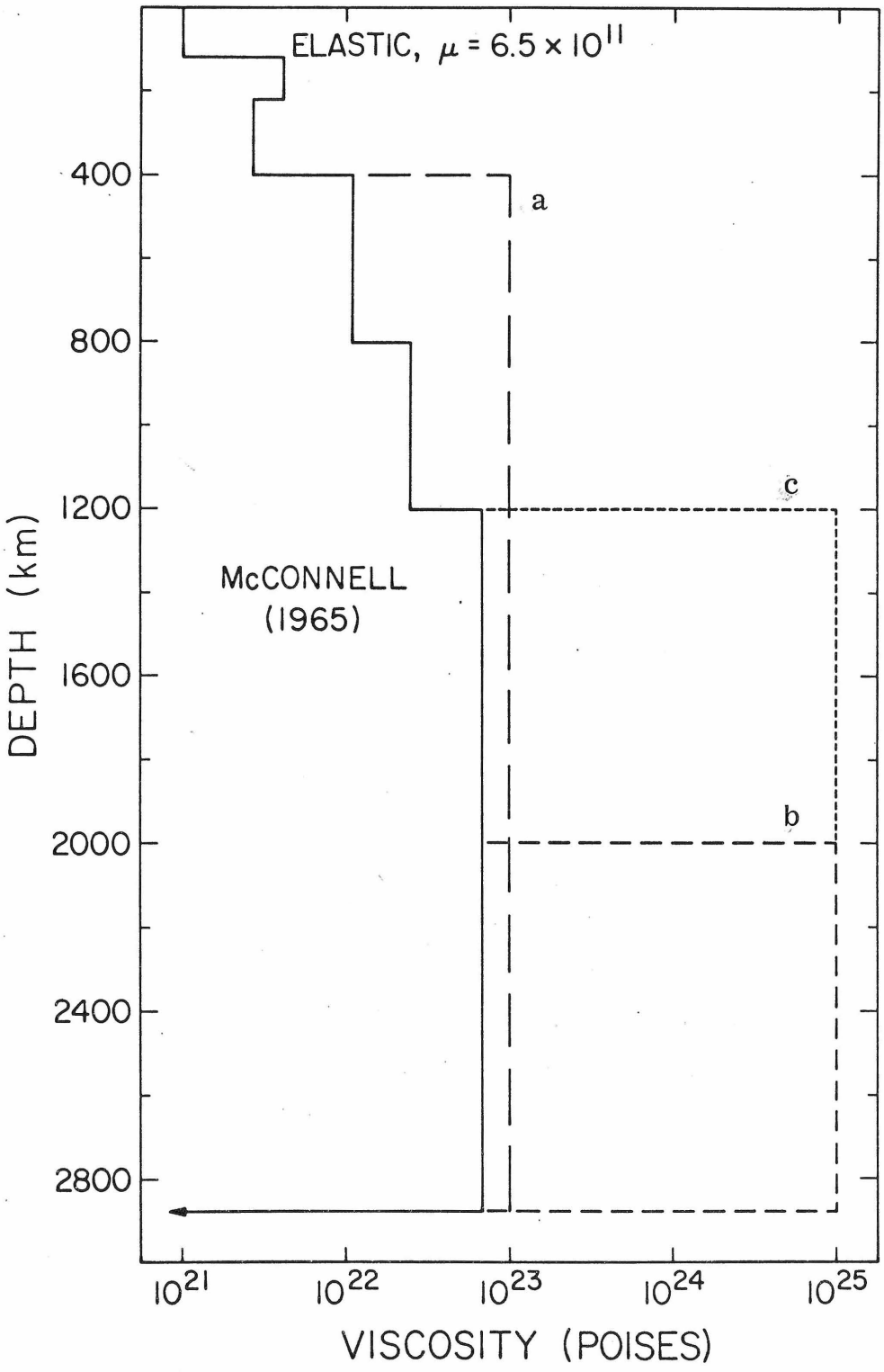
ELASTIC, $\mu = 6.5 \times 10^{11}$
a
c
b
McCONNELL
(1965)
DEPTH (km)
400
800
1200
1600
2000
2400
2800
10^{21}
10^{22}
10^{23}
10^{24}
10^{25}
VISCOSITY (POISES)

FIGURE 2

FIGURE 3

Relaxation time spectra for viscosity models of Figure 2. The effects of sphericity, the presence of a core and the density structure of the earth cause McConnell's model 62-12 to not fit the data for lower degrees (a flat earth solution of the same model fit the data). In order for this model to satisfy τ_2 = 3000 years, the lower mantle viscosity would have to be reduced to $\sim 2 \times 10^{22}$ p. It would then also fit the data for low degrees. Model a shows the effect of the viscosity at $\sim$ 800 km. depth on τ_{20}. Models b and c show that a high viscosity region confined to the lower mantle still significantly affects the relaxation times for low degrees.

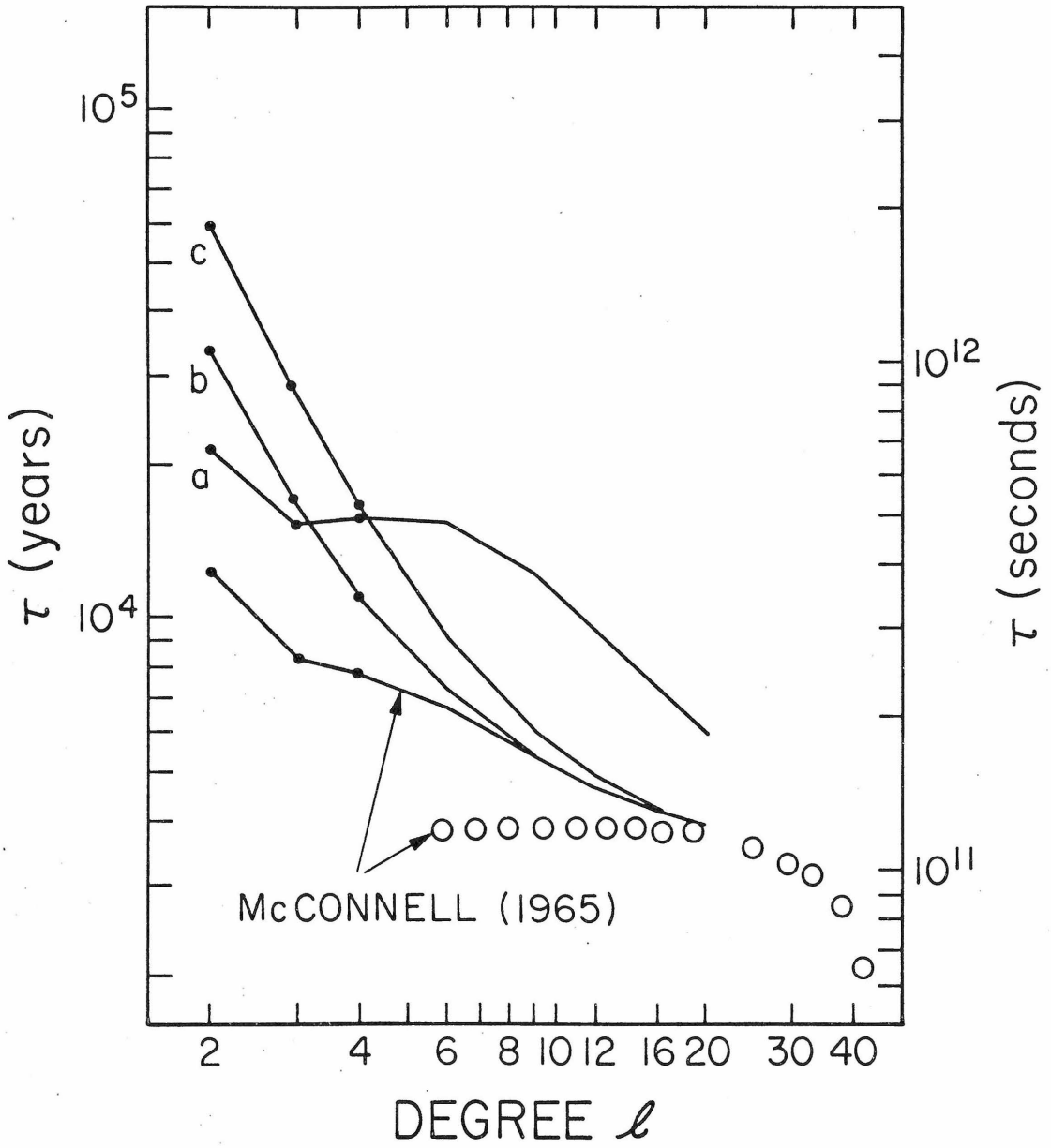
10^5
10^4
τ (years)
10^{12}
10^{11}
τ (seconds)
c
b
a
McCONNELL (1965)
2
4
6
8
10
12
16
20
30
40
DEGREE ℓ

FIGURE 3

viscosity would need to be $\sim 10^{22}$. This would result in a uniform viscosity, or only a very slight increase below $\sim$ 400-800 km. depth.

For degrees $\ell \gtrsim 20$, the spherical and half space solutions agree, as would be expected, since the scale of the deformations will then be much less than the radius of the earth, and only the upper mantle will be involved in the flow as isostatic readjustment takes place.

Also shown in Figures 2 and 3 are two models b and c, to determine to what extent a high viscosity lower mantle could be "shielded" by a lower viscosity upper mantle. As shown by model c, a high viscosity lower mantle below 1200 km. depth substantially increases the relaxation time for the lower degrees. Even a higher viscosity region confined to depths below 2000 km. depth (model b) raises the relaxation time for $\ell = 2$ by a factor of 3. Note that both these models with a high viscosity lower mantle agree with McConnell's model and data for $\ell \gtrsim 20$. This is because they all have the same structure in the upper mantle. Model a, on the other hand, has a different structure below 400 km. depth; and it has a higher relaxation time for $\ell = 20$ than the other models.

Conclusions from Model Studies

On the basis of the solutions of these models, we therefore conclude that a model of the mantle viscosity similar to McConnell's model 62-12 in the upper mantle, but with a lower mantle viscosity of $\sim 10^{22}$ will fit McConnell's Fennoscandia data and give a relaxation time of $\sim$ 3000 years for an $\ell = 2$ deformation.

We might inquire whether a simpler model could give an acceptable relaxation time spectrum. As mentioned before the spectrum from the Fennoscandia data by McConnell may be unreliable for lower degrees although for $\ell \sim 20$, it should be reliable. As shown by McConnell (1965), the spectrum for higher degrees greater than 20 can be altered for a given model by making changes in the elastic layer representing the lithosphere, or by making changes in the viscosity of the uppermost mantle; this can be done without seriously changing the spectrum for lower degrees.

We therefore take as controls on our spectrum, a relaxation time of $\sim$ 4000 years for $\ell = 20$, (from McConnell), and a relaxation time of from 1000 to 3000 years for $\ell = 2$ (from Figure 2 of Chapter I). The spectrum for degrees higher than $\ell = 20$ can be adjusted by changes in the uppermost mantle, so we shall not try to fit it. Rather, we shall concentrate on the relation between the upper mantle viscosity (at depths less than $\sim$ 1000 km.) which influences the relaxation time for $\ell = 20$, and the lower mantle viscosity which will influence the relaxation time for $\ell = 2$.

The simplest model is one with a uniform viscosity, the spectrum for which is shown as model 4 in Figure 1. This model gives a value for the ratio of the relaxation times $\tau_2/\tau_{20} = 0.76$, which is the same as one obtains with $\tau_2 = 3000$ years and $\tau_{20} =$ 4000 years. Thus a mantle with a uniform viscosity of $\sim 6 \times 10^{21}$ poise will result in acceptable relaxation times for both $\ell = 2$ and $\ell = 20$. (Note that for a uniform viscosity mantle, τ_ℓ is proportional to viscosity.)

A relaxation time for $\ell = 2$ of less than 3000 years will require a viscosity in the lower mantle less than that of the upper

mantle, conversely an increase in viscosity with depth will result in a larger ratio τ_2/τ_{20}, which would require a value of τ_2 greater than 3000 years. We are thus led to conclude that $\tau_2 \approx 3000$ years, and that the mantle may be characterized by a uniform viscosity of $\sim 6 \times 10^{21}$ poise, except for fine structure in the upper mantle at depths less than a few hundred kilometers.

The implications of this conclusion are considerable. Such a viscosity would permit convection in the lower mantle (Knopoff, 1964). With such a low viscosity, it is difficult to see how the lower mantle could statically support the low degree components of the geopotential (McKenzie, 1967b). Thus they must be supported by a dynamic process, such as convection. If this were so, changing patterns of convection would result in changes in the principle moments of inertia of the earth, thus changing the axis of the greatest principle moment of inertia. This could then result in polar wandering as suggested by Goldreich and Toomre (1969). The value of the viscosity we have calculated would permit polar wandering at the rate and in the manner that they suggest.

References Chapter III

Anderson, D. L., and R. O'Connell, Viscosity of the earth, Geophys. Journ. Roy. Astron. Soc.,14, 287-295, 1967.

Bullen, K. E., and R. A. W. Haddon, Earth oscillations and the earth's interior, Nature, 213, 574-576, 1967.

Coddington, E. A., and N. Levinson, Theory of Ordinary Differential Equations, McGraw-Hill, New York, 1955.

Gilbert, F., and G. E. Backus, Propagator matrices in elastic wave and vibration problems, Geophysics, XXXI, 326-332, 1966.

Goldreich, P., and A. Toomre, Some remarks on polar wandering, Jour. Geophys. Res., in press, 1969.

Gordon, R. B., Diffusion creep in the earth's mantle, Jour. Geophys. Res., 70, 2413-2418, 1965.

Knopoff, L., The convection current hypothesis, Rev. Geophys., 2, 89-122, 1964.

McConnell, R. K., Jr., Isostatic adjustment in a layered earth, Jour. Geophys. Res., 70, 5171-5188, 1965.

McConnell, R. K., Jr., Viscosity of the mantle from relaxation time spectra of isostatic adjustment, Jour. Geophys. Res., 73, 7089-7105, 1968.

McKenzie, D. P., The viscosity of the lower mantle, Jour. Geophys. Res., 71, 3995-4010, 1966.

McKenzie, D. P., The viscosity of the mantle, Geophys. Jour. Roy. Astron. Soc., 14, 297-305, 1967a.

McKenzie, D. P., Some remarks on heat flow and gravity anomalies, Jour. Geophys. Res., 72, 6261-6274, 1967b.

Takeuchi, H., and Y. Hasegawa, Viscosity distribution within the earth, Geophys. Jour. Roy. Astron. Soc., 9, 503-508, 1965.